United States/People's Republic of China

Flood Forecasting Symposium/Workshop Volume One

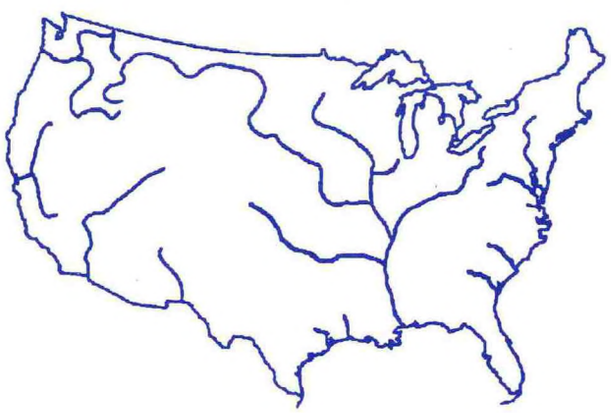

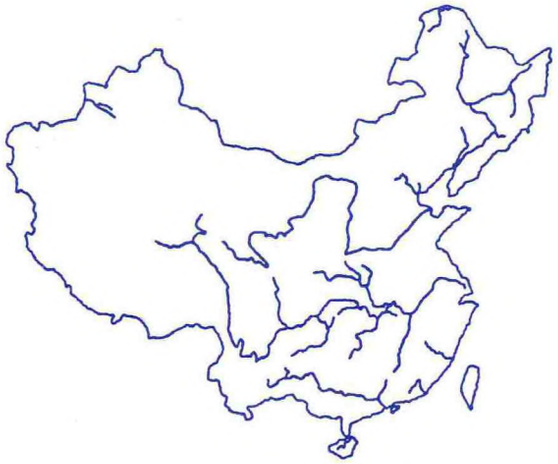

Symposium March 29-31, 1989
Workshop April 3-4, 1989

Red Lion Inn
Columbia River
1401 North Hayden Island Drive
Porland, OR

Office of Hydrology
National Weather Service
National Oceanic and Atmospheric Administration
U.S. Department of Commerce

UNITED STATES/PEOPLE'S REPUBLIC OF CHINA
FLOOD FORECASTING
SYMPOSIUM/WORKSHOP
Portland, Oregon
March 29 - April 4, 1989

VOLUME ONE

Table of Contents

==========

Theme II - Hydrologic Models

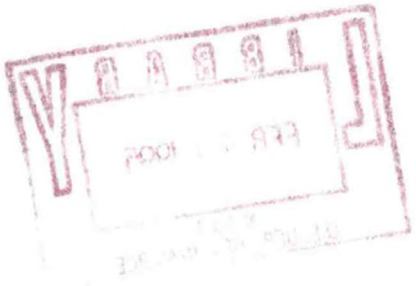

VOLUME TWO

==========

Theme III - Forecasting

==========

*Papers giving additional enlightenment on these themes received after the symposium/workshop

==========

Workshop

UNITED STATES/PEOPLE'S REPUBLIC OF CHINA FLOOD FORECASTING
SYMPOSIUM/WORKSHOP
Portland, Oregon
March 29 - April 4, 1989

VOLUME ONE

Table of Figures

HYDROLOGICAL INFORMATION AND FORECASTING IN CHINA

DEVELOPMENT AND OPERATION OF THE SNOWPACK TELEMETRY (SNOTEL) SYSTEM IN THE WESTERN UNITED STATES

TECHNICAL DEVELOPMENT AND EXPERIENCE OF HYDROLOGICAL INFORMATION AND FORECASTING ON THE YANGTZE RIVER

AUTOMATED DATA ACQUISITION TECHNIQUES FOR FORECASTING PACIFIC NORTHWEST RIVERS

THE SIMULATION OF THE CATCHMENT RUNOFF PRODUCTION COMPUTATION

USE OR MISUSE OF QUANTITATIVE PRECIPITATION FORECASTS (QPF)

A COMPARATIVE STUDY ON HYDROLOGICAL FORECASTING MODELS

FLUVIAL-12, MATHEMATICAL MODEL FOR ERODIBLE CHANNELS

APPLICATION OF THE VARIABLE ISOCHRONE METHOD

NUMERICAL FLOOD ROUTING MODELS USED IN NWS

INTEGRATION SOLUTION OF THE MUSKINGUM SUCCESSIVE ROUTING METHOD AND THE LAG-AND-ROUTE METHOD

IMPORTANCE OF THE HYDROLOGIC RAINFALL ANALYSIS PROJECT (HRAP) GRID FOR OPERATIONAL HYDROLOGY

THE XINANJIANG MODEL AND ITS APPLICATIONS

VOLUME TWO

THE IMPROVED MUSKINGUM METHOD AND ITS APPLICATION IN CHINA

A RESEARCH ON GEOMORPHOLOGIC INSTANTANEOUS UNIT HYDROGRAPH (GUH) MODEL FOR RESERVOIR REGION

A RUNOFF MODEL OF KARST REGIONS IN GUANGXI

A HYDROLOGIC MODEL OF SEMIARID REGIONS

IMPROVEMENT AND APPLICATION OF THE XINANJIANG MODEL

DAMBREAK FLOOD WAVE ROUTING BY USING TOTAL VARIATION DIMINISHING SCHEME

FLOOD FORECASTING METHODS UNDER CONDITIONS OF MOVING RIVER BED AND PROTECTIVE DIKES ON THE DOWNSTREAM OF THE YELLOW RIVER

FORECASTING FOR FLOOD CONTROL OPERATIONS IN THE COLUMBIA RIVER

REDUCING RISK IN THE DEFINITION AND IMPLEMENTATION OF THE NWS AWIPS-90 HYDROLOGIC COMPONENT

A STUDY OF NUMERICAL FORECASTING TECHNIQUES FOR TYPHOON SURGE ALONG THE FUJIAN COAST

PARAMETER UPDATING WITH A SINGLE EVENT REAL-TIME FLOOD FORECASTING MODEL

USING RADAR DATA PROCESSOR (RADAP II) AND INTERACTIVE COLOR RADAR DISPLAY (ICRAD) FOR FLASH FLOOD FORECASTING

WELCOME

I would like to welcome everyone to Portland, Oregon and the United States/People's Republic of China Flood Forecasting Symposium/Workshop. First, it is with great pleasure that I officially welcome our visitors from the People's Republic of China (PRC) to the United States. Second, I wish to acknowledge our participants from the Federal water resources agencies, as well as the representatives from the universities. Last, I am gratified by the sizeable delegation from the National Oceanic and Atmospheric Organization/National Weather Service. In particular, I want to acknowledge the efforts of Mr. Charles Orwig, Hydrologist-in-Charge, Northwest River Forecast Center, and his staff. Without their assistance (in handling the local arrangements), this international symposium and workshop would not be possible.

We have an extremely ambitious agenda for both the symposium and the workshop and some ground rules need to be established. The symposium is composed of three themes, data collection and dissemination, hydrologic models, and forecasting, and the papers have been grouped appropriately. During the symposium, each speaker will have 25 minutes for their presentation and 10 minutes for questions and discussion. Unresolved issues will be considered for inclusion at the workshop scheduled for April 3-4. The United States participants are requested to speak slowly for the benefit of our Chinese delegates.

Before beginning the symposium, we should address briefly the history of United States/People's Republic of China involvement in hydrologic information and flood forecasting.

In 1981, the National Weather Service (NWS) agreed to take the lead in providing consulting services for the World Meteorological Organization (WMO), a United Nations sponsored program for the People's Republic of China Ministry of Water Conservancy and Electric Power for the purpose of improving real-time telemetering and flood forecasting on the San-Hua reach of the Yellow River. In November 1983, the telemetry system and base stations became operational. The NWS has also provided technology for improving hydrologic forecasting by

the introduction of NWS forecasting techniques and assisted WMO in the selection, procurement, and installation of computers for the project. In 1983, David Street of the NWS Office of Hydrology instructed the PRC staff on the operation of the PRIME computer. Forecasting techniques have been implemented, including early warning forecasting capabilities, at the Luhun Reservoir data collection site. In August 1984, Larry Brazil visited China and loaded National Weather Service River Forecast System (NWSRFS) software on the Yellow River Conservancy Commission (YRCC) PRIME computer and gave several lectures on numerous topics related to NWSRFS. Daily workshops and discussions were held on possible alternatives for modeling the Yi He River Basin. Mr. Brazil visited Zhengzhou in September 1985 to provide follow-up consultation and training on the implementation and calibration of the NWSRFS. The principal objectives of the trip were to discuss YRCC organization of historical and real-time data, discuss the status of implementation and YRCC calibration work with NWSRFS, discuss development of Xiananjiang model, and to present lectures on real-time forecast updating using Kalman Filtering.

The Department of Hydrology of the Chinese Ministry of Water Resources and the U.S. Geological Survey signed a 5-year agreement in 1981, entitled "Scientific and Technical Cooperation in the Study of Surface-Water Hydrology." This protocol contains seven annexes with Annex 5 identified as Hydrological Information and Forecasting and the responsibility of the NWS. Annex 5 covers cooperative research on hydrological information and forecasting; including studies and the exchange of experience on real-time data collection, on-line and off-line methods of hydrological forecasting computer applications to hydrological information and forecasting, flood forecasting for control of water conservancy and hydropower projects, and flood warning. This annex was signed on April 10, 1985, by the U.S. Permanent Representative, Dr. Richard G. Hallgren, officials of the PRC, and the USGS. An initial visit to the U.S. by five Chinese hydrologists during the period October 15-30, 1986, was followed by a U.S. team reciprocal visit in the spring of 1987. During these visits, both countries described their respective roles on hydrological information and forecasting. At the conclusion of the spring 1987 meeting, the People's Republic of China and the

United States developed plans for two symposiums and workshops on hydrological information and forecasting. In September 1988, U.S. annex co-leader, Dr. Hudlow, met with PRC annex co-leader, Mr. Wang, in China to finalize plans for the Bilateral Flood Forecasting Symposium. This symposium is the result of that meeting and a similar symposium and workshop will be scheduled in China in the near future.

This symposium will conclude in late afternoon on March 31. A field trip is planned on April 1 to Mt. St. Helens and the Toutle-Cowlitz area. On April 2, another field trip is planned to Mt. Hood. All participants are invited to attend one or both field trips since these bilateral sessions offer an excellent opportunity to exchange technical and cultural experiences between the two countries. On Monday, April 3, a two-day workshop is planned to focus in depth on substantive issues raised during the symposium. We plan to publish the symposium papers and a summary of the workshop.

Again, I want to welcome everyone to the Pacific Northwest and to encourage all participants to talk freely during the coffee breaks, lunches, and social functions. These unofficial technology transfers play a valuable part in fostering an open exchange between our two countries. Thank you all for coming. I wish everyone the best towards a successful symposium and workshop.

OPENING REMARKS OF THE SYMPOSIUM

Ladies and Gentlemen,

Today, the Sino-American Bilateral Symposium on Hydrological Information and Flood Forecasting has formally opened. We have anticipated the symposium and workshop for a long time. The Chinese delegation is very happy to attend the symposium with our American friends here in such a beautiful country. Of course, it is the first bilateral symposium in Sino-American history in this field, and I wish it to be a complete success.

America and China are very similar in natural and hydrologic conditions. Both of them have vast territories and famous rivers of the world. For example, in America there is the famous Mississippi, in China there are the Yangtze and Yellow Rivers; in America there is a threat of flash floods from medium- and small-sized rivers, while in China there often happen serious calamities of mountain floods in mountain areas. America is often affected by hurricanes while China is threatened by typhoons. Both countries have also been hit by storm-surges along their long coastlines; and they often suffer from severe droughts. Every year America and China sustain heavy losses from floods and droughts. This is despite the construction of many reservoirs in both countries. To summarize, what we are facing is how to decrease flood damage, put water resources to more efficient use, and bring additional benefits to mankind.

Functioning as eyes and ears, hydrologic information and forecasting is of the utmost importance and has played a significant role in the struggle for water control in both of these countries. Therefore, the hydrologists have an interest in the development and improvement of hydrologic information and flood forecasting. As a developed country, America has advanced equipment and rich experience in hydrologic information and forecasting. As a country with a long history, China has accumulated a wealth of experience in hydrologic information and forecasting, especially, the most recent advances. We believe

there is a bright future of extensive cooperation between America and China. Of course, there's much in the American hydrologists experience that our Chinese hydrologists should learn and make use of.

Today, hydrologists from both America and China have happily gathered under the same roof to exchange experience, discuss interesting hydrological techniques, improved measurement, and the future direction of hydrology. All of this will certainly push forward the development of hydrological information and forecasting of both our countries, and will make many contributions to humanity. Of course, the symposium will be a milestone in the history of cooperation between America and China in hydrological information and forecasting.

As the host, the National Weather Service has made a most satisfactory arrangement and offered a good location for the symposium, and has given our Chinese delegation a warm welcome. Here, let me express heartfelt thanks on behalf of the Hydrological Forecasting and Water Control Center. Thank you very much.

HYDROLOGICAL INFORMATION AND FORECASTING IN CHINA

Wang Juemou, Sun Guihua
Hydrological Forecasting and
Water Control Center
Ministry of Water Resources, PRC

Abstract. This paper provides an introduction to the natural and hydrological characteristics in China. Due to the uneven distribution of precipitation, strong rainstorms and frequent calamity of flood and drought, the work of hydrological information and forecasting, functioning as the eyes and ears, is of the utmost importance in China. This work has played a significant role in the struggle for flood control and water resources management over the years, getting great attention from the Government and society. This paper reviews the history of hydrological information and forecast development in China. It is reported that the system of reporting rainfall started in 206 B.C. and that sending hydrological information downstream by horse and the estimation of water rising and falling, based on flow, was in limited use by 1573 A.D. In recent years, hydrological information and forecasting has developed rapidly. This paper also shows the structure of hydrological information and forecasting services/systems, including the collection and processing of hydrological information. These are considered as they apply to conditions concerned with hydrological forecasting in China. We currently have a network consisting of more than 8,500 hydrological information stations with telegraph and computer systems for hydrological information receiving and processing. Recent improvements in hydrological forecasting have included development and implementation of new hydrologic procedures and models which consider specific

hydrometeorological characteristics in China. In addition, considerable progress is being made toward computerizing the forecasting system. Recently, the hydrological departments, from the central government to the provinces (municipalities and autonomous regions), have been equipped with VAX-11 computers. IBM-PC computers have been implemented in many basic hydrological units. This creates favorable conditions for more effective use of available hydrological information and procedures for forecasting. As a developing country, China is still behind in the state of the art in dealing with hydrological observation and communication which adversely limits forecast effectiveness for extreme rainstorm floods (especially mountain torrents and mud/debris flow). As a result, we have much to gain from the more advanced experiences from other countries. This suggests that great value should arise from close cooperation between America and China in hydrological information and forecasting.

I. HYDROCLIMATOLOGY AND DEMOGRAPHICS

China is a country with a vast territory and numerous rivers, of which over 1500 have watershed areas larger than 1000 sq. km. Average annual precipitation is about 648 mm with an average annual runoff of about 2700 billion cubic meters. Annual precipitation varies between regions with a progressive decrease from the southeastern coast to the northwestern inland; the change ranges from 1800 mm (in some areas, it can reach more than 2000 mm) to less than 200 mm (in some areas, it can be below 20 mm). While precipitation varies from year to year, it is distinctly concentrated in four consecutive months, amounting to 50-70 percent of the year's total in southeast China and 70-80 percent of the year's total in other areas. Year-to-year variability indicates that maximum annual precipitation is two to three times more than the minimum in the southern part of China and three to six times in

the northern part. There are successive abundant water years and successive dry water years. China suffers often from typhoon damage with many such storms exhibiting great intensity. The maximum 24-hour rainfall is 1060 mm; the maximum 4-hour rainfall is 830 mm. Clearly, disasters of great proportion resulting from floods and droughts occur frequently.

China is densely populated in its eastern plains. The areas in the middle and lower reaches of the seven major rivers (the Yangtze, Yellow, Huai, Hai, Liao, Pearl, and Songhua Rivers) cover approximately 1 million sq. km. With many important cities, such as Beijing, Shanghai, Tianjin, Guangzhou, and Wuhan and more than half of the country's population, this region has evolved to form China's principal political, economic, and cultural centers. However, the land surface elevations of many major populated areas within this region are below the flood levels in the river. Consequently, they have to be safeguarded by dykes. The dykes are of poor quality and deposition on the river beds owing to serious soil erosion and high sediment on the middle- and lower-reaches of the rivers have increased the risk of flood damage. In a word, flood damage is a serious problem in China.

Damage from ice-jam dams and resulting floods often occur in the rivers of the northern part of China and some cities in that region are seriously deficient in water resources. Proper control and protection of water resources (including the 87,000 reservoirs throughout China) through hydrological information and forecasting (including considerations of flood, drought, ice regime, sediment, water quality and ground water) are extremely important. Meanwhile, as the "eyes and ears" in the struggle against flood and drought, hydrological information and forecasting are also helpful in measures involving flood storage, flood diversion, and in the transferring of people and property so that flood damage can be held to a minimum.

Flood forecasting facilitates the implementation of effective flood mitigation measures as well as the management of conservancy projects and irrigation, navigation, water supply and water quality management. Flood information and hydrological forecasting have played an important part in flood control as well as overall water management in China. For example, owing to a flood forecast in 1975, the height of the dam of the Boshan

Reservoir (earthen dam, total reservoir capacity of 0.62 billion cubic meters) in Henan Province was increased in time to prevent overtopping. Flood forecasting led to timely evacuation in 1981 of 220,000 residents and factory and government workers along the Yangtze River to a safe area under the leadership of the Chongqing City Government. In 1979, the gate of the Sanmenxia Reservoir was closed to control an ice-jam flood in the Yellow River.

II. HISTORIC DEVELOPMENTS IN HYDROLOGIC FORECASTING IN CHINA

The history of flood information and forecasting in China goes back some 2,000 years. The agricultural law of the Qin Dynasty (221-206 B.C.) required localities to make rainfall reports. However, it was not until 1573 A.D., during the Ming Dynasty, that the beginning of a flood information system was institutionalized. Flood information was transmitted by horse-back couriers, from post to post, set 30 km apart along the Yellow River, to its lower reaches. The rise and fall of the Yellow River was forecast from the appearance or non-appearance of water bubbles, respectively. However, hydrological forecasting remained at a standstill for a long time in later history. By 1949, there were only some 300 hydrological information stations but no routine hydrological forecasting. Since 1949, the Chinese Government has made great strides in the building of water projects and in the application of hydrological information and forecasting, in order to decrease the damage from floods and droughts. In the early 1950's, a standard reporting method for hydrological information was initiated in the country and the number of stations was increased to more than 8,500. Hydrological information and forecasting agencies have been established in flood control departments at all levels, from the central government down to river basin authorities, provinces (municipalities, autonomous regions), prefectures, most counties and important water projects, to form a fairly thorough and organized system to gather hydrological information and to carry out forecasting for flood control and water management. The organization of the Ministry of Water Resources and associated infrastructure responsible for gathering hydrological information and preparing hydrologic forecasting are shown in Figs. 1-4.

Feasible standards have been established for stages and periods when telegrams about hydrological information are transmitted. According to the requirement of flood control and water resources management, the hydrological station network includes both stations which send telegrams for the entire year and stations which send telegrams only during flood periods. The daily number of telegrams is determined according to the characteristics of the river basin, the function (for hydrological forecasting or monitoring), and the importance of the hydrological information in flood control. In large river basins the stations for hydrological forecasting will send telegrams four times a day (i.e., 6-hour time intervals); in medium- or small-sized river basins they will send telegrams 8-12 times a day. For the monitoring stations, a standard for increasing the sending of telegrams according to water level discharge or rainfall should be determined. Usually, one telegram (or none) is sent per day. If the standard is exceeded, the telegramming will be increased. Different hydrological stations have various reporting intervals. During emergency flood-control conditions, some stations should send a telegram every hour or every half hour. The contents of the telegram include water level, rainfall, discharge (observed discharge), sediment, ice regime, water temperature, reservoir capacity, gate operations, dam-break potential, ice-jam damming situations, etc.

Every hydrological station has its observers, who, on getting flood information, immediately send coded telegrams to county, prefecture, and province authorities through the postal and telecommunication departments. The Communication Ministry of PRC has ruled that hydrological information telegrams fall in the extra urgent category of the "R" kind. Transmission times can not exceed 90 minutes. In some important hydrological stations, specific shortwave radio transceivers have been installed to increase the speed of hydrological information transmission. After the 1975 flood in the Huaihe River Basin, a radio communication network has been partially established by the water resources agencies in order to raise the reliability and speed of information transmission. There are some 10,000 transceivers currently installed in the country. Automatic systems for flood forecasting and warning have been established gradually in more than 30 important areas for flood control and in important conservancy projects. They have been put

into operation in such places as the Puyangjiang River Basin in Zhejiang Province, in the Guanting gorge at Beijing, in the Xizhijiang River Basin in the Guangdong Province, at the Danjiangkou and Luhuen Reservoirs, and at the Baishan and Fangman Hydropower Stations. In recent years, experiments in the use of meteor burst technology for the transmission of flood information in the river basin above the Danjiang Reservoir have been undertaken. Similarly, satellite communication technology is being employed in the Three-Gorges area of the Yangtze River. Experiments in sharing hydrological information by long distance computer retrieval are being undertaken in some departments which have communication facilities such as the central agency, river basin authorities, province and prefecture hydrological agencies. Testing with weather radar has started in order to get precipitation information in more detail over larger areas. In some river basins, identifying the range of water surface fluctuation and rainfall distribution by remote sensing techniques has been started (as shown in Fig. 5).

Traditional hydrological information processing and transmission are dependent on manpower. By using computers, China has developed a system for processing hydrological information in real time. This has been accomplished by receiving and translating hydrological information telegrams using VAX-11 and IBM-PC computers as the foundation. The system consists of data receiving, processing, storing, retrieving, and application functions which are linked to a program library and a real-time data base. With this system, a terminal can be used at any time to retrieve the hydrological data and warning data in any river basin from any hydrological station. The user can retrieve:

- charts of rainfall distribution in various river basins,
- flood information distribution and water level-discharge hydrographs at various hydrological stations,
- and various statistical and analyzed data.

The data and charts can be displayed on large screens and printed out as bulletins of hydrological information and rainfall distributions. The real-time hydrological information processing system is shown in Fig. 6. Computerization has vastly improved data processing and flood forecasting

efficiency, met the needs of various concerned departments, and formed the basis for on-line hydrological forecasting in real time.

III. CONCLUDING REMARKS

Offices have been established in the flood control departments at all levels, forming a fairly thorough organization to carry out the mission of hydrological forecasting. More than 1000 basic hydrological stations issue local hydrological forecasts about rivers and reservoirs. Hydrological forecasting is very useful in managing water projects. Hydrological forecasting has extended from forecasting floods to forecasting low flows, ice regimes, droughts, sediment and water quality. Some hydrological agencies have undertaken research on medium- to long-term forecasting and on potential improvements in hydrological forecasting that may be gained by incorporating climate analyses and meteorological forecasting.

Although much work remains, China has achieved great progress in hydrological forecasting capability. Chinese hydrologists have improved the traditional methods of relating water level (discharge) and Muskingum discharge routing through physical consideration of river flood-wave movement. This approach considers continuous discharge routing in separate sections and non-linear solutions according to the characteristics of the natural conditions and practical experiences. This method increases calculation precision and can be used in areas with no discharge data. This method of routing floods can be adapted to consider further complexities such as the effects of high sediment concentrations which exist for some rivers in China. In the forecasting of rainfall-runoff, a natural storage model has been established which is suited to the humid areas of China and another model is being developed for the arid areas. For the calculation of watershed concentration, a hydrological model suited to the river basins of China has been developed. The reliability of the basic assumptions involved in the unit hydrograph method has been studied. The accuracy of the method has been improved by treating the system as non-linear which can deal more accurately with the problems of uneven rainfall, different runoff sources, different flood regulation and storage functions, intervening lateral inflows and

non-linear variations. Conceptual models and "black-box" models from other countries have been improved and adapted to the conditions in China. In order to meet forecasting requirements for medium and small reservoirs, some simple flood-routing methods have been developed. Also, methods for ice regimes, drought forecasts, groundwater, storm surges and medium- to long-term forecasting have been tried and have achieved good results. Some books on hydrological forecasting methods on these and other subjects have been published.

In operational hydrological forecasting, Chinese hydrologists have used:

- the method of relating water level to discharge (Muskingum method of successive routing in subreaches for large rivers),
- rainfall-runoff relationships and the unit hydrograph approach for medium and small rivers and for the inflows to reaches of the larger rivers.

Meanwhile, the Xinanjiang, SCLS, Sacramento, and TANK models have been used for some areas. In the 1950's and 1960's, operational hydrological forecasting in China was manpower-intensive. Hydrologists began to implement operational hydrological forecasting schemes on computers in the early 1970's. At present, China has established a hydrological forecasting system which can be used by the various levels of government and hydrologic agencies on available mini- and micro-computers. The system is now widely used. Its characteristics are:

- complete functions -- calibrated model with real-time forecasting provisions capable of including adjustments and various data and information sources (such as from quantitative precipitation forecasts);
- strong adaptability -- covers many models, suitable for any watershed and region; high degree of automation with provisions for processing, interpolation and correction of historical or real-time data; capability to automatically incorporate new or changed model calibration coefficients into the real-time modelling and forecast systems;
- strong common use -- standard input and output file formats; and

- speedy calculation -- obtainable in a few minutes.

In 1985, based on experiences to that time, the Ministry of Water Resources and Electric Power produced "The Standard for Hydrological Information and Forecasting," which provides a good foundation to further improve the quality of hydrological information and forecasting.

As a developing country, China is still behind the state of the art in technical equipment, especially in hydrological information collection and processing and flood information communication, and can not adequately deal with extreme rainstorm floods (especially mountain flood and mud/debris flow). As a result, we have much to gain from the more advanced experiences from other countries. This suggests that great value should arise from close cooperation between American and Chinese in hydrologic information and forecasting.

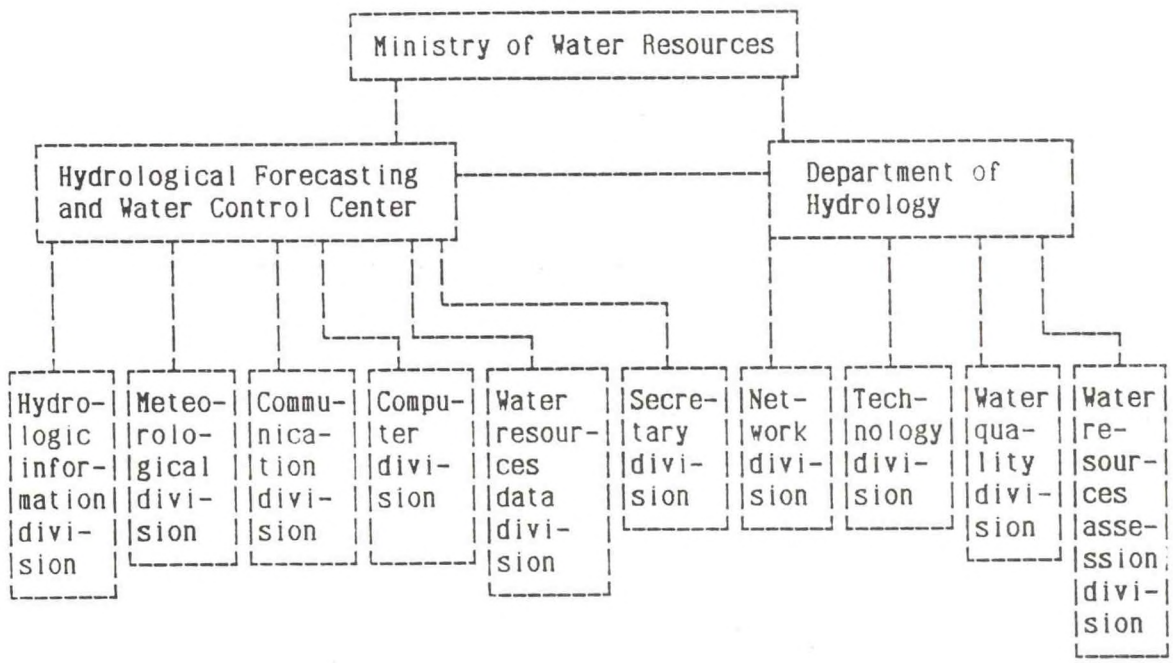

Fig. 1. Hydrology Agencies in the Ministry of Water Resources

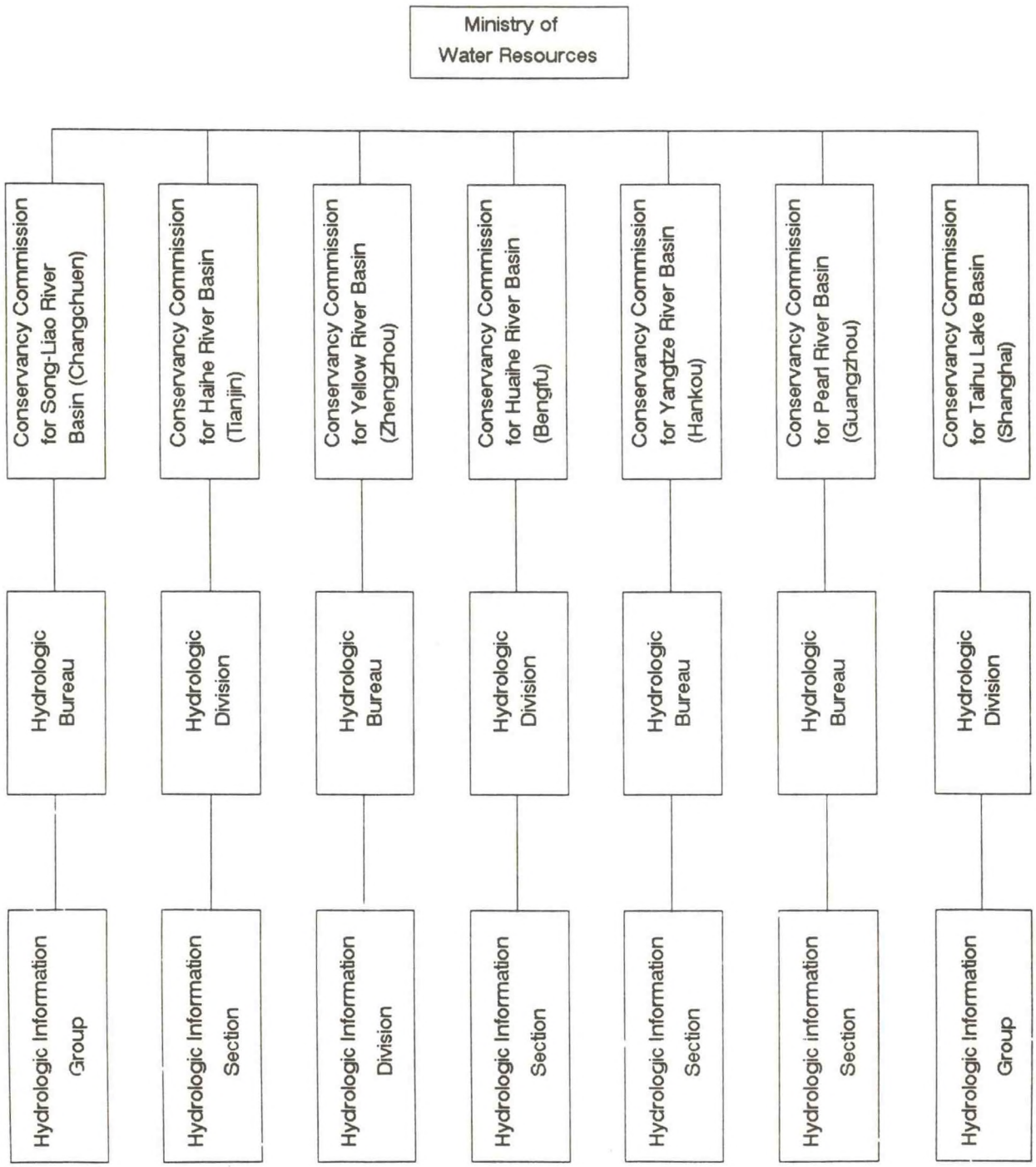

Fig. 2. River Basin Agencies under the Ministry of Water Resources

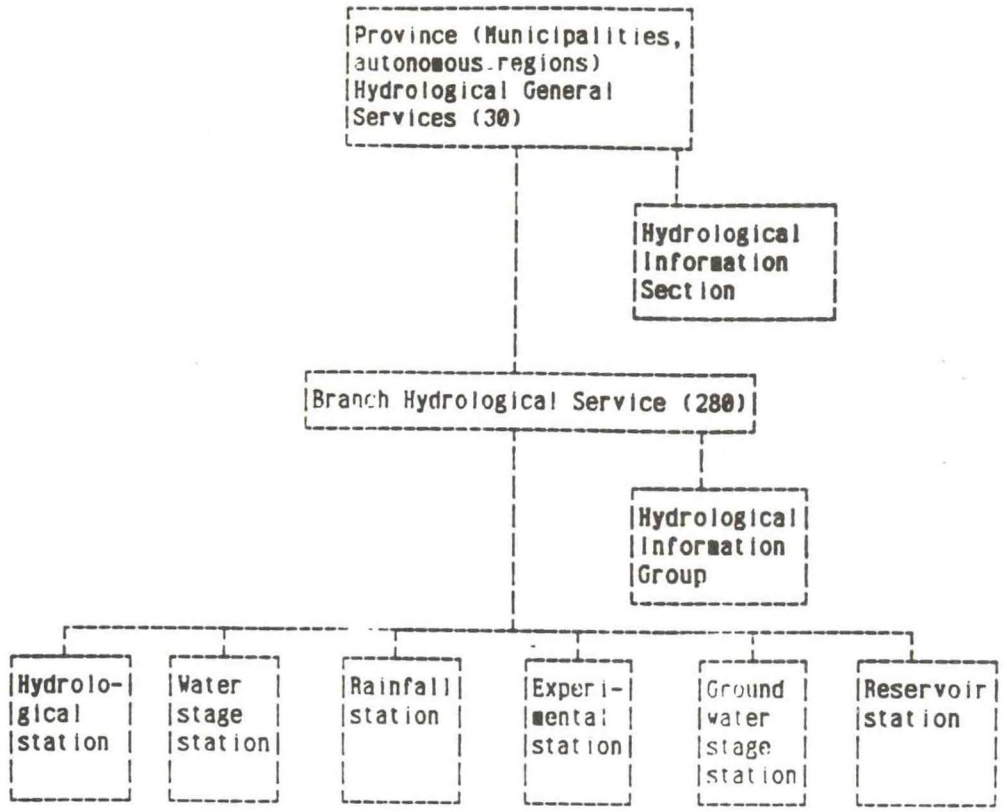

Fig. 3. Local Hydrological Agencies

Type of Station	Hydrological Station	Water Stage Station	Experimental Station	Rainfall Station
Station Number	3384	1420	63	16406

Terms of Observation	Discharge	Rainfall	Sediment	Evaporation	Ice Regime	Ground Water
Number of Terms	3384	20256	1583	1405	1260	2188

Fig. 4. National Network of Hydrological Stations

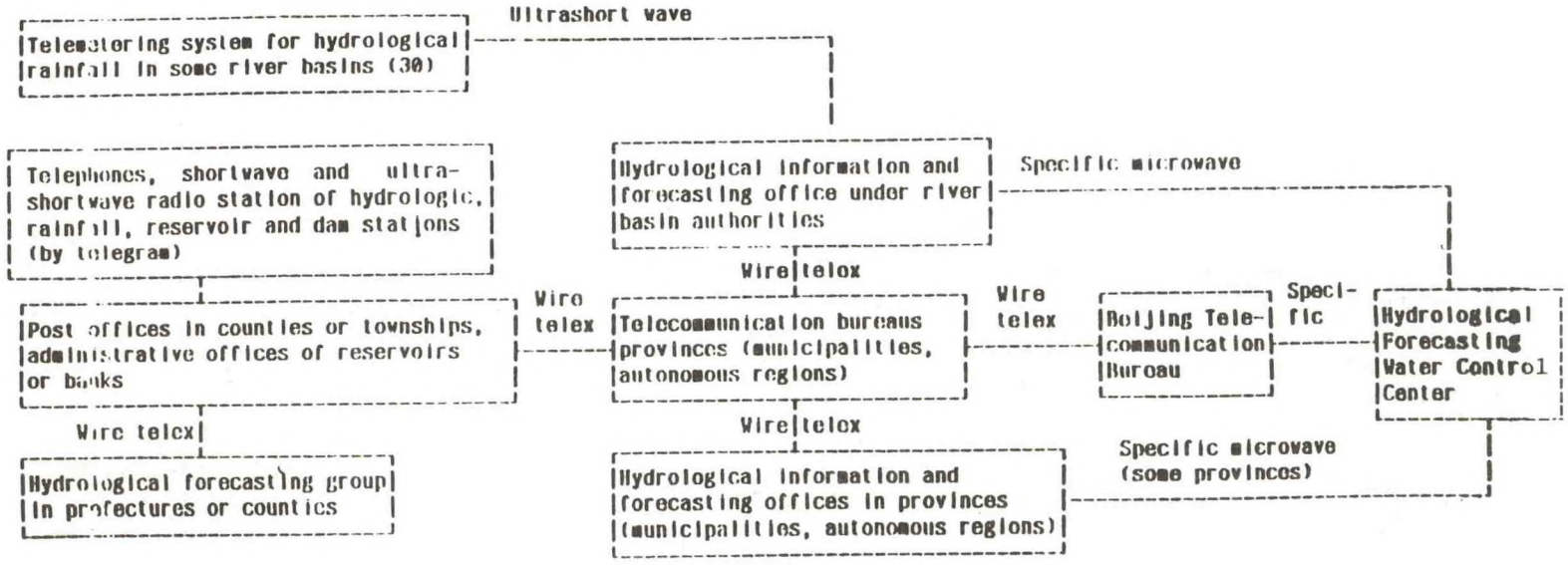

Fig. 5. Hydrological Information Transmission System

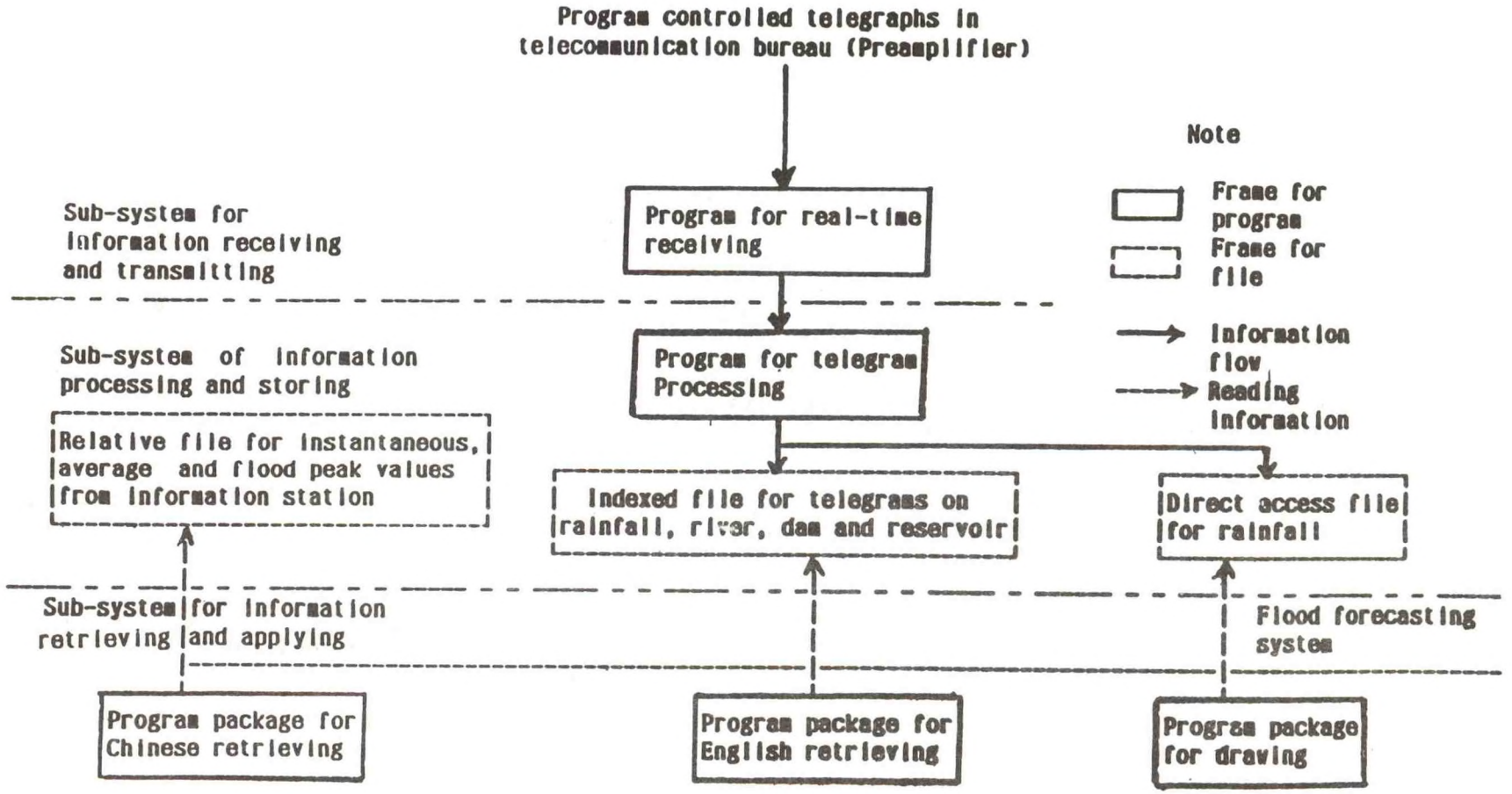

Fig. 6. The Automatic System for Real-Time Hydrological Information Processing

HYDROLOGICAL INFORMATION AND FORECASTING IN THE USA

Robert A. Clark
Retired Director, Hydrology, National Weather Service
Silver Spring, Maryland

Evolution of the bilateral program is discussed along with a brief history of hydrologic forecasting by the National Weather Service (NWS) in the United States. The development of forecasting models currently in use by the NWS and the importance of timely data and applications of these data to conceptual models which utilize computer technology is discussed next. Special hydrological problems also are presented, such as those associated with "dam breaks" and with unusual events like Mt. Saint Helens. Finally, future activities of the NWS and their impact on the hydrologic forecasting program are discussed.

I. EVOLUTION OF THE BILATERAL PROGRAM

The bilateral program has developed from a number of exchange programs between engineers in several of the water related agencies in the United States (USA) and similar groups in the Peoples Republic of China (PRC). Instrumental in the current program was an Annex to a Protocol developed between the Ministry of Water Resources, PRC and the Geological Survey and the National Weather Service, USA. Initial contacts were made during the 1970's when several visits were made to the PRC by engineers representing the Bureau of Reclamation, Corps of Engineers, Geological Survey, Soil Conservation Service and several universities. Later visits by Chinese engineers to the USA in the early 1980's from the Ministry of Water Resources and universities specializing in water development strengthened these contacts. Similarity of water problems facing engineers in both the USA and PRC has provided an important link between the two countries.

II. HYDROLOGIC FORECASTING BY THE NATIONAL WEATHER SERVICE

Federal legislation in 1890 authorized the Weather Bureau (now the National Weather Service - NWS) to provide forecasts of river flow for benefits related to commerce, irrigation, and flooding. Initial efforts were concentrated

primarily on the big rivers, e.g., Mississippi, Missouri, Ohio, and Columbia. Because of fragmented efforts it was decided in the late 1940's to establish forecast centers specifically for flow forecasting at several locations along the major river systems, viz., Cincinnati, Saint Louis, Kansas City, and Portland. Although major flood damage was usually observed along the large rivers, deaths related to flooding were frequently observed on the minor streams. As a result, forecast centers were established later in such places as Ft. Worth, Tulsa, Atlanta, Sacramento, Hartford, and Harrisburg.

In recent years, the emphasis has shifted even more to problems associated with flash floods (usually defined as those floods occurring over time intervals of six hours or less between the rainfall event and the flood peak) and with water supply forecasting which defines the utilization of water for irrigation, power, navigation, domestic water supply, recreation, and related activities. Forecast centers in Salt Lake City, Anchorage, Slidell, and Minneapolis were the last created.

III. HOW ARE FORECASTS MADE

Initially, forecasts were primarily related to the movement of water down major river systems. Early studies were associated with the attenuation or non-attenuation of flood peaks as significant floods occurred on the big rivers. These were, of course, very important since many of the major cities in the USA, viz., Pittsburgh, Cincinnati, Louisville, Kansas City, Saint Louis, Memphis, New Orleans, and Portland, were located on major rivers. Since most of these cities lie in a flood plain, they are vulnerable to extreme flows.

Increased emphasis on flood control during the 1930's by the Corps of Engineers, U.S. Army, and involvement of the "Weather Bureau" in these activities was instrumental in the creation within the Weather Bureau of a hydrometeorological group who were primarily responsible for estimating heavy precipitation potential, and related runoff. Early studies indicated a strong relationship between soil moisture conditions and runoff resulting from storms of various intensity. During the 1940's and 1950's a model was developed which utilized an antecedent precipitation index (API) and rainfall collected

at 6 hour or 24 hour intervals from a reasonably dense network to predict rainfall excess. Although this model was primarily an "event" based model, i.e., each rainfall event was analyzed separately, it proved very effective and is still used widely.

In the late 1950's and early 1960's, Professor R.K. Linsley and a number of his graduate students at Stanford University developed a conceptual model (known as the Stanford Watershed Model) whose primary advantages were that it was a continuous-process model that allowed monitoring of variations in infiltration, soil moisture, evaporation, and evapotranspiration. The model also was able to estimate overland flow, interflow, and the contribution to streamflow from the groundwater. This model was, of course, somewhat difficult to use and required an experienced hydrologist to use it properly.

At about the same time, D.M. Rockwood of the Corps of Engineers in Portland, Oregon, developed the Streamflow Synthesis and Reservoir Regulation (SSARR) model to meet their needs in the Columbia River basin. This model was later adopted by the NWS River Forecast Center in Portland. The basic model was not as complicated as the Stanford Model, however, it was continuous and did a reasonably good job of accounting for most of the same processes. Calibration of this model also required an experienced/or well-trained hydrologist.

Late in the 1960's and during the early 1970's, hydrologists R.C. Burnash and R.L. Ferral of the NWS River Forecasting Center in Sacramento and R.A. McGuire of the California Department of Water Resources developed a soil moisture accounting model similar to the Stanford Watershed Model (SWM), but with some distinct advantages for flood forecasting which has become known as the Sacramento Model. This was a continuous simulation model which also included algorithms for the same processes as both the SSARR and SWM. It was adopted in 1974 as the standard soil moisture accounting model by the NWS. Accounting for moisture in the lower zone was somewhat complicated; however, the model appeared to account for long dry spells more efficiently and modifications to the complete model seemed easier to make.

Flash floods have proved to be a major source of weather related damage and deaths in the United States in recent years. Conventional flood forecasting procedures do not provide adequate warnings for these floods. Emphasis in the

past 20 years has been primarily on the rapid collection of data to provide an indication of flash flood conditions. Several approaches have been used:

(1) Flash flood alarm systems that are simple stream gages that indicate an unusual rise in water stage,

(2) remote sensing techniques such as radar and satellite which can be used to identify very heavy rain producing storms,

(3) the implementation of a network of rain gages over a specific basin which report either by voice using telephone or radio or automatically through the same technology, and

(4) meteorological forecasts of areas of potentially severe local storms.

The various forecast centers in the NWS also analyze current soil moisture conditions and, based on standard hydrologic forecasting procedures, estimate the flood potential for selected basins based on heavy rainfall which might occur over selected time intervals.

IV. IMPORTANCE OF DATA

Data are, of course, critical to the implementation of all flood forecasting systems. Initially, 30 or 40 years ago, data were collected utilizing the basic meteorological collection system which provided data at only a thousand or so stations. These stations provided only a limited amount of data over the approximately 3 million square miles in the United States. To supplement these stations, a cooperative observer network was established in the 1940's to telephone or radio into selected base stations their rainfall observations. This source of data would be expensive if used for collection at the frequency and resolutions required to satisfy all requirements. As a result, this approach is not always too effective. In the past, the standard procedure was to report only rainfall amounts in excess of 0.50 inches in some set period, e.g., 3, 6 or 24 hours. In addition to reporting rainfall data, a large number of observers were employed to provide river stage data. Again, unfortunately, these data were not provided in many cases continuously so that maintenance of any continuous hydrologic model is difficult.

In recent years, a large number, several thousand, automated stations have

been installed in the United States. These stations utilize various convention technologies including: (1) direct radio communication, (2) telephones, (3) satellite relay, and various communications technologies including (4) meteor burst relay. Except for telephones which tend not to work during some weather condition, all have proved fairly reliable. Depending on the sophistication of the stations, they normally cost $3,000 and up to install. Annual operational and maintenance costs can easily average 10 to 20 percent of the costs of the stations. Nevertheless, these costs often prove minor compared to the benefits derived from improved operation of forecast systems.

An area of very rapid development of data collection has been the implementation of a very large number of automated rainfall stations for flash flood detection. These systems are frequently referred to as "ALERT systems" and normally employ radio transmission (UHF/VHF) to relay data. They can employ storage of information that is forwarded either on request or timed or can relay information at the time of the occurrence, e.g., when a total rainfall of 1 mm is received. Data from these stations are collected normally in the weather service office responsible for watches/warnings in a given geographic area or in the offices of some local civil defense agency.

V. COMPUTER USAGE

The importance of computer technology was apparent in the early 1960's for use in flood forecasting. Over a period of about 30 years the number of forecast points has increased from approximately 1000 to 4000. Many of these points require not only forecasts of individual floods but also continuous flow forecasts for water supply, power generation, navigation, pollution control, and other water related information. Currently, in addition to a large amount of data collected from individual observers, data are obtained several times a day from probably 5000 meteorological and hydrological gages that are automated. Compilation and processing of these data is a very large task. The 13 river forecast centers with an average of approximately 10 hydrologists could not cope with this large amount of data and the many computations required, without heavy reliance on computers.

In the early 1960's small computers were installed in most of the river forecast centers to expedite data collection and processing. By 1973, it was apparent that these computers were not adequate to handle an increased work load. At that time most of the stations were given access to the NOAA centralized computer system. Although the system was very fast, there are many distinct disadvantages in using essentially a "batch" processing system. Regardless of the rather high state of hydrologic technology in the 1970's, the system in use did not allow for interactive processing of data which is still necessary for making good hydrologic forecasts. A good hydrologist is still required to recognize when model calibration goes astray. In addition, it is not always possible to program a computer to recognize erroneous data.

Recent trends have been to move to "in-house" computer usage with main frame central computers being used only for major forecasting applications which are non-time critical and/or extremely computer intensive.

VI. SPECIAL PROBLEMS

A. Dam Breaks

The failure of a number of dams over the past 30 years has placed increased emphasis on forecasting the results of such a failure. Instrumental in the development of these programs has been Dr. D.L. Fread, now the Director of the Hydrologic Research Laboratory in the Office of Hydrology, NWS. Computerized procedures for estimating dam failures have been developed and are available to all NWS offices. In addition, a catalog has been developed, from which estimates of flood potential from possible failure at more than 50,000 dams can be obtained. In the event of a possible failure, the weather service office in the appropriate area can rapidly obtain a "first guess" on what might happen. These programs have also proved useful to the Corps of Engineers in their "Safety of Dams Program" and to other federal and state agencies responsible for the dams under their jurisdiction.

B. Mount Saint Helens

The eruption of this volcano in the southwestern portion of Oregon created a unique hydrologic problem. Large amounts of sediment were deposited in the several streams lying to the north and west of Mount Saint Helens. Because of the reduced channel capacity of these streams, their potential for flooding was greatly increased. As a result, the NWS was asked to augment the existing flood forecasting system in that region with an enhanced system which was capable of alerting the more than 100,000 people living along the streams in that area to potential flooding within a few hours. A network of more than 40 automated gages (ALERT Type) was established within about 4 months of the eruption.

C. Other Specialized Systems

Serious flood problems on the Susquehanna River in June 1972 and on the Colorado River in 1983 required early resolution. Flooding in the Susquehanna Basin was very serious as a result of Hurricane Agnes. Over a period of several days more than 18 inches of rain fell in central Pennsylvania. Radar and satellite coverage was not adequate to pinpoint the very intense rainfall centers. Flood damages exceeded more than 3.5 billion dollars and 118 lives were lost. Although the dollar damages and loss of life was not as serious in the Colorado River basin in 1983, runoff from a very large snow pack and heavy spring rains filled to overflowing the numerous reservoirs on the Colorado River systems. Damages to the spillway system on Glen Canyon Dam and to the Colorado River below Hoover Dam were extensive due to very large flows. Specialized data collection networks in addition to enhancement of the river forecast centers in Harrisburg, Pennsylvania and Salt Lake City, Utah have greatly increased the ability of the NWS to forecast streamflow in these basins. It is anticipated that similar enhancements will be made in other hydrologically critical basins in the future.

VII. THE FUTURE

The hydrologic forecasting service in the United States is a component of the National Weather Service. Since the weather service is highly dependent

on "real time" data collection, improvements in the collection of meteorological data also greatly improve hydrologic data collection. For example, the planned radar program (NEXRAD) will not only enable the NWS to identify areas of potential tornadoes but also delineate areas where heavy rainfall is occurring. The new radar system will provide estimates of rainfall intensity with increased accuracy in many situations, especially for those areas and times inadequately covered by rain gages.

Other programs such as improved communications and information processing systems (AWIPS) and increased automation of the surface observing system (ASOS) will provide the hydrologic service with improved tools for streamflow forecasting. On-site computer facilities will enable the hydrologists in each river forecast center to work interactively with their computers and provide better control and calibration of their various forecast models. Although the accuracy of water stage forecasts may improve more slowly, the "timeliness" of these forecasts should improve considerably. Probably 50 percent or more of flood warnings for small streams are issued after the flooding has already begun. While such delayed information is often useful, it is frequently too late to evacuate people and goods to provide the maximum benefits possible. Clearly improvements in forecasts and warning procedures are warranted since these instances are less than one-tenth of the resulting benefits from savings of life and property.

DEVELOPMENT AND OPERATION OF THE SNOTEL SYSTEM IN THE WESTERN UNITED STATES

Garry L. Schaefer and David E. Johnson, P.E.
Soil Conservation Service,
Portland, Oregon

ABSTRACT. Snowmelt runoff is the major component of the annual streamflow in the arid western United States. Accurate forecasts of this runoff are vital to many sectors of the economy in the West. The Department of Agriculture, Soil Conservation Service (SCS), began using meteor burst telemetry communication for collecting hydrometeorological data in 1977. The snowpack telemetry (SNOTEL) system consists of two master stations which initiate interrogation, receive data transmissions from remotes, and forward data to the central computer system located in Portland, Oregon. A typical remote data site is equipped with sensors which provide snow water equivalent (SWE), accumulated precipitation, and maximum, minimum, and average daily temperature data. SNOTEL supplements and, to a large extent, replaces the manual data collection network.

The SNOTEL system installation was scheduled over a 5-year period with SCS crews preparing sites and installing sensors. A contractor installed and maintained the electronics. In 1981, SCS assumed full maintenance responsibility for all electronic and meteor burst communications equipment. In 1987, the SCS began a SNOTEL upgrade program to replace old equipment and expand the network's capabilities.

Meteor burst communication has proven to be a reliable alternative to other types of telemetry systems. After 10

years of experience with SNOTEL, the SCS and other agencies are placing high reliance on the system.

I. INTRODUCTION

Snowpack telemetery (SNOTEL) is the project name for a meteor burst hydrometeorological data collection system operated by the U.S. Department of Agriculture, Soil Conservation Service (SCS), in the mountainous western United States. The primary purpose for SNOTEL is to forecast spring and summer streamflows. These forecasts aid water users in the management of the region's limited and seasonally variable water supplies.

Snow measurement activities began in the early 1900's and intensified in the 1930's due primarily to a severe drought experienced throughout the region. When SCS was charged with coordination of the program, its character changed from project-oriented to a region-wide activity. By 1960, there were over 1,600 individual snow courses being regularly measured manually by a number of cooperating agencies and organizations.

In 1974, the U.S. Congress approved the initial funding for the SNOTEL automated system to replace the costly, time-consuming, and often dangerous practice of manually measuring snow courses. In 1975, the first contracts were awarded; in 1977, the first data transmitted; and by October of 1980, there were 465 remote sites providing daily data to forecasting hydrologists. Since that time, SNOTEL remote sites have been added to the system, bringing the current operational total to about 540 (Crook and Beard, 1987).

Ten year's experience covering the design, construction, operation, and modernization of this extensive meteor burst data collection system yields information useful in designing and operating similar systems. The information has been divided into five areas of interest: (1) design, (2) installation, (3) maintenance, (4) modernization, and (5) performance.

II. SYSTEM DESIGN

The SNOTEL system covers the area of the western United States shown in fig. 1. This region extends approximately 1,800 km north and south from latitude N32° to N49°. It measures about 1,700 km east and west. The area encompasses large variation in topography and climate.

The manual data collection network of over 1,600 snow courses was designed to provide a comprehensive index of the water production zones. Courses were located to represent elevational, aspect, and exposure variations within a watershed. Attention was also given to the accessibility of these snow courses.

When the SNOTEL system was designed, about 465 sites were selected to represent that number of key manual snow courses. The key courses were usually determined to be of high value because they correlated well with streamflow volumes over a long period. In selecting SNOTEL site locations, consideration was also given to where streamflow forecast points were required to meet the needs of downstream users. In addition, emphasis was given to automating those key manual snow courses that were particularly hazardous or costly to access. The Upper Del North watershed on the Rio Grande River Basin is an example of a typical SNOTEL network density. This 3,419 sq. km watershed is gauged by four SNOTEL sites ranging in elevation from 2,437 meters to 4,215 meters.

Currently, over 540 SNOTEL sites have been installed. The additional 75 sites were added in areas where more data proved to be necessary for accurate forecasts. The system is designed to support a network of up to 1,000 remote sites. As the use of process simulation models replaces regression equations for water supply forecasting, some expansion of the SNOTEL system will be required. These models require minimum, maximum, and average daily temperature; snow water equivalent; precipitation and other data; and they need it daily or more frequently.

Remote sites are typically located in high mountain meadows. They are subject to climate extremes, and access is difficult and expensive. The transceiver (transmitter/receiver) for the remote site must be fully

functional and operational for a temperature range from -30° to +60°C, and humidity range from 0 to 95 percent. The principal structural design requirement was dependable routine performance; a second requirement was the ability to respond to occasional special demands. Figure 2 shows the SNOTEL system architecture including the Centralized Forecasting System computer where SNOTEL data is analyzed and forecasts prepared; the SNOTEL central computer; the data base archive facility (FCCC); and the interactive user terminals (Crook & Johnson, 1987).

SNOTEL operates in a near real-time mode with the remote sites collecting, processing, and storing physical parameters from up to 16 sensors for subsequent transmission. Figure 3 shows a conceptual diagram of a typical remote site. A system-wide poll of the remote sites is conducted daily from 0500 to 0800 hours to transfer data via one of the two SNOTEL master stations to the SNOTEL central computer. Data can be stored at the master stations for up to 3 days. The design goal was for 95 percent of the remote sites to respond to a poll within 1 hour. The system also has the capability to conduct special polls and regularly monitor the condition of each remote site and system performance. It can also send and receive 16-character text messages by using a portable operator console.

The remote sites transmit at 41.530 MHz and receive at 40.530 MHz with phase shift keying modulation. Receiver sensitivity is at least -121 dBm with a bit error rate of less than 1×10^{-4} The data rate is 2,000 bits per second operating in half-duplex mode. The sites are battery powered with solar panels used for trickle charging.

The two identical master stations are located at lower elevations near cities in a somewhat less harsh environment with approximately 430 km separation. Electrical power, telephone lines, and all-year road access are available. The greatest distance between a remote site and the nearest of the two master stations is about 1,000 km. Each master station operates unattended in a climate-controlled environment. An omnidirectional transmit antenna energized at 2 kw is used to transmit interrogation signals. Four receive antennas, each covering approximately one quadrant, monitor remote site transmissions. A computer in each master station receives commands from

the SNOTEL central computer and, in response, initiates communication with remote sites. The two master station communicate with the SNOTEL central computer and with each other on dedicated telephone lines. Normal operations use both master stations, but the system will operate with only one. Two master stations are employed to provide redundancy and allow more optimal aiming of remote site antennas. Figure 4 shows the current configuration of a SNOTEL master station.

III. SNOTEL INSTALLATION

The location of each remote site is based on specific hydrologic, microclimatic, and access considerations. Some remote sites are unavoidably located close to power lines, microwave relay stations, and antenna farms. All sites are as inconspicuous as possible for environmental concerns and to reduce vandalism. The master stations are located to optimize meteor burst communications within the network.

The complete system installation was scheduled over a 5-year period with SCS crews preparing sites and installing sensors, and the vendor installing the electronics. The short construction season, high elevation, and often difficult access complicated operations. Off-road travel was necessary to reach most sites, and helicopters were required for some locations. Experience with meteor burst remote systems was limited so there were inefficiencies associated with not having a precedent for many aspects of the installation. A summary of original SNOTEL costs is presented in table A (Crook & Beard).

Experience gained during the early stages of installation resulted in revised equipment and procedures for the later stages. The frustrating effects of moisture were countered with improved cables and connector. Descant packets were added to the housings enclosing the transceivers. The shelter house at each site that contains the transceiver, battery, and other components (and also provides shelter during winter maintenance and for emergencies) went through several design changes. The higher cost but longer life of fiberglass shelters compared to plywood proved to be reasonable for sites with difficult access. Rodent damage was greater than had been

Table A

SNOTEL PROJECT COSTS

Item	1976 Purchase Cost($)	Installation (1976-79) Staff days	Cost ($) Travel	Wages
Typical Remote Site				
Sensors & support fac.	4,000	6 -8	760	850
Supplies	300			
Electronics	6,000	2	300	300
Master Station Housing & facilities	15,000	10		1,000
Electronics	202,000	(Included in purchase)		
Central Comp. Facility Hardware	150,000	(Included in purchase)		
Software	300,000			

Note: The above referenced purchase and installation costs are expressed in U.S. dollars. They are based on original project contracts and practices and do not necessarily reflect current prices.

anticipated; wire mesh was wrapped around the plywood shelters, and cables were placed in conduits to minimize rodent damage.

Experiments were conducted with various antenna configurations and tower heights during installation. An antenna height of about 6 to 10 meters above the ground proved practical and resulted in high performance. A 3-element, 5 db gain, horizontally polarized yagi antenna gave good performance at a reasonable cost, and they were used in most locations. Where increased gain was required, the added expense for the 5-element antenna was justified, but wind and snow loading problems are increased by antenna towers to maximize

solar exposure during low sun months. Other locations required two or more panels to generate an adequate charge. These problems occurred most often in high forests and on north-facing slopes.

IV. SYSTEM MAINTENANCE

Maintenance of sensors and physical facilities at remote sites, non communications equipment at master stations, and all central computer facilities has been the responsibility of SCS since the project began. Communication system maintenance of remote sites and master stations was initially performed under contract with the original vendor. Because of occasionally hazardous winter access and low commitment to data collecting priorities, the maintenance service was inadequate. To correct this situation, in 1981 the government assumed maintenance responsibility for all electronic and meteor burst communication equipment at the remotes. Ten electronics technicians are employed with primary duties of field maintenance and in-shop repair.

The original concept of preventive maintenance for SNOTEL was to fully check, adjust, and fine-tune communication equipment at each site on an annual schedule, with remedial repair work done as required throughout the year. However, accumulated evidence indicated that this annual preventive maintenance procedure stressed certain components within the electronics system, causing the site to fail during maintenance or shortly thereafter. As a result, routine, exhaustive maintenance has been discontinued. Now, the procedure is to do an annual abbreviated check of battery condition, solar panel output, and sensor output. If this check indicates the system is operating properly, no other diagnostics are performed. Coaxial cable integrity, cable connections, antennas, and grounding are also checked, particularly if the site has a history of intermittent performance.

Master station electronics are checked during intermittent visits to the stations, and a full electronics preventive maintenance check is performed on a 6-month frequency. In addition, air conditioning equipment is serviced every 2 to 3 months during the warmer part of the year, and the computers are

serviced regularly each month. Central computer equipment is regularly maintained in accordance with the manufacturer's recommended schedule.

Remedial maintenance of remote sites is usually performed as soon as the site evidences a serious problem such as errored data or sustained non response to polling. However, the schedule is heavily influenced by the availability of electronics technicians, weather, and budget (some locations are so remote as to require large expenditures for helicopter transportation). During the short summertime access period, it has proven very important to adhere to a strict preventive maintenance master schedule to assure that the planned work can be completed before winter again limits access. Thus a site needing remedial service may not be visited immediately in the summer until its scheduled preventative visit, or until a technician is available without compromising the master schedule. During the past several years, approximately 20 percent of the remote sites have required remedial electronic maintenance each year.

A typical remedial maintenance visit requires 1 to 3 hours of pretrip diagnostic study and preparation and about 1 hour of post trip documentation and other house keeping. Travel time to and from the remote site is obviously dependent on location and time of year; 2 days are frequently required from start to finish. While at the site, if it is a wintertime visit, the repair work is usually confined to the immediate problem and averages about 1 hour. A summertime visit normally will be combined with any other work that is necessary, and takes about 4 hours on the average.

Six year's experience in site maintenance has provided the basis for systematic resolution of electronic problems and generated many system improvements. In Table B, the relative frequency of occurrence of various problem sources is listed (Crook & Beard, 1987). Some frequencies of problems are very environmentally dependent. For instance, coaxial cable connectors collect moisture and short out much more frequently in the predominantly damp climate of the Pacific Northwest than in the drier Rocky Mountain region. A major improvement in site reliability was obtained in Oregon and Washington by concentrating trouble shooting on the coaxial cables. Moisture absorption also caused power degradation problems in early solar panels that had cells

Table B

INCIDENCE OF REMOTE SITE FAILURE

Category of Problem		Percent of Occurrence
Battery Voltage (Includes low and dead)		40%
Transceiver Unit		30%
Transmitter	(12%)	
Receiver	(7%)	
Control Logic Board	(6%)	
Data Acquisition Board	(5%)	
Power Control Unit		10%
Sensor Interface Card		5%
Coaxial Cable and Connections		5%
Solar Panel		5%
Solar Panel Regulator		2%
Physical Damage (Falling trees, etc.)		1%
Other		2%

sealed with a silicone rubber compound. Improved models with glass cases resolved the problem and also proved less likely to accumulate a snow cover.

V. SNOTEL MODERNIZATION

As the anticipated 10-year life of the original transceivers approached, maintenance problems increased and replacement parts became more difficult to obtain. SCS launched a 5-year, $5 million upgrade program for SNOTEL in 1987. Beginning with the first stages of SNOTEL installation, opportunities for improvements became apparent. Operational demands and maintenance experience continue to generate a list of changes and desired new features.

Major emphasis for modernization was placed on the requirements for the "next generation" transceivers. Prior to initiating the uppergrade program, a decision was made to use 100-watt, 36-volt original equipment. Performance is similar, and battery requirements are significantly reduced. Miniaturization and improved design allowed the physical dimensions and weight of the transceivers to be reduced. About 10 percent of the network currently uses the 100 watt units.

The new transceivers have numerous improvements to support future SNOTEL operations such as process simulation modeling for water supply forecasting.

These models required more data more frequently than current forecasting procedures need. The number of sensors that a site can monitor was increased from 16 to 48, and the capability to handle physical sensor processing was enhanced in the transceiver microprocessor. For example, sites previously reported air temperature at the time they were polled. The new transceivers can now report minimum, maximum, and average air temperature for a 24-hour period.

A. Remote Site Polling

The original design divided the remote sites into eight polling groups for responding to master station polls. Each site was assigned a specific polling address to which it responded. Sites with less than 80 km separation were assigned to different polling groups to avoid attempted simultaneous responses. In a routine probe, each group was polled in turn for 8 minutes and then for a second 8 minutes (for 128 minutes total). The new design does not use polling groups. Each remote site, in response to a general probe, transmits once out of every seven signal occurrences as measured from a randomly selected start time.

The desired ability to poll a specific site without initiating responses from other sites was not obtained as planned with the original transceivers. This resulted in a reluctance to use very many special polls because of battery power limitations at the remote sites. Operational experience and improved batteries and solar panels have reduced this concern. The new SNOTEL transceivers can communicate with the master stations in response to a specific probe using the 10 bit unique address at each remote site. Other sites not being addressed will not respond.

The command probe is a new capability that will be available when the total system has been modernized. The command probe allows certain remote site operational characteristics, such as polling frequency or sensor activation, to be changed by central computer command via the master stations. This feature will replace the need to make physical changes at the site, reducing costs and increasing the flexibility of system operations.

B. Remote Maintenance Parameters

An important new feature of the most modern transceivers is the monitoring and reporting of certain remote site maintenance parameters (RMP). Acquisition of these parameters enables SCS personnel to regularly evaluate the behavior and operational integrity of the remote site, and they can be better prepared before leaving for the field to perform indicated maintenance. RMPs are comprised of eight data values representing the critical performance parameters at the remote data site. Under normal operation, these values are reported to the master stations once per day and reflect site performance during the previous 24 hours ending at midnight. Special polling requests can also retrieve current RMP transmissions (Crook & Johnson, 1987).

Acknowledge Count

When a master station receives a complete and error-free message from the remote, it transmits an acknowledgment (ACK) back to the remote. The remote, upon receipt of the ACK, reverts to a quiescent state and will not transmit in response to further probing for a preset time period (usually 2 hours). The ACK is transmitted on the same meteor trail path that the probe receipt and remote site response used. Loss of path during any of the segments can curtail or degrade the transmission. Thus, only a percentage of the replies from the remote are received by the master in a complete and error-free form, and not all ACKs of good messages are received by the remote. Examination of the ratio of synchronizations, transmits, and ACKs provides very useful information regarding the site and system health; a ratio of transmits to ACKs greater than 5:1 indicates a problem.

Transmit Count

The number of times the remote unit is transmitted during the previous 24-hour period in response to a valid master station poll.

Receive Signal Detection Count

This parameter is based on the 24-hour count of detected Radio Frequency

(RF) carrier signals which exceed a predetermined strength level.

Receive Sync Detection Count

This parameter is an hourly count of the number of times the master stations send a synchronization pattern bit sequence.

In addition to the signal counts, RMPs include RF activity, battery voltage during transmissions, and forward and reverse transmit voltage.

C. Master Stations

The eventual modernization of the master stations depends on technology currently being developed. The SNOTEL system recently replaced its vacuum tube driven 2 kw transmitters with newer models of similar design. A future conversion to solid-state design would reduce the continual heat dissipation problems in the master stations.

Major progress was made in improving communications and reducing RF noise by converting each master station from four transmit antennas rated at 500 watts each to one omnidirectional 2 kw antenna. The four antennas had been colocated on the same towers with the four receive antennas and served an approximate quadrant. The colocation had also required the use of duplexer cavities, another source of noise.

VI. PERFORMANCE

A measure of the reliability of an individual remote site is the simple count of its responses to polls. A summary of the responses from all sites during the period October 1, 1986, to January 22, 1987, is shown as fig. 5 (Crook & Beard, 1987). About 42 percent of the sites, 225 by count, responded to each of the 114 daily polls. Eighty percent missed four or fewer polls, and 88 percent responded to at least 90 percent of all polls. An examination of these performance records indicates that chronically poor responses constitute a minority. Their performance is due to site-specific hardware or tuning problems, rather than being random in nature, which would indicate a systematic problem with either the meteor burst link or the design.

SNOTEL system reliability is continuously monitored by compiling statistics on several performance characteristics. Figure 6 shows a 3-month moving mean of remote site response to the daily system-wide poll. The moving mean provides a better visualization of trends. System performance has improved steadily since 1981 when SCS assumed full maintenance responsibility. The improvement is a reflection of the increasing skill levels of the technicians, enhanced diagnostic capabilities, improved transceiver design, improved batteries and solar panels, and the gradual elimination of poor performance problems by "fine-tuning" the sites. The sharply reduced response from October 1983 through June 1984 was the result of performance monitoring problems. The 1987 water year (beginning October 1986) averaged above 96 percent response.

A. Annual Variations

Figure 6 also shows the annual variation in site response. This variation reflects the annual periodicity in the presence of meteor trials available for signal reflection or reradiation. Typically for SNOTEL, the performance in July and August is 5 to 10 percentage points higher than the February response rate. An examination of response times (the system-wide average time elapsed between the first possibility to respond to a probe and the actual response) indicates that the average for mid-January to mid-February is about double the average response times for August to October.

B. Diurnal Variation

Technical discussion of meteor burst technology includes references to the diurnal characteristics of meteor availability. There is an approximate 4:1 ratio of available incoming meteors from early morning to evening (Leader, 1974). A measure of the diurnal effect on SNOTEL communications is illustrated by the results of a series of polls conducted in August 1986. During a 10-day period, special, 2-hour, system-wide polls were made beginning at 1100, 1500, and 2000 hours in addition to the regular 0500 hour poll. The average rate of responses during these polls is shown in table C.

The presence of a significant diurnal perdiodicity was confirmed, but it did

not result in large magnitude changes of system performance.

Table C

TEN DAY AVERAGE DIURNAL RESPONSE

Polling Hours		Percent Response
0500-0700	=	95.9%
1100-1300	=	91.7%
1500-1700	=	90.0%
2000-2200	=	90.0%

C. Influence of Solar and Geomagnetic Activity

Solar flares and geomagnetic storms are relatively common occurrences which alter the earth's magnetic field causing varying degrees of RF interference. For several years, SNOTEL analysts have observed a correlation between system response and these occurrences which are forecast and observed by the National Oceanic and Atmospheric Administration-U.S. Air Force Space Environment Services Center in Boulder, Colorado.

These disruptions are seen as increased noise levels on the receivers at both the remote sites and at the master stations. Depending upon the severity of the disturbance, some alteration of system performance can be seen. During these times, the remote site receivers see an elevated noise level and detect RF, making it harder for the unit to identify valid master station transmissions. Because SNOTEL only requires one valid transmission sequence per polling period, it is highly likely that unless noise completely saturates the receiver, the necessary transmission will eventually occur. Therefore, when most geomagnetic storms and solar flares happen, little change can be seen in system performance or in the number of remote sites responding to a poll.

Very intense storms, such as the one that occurred on November 8, 1986, can show significant system degradation. During this period, SNOTEL performance dropped 10.7 percent.

The master stations interpret this noise only as good remote site transmissions or as bad ones, with or without valid sync characters. Monitoring these statistics during polling allows SNOTEL operators to determine the amount of noise actually present. For example, on February 8, 1986, an extremely strong geomagnetic storm occurred. Noise levels elevated to 13 times normal at the master stations and system-wide response dropped 5.3 percent. Although there may have been other contributing factors, the system did not completely return to normal for 5 days.

VII. SUMMARY

The SNOTEL experience can be taken as an empirically based endorsement of meteor burst communications for the continual collection of hydrometeorological data year after year. It is ideally suited to operations in remote high-mountain regions where conventional communications are difficult. With proper design, the system operates satisfactorily in extremely adverse environments and under the full range of meteor availability.

The installation of SNOTEL was complicated by the short working season, difficult access, and the lack of an experience base for constructing comparable meteor burst networks. The first two problems remain, but the installation of SNOTEL, and subsequent systems by others, has generated a body of experience benefiting new system installations.

Maintenance is also complicated by the remoteness and harsh environment of SNOTEL sites more than by any unique characteristics of a meteor burst system. Dedicated, skilled, experienced technicians and adequate diagnostic capabilities, such as SNOTELs remote maintenance parameters, are the necessary components of a successful maintenance operation.

SNOTEL modernization, in providing for the planned replacement of obsolete components, also presents an opportunity to make equipment and system revisions. In addition to improving performance and reliability, the capabilities of SNOTEL are being expanded in the upgrade program to meet continually developing natural resource needs for data and related products.

Performance characteristics unique to meteor burst communications systems are measured in SNOTEL, and they show that the system is in comformance with the design and exceeds operating requirements. These statistics also show steady improvement in performance. It can be concluded that, by any measure, SNOTEL is completely successful.

REFERENCES

Crook, Arthur G., Beard, G.A., and Helseth, E.S. "Practical Experience in Data Acquisition System Operations--SNOTEL." Proceedings of the World Meteorological Organization Workshop on Telemetry and Data Transmission for Hydrology. 1987.

Crook, Arthur G. and Johnson, D.E. "Characteristics of the SNOTEL Data Acquisition System." Proceedings of the World Meteorological Organization Workshop on Telemetry and Data Transmission for Hydrology. 1987.

Leader, Ray E. "Meteor Burst Communications." Proceeding of the 42nd Western Snow Conference, pp. 29-36, 1974.

Figure 1. Geographical Extent of the SNOTEL System

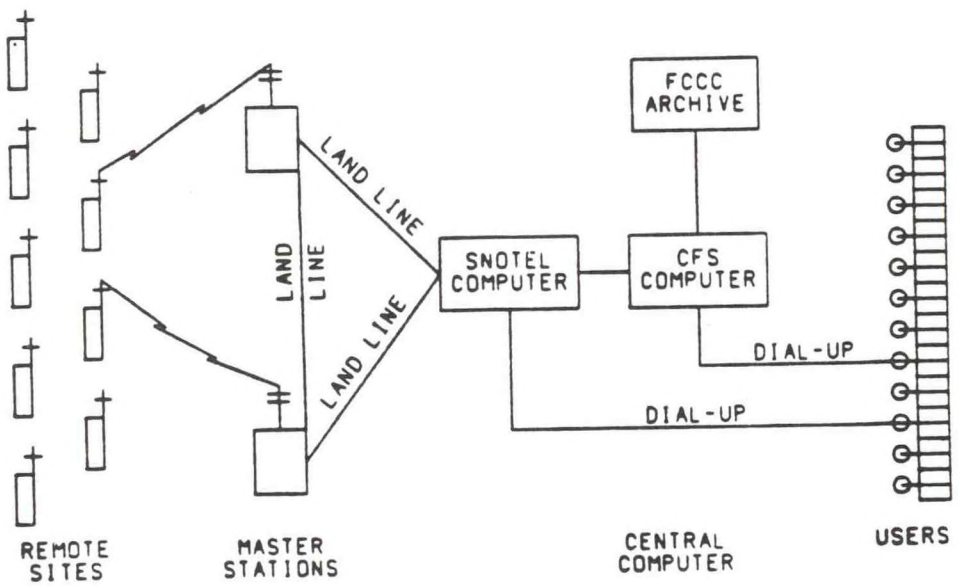

Figure 2. SNOTEL System Architecture

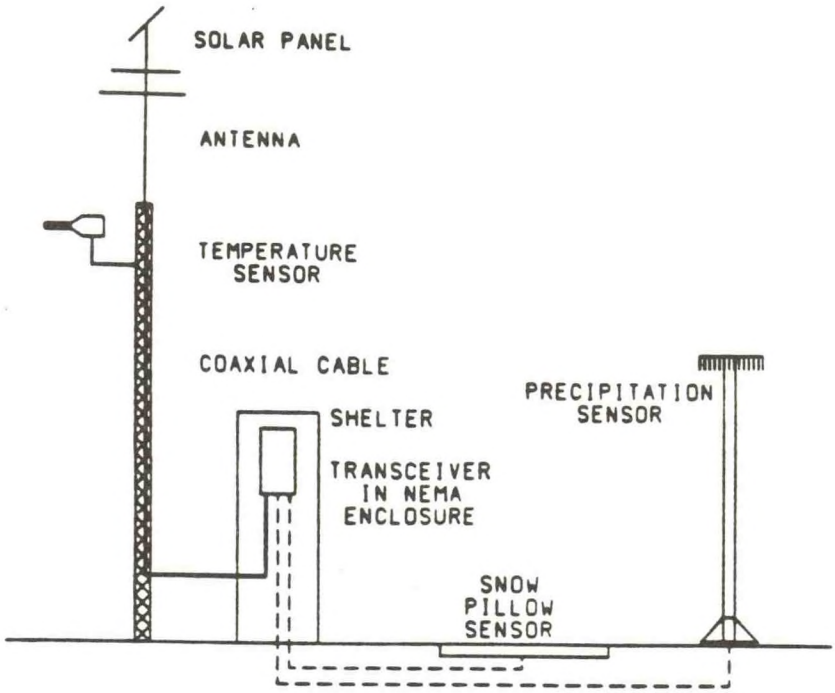

Figure 3. Typical SNOTEL Remote Site Configuration

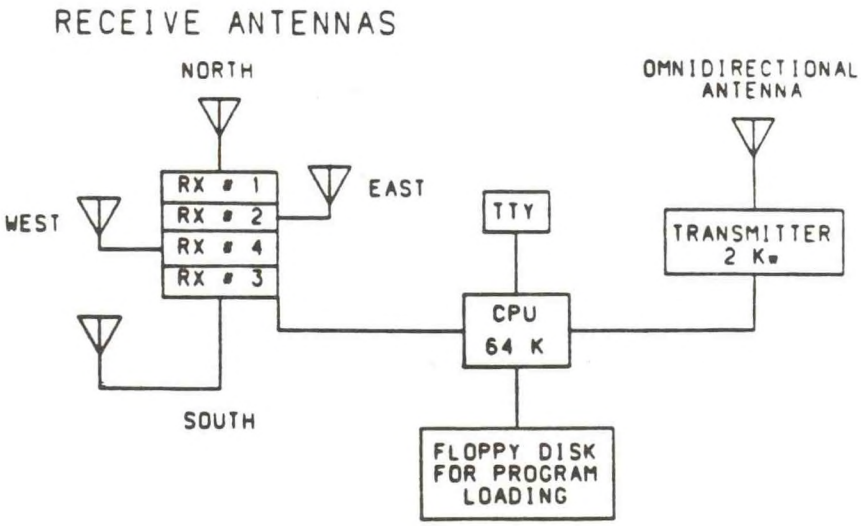

Figure 4. Typical Master Station Configuration

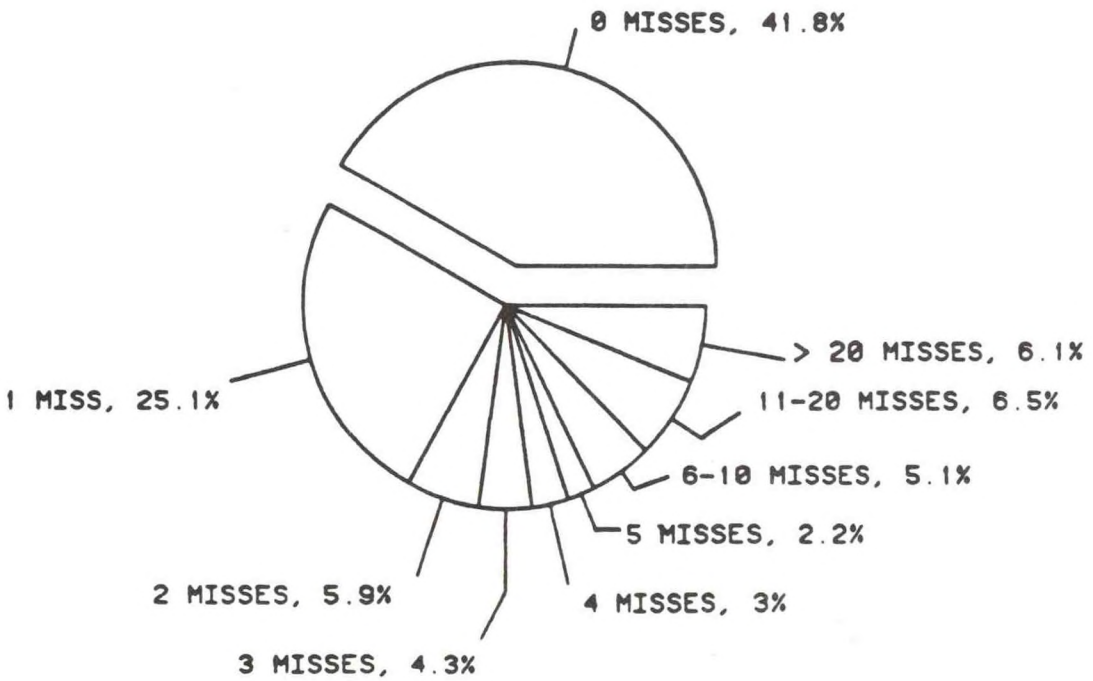

Figure 5. Individual Remote Site Responses

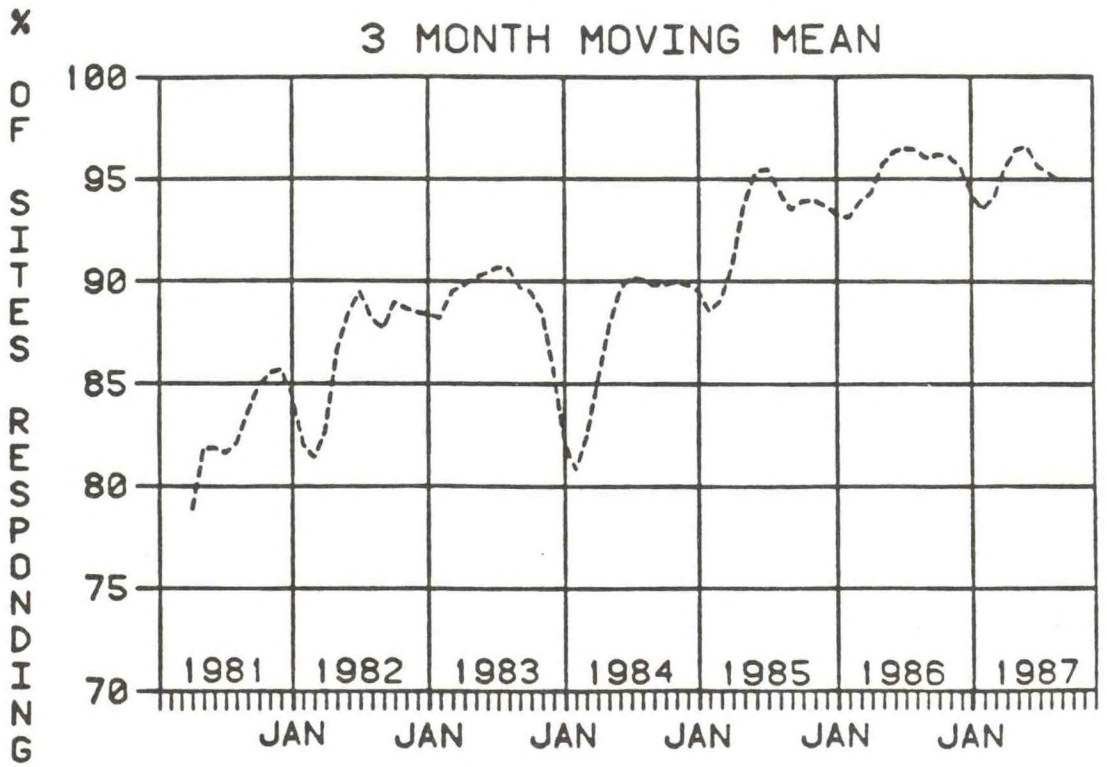

Figure 6. SNOTEL Systemwide Performance

TECHNICAL DEVELOPMENT AND EXPERIENCE OF HYDROLOGICAL INFORMATION AND FORECASTING ON THE YANGTZE RIVER

Chen Jinrong and Wang Qinliang
Yangtze Valley Planning Office
Ministry of Water Resources

ABSTRACT. A brief introductory review is provided of the historical development and present status of the hydrological information and forecasting on the Yangtze River. The Yangtze is a rainfall-flood river which leads to frequent floods, droughts, and waterloggings. Since the founding of the People's Republic of China, our government has attached great importance to flood prevention as it has important bearing on the life and property of the people. The hydrological information and forecasting on the Yangtze River, as a non structural measure, has been developed rapidly and has achieved remarkable success, which is usually called an "ear and eye" and "advisor" for flood control and becomes an essentially professional work. Meanwhile, the forecasting techniques and methods have been improved and promoted on the basis of practice in the struggle against flood for nearly 40 years. This paper presents some advances in corresponding stage/discharge relationship, streamflow routing, rainfall-runoff forecasting, computer applications, on-line forecasting, and long-term hydrometeorological forecasting, respectively. The forecasting service and benefit are also covered, including the forecasting items and the range and way of service. Several extraordinary floods that have occurred in the past 40 years are taken as examples to show how the hydrological information and forecasting plays a significant role in flood control on the Yangtze River. Finally, some major knowledge and understanding are proposed based on our practical experiences for the past 40 years.

I. INTRODUCTION

The Yangtze river is the largest river in China, and is also one of the largest rivers in the world. It originates from the northern slopes of the Tanggula Mountain Range on the Qinhai-Tibet Plateau and flows through 10 provinces (autonomous regions and municipalities) into the East China Sea, with a total length of 6,300 km. The tributaries of the Yangtze extend to 10 provinces (autonomous regions). Its drainage area is 1.8 million km^2, equal to about one-fifth of the total country.

The Yangtze basin is rich in water, hydropower, mineral, forestry, and aquatic resources. The value of industrial and agricultural output amounts to about 40% of the nation's total. The population is about 1/3 of the total country. Many industrial and commercial cities are located along the river banks. Therefore, the Yangtze occupies a very important position in the development of the economy of China.

The Yangtze basin extends between 24°N and 26°N, belonging to the subtropical monsoon region. The climate in most parts of the basin is mild with abundant precipitation. The annual mean rainfall over the whole basin is about 1,100 mm. The annual mean flow volume is about 1,000 billion m^3.

Floods from the Yangtze basin, with the exception of the headwaters region on the upper reach of Jinshajiang, are the direct outcome of rain only events. Rainfall over the Yangtze basin is related with both monsoon activity and seasonal movement of the subtropic high. The wet season falls between May and October. The distribution of precipitation within a year is quite nonuniform and the amount of precipitation in the rainy season usually comprises about 70-90% of the annual total. The precipitation also varies widely from year to year. The nonuniformity of rainfall distribution in space and time and the prematurity or delay of the rainy season, lead to frequent floods, droughts, and waterloggings.

According to historical records, more than 210 disastrous floods occurred in the 2,000 years from the beginning of the Han dynasty (185 B.C.) to the end of

the Qing dynasty (1911 A.D.), or once in every ten years on an average. Since 1921, 11 unusual floods have occurred, with an average of once in every 6 years.

In the past, hydrological forecasting was nill basically and very little use was made of the hydrological information available in the Yangtze basin. After the founding of new China, governments at all levels have devoted much attention to flood prevention as it is of vital importance to the life and property of the people. The hydrological information and forecasting, functioning as eyes and ears for flood control, has been expanding by leaps and bounds and has yielded enormous benefits to both the society and the economy of new China.

In this paper, we will briefly review the historical development and the present status of the hydrological information and forecasting on the Yangtze River, and introduce some advances in forecasting techniques and methods. The benefits of improved forecasting procedures will also be demonstrated. Finally, some understanding and knowledge will be proposed based on our practical experiences over the last 40 years.

II. DEVELOPMENT IN HYDROLOGICAL FORECASTING ON THE YANGTZE

A well-developed network of reporting stations for forecasting operation has grown up from only 20 plus points along the river in the early 1950's to 752 stations over the entire basin now. There are 193 stations for water level, 143 for discharge and 707 for rainfall. The rationally-distributed network can strictly monitor the rain and river regimes, and basically meet the demand for forecasting operation. In order to improve the reliability and to save time in transmitting observational data from stations to the forecasting center, several automatic systems for hydrological data collection and transmission have been installed recently such as the system with ultra short wave transmission on the Lushui basin in the middle Yangtze; the testing system with meteor-burst trail technology in the upstream area of Danjiangkou Reservoir on the Han River; an unattended hydrological network for some stations in the Three Gorges region; and the Daning River basin with satellite transmission under testing. Furthermore, on the Jingjiang stretch of the

Yangtze and the middle-lower stretch of the Han River, which are the most important areas for flood control, the automatic systems are ready to be installed.

The short-term flood forecasting on the Yangtze started soon after the founding of new China. The forecasting was provided for the Jingjiang stretch and the middle-lower Han River which were urgently needed for flood control. An extraordinary flood, greater than a one-hundred-year flood, occurred in the Yangtze basin in 1954. According to the actual demands of flood control, the content and scope of flood forecasting was enhanced rapidly. Through two month's practice in the struggle against the flood, experiences of flood forecasting were greatly enriched. In 1958, a book Technical Experiences of Hydrological Forecasting on the Yangtze River was summarized and published (YVPO, 1958). On this basis, going further for the whole mainstem, some large tributaries and local areas, a complete systematic set of forecasting schemes was made.

The short term weather forecasting service was formally instituted in the late 1950s. Apart from meteorological departments, our efforts were made to predict the mean areal rainfall for each of the drainage areas so that it could be directly incorporated into hydrological forecasting for the purpose of increasing the lead time of forecasts.

At the same time, the long-term forecasting for yearly and monthly hydrological characteristic values was also carried out. As the construction of several large scale projects, such as Danjiangkou, Yahekou, Lushui, and Gezhouba project, the construction forecast for reservoirs had been made.

Since the 1970's, the emphasis of research has been on runoff formation, flow concentration model, real time on-line forecast, regularity of flood and drought, and long term forecasting methods. In 1979, a book Hydrological Forecast Methods in China was published and compiled principally by the Yangtze Valley Planning Office (YVPO, 1979). Nearly 30 experts, scientific researchers and professors over the country participated in writing and reviewing the book. This book systematically summed up the techniques and methods for short-term forecasting on rivers, lakes, and reservoirs in China, including the Yangtze River. At the same time, another book, Collected Works

in Medium and Long Term Hydrometeorological Forecasting, compiled by YVPO was published (YVPO, 1979).

Now, YVPO undertakes the task of hydrological forecasting for the main stem and important tributaries of the Yangtze River with a length of up to 3,400 km. There are more than 50 forecasting stations and points. The forecast periods include short term, medium term, and long term. According to statistics of errors in short-term operational forecasts for years, the assurance ratio curves for water level forecasting error in the different forecasting periods are plotted, as shown in fig. 1. As for the accuracy of short-term rainfall forecasting, taking the upstream region of the Han River (the drainage area is 95,200 km) as an example, it is 77 percent for the 24-hour-ahead forecasting and 67 percent for the 48-hour-ahead forecasting. The medium term forecasting for rainfall is now being tested. The qualitative accuracy of long-term forecastim ng about 70 percent.

III. TECHNICAL DEVELOPMENT

With the practical experiences of nearly 40 years, the techniques and methods for hydrological forecasting on the Yangtze River have been significantly promoted and developed. These are mainly summed up as follows:

A. Methods of Corresponding Stages (Drainages)

This method is an old and simple method, used on the Yangtze River beginning in the early 1950s. Through continuously and perfectly summerizing, a complete set of forecasting schemes for river systems has been established, so the successive forecasting from the upperstream Cuntan station to the downstream Datong station can be carried out.

In order to treat some complicated problems such as, confluences with tributaries, flows from local districts, and effects by backwater, effective methods have been developed. For example, on the reach from the Cuntan station to the Qingxichang station in the upstream Yangtze, a main tributary of the Wujian River is joined (fig. 2). For the development of the crest relation between these two stations, the stage of Wulong station on the Wujiang River should be taken as a parameter, as shown in fig. 3. The next

example is the middle stretch of the Yangtze, from the Yichang station (the outlet of the Three Gorges) to the Luoshan station (at the confluence of Yangtze with the Dongting Lake). The tributaries of the Qingjiang River feed into the main stem and the Xiang River, Zi River, Yuan River and Li River feed into Dongting Lake (fig. 4). Due to the complication of the confluences, the method of summed discharge is used for establishing forecasting relation (fig. 5). In addition, for forecasting the stage of Jianli station, upstream of the confluence of Yangtze stem and Dongting Lake (fig. 4), which is frequently influenced by backwater from the lake, the different relation curves are plotted for the various conditions, the example being shown in fig. 6. As for the forecasting of tributary reach affected by the backwater from the stem, the relevant relation can be made by taking the stage of the downstream station as parameter (fig. 7).

In short, the relation of corresponding stages (discharges) is based on the principle of flood wave movement in channel, and practically is a kind of empirical model for river routing. The method is simple and easy, and can be used to avoid the existing trouble of transforming the discharge into stage. When it is used in operational forecasting, cooperating with the present-time adjustment technique and the practical experience of skilled technicians, it can still be regarded as an effective forecasting method for river stage.

B. Methods of Flow Routing

In the 1950's, an extensively used method was the Muskingum method. Its application and problem was examined. Early in the 1960's, the method of basin flow concentration computation suggested by Zhao Renjun (1962) was applied to the computation of river flow concentration. On the basis of finite difference solution of Muskingum method by successive routing, the general equation for the flow concentration coefficient was derived as follows:

$$P_{o_n} = C_o^n \qquad (m - 0)$$

$$P_{mn} = \sum_{i=1}^{n} \beta_i C_o^{n-1} C_?^{m-i} \alpha^i \qquad (m>0,\ m-i\geq 0)$$

in which,

$\alpha = C_1 + C_0 C_2$

$\beta = n!\cdot(m-1)! \;/\; [i!\cdot(1-1)!\cdot(n-1)!\cdot(m-1)!]$

here, m is the number of time intervals;

n is the number of reaches;

C_0 , C_1, C_2 are Muskingum coefficients.

With regard to the theoretical basis of the Muskingum method, and the significance of parameters and the problem of negative response, the studies were made through the hydraulics and systematic theory. The result has shown that the Muskingum model for multiple river reaches may be a lumped "strong approximation" to the quasi-diffusion wave (Wang, 1988, Wang and Luo, 1989).

The quasi-diffusion equation may be written as:

$$\frac{\partial Q}{\partial t} = \frac{1}{w_0} \frac{\partial Q}{\partial x} + \frac{v_0}{w_0} \frac{\partial^2 Q}{\partial x \partial t}$$

By integrating over the river reach and applying the composite trapezoidal quadrature formula, the storage equation is obtained as:

$$S(t) = \sum_{m=1}^{n} \{K_0[Q(\frac{m-1}{n} L, t) + (1 - \theta_0) Q (\frac{m}{n} L, t)]\}$$

The truncation error is:

$$R_n(Q) = - \frac{1}{12} \cdot \frac{L^3}{n^2} \cdot \frac{\partial^2 Q(x,t)}{\partial x^2} \Bigg|_{x = n} \qquad n \varepsilon [0,L]$$

The analytical solutions derived for the quasi-diffusion wave and the multiple Muskingum model are respectively:

$$u(x,t) = \exp(- \frac{x}{v_0}) \delta(t) - \sum_{\lambda=1}^{\infty} (- \frac{x}{v_0})^{\lambda} \frac{1}{\lambda} \cdot \frac{w_0}{v_0} \exp(- \frac{w_0 t}{v_0}) L_{\lambda-1}^{1}(\frac{w_0 t}{v_0})$$

$$u(t) = (- \frac{\theta_0}{1-\theta_0})^n \delta(t) - (- \frac{\theta_0}{1-\theta_0})^n \frac{1}{K_0\theta(1-\theta_0)} \exp[- \frac{t}{K_0(1-\theta_0)}] L_{n-1}^{1}[\frac{t}{K_0 o_0 (1-\theta_0)}]$$

which display a good similarity. In the above equations,

w_0 = kinematic wave velocity;

u_0 = diffusion coefficient;

$v_0 = u_0/w_0$; $K_0 = L/(nw_0)$;

n = number of river reaches; $\theta_0 = 1/2\ nv_0/L$;

$L_m^1()$ = generalized Languerre polynomials.

It can be shown that the negative response of the Muskingum method is eliminated when the successive routing method by subreaches is applied with $n \geq L / 2v_0$.

After the construction of the Danjiankou reservoir, the hydraulic characteristics of middle/lower reach of the Han River have been evidently changed. In the propagation of flood wave resulting from the release of the reservoir, the effect of translation is outstanding. Thus, a conceptual model, called as the model of lag-instantaneous flow concentration or the successive lag-and-route model, was proposed in the 1970's (Wang, 1982; Luo, 1987). With the concept of linear channel and linear reservoir by J.C.I. Dooge, the storage equation and the water balance equation were found as follows:

$$S(t) = \int_0^t [I(t) - I(t - \tau)]dt + ko(t)$$

$$I(t) - o(t) = dS(t)/dt$$

From which the integration solution of the lag-and-route model for n reaches was derived as:

$$u(t) = \begin{cases} 0 & 0 \leq t \leq n\tau \\ \frac{1}{k_r(n)} \cdot \left(\frac{t-n\tau}{k}\right)^{n-1} \exp\left(-\frac{t-n\tau}{k}\right) & t > n\tau \end{cases}$$

The relations between the parameters and the moments were also obtained. Moreover, the good results were achieved in actual forecast.

C. Forecast of Runoff From Rainfall

In the early 1950's, the Snyder method and the trial and error method were applied for the determination of the runoff hydrograph from rainstorm over the ungaged areas of the Three Gorges region, and the synthetic forecasting scheme for the Wanxian-Yichang stretch was made. For the tributaries of the Ming, Tuo, Jialing, and Wu rivers on the upstream Yangtze and the Dongting river system of the Xiang, Zi, Yuan, and Li rivers, the runoff was forecast by the methods of rainfall-runoff relation or runoff coefficient.

In 1954, an extraordinary flood occurred. On account of the excessive complication of the state about the flood diversions, the burst open of levees in a natural or planned way, and the river and lake flooding as a whole, the lake routing method was utilized to forecast the outflows from some major cross-sections and the results were satisfactory.

The rainfall-runoff relation is frequently used in operational forecasting. The main factors which are usually considered in the development of rainfall-runoff relations are antecedent, effective rainfall; season; rainfall duration or rainfall intensity; rainfall pattern; and location of the storm center. The selection of factors depends on the concrete condition of the river basin. The correlation diagrams can be made with three variables, four variables, or five variables.

The unit hydrograph is mainly adopted for forecasts of the basin flow concentration, and some adjustments are made based on the characteristics of storms and floods for each basin. For example, to consider the nonlinear effect, the rainfall patterns are assigned according to the storm center location or the rainfall intensity.

When drawing up the inflow forecasting scheme for the Danjiangkou reservoir, it is necessary to take the non-uniform areal distribution of rainfall and runoff since the drainage area above the reservoir is rather large (95,200 km). The solution is the division of the whole basin into subareas according to the tributaries and local districts and developing the forecast schemes of the runoff formation and the flow concentration for each of the subareas. The flow concentration in the channel is then computed one section after another.

In addition, for the conceptual rainfall-runoff models such as the API model, the model of runoff formation at natural storage, the Stanford watershed model, the Tank model, and the Sacramento model, etc., many studies and tests have been taken for application.

D. Computer Application and On-Line Forecasting

In the early 1960's, YVPO developed an electronic analog for flood routing in channel. As the electronic techniques developed, the forecasting scheme came to be drawn up with a digital electronic computer in the 1970's.

In recent years, the on-line flood forecasting for river systems have been particularly studied and established. Since most of the real-time data are transmitted from the field stations to the forecasting center at present, by means of telegram or telephone through the communication system of post and telecommunication department, the pre-processing of data will include the automatic translation of telegram, format transformation, data quality examination, error rejecting, data processing and tabulation, and filing forming. For all forecasting schemes in operation, the general programs are worked out. Based on the preprocessed real-time information of river and rainfall, the on-line forecasting in river systems can be done immediately (figs. 8 and 9).

At the same time, to take further steps to establish the real-time on-line forecasting system, the state estimation and stochastic approximation theory are applied to solve the problem of the real-time adjustment for forecasting, and the least square dynamic identification and Kalman filter method are applied to self adjust the parameters at real time.

E. Techniques and Methods of Long-Term Forecasting

Since the 1950's, the business of long-term forecasting have been regularly taken by YVPO, and the technical level has been obviously raised, gradually forming a frontier course with a close combination of hydrology, meteorology, oceanology, astronomy, geography, and mathematics. The forecasting techniques can be summed up as the following categories: the synoptics technique, the statistics technique, the interaction of ocean-atmosphere and earth

atmosphere, the relation of solar-earth, and the analysis of geophysical factors. The long period variations of weather for the flood or the drought in the wet season on the area of middle and lower Yangtze are emphasized to be studied. Two circulation patterns for the rainy years and the dry years are presented. Considering the effects of the surface temperature on the Pacific Ocean and the thermal condition of the Qinghai-Tibet Plateau to the long period synoptic course, the forecasting model for flood and drought is established. Moreover, relating to the index of solar activity such as the relative number of sunspot and the radiant discharge 10 cm from the sun, to the geographical factor such as shifting of earth pole, variation of rotation speed of the earth, geomagnetism, and volcanic eruption, the corresponding analysis with the variation in water volume on the Yangtze is carried out to provide the background of long period developing trend for the drought or waterlogging forecasting in the flood season. However, the techniques used on long-term forecasting are mostly the methods of probability and statistics, such as, correlation analysis, multivariate regression, progressive regression, autoregression (AR), autoregression moving average (ARMA), autoregression integration moving average (ARIMA), discriminatory analysis, cluster analysis, harmonic analysis and orthogonal function expansion.

IV. FORECASTING SERVICE AND BENEFIT

The items of service are mainly as follows: (1) short-term river forecasting including the forecast of flood fluctuation, peak stage (discharge) and occurred time, with the forecasting period of 1-5 days; (2) forecasting for the inflow to and the pool stage of large-scale reservoir; (3) special water-regime forecasting for flood diversion and levee burst; (4) forecasting of mean velocity in individual cross section; (5) construction forecasting for large scale project; (6) short-term precipitation forecasting for the regions; (7) extended forecasting for synoptic situation and precipitation trend; (8) long-term hydrometeorological forecasting including the trends of flood or drought regime in whole year, and the yearly and monthly hydrological characteristic values of main stations on the Yangtze stem.

Among the forecasting service units, there are more than 200 for the short period, and 120 for the long period. These units relate to flood control and drought resistance, reservoir construction and management, electric power regulation, navigation, communication, transportation, water supply, industry, commerce, insurance, wharf and store house.

Using the telegram and telephone, the results of operational forecast are transmitted to the users. During the flood season, the Bulletin of Flood Information and Forecasting on the Yangtze is specially released once every two or three days. If there are some important water regimes or synoptic developments, the analysis and forecast will be made and reported promptly to the National Flood Control Headquarters, informing all headquarters of the provinces along the Yangtze River. Moreover, the prevention measures probable adopted will also be proposed and consulted by YVPO. As for the long term forecasting of flood season (May-October) and dry season (November-April), the announcements will be made in April and October, respectively.

As mentioned earlier, the Yangtze River is a rain-and-flood river. The flood hazards are frequent and serious. Especially in the plains area along the middle and lower reaches where the industry and agriculture are flourishing and the population density is rather high. However, the surface elevation is generally lower than the flood water level of the river, so that the areas are all protected against floods by levees. Obviously, how to bring the serious river flood under control is a major problem. In addition, a vast number of water conservancy projects have been built and are under construction on the main stem and tributaries of the Yangtze River. The reasonable regulation and operation of reservoirs and their safety are also very important. As a result, the hydrological information and forecasting, as a non-structural measure, has played a vitally important role in the struggle against the floods over the years.

For example, a major flood occurred in 1954. The flood levels in the middle and lower Yangtze from Zhijiang to Zhenjiang all exceeded over their historical observed records. The flood from upstream was high, carried great volumes of water, and lasted a long time. The hydrologic information and forecasting provided a reliable basis for the flood prevention and emergency

repairs along the river, the operation of the sluice gate of Jingjiang flood diversion project, and the rational operating schedule for retarding basins and flood storage areas. The total volume of flood water diverted in the middle and lower area of the Yangtze River was 1,023 billion m^3 during the flood of 1954. The result was that the Jingjiang Levee and the cities of Shashi, Wuhan, and Nanjing were kept in tact.

In the last ten days of June, 1964, the Lushui basin of a tributary of Yangtze was hit by a heavy rainstorm, which caused a serious menace to the construction of the Lushui Project and the downstream Beijing-Guangzhou railway. The peak stage forecasted could approach the elevation of the upstream cofferdam. In this critical time, a decision must be made, either the cofferdam to be broken or the flood prevention to be kept consistent, which, of course, depended on the future development of the rainfall and subsequent flow. This proved to be a severe test of our forecasting ability. The flood forecasting was produced in combination with the weather forecasting, and proved to be highly effective. The flood passed without causing any significant damage.

The third example is the 1981 flood which occurred on the upper area of Yangtze in the middle of July. The extraordinary flood seriously threatened the safety of the Jingjiang Levee and the construction of the Gezhouba Project. As the forecasted crest stage at Shashi closed with limited space for flood control, the situation was critical. Based on the analysis and forecasts of rainfall and water regimes, the leading authorities made a decision of not using the Jingjiang flood diversion project and organized about 300,000 masses and army men to take part in protecting the levee. The forecasts were extremely accurate. For the crest stages, the five-day predictions at Yichang and Shashi agreed with the observations, and the forecast errors were only 2 cm and 6 cm, respectively. Thus, not only was the safety of the Jingjiang Levee (protecting 8 million mu farmland and 5 million people in the plain area on the northern bank) ensured, but also the heavy losses of both temporary relocation of 400,000 inhabitants and inundation of 600,000-mu cultivated land in the Jinjiang dentention basin were averted. The

Chongqing City received our forecasting report and immediately withdrew 220,000 people to a safe area (Chen, 1981).

So many facts can be stated, but considering the limited space of the paper, it will not go into detail to cover additional examples.

V. MAJOR KNOWLEDGE AND UNDERSTANDING

Based on our practical experiences in the hydrological information and forecasting on the Yangtze River for years, some knowledge and understanding are synthesized as follows:

1. Hydrological information is an essential prerequisite for flood forecasting, and also a fundamental link in information-forecast-service systems. Without accurate and timely information, the forecasting is difficult to accomplish. Thus, the management of hydrological information is most important.

In addition to having an optimized hydrological network and deciding on a scientific and reasonable standard of reporting time intervals, a set of strict rules and measures is required for the management of hydrological information, such as, working out the assignment and entrustment for river and rainfall information, defining the task and requirement of reporting for each of the stations, compiling a summarized table and service cards for reporting stations and filing into the computer for retrieval and checking, and establishing "Rules for testing and assessing quality" and "System of personal responsibility."

At present, the data collection-transmission-processing is still in manual operation, and there are so many circulation links not only paying for time but also affecting the reliability. This is a major obstacle for increasing the effective forecasting period and raising the forecasting accuracy. For this reason, it is desirable to set up the automatic systems for hydrological information and forecasting, especially in some key areas for flood control. We plan to gradually update measures of data transmission by means of radio, satellite and meteor-burst technology.

Meanwhile, scientific research should continue to be enhanced for advancing and raising the theoretical and technical level of hydrological forecasting. Our research efforts will concentrate on the physical mechanism and basic principle analysis for the runoff formation and flow concentration, the real-time on-line forecasting system, the synthesis automatic system for the reservoir inflow forecasting and regulation, the local-inflow forecasting, the precipitation quantitative forecasting, and extended forecasting.

2. Dealing with many uncertain factors, the flood forecasting should proceed from actual conditions and place strong emphasis on analysis in order to increase the ability of flood prediction. There is no doubt that the forecasting scheme (model) is an important tool and the basis of operational forecasting. However, because the change of river characteristics, the effect from human activities, the different time-spatial distribution of rainstorms, the different flood composition, and the specific characteristics of various floods, the forecasting scheme should not be applied mechanically.

In a forecasting operation, based on the consideration of common law (general character) of floods, much attention should be paid to the analysis of particularity (individual character) from which the greatest error in forecasting is usually a result. During the extraordinary flood, the situation is very complicated because of flooding over the flood plain, flood diverting and levee breaches; therefore, carefully considering these factors and taking the key point is important for improved accuracy in forecasting.

In our forecasting practice, care has been taken of the investigation by the forecasters and the forecasting will be achieved with the help of the following measures as; collecting relevant data, keeping informed on the variation of river characteristics, summing up the imperical lesson on flood forecasting, and establishing the essential forecasting card thereafter.

3. The hydrological forecast must be coordinated with the meteorological forecast to a maximum as it is an important way of extending the forecasting period and increasing its benefit. Hydrological forecasting gives us a reduction to the blindness on flood understanding. If the hydrological forecast is organically cooperated with the meteorological forecast, the foresight on flood can be markedly improved.

The formation of each flood on the Yangtze River, the sizes of peak and volume, the length of duration, the sharpness of flood peak, and the effect of rainfall on local districts all depend upon the synoptic situation and the rainfall characteristics to a great extent. Coordination of hydrology and meteorology forecasts is shown clearly by the following facts: a forecasting of floods from rainstorm on the Lushui reservoir in April 1964, a forecasting of extraordinary floods on upstream Yangtze in July of 1981, and a forecasting of floods from rainstorm on the Yahekou reservoir of the Tangbehe River, and the Han River system in April, 1975.

4. Flood forecasting should be coordinated with flood control and regulation for maximum benefit. At present, the basic means for flood control on middle and lower Yangtze depends upon the structural measures on the levees, building and repairing levees in emergency work, and choosing optimal timing for flood diversion and gap diggings, all rely on flood forecasting. In turn, the value of flood forecasting is really expressed under the response of flood prevention. Thus, after working out the flood forecasting, the advise and suggestion should be proposed for the measures of flood prevention to be adopted. The forecasting in combination with flood prevention and regulation, can play a more important role as an advisor.

For example, on the Han River a major flood occurred in October, 1983. The rainfall began on the 3rd of October. According to the forecasting, 210 million m^3 of reservoir storage should be pre-empted from the Danjiangkou reservoir. In order to meet the requirement for flood regulation of reservoir and on the basis of the development of water and rainfall situation, the forecasting of rainfall-runoff and reservoir inflow were made several times, so the reservoir discharging was gradually increased. As for the stretch downstream from Danjiangkou reservoir, forecasting of the peak levels for the stations along the middle-lower Han river was issued timely. At the same time, because of the flood exceeding the downstream discharge capacity, we decided to operate the Dujiatai flood diversion project for storing up 2.3 billion m^3 of flood volume and breaking two embankments of diversion areas for storing 0.88 billion m^3 of flood volume. As a result, the peak stages on the middle and lower stretch of the Han River were lowered.

For the flood, due to the close coordination of hydrological forecasting with flood-control regulation, the dam of Danjiangkou Reservoir and the 400-km-long main and distant levees on both banks along the middle-lower reach of the Han River were safeguarded so that more than 5 million inhabitants living on 10 million mu (0.67 million hectares) of farmland were protected from disasters and the threat of this flood against the safety of Wuhan City was alleviated as well.

REFERENCES

Bokun, Luo "Theory and Application of Lag-and-Route Method and the Comparison with Other Flood Routing Methods," Journal of Hydraulic Engineering, Beijing, China, Vol. 6, pp. 17-25, 1987.

Jinrong, Chen, "Forecasting of Extraordinary Flood on Upper Yangtze," China Water Resources, Beijing, China, Vol. 4, July 1981.

Qinliang, Wang, "The Model of Lag-Instantaneous Flow Concentration,` Hydrology, Beijing, China, Vol. 1, pp. 13-19, 1982.

Qinliang, Wang, "Quasi-Diffusion Wave and Its Lumped Approximation," National Symposium on Hydrological Forecasting, Xian, China, May 1988.

Qinlilang, Wang and Bokun, Luo, "Integration Solution of the Muskingum Successive Routing Method and the Lag-and-Route Method," China U.S. Bilateral Symposium of Hydrological Forecasting, March 1989.

Renjun, Zhao, "Method of Estimation for Runoff Concentration of River Basin," Journal of Hydraulic Engineering, Beijing, China, Vol. 2, 1962.

Yangtze Valley Planning Office (YVPO), Technical Experiences of Hydrological Forecasting on the Yangtze River, China Water Resources and Electric Power Press, Beijing, 1958.

YVPO, "Research on Several Methods of Flow Concentration with Particular Reference to the Reach from Wanxian to Yichang in the Three Gorges Region," National Symposium on Hydrological Forecasting, Wuhan, China, April 1964.

YVPO, Hydrological Forecast Methods in China, China Water Resources and Electric Power Press, Beijing, 1979.

YVPO, Collected Works in Medium and Long Term Hydrometeorological Forecasting, China Water Resources and Electric Power Press, Beijing, 1979.

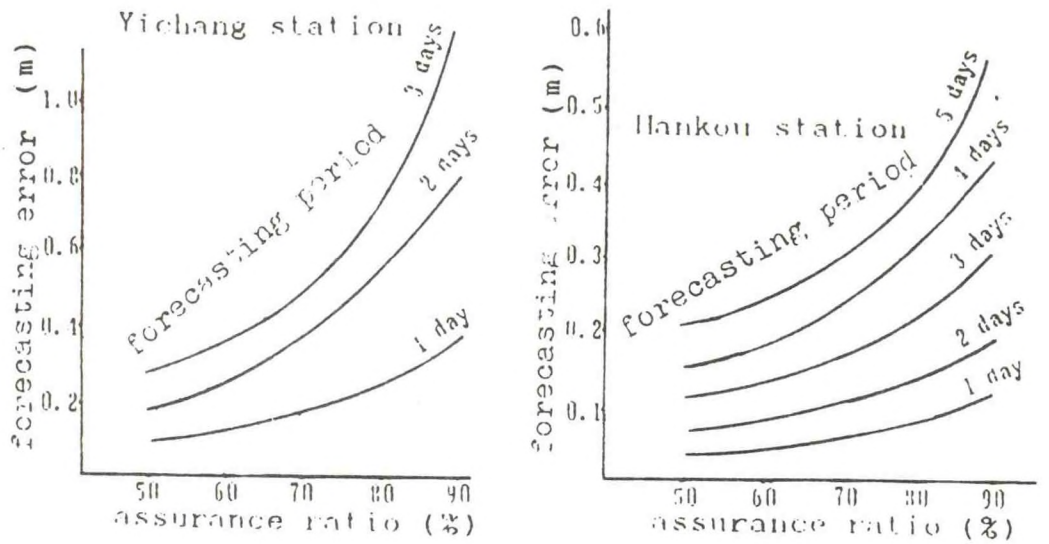

Fig. 1. The assurance ratio curves for water level forecasting error at Yichang and Hankou stations on the Yangtze River

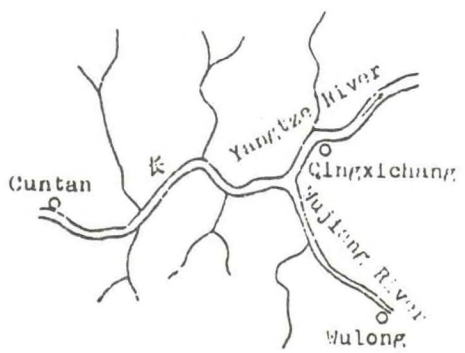

Fig. 2 Diagram of the forecasting reach from Cuntan to Qingqichang on Yangtze

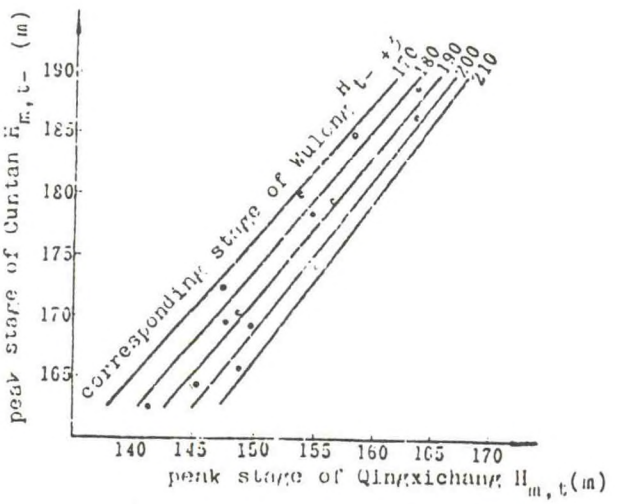

Fig. 3. Peak stage relation for Cuntan-Qingqichang, the Yangtze River

Fig. 4 Diagram of the Yichang-Luoshan reach, the Yangtze River

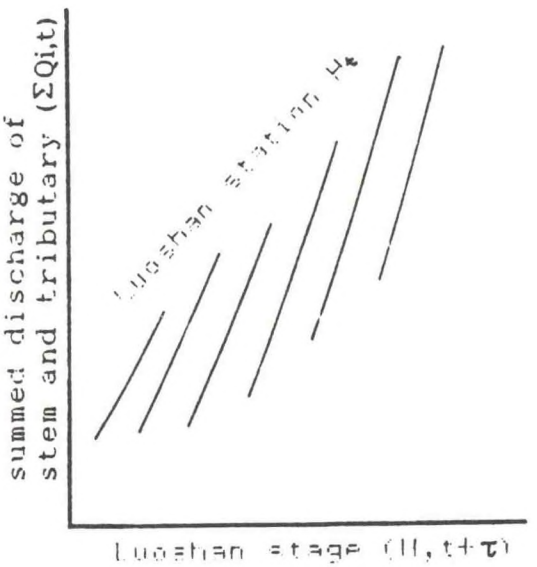

Fig. 5 Relation between the sum of discharges at upstream stations and water level at Luoshan station using Luoshan stage at the time of the forecast issue as parameter, the Yangtze River

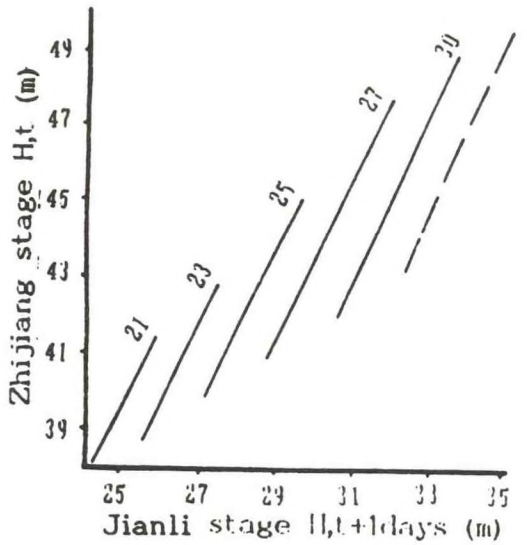

Fig. 6 Guage relation for Zhijiang-Jianli with simultaneous stage of Chenglingji as parameter, the Yangtze River

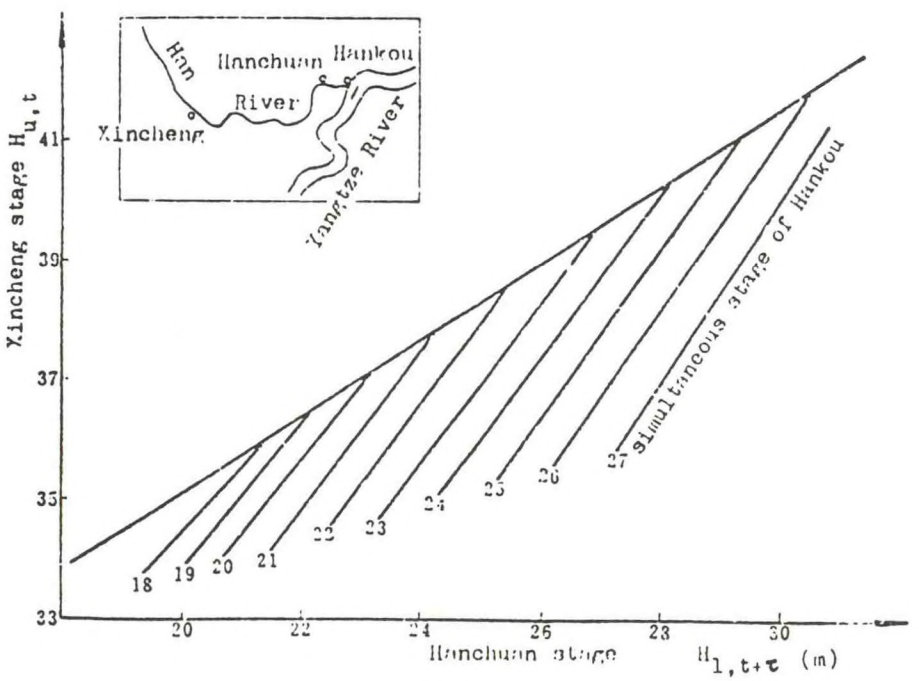

Fig. 7 Gauge relation for the Xincheng-Hanchuan reach (subjected to backwater); Han River

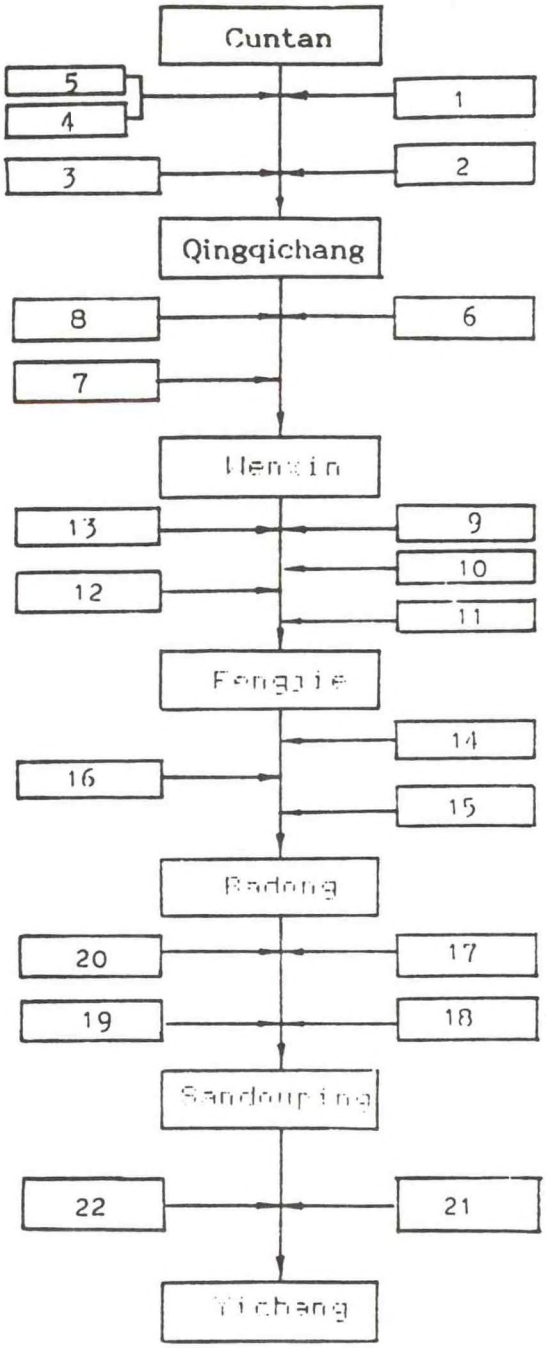

Fig. 8 River system forecast for the local districts in the Three Gorges of Yangtze

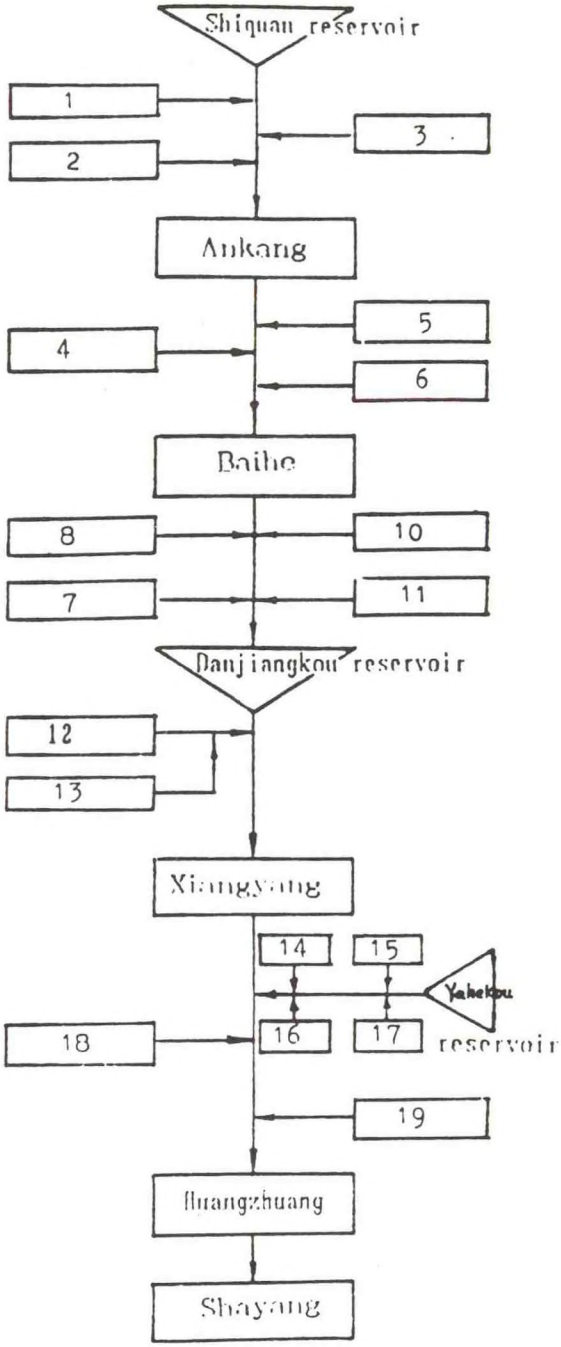

Fig. 9 River system forecast for the Han River

REFERENCES

A MODULAR WATERSHED MODELING AND DATA MANAGEMENT SYSTEM

G.H Leavesley and L.G. Stannard
U.S. Geological Survey
Lakewood, Colorado

ABSTRACT. A modular watershed modeling and data management system that provides a range of hydrologic simulation and data analysis capabilities has been developed. The watershed model component is the U.S. Geological Survey's (USGS) Precipitation Runoff Modeling System (PRMS). PRMS is a modular design, physical process based, distributed parameter watershed model. Data management and analysis components are provided by the USGS data management program ANNIE (not an acronym). ANNIE is an interactive program that accepts and reformats data from a variety of sources for model application. ANNIE also includes a number of statistical, graphical, and data management functions for analysis of measured and simulated data. Hydrologic forecasting capabilities are provided by a modified version of the National Weather Service's Extended Streamflow Prediction (ESP) program. ESP applications include short-term and seasonal forecasting for floods and water supply, and evaluation of the effects of land-use and climate changes on hydrologic response. Other modules, including a digital-terrain-analysis module for use in basin characterization and parameter estimation, a remote-sensing-applications module for use in basin characterization and parameter estimation, and a remote-sensing-applications module for incorporating remotely sensed snow covered area and snowpack water equivalent data in watershed simulations, are currently being developed and tested. The system operates on mainframe, mini, and micro (PC) computers. A fully interactive version of the system using a graphical and expert system interface is currently

being developed and tested on a 32-bit engineering work station.

I. INTRODUCTION

A major problem that affects most model users is the selection of the appropriate model for a specific application. The variety of applications -- ranging from single objective problems such as flood forecasting, to more complex multidisciplinary problems such as simulating the detachment, transport, and deposition of sediment, nutrients, and pesticides -- has resulted in the development of a large number of hydrologic models. Problem objectives, data limitations, scale of application, costs, and time available all are factors that need to be considered in selecting the most appropriate model for a specified application. Given the wide variety of available modeling approaches, model selection can be difficult.

Studies comparing different models using common data sets have been conducted (WMO, 1975; WMO, 1986). However, a common problem in these studies is that the intercorrelation of model components prevents the direct comparison of specific model processes of interest. One approach to address the problems of model comparison and selection is the development of a modular designed modeling system. The modular system uses the concept of a master library which contains compatible subroutines simulating most components of the hydrologic cycle. Alternative or new simulation procedures for selected process components can be compared directly while keeping the remaining process components the same. The use of a standard set of statistical measures, maintained within the system framework, provides a common basis on which to compare component performance. Results of this comparison can be used to make objective decisions regarding the most appropriate combination of simulation procedures, rather than having to select the existing model that most closely meets the user's needs.

The modular concept also provides a system with operational and research modeling capabilities. The use of a standard model framework and data structure enables researchers in a variety of disciplines to develop and test

model components in their areas of expertise without having to develop the entire model. Advances made in hydrologic simulation or data management techniques can be incorporated directly into an operational model.

A modular modeling system is currently being developed to provide the operational and research tools needed to develop, test, and evaluate process simulation techniques and alternative modeling approaches for a wide range of applications. The initial system has been developed from existing software. The major components of the system are: the U.S. Geological Survey's (USGS) Precipitation Runoff Modeling System (PRMS) (Leavesley et al., 1983); the USGS' interactive data management and control program ANNIE (A. M. Lumb, USGS, written commun. 1989); a modified version of the National Weather Service's (NWS) Extended Streamflow Prediction (ESP) program (Day, 1985); and a set of digital-terrain-analysis programs for use in basin characterization. Together they form a complete system that enables a user to reduce, analyze, and prepare data for model application; simulate and forecast watershed response; and statistically and graphically analyze model results.

The purpose of this paper is to provide an overview of the modular system concept, to briefly describe the specific components that make up the initial system, and to discuss future developments. More detailed discussions regarding individual components can be found in cited references for each component. The major components of the system and the data transfers among these components are depicted schematically in fig. 1 and described hereafter.

II. ANNIE

ANNIE is a modular design interactive program that provides the data management and analysis functions of the system. Data from a variety of sources are reformatted by ANNIE to a system-compatible file structure. Meteorologic and hydrologic data are placed in a direct-access file structure called the Watershed Data Management (WDM) file. Data in the WDM file can be analyzed using a number of statistical, graphical, and data management functions. Model- and watershed-specific data can be entered interactively into ANNIE to construct the required input files for PRMS.

ANNIE is a system of software modules designed to help a user interactively create, check, and update input to hydrologic models, and to provide statistical and graphical tools to assist in the analysis of model input and output. The design of the user interactions in ANNIE is a hierarchical system of branches. Branches are selected by the use of menus. Each response moves the user farther down the hierarchy until the desired operation is reached. A user response of a question mark to any menu item produces a help message with additional information about the question and alternative responses. The major branches of ANNIE are depicted schematically in fig. 2. Descriptions of these branches are presented hereafter.

A. Model Input Preparation

This component assists in the preparation of input files for PRMS. Model parameters and variables, watershed characteristics, and model options are contained in these files.

B. Data Management

WDM. The WDM component is used to create a WDM file, define the data sets in the WDM, and perform a variety of data-management functions on the data sets. After the WDM file is created, data sets are added by specifying the data-set number and the attributes associated with each data set. Attributes describe the type, geographic location, and other characteristics of the data set.

Reformat

Reformat converts meteorologic and hydrologic time-series data from a number of different sources into the system-compatible, direct-access WDM file structure. Input from the NWS' climatic data files, USGS' National Water Data Storage and Retrieval (WATERSTORE) system (Hutchinson, 1975), and the U.S. Soil Conservation Service's (SCS) Centralized Forecast System (CFS) (Shafer and Huddleston, 1986) currently (1989) are supported.

Generate

Generate provides the capability to create new data sets. One procedure generates a new data set by applying a mathematical operation to one, or selected combinations of two, existing data sets. Twenty-three different mathematical operations are available for use. Mathematical functions include: log transformations; power transformations; weighted sums; and the addition or subtraction of, and multiplication or division by, constants. A second procedure generates a new data set by changing the time step to an existing data set. A disaggregate transformation expands a time series into shorter time steps. An aggregate transformation condenses a time series into longer time steps.

Logger

Meteorologic and hydrologic data, collected using digital data loggers, can be directly entered into a WDM file. Procedures currently (1989) available were developed to work with data collected using Campbell Scientific CR-21 and CR-21x data loggers*.

C. Statistics

Statistical analysis capabilities are provided by both internal and external application programs. Commonly used statistical procedures such as the computation of means, standard deviations, correlations, and simple linear regressions are done in ANNIE. Error analysis also is supported in ANNIE. More complex statistical procedures are accommodated by reformatting (WDM) data sets to a sequential flat file that is compatible with statistical packages external to ANNIE.

D. Plot

The plot component provides the graphic capabilities in ANNIE. Data sets in the WDM file, results of selected statistical analyses, and PRMS results placed in a PLOTGEN file can be displayed graphically on a monitor or on a pen

* The use of trade-names is for descriptive purposes only and does not constitute endorsement by the USGS.

plotter. Graph formats include time-series plots of one to five data sets, x-y plots of selected data sets, frequency plots, flow-duration plots, and scatter diagrams.

III. PRMS

PRMS is a modular design, distributed parameter, physical process watershed model that was developed to evaluate the effects of various combinations of precipitation, climate, and land use on watershed response. Watershed response to normal and extreme rainfall and snowmelt can be simulated to evaluate changes in water-balance relations, flow regimes, flood peaks and volumes, soil-water relations, sediment yields, and ground water recharge. Parameter optimization and sensitivity analysis capabilities are provided to fit selected model parameters and to evaluate their individual and joint effects on model output.

Watershed response can be simulated at both a daily and a storm time scale. The daily mode simulates hydrologic components as daily average or total values. Streamflow is computed as a mean daily flow. The storm mode simulates selected hydrologic components at time intervals shorter than 1 day. The minimum time interval is 1 minute. The storm mode computes storm hydrographs and sediment yields for selected rainstorms. Sediment modeling capabilities are currently (1989) provided only in the storm mode.

Distributed parameter capabilities are provided by partitioning a watershed into units using characteristics such as slope, aspect, elevation, vegetation type, soil type, and precipitation distribution. Each unit is assumed to be homogeneous with respect to its hydrologic response and to the characteristics listed above; each unit is called a hydrologic response unit (HRU). A water balance and an energy balance are computed daily for each HRU. The sum of the responses of all HRUs, weighted on a unit-area basis, produces the daily watershed response.

A second level of partitioning is used for storm-mode computations. The watershed is conceptualized as a series of interconnected flow-plane and

channel segments. An HRU can be considered the equivalent of a single flow plane, or it can be delineated into a number of flow planes.

The conceptualized watershed system and its inputs are schematically depicted in fig. 3. Brief descriptions of the components that comprise major hydrologic process subsets of the watershed system and that provide mode support capabilities are presented hereafter.

A. Daily-Mode Components

The daily mode components simulate the daily accretion, depletion, storage, and movement of water in an HRU. The rates and volumes of these processes are a function of HRU physical, hydrologic, and climatic characteristics.

Climate Components

Model inputs are daily precipitation, maximum and minimum air temperature, and solar radiation. Precipitation in the form of rain, snow, or a mixture of both is decreased by interception, and it becomes net precipitation delivered to the watershed surface. The energy inputs of air temperature and solar radiation are used in the computation of evaporation, transpiration, sublimation, and snowmelt.

Daily climate data are extrapolated to each HRU using a set of user-defined adjustment coefficients developed from regional climate data. Maximum and minimum daily air temperature data are adjusted using monthly lapse rates and the elevation difference between the climate station and each HRU. An additional correction is applied to adjust for variations in HRU aspect.

Precipitation volume on each HRU can be adjusted to account for changes with elevation and deficiencies in gage catch due to the effects of wind, gage location, and other factors. Separate adjustment coefficients can be applied to summer and winter periods to account for changes in storm characteristics. Precipitation form (rain, snow, or mixture of both) on each HRU is estimated from the HRU maximum and minimum daily air temperatures and their relation to a base temperature (Willen et al., 1971). For mixed events, rain is assumed to occur first. The precipitation form estimation procedure

can be overridden for days when the form is known; also, snowpack volumes on each HRU can be adjusted using measured snowcourse data.

Shortwave radiation, measured on a horizontal surface, is adjusted to estimate daily shortwave radiation received on the slope-aspect combination of each HRU using a method described by Swift (1976). If measured solar-radiation data are unavailable, two procedures to estimate daily solar radiation using air temperature, precipitation, and computed potential solar-radiation data are available (Leaf and Brink, 1973; Thompson, 1976).

Land Phase Components

The watershed system is conceptualized as a series of reservoirs, the responses of which combine to produce the total watershed response. The soil-zone reservoir represents that part of the soil mantle that can lose water through the processes of evaporation and transpiration. Average rooting depth of the predominant vegetation covering the soil surface defines the depth of this zone. Water storage in the soil-zone reservoir is increased by infiltration of rainfall and snowmelt and is decreased by evapotranspiration. The soil-zone reservoir is treated as a two-layered system. Losses from the upper zone, termed the recharge zone, occur from evaporation and transpiration; losses from the lower zone are assumed to occur only through transpiration. When the soil-zone reservoir reaches its storage capacity, a storage level assumed equivalent to field capacity, additional infiltration is routed to the subsurface and ground-water reservoirs.

Daily total precipitation occurring over an HRU is reduced in amount by interception to produce net precipitation. Interception is computed as a function of vegetation cover density and the storage available on the predominant vegetation of an HRU. Intercepted rain is assumed to evaporate at a free water surface rate. Sublimation of intercepted snow is assumed to occur at a rate that is expressed as a percentage of potential evapo-transpiration. In addition to sublimation, intercepted snow can be removed from the canopy by melting.

Net precipitation reaches the snowpack or soil surface where it accumulates in the snowpack or is available for surface runoff and infiltration. Daily

surface runoff from rainfall on pervious snow-free HRUs is computed using a contributing area concept (Dickinson and Whiteley, 1970; Hewlett and Nutter, 1970). The percent of an HRU contributing to surface runoff can be computed as either a linear or a nonlinear function of antecedent soil moisture and rainfall amount.

Surface runoff from snowmelt is computed only on a daily basis. Snowmelt runoff from pervious areas is assumed to occur only when the soil zone of an HRU reaches field capacity. At field capacity, a daily maximum infiltration rate is assumed. Any daily snowmelt in excess of this maximum infiltration rate is assumed to become surface runoff. For impervious areas, snowmelt first satisfies available retention storage, and the remaining snowmelt becomes surface runoff.

Net precipitation not becoming surface runoff infiltrates the soil surface. Infiltration first satisfies any moisture storage deficit in the soil-zone reservoir. Infiltration in excess of the storage capacity of the soil-zone reservoir is routed to the subsurface reservoir. After soil water accretions and routing are completed, evapotranspiration losses are computed.

Three procedures are available to compute potential evapotranspiration (PET). One procedure uses daily panevaporation data and a monthly panadjustment coefficient. A second procedure computes PET as a function of daily mean air temperature and possible hours of sunshine (Hamon, 1961). The third procedure is a modified Jensen-Haise technique (Jensen et al., 1961) that computes PET using air temperature, solar radiation, and two coefficients that can be estimated using regional air-temperature, elevation, vapor pressure, and vegetation data. Actual evapotranspiration is computed as a function of soil type, water currently available in the soil-zone reservoir, and the storage capacity of the soil-zone reservoir.

When the soil-zone reservoir reaches field capacity, infiltrated water in excess of field capacity moves to the subsurface and groundwater reservoirs. Recharge to the groundwater reservoir is removed first from the soil-zone reservoir excess and is assumed to have a daily upper limit. Water in excess of this limit is delivered to the subsurface reservoir. The subsurface reservoir simulates the relatively rapid component of flow that may occur in

the saturated-unsaturated and groundwater zones during periods of rainfall and snowmelt. The groundwater reservoir simulates the slower component of flow from the groundwater zone. The subsurface reservoir can be defined as being linear or nonlinear; the groundwater reservoir is assumed to be linear.

The vertical movement of water from the subsurface reservoir to the groundwater reservoir is computed as a function of the current volume of storage in subsurface reservoir and a linear routing coefficient. The movement of water through the groundwater reservoir to points outside the surface drainage boundary is treated using a groundwater sink. Movement from the groundwater reservoir to the sink is computed as a function of the current volume of storage in the ground-water reservoir and a linear routing coefficient.

Channel Reservoir Components

Channel reservoir components simulate the storage and routing response of channel reservoirs. Reservoir inflows are computed as the sum of the streamflow contributions from all HRUs and the parts of subsurface and groundwater reservoirs above the channel reservoir. Reservoir inflow can also include the outflow of up to three upstream channel reservoirs. Two types of routing procedures are available for simulating reservoir outflow. One is a linear storage routing procedure in which outflow is a linear relation of storage. The second is a modified Puls routing procedure (SCS, 1971).

Snow Components

The snow components simulate the initiation, accumulation, and depletion of a snowpack on each HRU. A snowpack is maintained and modified on both a water-equivalent basis and as a dynamic heat reservoir. A snowpack water balance is computed daily, and an energy balance is computed twice each day for two 12-hour periods (designated day and night).

The energy-balance computations are a combination of equations and functional relationships taken or derived from several sources. The conceptual model for the snowpack system and its energy relations is one described by Obled and Rosse (1977). The snowpack is assumed to be a two-

layered system. The surface layer consists of the upper 3-5 centimeters of the snowpack, and the bottom layer is the remaining snowpack. Heat transfer between the surface layer and the snowpack occurs by conduction when the temperature of the surface layer (Ts) is less than 0°C. When Ts equals 0°C, heat transfer occurs as conduction when the net energy balance at the air-snow interface is negative; but heat transfer occurs as mass transfer by surface melting when the net energy balance is positive. Heat transfer from the precipitation occurs as a mass-transfer process. Conduction of heat from the soil surface to the snowpack is assumed to be negligible compared to the energy exchange at the air-snow interface. The conceptual snowpack system and the components of the snowpack energy balance are shown in fig. 4.

The net shortwave and net longwave components of the energy balance are computed for each HRU using equations developed by the U.S. Army (1956). The net shortwave component is computed as a function of daily shortwave solar radiation, the transmission coefficient of the vegetation canopy above the snow surface, and the snow surface albedo. The net longwave component is computed as a function of the temperatures and emissivities of the snow surface, air, and vegetation canopy. Longwave energy radiated from these sources is computed using the Stefan-Boltzmann law. The latent and sensible heat component is computed as a simplified temperature-index value that is adjusted for the presence or absence of forest cover.

When the energy balance is positive, there is a net gain of energy to the snowpack. This energy melts snow in the surface layer, and the melt then transports heat into the snowpack by mass transfer. If the snowpack temperature is less than 0°C, the melt water is refrozen and decreases the cold content of the snowpack. When the snowpack become isothermal at 0°C, snowmelt is first used to satisfy the free-water holding capacity of the snowpack. Any remaining melt leaves the bottom of the snowpack to become infiltration or surface runoff.

Evaporation and sublimation from the snow surface are assumed to occur only when there is no transpiration from vegetation above the snowpack. Loss from the snow surface is computed as a percentage of the daily PET value. The daily percentage is a constant and is user defined.

B. Storm-mode Components

A watershed is configured into flow plane and channel segments for storm mode computations. An HRU can be considered a single flow plane, or it can be divided into 2 or more flow planes to account for variations in slope and surface roughness. Cascading flow planes are not currently supported, so all flow planes discharge into channel segments. The watershed drainage network is characterized as a system of channel, reservoir, and junction segments that jointly describe the drainage pattern. Each segment can receive upstream inflow from as many as three other segments. In addition, each channel segment can receive lateral inflow from as many as two flow planes (left bank and right bank).

Storm precipitation is reduced by interception, and the net precipitation is available for infiltration. On pervious areas, infiltration is computed using a variation of the Green and Ampt equation (Green and Ampt, 1911). Rainfall excess (net precipitation less infiltration) is then routed as surface runoff over the flow planes into the channel segments using the kinematic approximation to overland flow developed by Leclerc and Schaake (1973). Channel flow is routed through the watershed channel system using the kinematic wave approximation for channel flow described by Dawdy et al., (1978). Routing through channel reservoirs is computed using the same procedures as the daily mode but with shorter time steps.

Sediment detachment and transport from flow planes is computed using a rill-interrill concept approach presented by Hjelmfelt et al., (1975). The procedure considers rainfall and flow detachment processes and the subsequent transport and deposition of entrained sediment. Rainfall detachment is assumed to occur in the interrill areas and is computed as a function of rainfall rate and mean depth of overland flow. Flow detachment is assumed to occur in the rills and is computed as a function of the difference between transport capacity and the current transport rate for each time step. Transport capacity is computed as a function of mean depth of overland flow and the slope of the flow plane.

Sediment delivered from a flow plane is currently transported as a conservative substance in the channel system; detachment and deposition are

not included. The channel sediment routing component will be upgrade in the future with the addition of detachment and deposition capabilities.

C. Optimization and Sensitivity Analysis Components

Optimization components control the automatic adjustment of model parameters to obtain better agreement between observed and predicted runoff. A model parameter is broadly defined as a value that is used to represent a physical or hydrologic characteristic of a watershed and is held constant during a simulation run. This definition produces a large number of parameters for optimization and sensitivity analysis; however, the availability of a large number of parameters is not meant to encourage optimization of all of them. The parameters are available primarily for development work in the theory of errors for the modeling system and to permit model users to evaluate the sensitivity of each parameter and its interactions with others.

Two optimization techniques are available: one is the Rosenbrock technique (Rosenbrock, 1960); the second is a Gauss-Newton technique similar to the linearization method described by Draper and Smith (1966), but with the incorporation of the Box Kanemasu interpolation modification (Beck and Arnold, 1977). One of four objective functions can be selected for use with either technique.

Spatially distributed parameters have an initial value assigned to each HRU, subsurface reservoir, or groundwater reservoir. Temporally distributed parameters have an initial value assigned for each time increment. One, or any combination of parameters, can be selected for optimization. For each interaction of a distributed parameter, all values of the parameter are moved in the same direction at the same time. The amount that each value is moved can be selected as the same magnitude or as the same percentage of the initial value. A major assumption in this fitting procedure is that the initial estimates of the values of a given distributed parameter are correct with regard to their relative differences in space or time.

An option in the fitting procedure allows the user to adjust different subsets of a distributed parameter independently. A special case of this

option is that a distributed parameter may be adjusted independently on all HRUs.

Sensititivity analysis components allow the user to determine the extent to which uncertainty in the parameters results in uncertainty in the predicted runoff. When sensitivity analysis is coupled with optimization, the user also can assess the magnitude of parameter standard errors and parameter intercorrelations. Discussions of sensitivity analysis and its interpretation are presented by Mein and Brown (1978), and Beck and Arnold (1977).

IV. EXTENDED STREAMFLOW PREDICTION (ESP)

A modified version of the ESP program has been coupled to PRMS to provide forecasting capabilities. Given the simulated hydrologic conditions for a watershed at a specified point in time, the ESP procedure uses historic or synthesized meteorologic data to forecast future streamflow. When historic data are used, the procedure assumes that past meteorologic events are representative of future meteorologic events. Alternative assumptions about future meteorologic conditions can be made with the use of synthesized meteorologic data.

To implement the ESP procedure, the user defines a forecast period in PRMS, the meteorologic data set to be used, and the forecast variables of interest. The forecast period can vary from a few days to an entire water year. PRMS simulates to the start of the forecast period then stores all model variables that describe the state of the watershed system. A streamflow hydrograph for the forecast period is then simulated for each year in the meteorologic data base. PRMS is reinitialized at the start of each iteration of the forecast period using the previously stored variables. The simulation results obtained from this iterative procedure are termed the conditional simulation.

Streamflow variables of interest are extracted from each forecast hydrograph and stored in an ESP file. The variables that can be extracted are the maximum and minimum daily flow values, flow volume, and the date that the flow decreases to less than a selected threshold value. One variable, or any combination of variables, can be selected for a given model run.

The ESP program reads the ESP file, performs a frequency analysis on the variables, and produces a probabilistic forecast for each of the variable in the file. The Log-Pearson Type III probability distribution is currently (1989) supported, but other distributions can be added. Frequency analysis results for the conditional simulation are presented in tabular form and in a printer plot.

A frequency analysis also can be performed with ESP using the historic streamflow record or the simulation results obtained from running PRMS using the historic or synthesized meteorologic data without resetting the initial conditions each year. The results of this continuous simulation are termed the historic simulation when historic data are used. A comparison of frequency analysis results between the measured data and the historic simulation provides a measure of the adequacy of the PRMS calibration. Differences between the analyses reflect the effects of model and data errors on the historic simulation, and they also provide a measure of the bias in the conditional simulation results.

A continuous simulation using synthesized meteorologic data is termed the synthetic simulation. Differences between the analysis for the historic simulation and the synthetic simulation provide a measure of the effect of the assumed meteorologic changes in the synthesized record on streamflow.

The ESP component provides a valuable tool for a variety of hydrologic forecasting and analysis applications. These applications include short-term or seasonal forecasting for flooding and water supply, evaluation of the effects of land use changes on streamflow characteristics under a variety of meteorologic and watershed conditions, and the evaluation of the potential effects of climatic changes on streamflow under existing or future watershed conditions.

V. BASIN CHARACTERIZATION

Basin characterization is the discretization of a basin into HRUs based on topography, soils, vegetation, and other basin features for application in distributed parameter models. Some hydrologic parameters for these HRUs can be estimated from the basin features used in the characterization while others

require additional data. Historically, basin characterization was done manually and left to the interpretation of the model user. Manual characterization procedures are labor intensive and their subjective nature makes it difficult to develop standardized procedures that can be used by other modelers or that can be evaluated for the determination of an optimal technique.

To minimize the problems of manual characterization procedures, a set of programs have been developed to enable the application of automated characterization procedures (Jenson and Domingue, 1988). These programs compute basic topographic structure, drainage patterns, and subbasin areas using digital elevation data for a basin. Coupling these topographic delineations with overlays of geologic, soils, and vegetation data will incorporate additional physical measures to the characterization process and permit the estimation of selected hydrologic model parameters for the defined HRUs using these features.

Digital elevation data are processed into three utility data sets using a set of conditioning procedures. The first procedure conditions the data by filling depressions in the data set that would hinder flow routing in later procedures. Cells contained in the depressions are raised to the lowest elevation value on the rim of the depression. The second procedure builds a flow direction data set. The flow direction of each cell in the data is determined by examining the eight neighboring cells. The third procedure develops a flow accumulation data set in which each cell contains the value of the total number of cells that drain to it.

Basin characterization begins by selecting a point in the digital data set that represents the mouth of the basin. From this point, a program determines the complete basin boundary. The flow accumulation data set can then be used to construct the basin drainage network. Drainage network density is limited by the user specification of the minimum size of a subbasin area. Nodal intersections in the drainage net are then used by another program to assist in the definition of subbasin boundaries. The resulting characterization is a set of polygons that define HRU areas. The slope, aspect, and elevation of these HRUs can be computed, and the average or predominant soils and

vegetation of each HRU can be determined using map or satellite derived overlays.

These basin characterization tools can be interfaced with general purpose raster, vector spatial analysis, and relational data base management packages for use in the development and application of a variety of additional procedures. A number of geographic information systems (GIS) are being evaluated to provide this interface.

VI. REMOTE SENSING APPLICATIONS

One of the capabilities being developed using the basin characterization and GIS tools is the coupling of remotely sensed data to the modular modeling system. Initial development is being done to incorporate remotely sensed from data snow covered areas into snowmelt-runoff simulations. With a basin characterization stored in a GIS, remotely sensed measures of snow covered area and snowpack water equivalent can be registered over the basin. These measures can then be used to develop updated estimates of snow covered area and snowpack water equivalent on each HRU. Algorithms are currently (1989) being developed to incorporate point measures of snowpack water equivalent with remotely sensed snow covered area and snowpack water equivalent measurements from satellites and airborne gamma-ray spectrometry. Development and testing of these procedures are being conducted on several basins in the western United States.

VII. INTERACTIVE SYSTEM

The modular system as described above operates on mainframe, mini, and micro computers. ANNIE, PRMS, ESP, and the basin characterization components currently are stand-alone programs that run sequentially in a typical application. To provide more flexibility and to reduce the complexity of operation as more capabilities are added, an interactive version of the system is being developed. The interactive system uses a graphical user interface to display system options, data, basin characterizations, and model results and analyses. Expert system technologies will be used to assist users in system operations, model selection, parameter estimation, model calibration, and the

display, comparison, and analysis of model results. The interactive system is being developed for application on a 33-bit engineering workstation.

VIII. SYSTEM APPLICATIONS

The full modular system as discussed above is currently being tested in a variety of climatic and physiographic regions of the United States. Initial testing is being conducted predominantly in the western United States. Test basins include the Animas River in southwest Colorado, East Fork Carson River in east-central California, Weber River in north-central Utah, and Lower Willow Creek in west-central Montana.

Applications in other countries are also currently (1989) being developed. System application and testing is planned under annex 6 to the United States People's Republic of China Protocol for Scientific and Technical Cooperation in the Study of Surface Water Hydrology. Annex 6 deals with cold regions hydrology, snow, and ice. Proposed study areas in China include the Tien Shan, Chi Lian Shan, and upper Yellow River.

Studies also are being developed jointly with the Central Water Commission of India and the State Electricity Board, Himachel Pradesh, India. The system will be applied and tested on selected basins in the Himalayas.

Publications on system applications are forthcoming as selected stages of development and testing are completed. However, results of the applications of existing system components have been published. Reports on snowmelt runoff application of PRMS include Leavesley and Striffler (1979), Leavesley et al., (1981), Brendecke and Sweeten (1985), and WMO (1986). A summary of the application of PRMS to approximately 50 basins in selected regions of the United States to evaluate the hydrologic impacts of surface coal mining was presented by Stannard and Kuhn (1989). Application of selected storm-mode components, including sediment detachment and transport, to tephra deposits from the eruption of Mount St. Helens, Washington, were reported by Leasvesley et al., (1989). A review and application of the optimization and sensitivity analysis components was presented by Troutman (1985). Applications of ESP were reported by Twedt et al., (1977, 1978), and Day (1985).

IX. SUMMARY

A modular watershed modeling and data management system has been developed to provide a framework in which to develop and compare models and model process components, and to identify and apply the optimal approach to selected hydrologic problems. The modular system also provides a common framework in which to focus multidisciplinary research efforts on the solution of a variety of complex watershed modeling problems. In addition it is a framework in which maximum use of current and future advances in the fields of expert systems, geographic information systems, remote sensing, information management, and computer science can be readily applied. Much work remains to be done to determine which simulation approaches are best for various combinations of application problems and data constraints. However, as this work is completed the question of which model is best will be changed to a more appropriate question of which combination of process components is best.

REFERENCES

Beck, J.V. and Arnold, K.J., "Parameter Estimation in Engineering and Science," New York, John Wiley and Sons, Inc., 340-349, 1977.

Brendecke, C.M., and Sweeten, J.G., "A simulation model of Boulder's alpine water supply," in Proceedings of 53rd Annual Meeting of the Western Snow Conference, pp. 63-71, Boulder, Colorado, 1985.

Dawdy, D.R., Schaake, J.C., Jr., and Alley, W.M., "Distributed routing rainfall-runoff model," U.S. Geological Survey Water Resource Investment Report. 78-90, 1978.

Day, G.N., "Extended streamflow forecasting using NWSRFS," Journal of Water Resources Planning and Management, American Society of Civil Engineers, 111(2),157-170, 1985.

Dickinson, W.T., and Whiteley, H.Q., "Watershed areas contributing to runoff," IAHS Publ. no. 96, 1.12-1.28, 1970.

Draper, N.R., and Smith, H., "Applied Regression Analysis," New York, John Wiley and Sons, Inc., 1966.

Green, W.H., and Ampt, G.A., "Studies on soil physics, I--Flow of air and water through soils," Journal of Agricultural Research 4, 1-24, 1911.

Hamon, W.R., "Estimating potential evapotranspiration," Journal of Hydraulics Division, American Society of Civil Engineers, 87[HY3], 107-120, 1961

Hewlett, J.D., and Nuttaer, W.L., "The varying source area of streamflow from upland basins," in Proceedings of Symposium on Interdisciplinary Aspects of Watershed Management, pp. 65-83, Montana State University, Bozeman, Montana, 1970.

Hjelmfelt, A.T., Piest, R.P., and Saxton, K.E., "Mathematical modeling of erosion on upland areas," in Proceedings of Congress of the 16th International Association for Hydraulic Research, 2, pp. 40-47, Sao Paulo, Brazil, 1975

Hutchinson, N.E., compiler, "WATSTORE -- National water data storage and retrieval system of the U.S. Geological Survey -- User's guide," U.S. Geological Survey Open-File Report 75-426, 1975.

Jensen, M.E., Robb, D.C.N., and Franzoy, C.E., "Scheduling irrigation using climate-crop-soil data," in Proceedings of the American Society of Engineers National Conference on Water Resources Engineering, 20pp., New Orleans, Louisiana, 1969.

Jenson, S.K., and Domingue, J.O., "Software tools to extract topographic structure from digital elevation data for geographic information system analysis," Photogrammatic Engineering and Remote Sensing, 54(11), 1593-1600,1988.

Leavesley, G.H., Lusby, G.C., and Lichty, R.W., "Infiltration and erosion characteristics of selected tephra deposits from the 1980 eruption of Mount St. Helens, Washington," Hydrologic Science Journal, 34(3), 1989.

Leavesley, G. H. Lichty, R.W., Troutman, B.M., and Saindon, L.G. "A precipitation-runoff modeling system for evaluating the hydrologic impacts of energy-resource development," in Proceedings of 49th Annual Meeting of the Western Snow Conference, pp. 65-76, St. George, Utah, 1981.

Leavesley G.H., Lichty, R.W., Troutman, B.M., and Saindon, L.G., "Precipatation-runoff modeling system--User's manual," U.S. Geological Survey Water Resource Investment Report 83-4238, 1983.

Leavesley, G.H., and Striffler, W.D., "A mountain watershed simulation model, in Colbeck, S.C.," ed., Modeling of snow cover runoff. Hanover, New Hampshire, U.S. Army CRREL, 379-386,1979.

Leclerc, G., and Schaake, J.C., Jr., "Methodology for assessing the potential impact of urban development on urban runoff and the relative efficiency of runoff control alternatives," Massachusetts Institution of Technology Ralph M. Parsons laboratory Report 167,1973.

Mein, R.G. and Brown, B.M., "Sensitivity of optimized paramenters in watershed models," Water Resources Research 14(2), 299-303, 1978.

Obled, Ch. and Rosse, B., "Mathematical models of a melting snowpack at an index plot:" Journal of Hydrology 32, 139-163, 1977

Rosenbrock, H.H, "An automatic method of finding the greatest or least value of a function," Computer Journal, 3, 175-184, 1960.

Stannard, L.G., and Kuhn, G., "Watershed modeling, in Britton," L.J., Anderson, C.L., Goolsby, D.A., and Van Haveren, B. P., eds., Summary of the U.S. Geological Survey and U.S. Bureau of Land Management National Coal-Hydrology Program, 1974-84, U.S. Geological Survey Professional Paper, 1464, in press.

Swift, L.W., "Algorithm for solar radiation on mountain slopes," Water Resources Research 12 (1), 108-112, 1976.

Shafer, B.B., and Huddleston, J.M., "A centralized forecasting system for the western United States," in Proceedings of 54th Annual Meeting of the Western Snow Conference, pp. 61-70, Phoenix, Arizona, 1986.

Troutman, B.M, "Errors and parameter estimation in precipitation-runoff modeling," Water Resources Research 21 (8), 1214-1222, 1985.

Twedt, T.M., Burnash, R.J.C., and Ferral, R.L., "Extended streamflow prediction during the California drought," in Proceedings of 46th Annual Meeting of the Western Snow Conference, pp. 92-96,Otter Crest, Oregon, 1978.

Twedt, T.M., Schaake, J.C., Jr., and Peck, E.L., "National Weather Service extended streamflow prediction," in Proceedings of 45th Annual Meeting of the Western Snow Conference, pp. 52-57, Albuquerque, New Mexico, 1977.

U.S. Army, "Snow Hydrology," U.S. Army Corps. of Engineers, Portland, Oregon, USA, 1956.

U.S. Soil Conservation Service, "SCS National Engineering Handbook, Section 4--Hydrology," Washington, D.C., U.S. Government Printing Office, 1971.

Willen, D.W., Shumway, C.A., and Reid, J.E., "Simulationof daily snow water equivalent and melt," in Proceedings of 39th Annual Meeting of the Western Snow Conference, pp. 1-8, Billings, Montana, 1971.

WMO, "Intercomparison of conceptual models used in operational forecasting," WMO Operational Hydrol. Rep. no. 7, WMO Publ. no. 429, WMO, Geneva, 1975.

WMO, "Intercomparison of Models of Snowmelt Runoff," WMO Operational Hydrology Report no. 23, WMO Publication no. 646, WMO, Geneva, 1986.

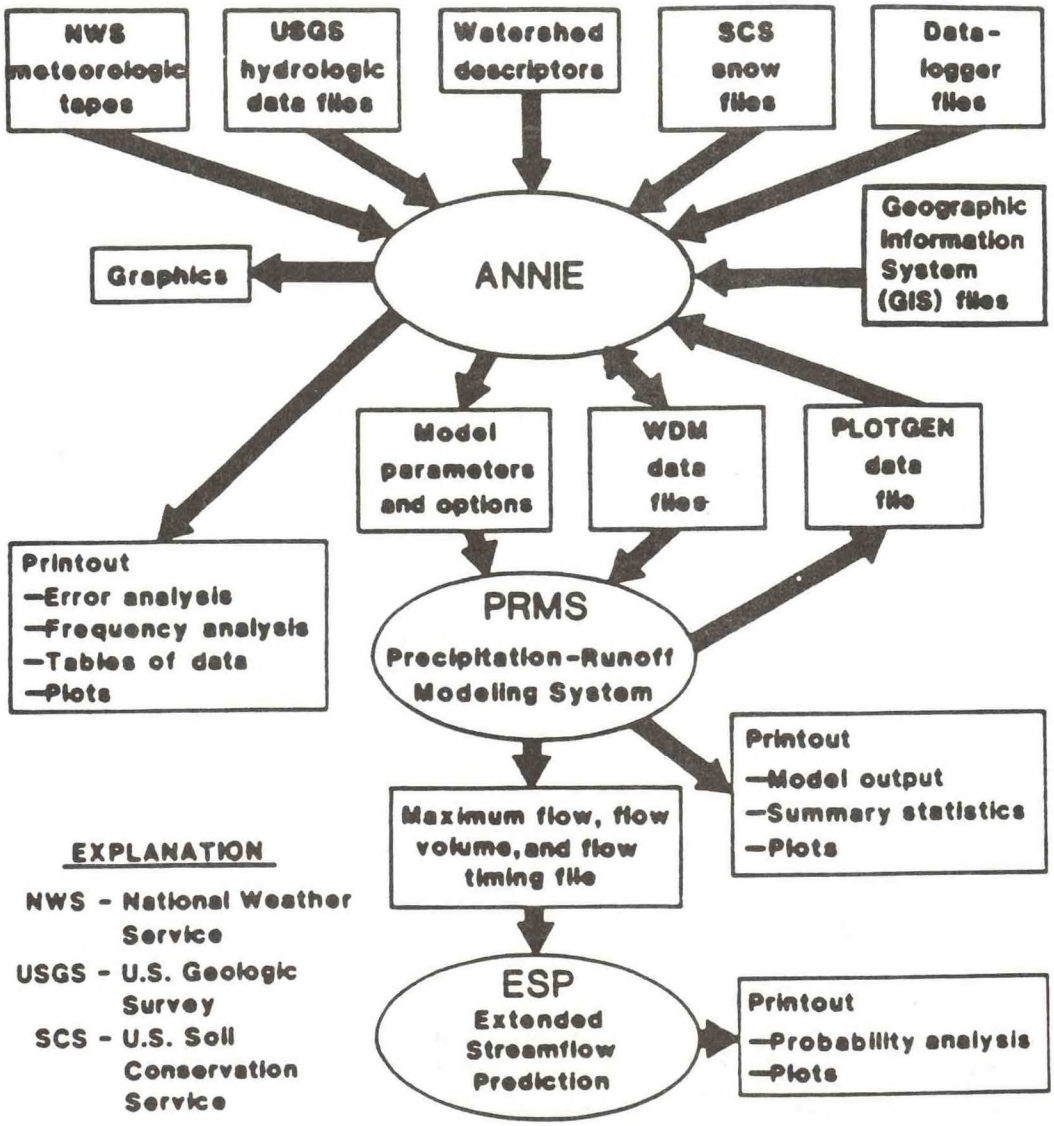

Figure 1. Schematic diagram of the data transfers in the modular watershed-modeling and data-management system.

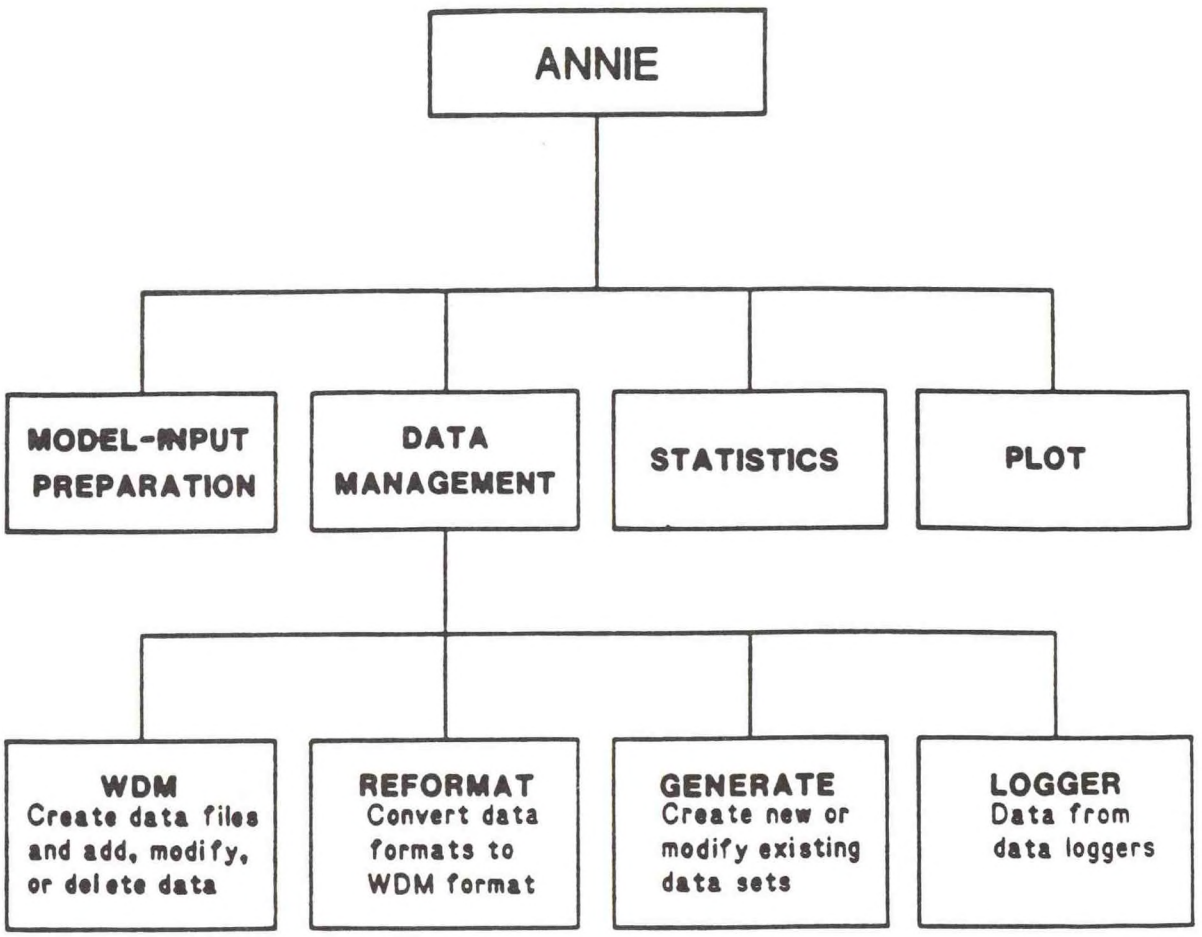

Figure 2. Schematic diagram of the major branches of the data-management and analysis program ANNIE.

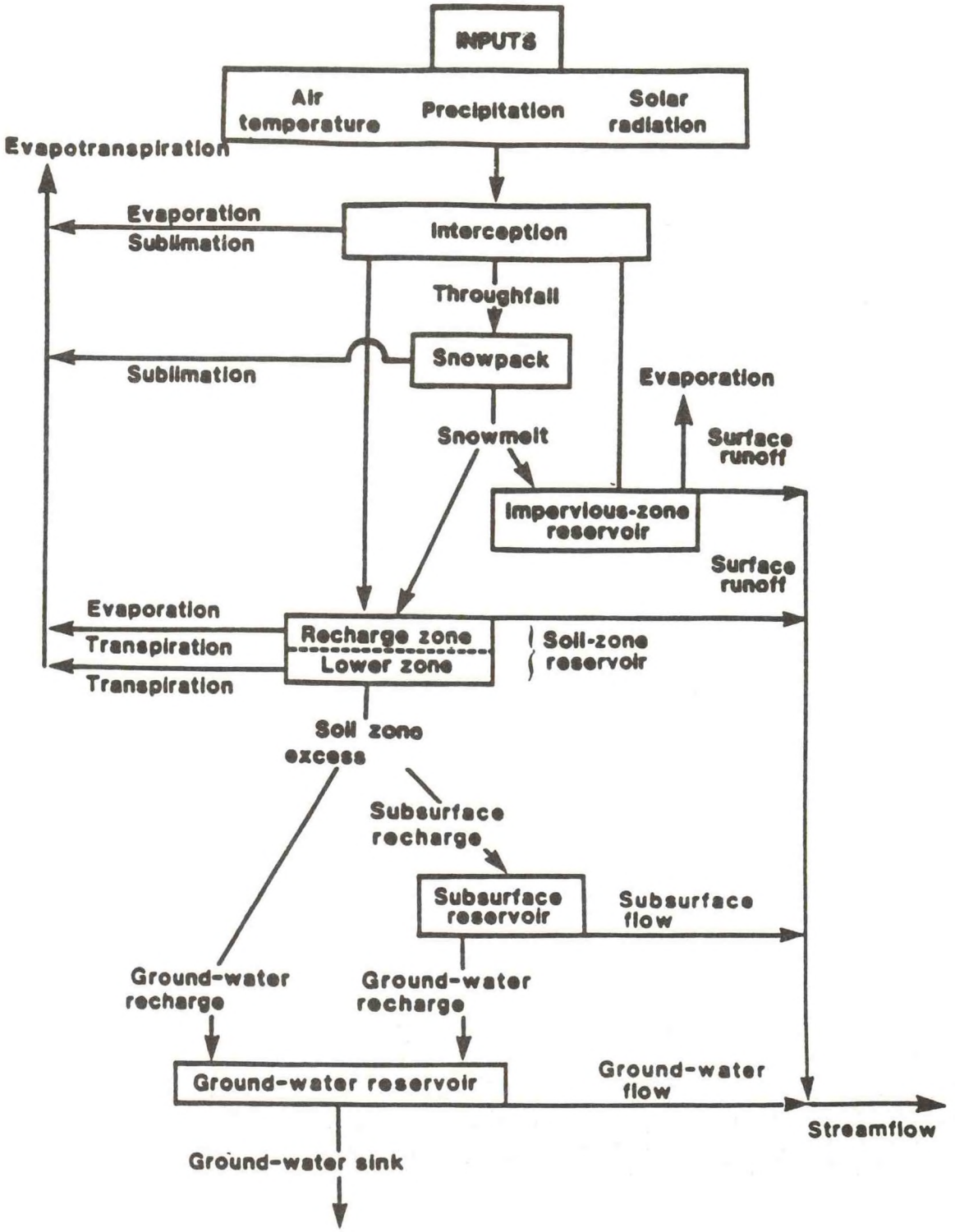

Figure 3. Schematic diagram of the conceptual watershed system and its inputs (modified from Leavesley et al., 1983).

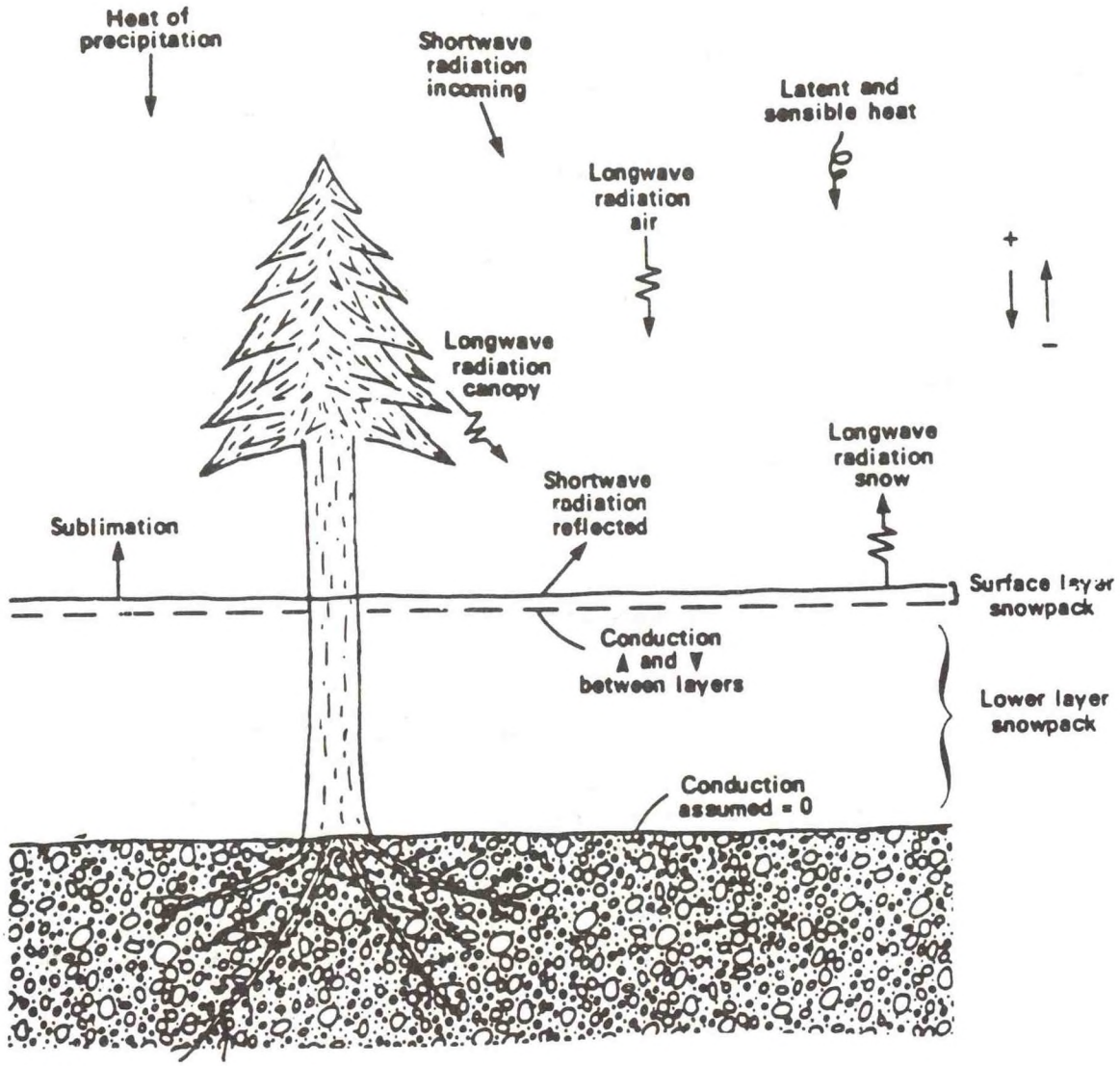

Figure 4. Components of the snowpack energy balance.

THE U.S. GEOLOGICAL SURVEY'S USE OF SATELLITE TECHNOLOGY FOR THE COLLECTION OF HYDROLOGIC DATA

William G. Shope, Jr.
U.S. Geological Survey
Reston, Virginia 22092, USA

ABSTRACT. The Geological Survey's Use of Satellite Technology for the Collection of Hydrologic Data Shope, W.G. (U.S. Geological Survey, 460 National Center, Reston, Virginia 22092; 7703-648-5364).

The U.S. Geological Survey maintains the basic hydrologic data-collection system for the United States. The Survey is upgrading the collection system with electronic communications technologies that acquire, telemeter, process, and disseminate hydrologic data in near real-time. These technologies include satellite communications, via the Geostationary Operational Environmental Satellite, data collection platforms in operation at over 2,500 Survey gaging stations, direct-readout ground stations at six Survey District Offices, and a network of powerful minicomputers that allows data to be processed and disseminated quickly. The Survey is moving rapidly toward making the satellite telemetry system an integral part of the national hydrologic data-collection network. Data telemetry provides valuable information to the water-user community on a timely basis, improves the operation of the data-collection network, and enhances the quality of the hydrologic data. Further enhancement of the data-collection system by the operational use of the telemetry throughout the network will be based on the needs of the water-data users and cost effectiveness.

I. INTRODUCTION

The U.S. Geological Survey (USGS) operates the basic hydrologic data-collection program that provides an information base to a wide variety of

water-resources planning and management activities in the United States. The data-collection program and information base are in transition to more automated technologies that will speed the flow and analysis of data from thousands of remote data-collection stations to user facilities. This transition includes upgrades to data-collection and recording equipment at hydrologic stations, telemetry systems for automated data retrieval, and networks of computers to analyze and distribute the data to users across the Nation. National economic growth has been accompanied by an increase in the number of hydrologic data users who operate hydropower generating plants and irrigation systems and who manage flood-damage prevention and navigational waterways. Growth also has generated interest from groups, such as environmentalists, who seek to prevent environmental degradation. These requirements for hydrologic information have been translated into a need for more hydrologic data on a more timely basis, which requires that data be collected and delivered to users through automated telemetry and computerized data processing and distribution systems. This paper describes the USGS' use of satellite telemetry for the collection and processing of hydrologic data.

II. GEOLOGICAL SURVEY HYDROLOGIC STATION NETWORKS

The USGS collects hydrologic data from about 12,600 water stage and discharge stations; 34,100 wells where water level and (or) pumpage data are collected annually or more frequently; and 3,200 surface-water stations; and 8,100 wells where water-quality data are collected. Data from the majority of these stations are collected through on-site visits by USGS personnel or observers who collect water samples and/or make hydrologic measurements. Where continuous data records are needed, data are collected by use of automated recorders supplemented by manual measurements that are used for calibration and correction. The USGS computes continuous discharge from stage (water-level) data records collected at 7,100 stream sites. Water-level data records also are collected at 700 lakes and reservoirs throughout the Nation. Continuous water-level records are also collected for about 2,400 wells and 600 stations (primarily surface-water) where water-quality data are obtained. For more information on the Water-Data Program of the Survey, the reader is directed to Gilbert and Buchanan, (1982).

III. TELEMETRY OF HYDROLOGIC DATA

The procedures for acquiring data from the hydrologic data-collection sites and manually entering the data into a computer are intensive and time consuming. These two factors are obstacles to providing more and timely data. The USGS is addressing the obstacles through the use of new automation and data telemetry technologies. The methods for automating the collection of data for continuous record stations have evolved over the past 40 years from spring or weight-driven mechanical devices to electronic instruments that use new communication and computer technologies.

The telemetry of data from remote data-collection sites is being accomplished by a variety of different methods. The major components of a telemetry system are: the sensors that measure or detect changes such as a rising or falling stream stage; encoders that convert the sensor output to forms suitable for transmission; a transmission system that provides the link from a remotely operated sensor to another location; and a data reception and distribution facility that receives, sorts, decodes, checks, and distributes the data system. The transmission media is the important component, and characterizes the communications system. Conventional telemetry methods applied over the past 35 years include land lines (telephone), high-frequency, and ultra high-frequency (microwave line-of-sight) radios. Extraterrestrial methods applied within the past 17 years include meteorburst and satellite data-collection systems. The reader is referred to Halliday (1979), for a more complete review of telemetry systems.

The selection of a telemetry system requires careful consideration of many factors such as cost, reliability, responsiveness, coverage, growth, and flexibility. The choice of a telemetry system for an area of limited size and uniform greographic characteristics could result in any one of the conventional or extraterrestrial systems. The telemetry system selected by the USGS must support a national hydrologic information system that meets the needs of a variety of water users and collects data over a wide range of geographic conditions.

The evaluations conducted by the USGS and many other Federal agencies have shown that satellite telemetry, when compared with other telemetry systems, is

generally cost-effective, reliable, easy to install and operate, able to cover vast areas, and extremely flexible in carrying a wide variety of data transmissions that can be scheduled to meet user needs. For reasons of compatibility with other Federal agencies, economics, flexibility, and large area coverage, the Survey has chosen to use the Geostationary Operational Environmental Satellite (GOES) Data Collection System (DCS) operated by the National Earth Satellite, Data, and Information Service (NESDIS). The GOES-DCS is provided at no cost to the Survey and other Federal, State, and local government agencies under a Memorandum of Agreement with NESDIS, which is a component of the National Oceanic and Atmospheric Administration (NOAA). This agreement specifies NESDIS as the operator of the satellites, primary ground receiving station, and a data-distribution center. The reader is referred to NOAA (1979) for detailed information on the GOES DCS.

IV. GOES DATA COLLECTION SYSTEM

The GOES DCS uses Earth-orbiting satellites to relay transmissions from networks of data-collection sites to one or more receiving stations. A satellite data collection system is made up of five major elements that include: (1) data sensors linked to (2) small radios called data-collection platforms (DCPs) that transmit data to (3) satellites which immediately relay the data to (4) Earth receiving stations that forward the data to (5) data handling and distribution facilities.

The commercially available GOES DCPs can satisfy most needs for collecting and reporting hydrologic data. These DCPs collect and temporarily store data from sensors at user-defined rates and transmit these data to the GOES satellite. Data collection from the sensors occurs at 15-, 30-, or 60-minute intervals and the DCP transmissions are normally scheduled by the users at 4-hour intervals. These self-timed transmissions consist of messages that contain, at a minimum, all data collected from the sensors since the last transmission. In some cases, the messages are extended to include data from one or more previous transmissions, thus providing redundancy in data transmission. Most of these DCPs also contain an alert feature that triggers unscheduled data transmissions within several minutes of the detection of a

data value that has exceeded a user-defined threshold or differential when compared with the previous sensor value. An example of this is a rapid change of stage or rate of precipitation during a critical hydrologic event. Alert messages normally contain the most recent set of values collected. DCPs developed in the mid 1980's, with costs below $3,000, have significantly increased capabilities. These DCPs provide an on-site data conversion and calibration and can perform statistical summaries and other analytical tasks.

Messages transmitted from the DCPs are received by GOES and are immediately retransmitted to Earth. Data are received from GOES by the NESDIS primary satellite ground receiving station at Wallops, Virginia, as well as user-owned and operated stations referred to as a Direct-Readout Ground Stations (DRGS'). The Wallops station is used by NESDIS as the centralized facility for all data reception and for monitoring, command, and control of the GOES spacecrafts.

Several users of the GOES system have turned to local passive (receive only) DRGS' in an effort to reduce system complexity, increase timeliness of the data, and reduce dependence on land lines. These DRGS', which cost $40,000-$80,000, provide a user with immediate access to the data relayed from GOES. A DRGS is comprised of: an antenna, radio receiver, decoding equipment, and a minicomputer that functions as a system controller. This controller is powerful enough to: manage the operation of the radio receiver, decode the DCP messages, flag and disseminate alert messages, store the decoded data in a temporary file, monitor the performance of the DCP transmissions, provide access for multiple users, and forward data to other computers collocated at the users' offices.

During the early 1980's, the USGS began to process and install satellite DRGS' at several offices. These DRGS' automatically acquire data from satellite transmissions and forward the data to user-defined destinations. Because these DRGS' do not transmit to the satellite, monitor its health, command it and its sensors, or copy imagery, they can be dedicated to serve the single requirement of collection of real-time telemetered environmental data. Because the DRGS' can be collocated with the user or data collection network field manager, responsiveness to user needs has been improved, control

of data-collection operations has been given to the field manager, and system flexibility has increased considerably. As a result of these and other factors, the use of DRGS' have become increasingly beneficial to users of the GOES telemetry system. The USGS is currently operating DRGS' at Harrisburg, Pennsylvania; Columbia, South Carolina; Denver, Colorado; Phoenix, Arizona; Fort Worth, Texas; and Tacoma, Washington. For additional information on the development of a distributive system for satellite telemetry see Shope and Paulson (1983).

The five major components of the USGS' satellite telemetry system are shown in fig. 1. Surface water-level data are collected at a continuous-record station and relayed, via the GOES satellite, to a user-operated DRGS. Data are continuously acquired from the DRGS by one of the Survey's primary computers located near the DRGS, entered onto the Survey's telecommunications network, and delivered to the offices that operate the data-collection stations. If the data are from stations operated by the office that also operates the DRGS, the data are processed locally with summaries forwarded (by all offices) to Reston, Virginia, to update the Survey's National Water Data Storage and Retrieval System and the National Water Data Index (NAWDEX). See Edwards (1980), for more information on NAWDEX.

V. COOPERATIVE ACTIVITIES BY THE U.S. GEOLOGICAL SURVEY AND OTHER AGENCIES IN THE USE OF SATELLITE TELEMETRY

Many of the cooperative data-collection programs that the USGS conducts with 900 Federal, State, and local government agencies, support the operation of automated hydrologic data-collection stream-gaging stations. The USGS normally constructs the stations, installs and operates the sensors and recorders, makes periodic measurements to determine the relationship between the streams' discharges and water levels, retrieves and processes the stage data to compute instantaneous and mean discharges, and publishes the daily mean-discharge values. The USGS has been marginally involved in telemetry operations that involve line-of-sight radio networks and land line telephone systems through data monitoring and providing space for the telephone or radios in the gage houses. The data collected by the traditional telemetry

systems are useful in monitoring conditions upstream and downstream of reservoir projects, but lack the content that the USGS requires for computing continuous records. For this reason, prior to the mid 1970's, the USGS did not actively participate in operating remote telemetry systems. The value of real-time data collection to the USGS has changed with the advent of the use of satellites to relay data from remote sites. Satellite relay not only provides the water-data user with the timely data, but also provides the USGS with an opportunity to automate its data-collection activities and to remotely monitor condition of on-site instrumentation.

VI. SUMMARY

The number of USGS data-collection stations supported by satellite telemetry has grown significantly over the past 10 years. At the end of 1978, the number of stations that used satellite telemetry was 120, and by the end of 1988, it was up to 2,500. Most of these stations are meeting the remote telemetry needs of cooperating Federal, State, and local agencies. About 30 percent of the USGS' automated hydrologic data-collection stations are reporting through GOES. The USGS is involved in the installation and operation of more than 75 percent of the telemetry located in Survey data-collection stations, with the majority of the telemetry equipment owned by the primary water-data user, such as the Corps of Engineers, the Bureau of Reclamation, or the National Weather Service.

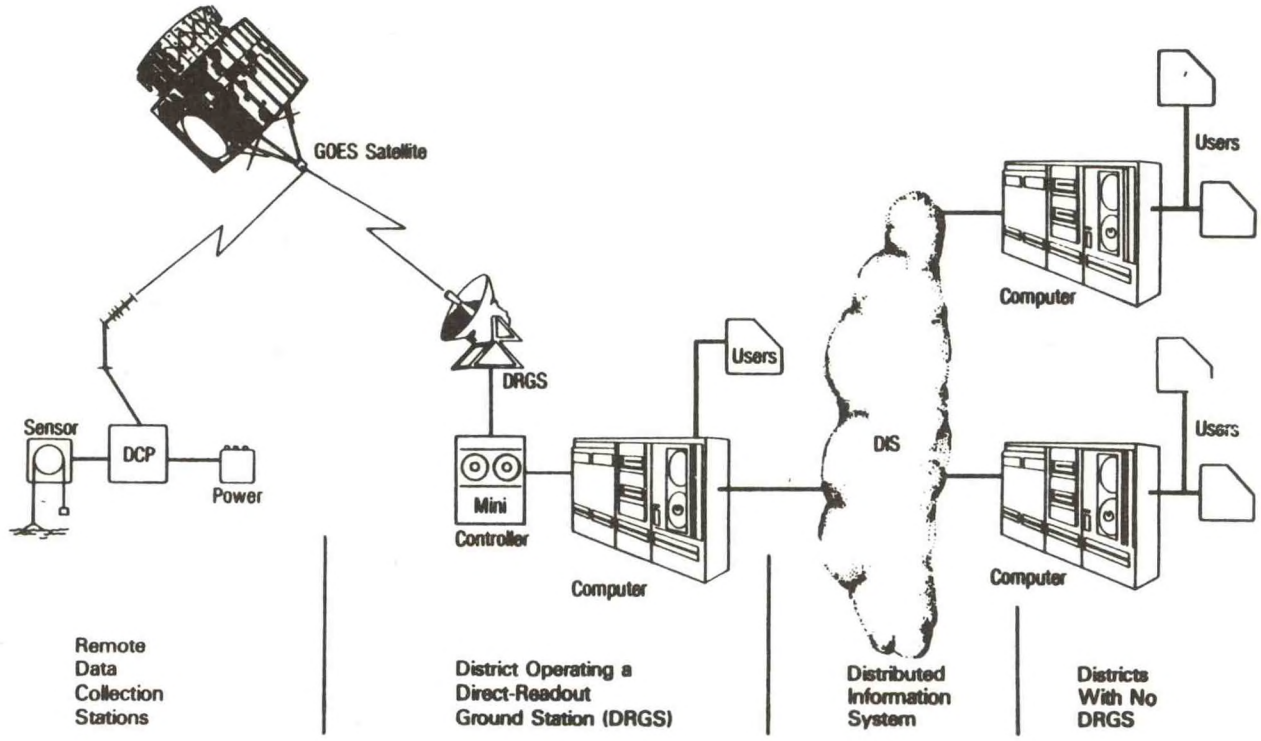

Figure 1. Hydrologic Data Collection by Use of Satellite Telemetry and a Distributed Information System.

APPENDIX - REFERENCES

Edwards, M. "NAWDEX: A Key to Finding Water Data," U.S. Geological Survey Pamphlet, Reston, Virginia, 15 pp., 1980.

Gilbert, B., and Buchanan, T., "Water Data Program of the U.S. Geological Survey," U.S. Geological Survey Circular 863, Reston, VA., 1982.

Halliday, R., "The Use of Satellites in Hydrometry," Hydrometry: Principles and Practices, R.W. Herschy, ed., John Wiley and Sons, Inc., New York, N.Y., pp. 427-447, 1979.

National Oceanic & Atmospheric Administration, "Geostationary Operational Environmental Satellite/Data Collection System," National Oceanic and Atmospheric Administration Technical Report NESS 78, Washington, D.C., 80 pp., 1979.

Shope, W., Jr., and Paulson, R., "Development of a Distributive System for Handling Real-Time Hydrologic Data Collected by the U.S. Geological Survey," presented at 1983 Hydrological Applications of Remote Sensing and Remote Transmission, Proceedings: Hamburg Symp., International Association of Hydrological Sciences Public, No. 145., 1983.

APPLICATION OF THE AUTOMATED FLOOD FORECASTING SYSTEM WITH PDP OR VAX SERIES COMPUTER

Xu Guanwu
Hydrological Forecasting and Water Control Centre
Ministry of Water Resources

ABSTRACT. The structure and function, as well as problems to be aware of in the application of the Automatic Flood Forecasting System (AFFS) is presented in this paper. The system has been applied to a number of river basins in China, such as the Yellow, Hanjiang, and Haihe River basins. The results show that it is not only suitable for the various types of basins, but also has the following advantages: simplicity and ease of use, saving time and manpower, use of advanced data processing, the speed of forecast computations, and the results of forecasting models used in the system has attained the timeliness and accuracy demanded by a practical real-time forecasting system.

The system introduced the software for processing historical hydrological data and the approach of Constrained Linear System (CLS) models, by E. Todini, A. Gabos, and M. Dichira of Italy (not referenced). Wang Juemou and Zhang Ruifang (1987) further worked on the model and proposed the use of the Synthesized Constrained Linear System (SCLS) model in China. Guan Huaimin (not referenced) took part in the work of model calibration.

I. SYSTEM STRUCTURE

The computer system used in processing real-time hydrological information and flood forecasting is a Programed Data Processor (PDP) or Virtual Address Extension (VAX) series computer by Digital Equipment Corporation (DEC)

consists of two relatively independent but related systems. They are: (1) Processor of Real-time Hydrological Information System (PRHIS), and (2) the Automated Flood Forecasting System (AFFS).

The PRHIS consists of three subsystems which are receiver, processor, and retrievor of information (fig. 1). The coded hydrological telegrams are transmitted by a post office computer and are received by the real-time receiver program of PDP or VAX computer at the hydrological information and forecasting offices in our country. The telegram decoder program converts the codes into the common hydrological elements such as rainfall, water level, discharge, storage volume of reservoir, etc. It then stores them in a real-time data base which consists of indexed files of rainfall, river stage, reservoir stages, releases and volumes, files of hydrological characteristic values, and direct access files of precipitation. Three packages: the English data retriever, Chinese data retriever, and the plotter package, are used to retrieve and display real-time hydrological information. Display output includes: tables of hydrological information, rainfall distribution charts, and hydrographs drawn on printer-plotters. Basin maps with rainfall distribution, warning messages of flood level and discharge, and hydrographs are available on color terminals and other output devices. In addition, the system supplies the processed real-time hydrological data to the AFFS.

The AFFS consists of four subsystems (fig. 2). The function of the historical and real-time hydrological data processor subsystem is to maintain a direct access file of rainfall and discharge data by entering the historical data from terminals manually and automatically retrieving and processing the real-time data from the PRHIS. These data are shared commonly among the packages of various forecasting models and forecasting schemes of the AFFS. Model calibration and real-time forecasting subsystems consist of several packages of forecasting models such as SCLS model; Optimized Sacramento (NSAC) model; Improved Tank (NTAK) model, and a corresponding file system required by the model. Each package includes calibration, parameter assembling, and real-time forecasting programs. SCLS includes five improved models which are formed by combining the CLS model with the Xinanjiang model and runoff from rainfall excess over infiltration model. In addition to the CLS model, NSAC

is a revised model by combining the CLS model with the Sacramento model. NTAK is also an improved model with common blocks of error statistic and data processing based on the original Tank model. The subsystem packages can perform the whole range of process from the model calibration to on-line flood forecasting.

In order to consider the effect of no uniform precipitation distribution and the difference in basin characteristics, the AFFS takes a disparity in the construction of the hydrological system. A large forecast basin will be subdivided into several smaller subbasins according to the general distribution pattern of rainfall, location of hydrological control stations, and specific subbasin characteristics during model calibration. Each subbasin can have any number of upstream inflow hydrographs and rainfall intervals. When calibrating a subbasin, in order to avoid the difficulties such as overelaborate procedures and the arbitrariness of separating the base flow out of flood events used in the traditional calibration method of a forecasting scheme, an approach of continuous computation of runoff and flow concentration of separated water sources at each calibrating time period and carrying the process through a rainfall event and the upstream inflow hydrograph/calibration is taken. This calibration is accomplished by meeting the minimum criteria of the sum of square of error between the observed and the computed discharge at the outlet of the subbasin for the calibration time period. The unit hydrographs or outflow and infiltration coefficients at the outlet of a subbasin for the input conditions of calibration can be obtained by optimization. The calibrated results of subbasins of a forecasting station produce a group of related parameter files, from which a parameter assembling program separates the fixed parameters and the variable parameters reflecting soil moisture conditions. The resulting files of fixed parameters and variable data are separated in the form of records with the assigned record number. The files are used in the real-time forecasting subsystem and are shared by the different control sections of the forecasting basin for the real-time forecast by the forecast model chosen.

II. SYSTEM PERFORMANCE

The model calibration programs complete the calibration of a subbasin with 6 years of records in 3-10 minutes by using the established input file. The calibration results of high accuracy as reflected by the confidence coefficient can be obtained by debugging all variable parameters of the input file one by one (debugging the parameters with high sensitivity in the model first used). However, after finishing each calculation for the computed results in the output file, verification analysis should be carried out, in order to determine the degree of agreement between observed and computed hydrograph of each flood event (particularly, what resulted from the rainfalls in subbasins), and the rationality of water volume distribution of three water sources and the working of unit hydrographs or outflow coefficients of tanks for the rainfall event. It is required that the result of a selected calibration scheme of each subbasin not only has a high confidence coefficient, but also agrees with the conditions of natural geography and the climate of the calibrated basin. After the completion of assembling parameter files of the forecasting basin, the reliability of applying the extension of calibrated parameters should be verified. The simulation test should be carried out by using the historical hydrological data of several years that are not used in the calibration. Only the verified forecasting scheme can be used.

When the real-time forecasting is being carried out, the subsystem of processing real-time hydrological data (fig. 3) is used every time. For a medium size basine with about 50 rainfall stations and 10 hydrological stations, the retrieving, interpolating and process of real-time hydrological data of several periods each day can be completed in 5 - 10 minutes.

Except CLS submodule of SCLS model among the various forecasting models of AFFS, there are 5 - 6 antecedent status variables of soil moisture, content. For SCLS Model, they are the outflow of ground water, storage volume of free water, drainage area, and storage volumes of upper, lower, and deep layers. For NSAC Model, they are tension storage volumes of upper and lower layers, storage volume of free water of upper layer, storage volumes of free water of fast draining and slow draining in lower layer, storage volume of temporary

impervious portion. For NTAK Model, they are storage volumes of four tanks and second soil moisture parameter. The above status variables approach the asymtolic values (approaches zero during a dry season and a large value during a wet season as in the case of antecedent precipitation index of simple API Model) and are difficult to chose their initial values. In order to obtain a better result of real-time forecasting, setting the initial condition as that of calibration should be taken when the initial forecast is carried out for the flood season every year. That is to say that the assembling of file of variable data of forecasting basin must be reassembled anew by running the parameter assembling program in order to set the status variables of soil moisture content to the values of calibration optimization, and begins the calculation of initial forecast each year.

By using the aforementioned file system, the data processor of the subsystem of processor of real-time hydrological data automatically retrieves and processes the real-time data of rainfall and discharge. It also retrieves the calibrated parameters and updates the variable data of all subbasins up-stream of the forecasting station in the assembled files, automatically. Then the rainfall runoff calculation and the flood routing calculation for any control section of the forecasting basin can be carried out from the upstream to the downstream, orderly, simply, and promptly.

Generally updating forecasts for each period, one by one, only needs a few minutes, but in the real-time forecasting program, several functional "switches" must be correctly selected in order to develop the system function sufficiently. This guarantees data renewal of assembling variable data file to be accurate and satisfactory forecasting results can be obtained.

A. Official Forecasting Switch

When daily rainfall is used to interpolate period rainfall and new discharge information of the control stations is used in current forecasts, the official forecasting "switch" is selected. Then the ending time of current forecasting calculation, corresponding calculated values of soil moisture, and real-time hydrological data of several periods before will be entered in the assembling variable data file as initial values of forecasting for the next time.

However, when forecasting is carried out by using incomplete data, a temporary forecast "switch" is selected, and the calculation results are not entered in the above assembling variable data file. Therefore, when the next forecast is carried out, the calculation results of the last official forecast are used for the initial values.

B. Updating Forecasting "Switch"

Usually, the updating forecasting "switch" is selected in order to increase the forecasting accuracy by carrying out an updating forecast for each period, one by one, using the new observed discharge messages just received for the forecasting section (when having autoregression input) and the upstream sections. Only when without the new observed discharge messages of upstream section used in forecast updates, then by starting nonupdating forecasting "switch," the forecasting is carried out for downstream sections based on the computed discharge hydrograph obtained by using rainfall data of upstream subbasins.

C. Restarted Running "Switch"

For the first forecast of each year, the initial operation mode is taken. For each forecast after this first forecast of the year, by starting run restart "switch," the forecast calculation is carried out based on the last calculated results stored in the assembled variable data file to shorten the forecasting calculation time.

D. Forecasting Rainfall "Switch"

During the urgency of flood control, by starting forecasting rainfall "switch," quantitative rainfall forecast values of several future periods for subbasins upstream of the forecast station are entered from terminal one by one, in order to extend forecast periods, and predict future possible flood processes by combining the hydrological and meteorological forecast for reference in making decisions for flood control and project management. Conversely, the regular forecast is carried out under the assumption of no future precipitation.

E. Forecasting Discharge "Switch"

By starting this "switch," the forecasted future discharge values of several periods at the inflow control stations or upstream reservoirs are entered from a terminal and used in the forecast calculations. Conversely, the value of the last observed discharge of the inflow control stations at upstream reservoirs will be used for the forecasting periods automatically.

F. Reservoir Operation "Switch"

By starting this "switch", the outflow hydrograph and corresponding water level of reservoir can be estimated from the computed inflow hydrograph according to the monthly optimum operational curves (when operating under the flood level control situation) and flood control rules (when operating in flood volume control). Conversely, outflow hydrograph of a reservoir for forecasting is given.

III. EXAMPLES OF APPLICATION

The 22 subbasins of different types used in the study are located on the reach downstream of the Sanmenxia Reservoir of the Yellow River with the hydrological control stations at Huayuankou near Zhengzhou, Henan Province, and on the reach of Guanting Gorge of the Yongding River near Beijing in the semiarid region, and upstream of the Hanjing River with a hydrological control station at Baihe, in the humid region (fig. 4). The results of calibration by using calibration programs of SCLS, NSAC, and NTAK are shown in table 1. The calibration accuracy of each model of AFFS is relatively high as shown in table 1. For the subbasins of single input of rainfall, the values of determination coefficient (DC) are about 0.9, and above 0.9 for the subbasins with multiple inputs of rainfall and discharge or single discharge input.

For the verification of model parameters calibration of Baihe station, Hanjing River, simulated tests for SCLS and NSAC were carried out by using the hydrological data of 1980 which was not used in the calibration. As seen by fig. 5, the hydrograph of computed and observed discharge are basically identical. Looking at the determination coefficient of whole flood season, for SCLS mode, the value of DC is 0.97, and nearly 0.99 for NSAC model. As

shown in table 2, the average absolute errors of three flood events of the above two models are 4-5 percent for peak discharge, and 3-4 percent for flood volume. The maximum error of peak discharge is 12 percent, and 8 percent for flood volume, which are all within the permitted range.

The reach downstream of the Sanmenxia Reservoir of the Yellow River (fig. 4) is a sandy one, frequently changing the river channel due to erosion and deposition, therefore it is difficult to make flood forecasts accurately. Four flood events occurred at the Sanmenxia reach in August 1988. The flood volumes coming from up Sanmenxia Reservoir are about 85 percent, 75 percent, and 70 percent, and about 15 percent, 25 percent, and 30 percent from Sanmenxia to Huayuankou interval for first, second and fourth, and third events separately. The most frequent flood events last for 15 days, and the flood flows contain a lot of silt, which cause obvious river-bed variation and inundate part of the flood plain.

During the above four flood events that occurred in August, 1988, real-time forecasts had been carried out by using the real-time forecasting programs of SCLS, NSAC, and NTAK for a total of 63 station-times. As seen by table 3, the average absolute errors of both peak discharge and volume are 2-4 percent. The maximum error of peak discharge is 10 percent, and 11 percent for flood volume, which are all within the permitted range. The comparison of computed discharge with the observed discharge at Huayuankou is shown in fig. 6. As shown in fig. 6, the degree of agreement between the observed discharge and the computed discharge of various models is very good.

The aforementioned results are the forecasting processes with a predicting period of 24-48 hours. The synthetic forecasting can be made by synthesizing forecasting results of various models, considering the trend of rise and fall of observed flood processes have been occurring at the forecasting sections upstream and revising the forecast with a reference to the past experiences. In fact, due to the advanced data processing and the high speed forecast calculation, the process of real-time data processing and forecasting calculation for each forecast can be finished within 10 minutes. By updating the forecast each period, one by one, higher accuracy in forecasts may be achieved than the results shown in table 3.

In summary, the following conclusions can be made:

(1) The forecast accuracy of forecast models of AFFS has achieved the level of a practical forecast scheme. The program packages and the file systems of AFFS can be applied to various basins with different conditions of natural geography and climate, and have the advantages of being a simple and easy use, efficient use of computing time and manpower, use of advanced data techniques, and high speed calculation.

(2) The subsystem of processing real-time hydrological data of AFFS can be shared. When the various forecast models and practical forecast schemes are used in a system, there is no increase in the amount of data processing and the forecast results of different models can be compared, checked, and then can replenish each other. The forecast value and the extendable forecast range given synthetically is an asset for the decision making in flood control and water resources.

(3) For other forecast models not included in the AFFS at present, the new common packages of forecast models can be created by developing specific blocks of runoff computation and flow concentration and assembling common blocks of optimization, error statistics and data processing of AFFS. The present forecasting schemes for various basins can be further improved by using advanced data processing and the construction of direct access file systems for the parameters used in AFFS.

(4) The main factor affecting forecasting accuracy is quantity and quality of real-time hydrological information rather than the differences between the various forecast models or the practical forecast schemes. By using the real-time hydrological information provided by the modern technology of telemeter and communications such as radar, microwave and satellite, and an AFFS to carry out the on-line flood forecasting, the forecast accuracy and speed of AFFS can further be improved that more potential social and economic benefit can be obtained from the accurate forecasts.

(5) The block of optimization of model calibration subsystem of AFFS is only used to optimize the unit hydrographs at present, while the model parameters of input file must be debugged repeatedly through a trial and error method. There are the groups of parameters restricted and related to each other which satisfy the given constrained conditions. To find an optimum calculation method of model parameters satisfied several constrained conditions will be researched and solved in the future so that the calibration results agreeable to the natural geography and climate conditions of forecasting basin can be obtained more easily.

REFERENCES

Renjun, Zhao, "Watershed Hydrological Modeling," Press of Water resources and Electric Power, Beijing, China, 1984.

Todini, E., and Walls, J.R., "Using CLS for Daily or Longer Period Rainfall-Runoff Modeling," Publication 13, Institute of Hydraulics, University of Pavia, 1974.

Natale, N., and Todini, E., "A Constrained Parameter Estimation Technique for Linear Models in Hydrology," Publication 13, Institute of Hydraulics, University of Pavia, 1974.

Burnash, R.J.C., "A Generalized Streamflow Simulation System Conceptual Modeling for Digital Computers," 1973.

Sugawara, M., "TANK Model and its Application to Bird Creek, Wollombi Brook, Bikin River, Kitsu Rivers, Sanaga River and Nam Mune," 1974.

Wang, Juemou, Ruifang, Zhang, and Guanwu, Xu, "Synthesized Constrained Linear System (SCLS)," Journal of Hydraulic Engineering, No. 7, 1987, Beijing, China.

Guanwu, Xu, and Zhaohui, Chen, "The System of Real-time Hydrological Information Processing and Flood Forecasting with PDP or VAX Series Computer," Hydrology, No. 4, 1988, Beijing, China.

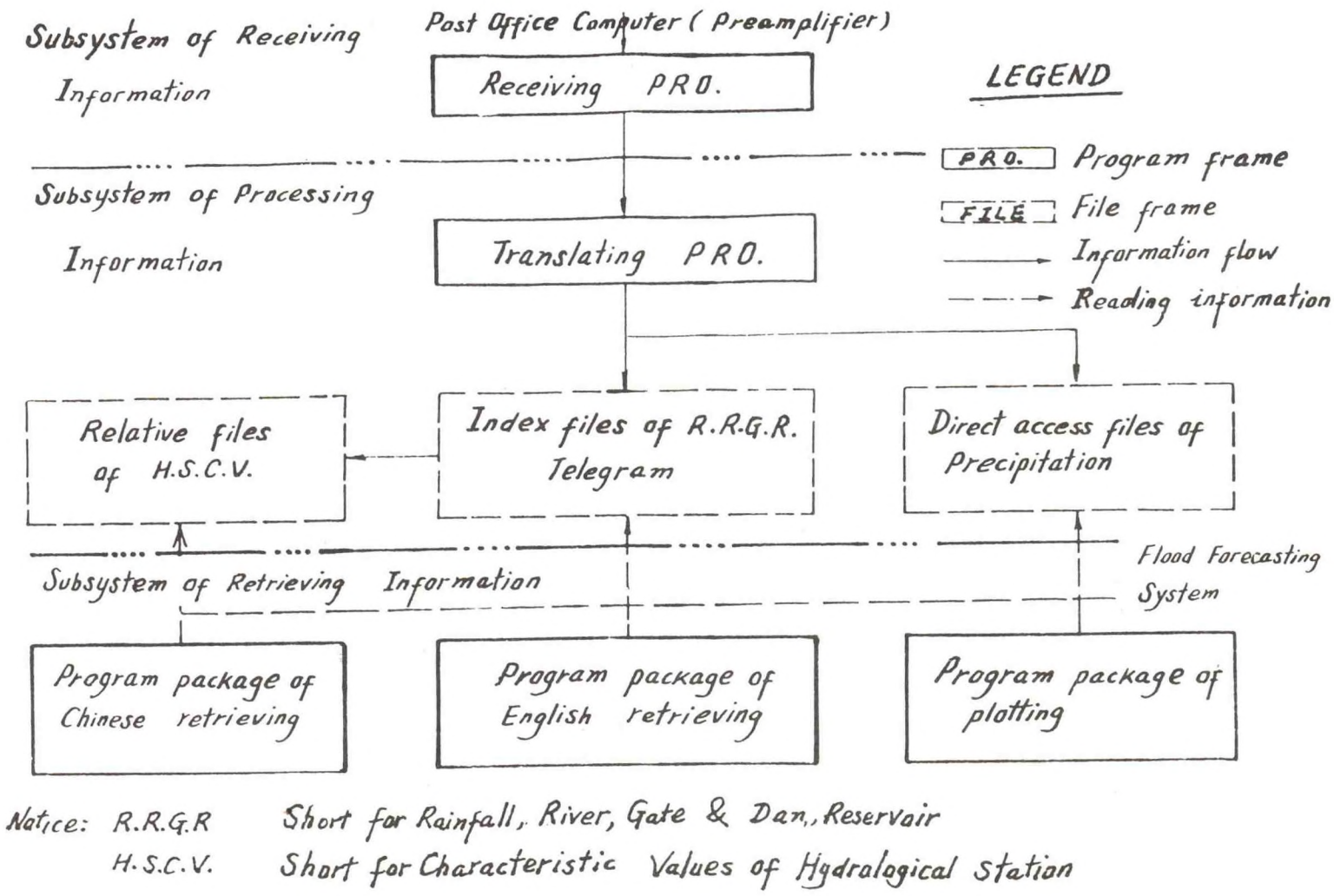

Figure 1. The Flow Chart of the System of Processing Real-time Hydrological Information

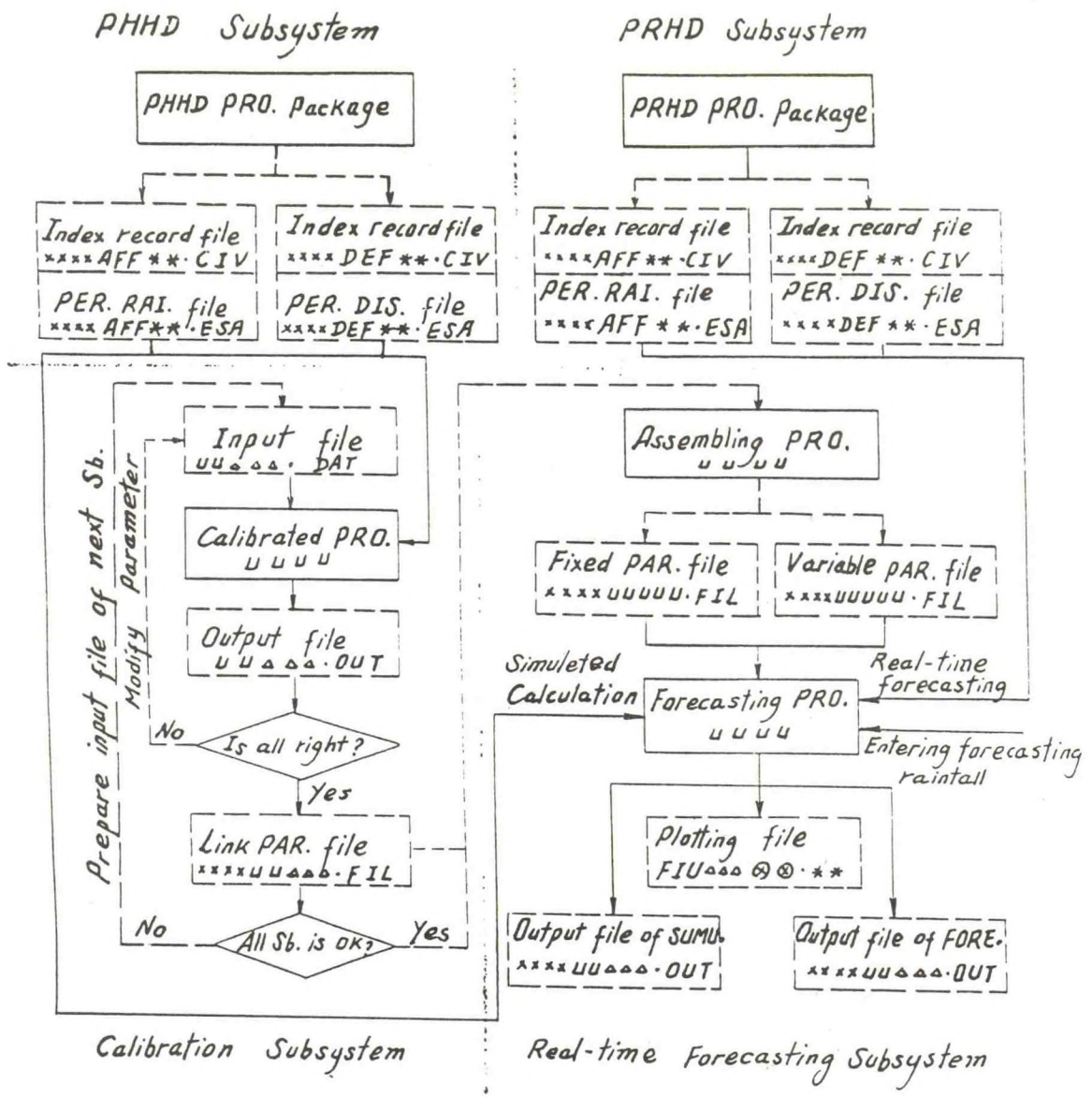

NOTICE: PRO. Program frame; FILE File frame; ×××× Basin Code; ΔΔΔ Station No.; ** Year No.; ⊗⊗ When UP. Stand for updating file; When Nu, Stand for no updating file.

→ Data flow; - - → Contral flow;

u u The Characters of program and file changed according to model.

PHHD: Precessing Historical Hydrological Data

PRHD: Precessing Real-time Hydrological Data.

Figure 2. The Flow Chart of Automatic System of Flood Forecasting of Series PDP and VAX Computers

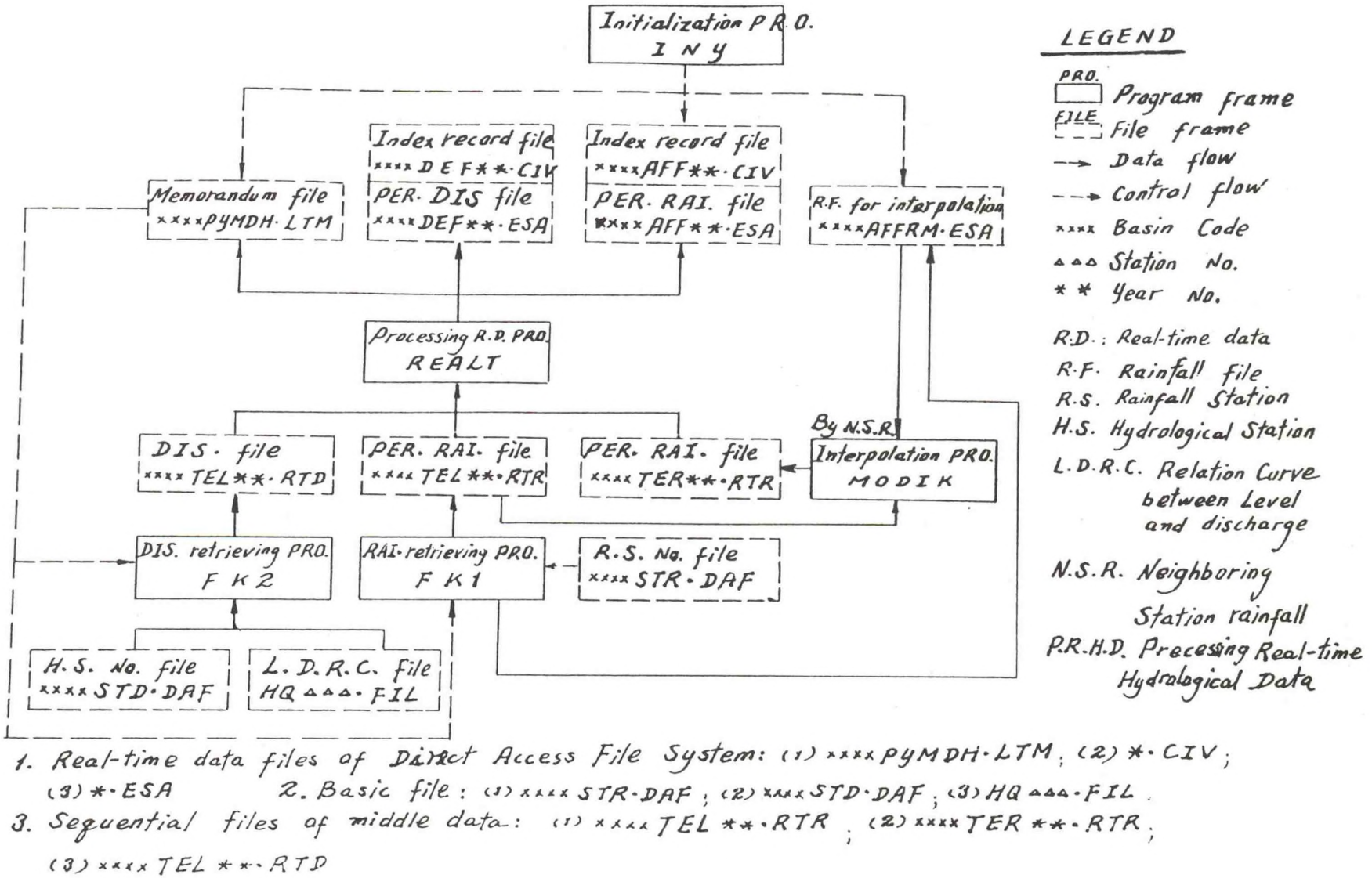

Figure 3. The Flow Chart of Data and Control Flow of the Subsystem of PRHD

Fig. 4(a) The Subbasins of Guanting Gorge of Yongding River

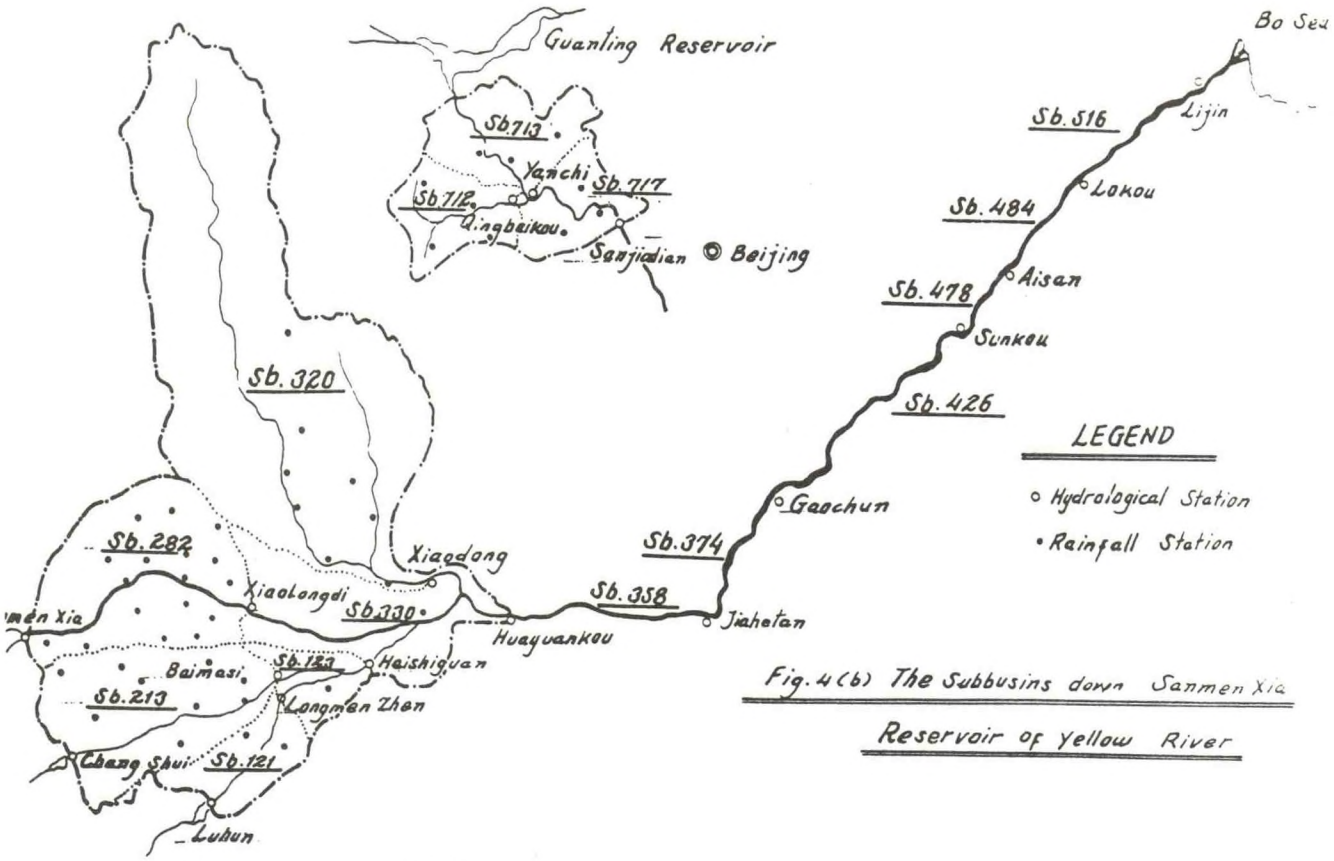

Fig. 4(b) The Subbasins down Sanmen Xia Reservoir of Yellow River

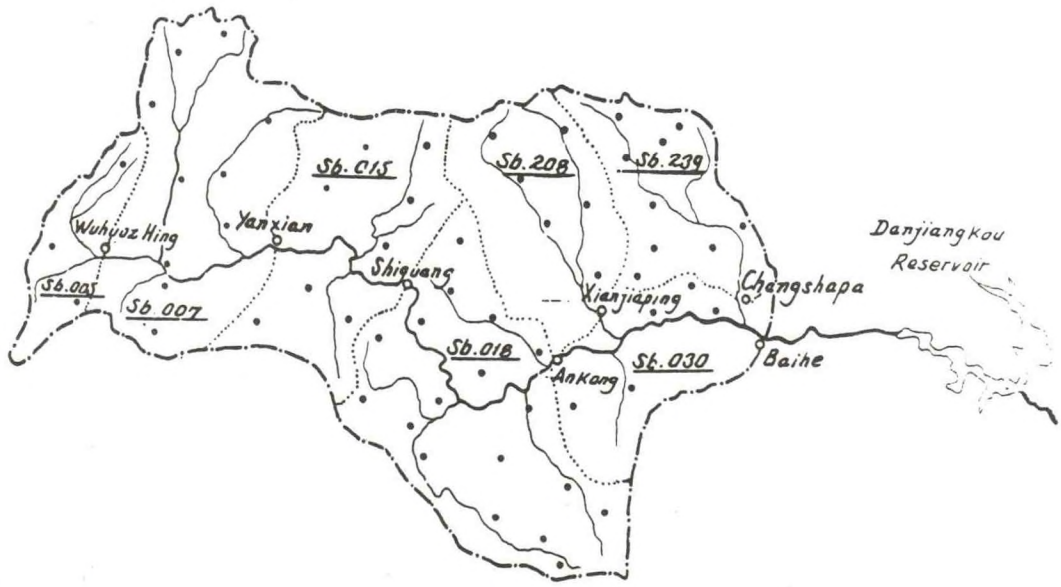

Fig. 4(c) The Subbasins up Baihe Hydrological Station in Hanjiang River

Figure 4a, b, c.

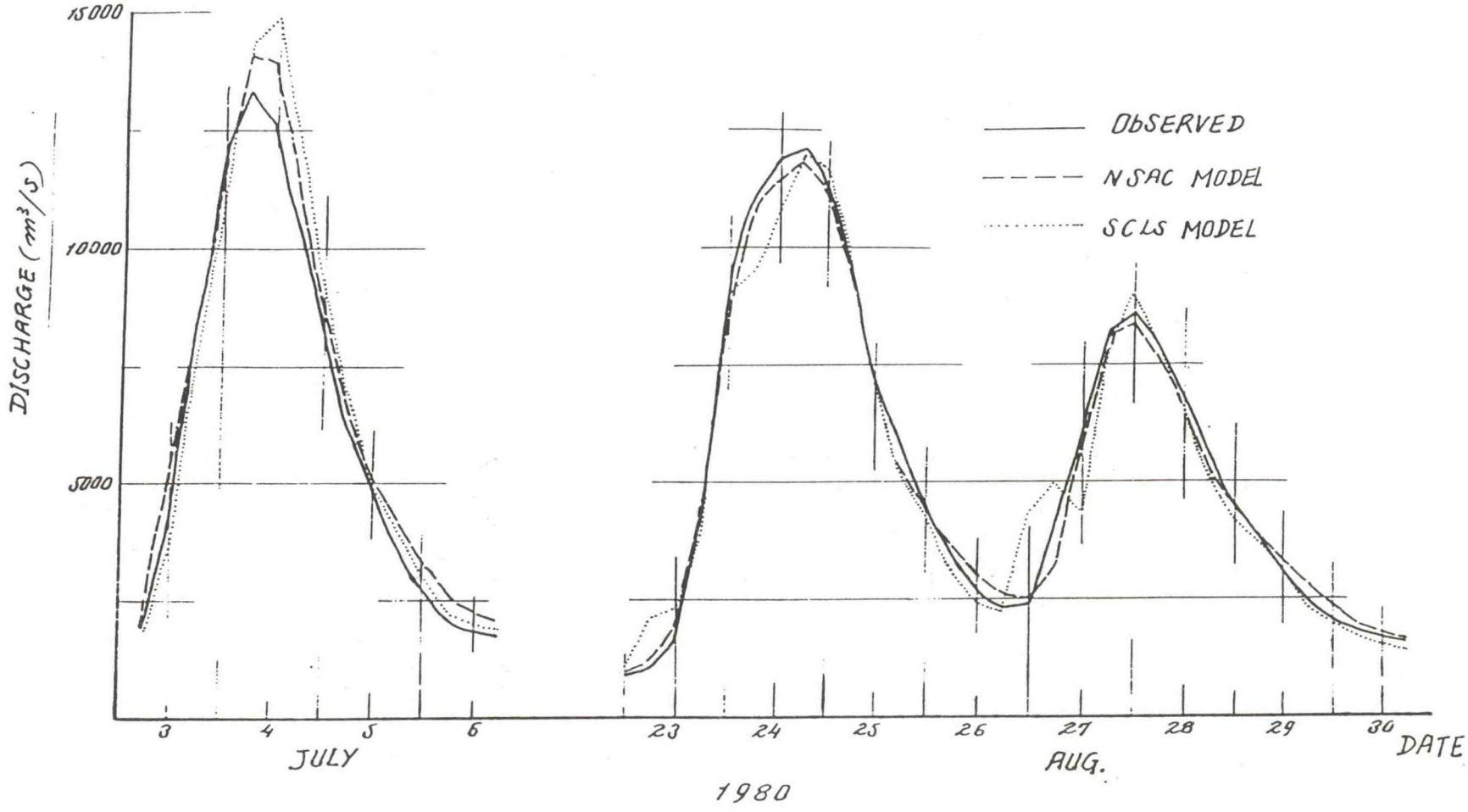

Figure 5. Comparison of Observed and Calculating Discharge in Baihe Station

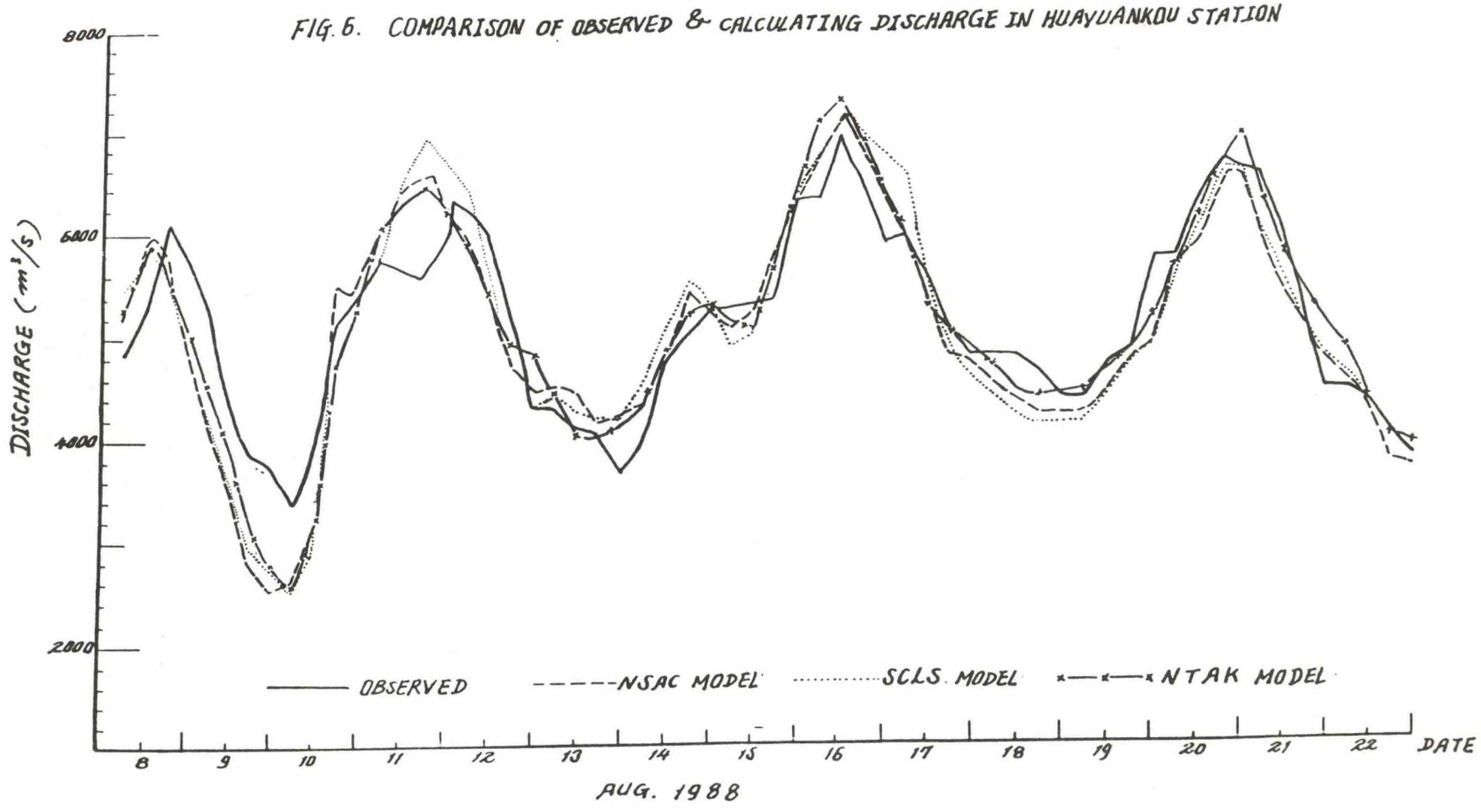

Figure 6. Comparison of Observed and Calculating Discharge in Huayuankou Station

CORPS OF ENGINEERS REAL-TIME WATER CONTROL SYSTEMS

Ming T. Tseng and Earl E. Eiker
U.S. Corps of Engineers, Washington, D.C.

I. INTRODUCTION

The Corps of Engineers (COE), through its Civil Works Program, carries out a comprehensive water resources planning, construction, and operations mission in the United States. The Civil Works Program is directed toward the coordinated management of water resources in a manner that will lead to the satisfaction of both immediate and long-range water related requirements established by Congress. These requirements include: flood control, navigation, hydropower generation, water supply, water quality control, recreation, and fish and wildlife enhancement. The Corps owns and operates some 600 water projects in the United States. In addition, the Corps has the responsibility for prescribing flood control and navigation regulations for 96 reservoir projects owned by other Federal, State, local government, or private agencies.

Management and operation of these projects are carried out by the COE 10 division and 32 district offices throughout the continental United States. District offices are generally responsible for day to day water control management, while the division office provides oversight, technical support and direction to the districts. Corps Headquarters is responsible for development of policy and technical guidance and overall monitoring of water control management activities. Continuous coordination and communication, particularly during periods of flooding and other emergencies, are maintained under the organizational structure.

II. RECENT EMPHASIS IN WATER CONTROL MANAGEMENT

Over the past two decades, construction of new projects has decreased while public demands on the Nation's water resources have continued to rise. As a result, increased emphasis has been placed on more efficient and effective operation of existing reservoirs and reservoir systems to increase project benefits. Existing projects are called upon to provide for additional flood control, increased water supplies, more water-related recreation, and to

accommodate add-on hydropower development. In addition, special regulations have been sought by special interest groups for a myriad of purposes never envisioned in project planning or authorization. These include protection of rare and endangered species of birds nesting along the rivers, drought regulation, fish passage, improved dissolved oxygen, pollution abatement, white water rafting, water temperature control, oil or fuel spills, deep draft vessels, and other domestic and environmental concerns. These demands have exerted additional pressure on water control managers in making difficult management decisions needed to minimize conflicts among project beneficiaries. In response to these challenges, the COE has developed strategies to improve capabilities in data collection and analysis, evaluation of project regulation alternatives, and management decision making.

III. REAL-TIME DATA COLLECTION

To effectively operate projects, the Corps must gather, process, and analyze a wide variety of field data in real-time. Four major types of real-time data are used by the Corps: (1) project data to monitor project performance and safety; (2) hydrologic data to determine basin rainfall and streamflow conditions; (3) meteorological data to forecast precipitation and runoff potentials; and (4) water quality data to assess environmental effects of project activities and to provide an operational basis for water quality control.

Generally, data are collected at intervals from 4 to 24-hours, whereas, during emergencies intervals as short as 15-minutes may be required. Currently, there are about 7,600 gaging stations nationwide at which data are collected in support of Corps water control management activities. The Corps owns or finances about 4,960 of these gage sites and the remaining 2,640 are owned by states and other Federal agencies. Under normal conditions, about 30,000 measurements are made daily at these stations. Because of its timeliness and reliability, the Geostationary Operational Environmental Satellites (GOES) data collection system has been chosen by the Corps as the primary real-time data telemetry system. Today, the Corps has deployed about

2,200 data collection platforms (DCPs) and installed eight ground receiving stations to transmit data via the GOES system.

IV. WATER CONTROL DATA SYSTEM

The complexity of Corps water control management activities requires the collection, processing, interpretation, display and dissemination of large volumes of information; a process ideally suited to automation. With the increase in ability to collect large amounts of data through implementation of new technology, there arose a parallel need to increase capability to manage the data. Accordingly, in 1978 the Corps Headquarters directed each division office to develop a Water Control Data System (WCDS) master plan which would fully integrate the data collection, data management, and communication needs of the division office and its districts. These master plans provided the basis for the continued acquisition of data collection/transmission hardware and automatic data processing equipment, and also defined broad software development needs. The master plans are considered to be "living documents" and are updated periodically to allow adjustments for continually changing requirements. Implementation of the master plans has been accomplished in two phases - hardware acquisition and software development.

A. Hardware Acquisition

Most division master plans clearly established a requirement for improved automatic data processing equipment (ADPE). Taken as a whole, 7 out of 10 divisions recommended acquisition of new dedicated mini-computers as a vital component of their overall water control management capability. A total of 23 (22 mini and 1 main-frame) computers were needed to satisfy Corps-wide requirements. The equipment was installed and operational by the fall of 1985.

B. Software Development

As a result of the hardware acquisition, the Corps made great strides in improving its data collection and processing capabilities. In order to make maximum use of these capabilities, however, it was necessary to establish an

orderly plan to provide for development of the software that was required to fully realize this new potential.

Development of software for Corps-wide use has been carried out by several Corps offices and private contractors, while development of software that is division or district specific has remained the responsibility of each local office. This process has allowed for a more effective allocation of scarce research and development funds and has avoided potential duplication of effort. Technical oversight and tracking of development activities has been accomplished by the Corps Hydrologic Engineering Center (HEC) in Davis, California.

The system applications software is divided into three distinct groupings: data acquisition, data base utility, and analysis. In addition, there is system support software that integrates all of the components into a user friendly system. The system support software includes routines for program and computer control, data base interface, and monitoring of system operations.

The data acquisition group includes programs to receive data from the GOES system, over landlines and radio networks, from the National Weather Service River Forecast Centers and other computer systems, and through manual entry. All data received is processed through a preliminary screening program prior to placement in the data base. Work is presently underway to develop the software to accept satellite imagery data and radar imagery data.

The data base utility group includes programs to generate reports, archive and retrieve data, compute summaries and statistics, generate graphics, send data to other computer systems, and perform other routine tasks.

The applications grouping includes streamflow forecasting models and real-time reservoir systems operation models. Work is presently underway to develop software to perform high level data screening and validation prior to application or dissemination of the data. Future developmental efforts are envisioned in the areas of economic analysis of flood related damages and damage prevented, water supply accounting, power demand evaluations, water surface profiles, and sediment transport.

V. SYSTEM IMPLEMENTATION

The real-time water control system is at various stages of implementation by the COE offices throughout the country. Some of these offices have developed an integrated system of data acquisition, data processing, and information capabilities for their projects. The Data Storage System (DSS) software developed by the HEC has been used extensively at those Corps offices equipped with mini-computers for real-time data management. The Corps main-frame computer at the North Pacific Division in Portland, Oregon, uses a unique data management system developed by the division water control managers.

The most popular models that have been applied by the Corps offices for real-time watershed runoff forecasting are the COE HEC-1F and Streamflow Synthesis and Reservoir Regulation model (SSARR). At some Corps offices these models are run for real-time runoff simulation, therefore, model parameters are constantly updated with real-time data, requiring minimum initial model calibration for flood runoff forecasting. HEC-1F is also used by several Corps offices as an interactive model for evaluation of alternative operational scenarios for flood releases.

Since the completion of the Corps of Engineers water control data system in late 1985, the system has undergone critical tests both for flood and drought operations. In 1986, record floods occurred along the Pacific Coast and in the midsection of the country. In February 1986, a large and powerful storm system produced record amounts of precipitation over much of northern California and western Oregon. The storm system resulted in record high flood stages in the Sacramento River basin in California. In the Willamette River basin in Oregon, heavy rainfall in combination with snowmelt due to warm temperatures, caused rivers to rise above flood stages. Regulation of reservoirs in the Willamette Valley and the reservoirs and extensive levee system on the Sacramento River prevented major damages to metropolitan areas.

Record storms and flooding also occurred in the nation's midsection during early October 1986. Remnants of Hurricane Payne, carrying large amounts of moisture, produced record amounts of rainfall over a wide area in Oklahoma, Missouri, Kansas, and adjacent states. As much as 22 inches of rain were measured over a 6-day period in some areas of Oklahoma. Regulation of COE

reservoir projects in the Arkansas, Osage, and lower Missouri River basins, during the flood events, substantially reduced flood stages downstream from Corps reservoirs. All of the Corps' water control data subsystems performed their functions well during the 1986 flood events. HEC-1F was used extensively by the Tulsa district during the flood operation of October 1986.

In 1988, about 70 percent of the Nation experienced some level of drought. Extreme drought occurred in the West, Midwest, Southeast and Ohio Valley areas. Many COE storage projects suffered record drawdowns, which resulted in profound impacts on hydropower generation, navigation, recreation, and other project purposes. The COE, one of the principal water resources development agencies for the Nation, was required to keep the executive and legislative branches of the Federal government as well as the general public informed of Corps drought management activities. In order to meet these requirements, substantial amounts of field data were provided to Corps headquarters for preparation of daily drought briefings. A data base management program called Real-time Data Exchange (RTX) was established on the HEC mini-computer for Corps-wide access. RTX proved to be extremely valuable for timely exchange of drought information within the Corps.

VI. SUMMARY

Automation of real-time water control management activities has enabled the Corps to keep pace with an ever increasing workload in a time of fiscal constraint and reduced manpower. Where manual procedures were recently the norm, the entire process is now automated. Data are collected automatically in the field, transmitted through satellites to ground receiving stations, and relayed to the office mini-computer to be processed. Once into the computer, the data are analyzed and used for evaluation of alternative management strategies to form a basis for water control decisions. The processed data are then disseminated and ultimately stored for future analyses. The entire process permits more data to be collected, more alternative operations to be evaluated and, as a final result, leads to better management decisions. The COE water control system has experienced critical tests for flood and drought operations since its completion in late 1985. The system performed reasonably well during these severe hydrologic extremes.

DEPENDENCE OF SEASONAL PRECIPITATION AND RUNOFF VOLUMES IN THE PACIFIC NORTHWEST ON AN INDEX OF THE EL NINO SOUTHERN OSCILLATION

Roy W. Koch
Department of Civil Engineering
Portland State University
Portland, Oregon

ABSTRACT. Water supply forecasts are an important source of information in the operation of water resource systems in the western United States. Current practice requires estimates of future precipitation for input to the forecasting models, which represents a major source of uncertainty in the forecast. Recent research in large scale climate behavior suggests that climate features on the global scale are related to regional climate and may provide information for water supply forecasts. The El Niño Southern Oscillation (ENSO) is the feature which has, perhaps, the strongest signal in the global climate system. Further, the relationship of ENSO to the climate of the midlatitudes has been established.

The dependence of precipitation and runoff volumes on the occurrence of ENSO events and an index of its intensity are examined. Seasonal precipitation and streamflow data for several drainage basins in the western United States were evaluated using split sample and correlation analysis. The results show a pattern of dependence on ENSO which is both seasonally and spatially variable. Two areas, one located in the Pacific Northwest and the other in the desert Southwest, are most strongly related to ENSO. During an ENSO event, the Pacific Northwest tends to have below average precipitation and streamflow, while the desert Southwest has the opposite response. The response is also seasonally variable. Indications are that this line of inquiry may prove useful in improving estimates of future precipitation used in water supply forecasts.

I. INTRODUCTION

Forecasts of the volume of streamflow to be expected in the upcoming runoff season, called water supply forecasts, are an important factor in the operation of many reservoirs. Water supply forecasts are issued on a monthly basis through the cooperative efforts of the National Weather Service (NWS) and the Soil Conservation Service (SCS) beginning in January each year. The forecasts are limited to those areas of the western United States where snowmelt represents a significant fraction of the runoff. In fact, it is the accumulation of moisture in the snowpack which makes these forecasts possible. Although newer methods are under development, water supply forecasts are currently based on regression models relating seasonal runoff volumes to seasonal indices of snow water equivalent, precipitation and antecedent moisture conditions. These procedures require estimates of precipitation and snow water equivalent which will occur in months subsequent to the forecast date as input to the regression models. Due to the uncertainty of these values, the forecast error, early in the season, is quite high.

Accuracy of water supply forecasts produced using these regression procedures depends on the fraction of seasonal streamflow volume that is due to snowmelt, variability in the local climate, and the date of the forecast. An evaluation of the forecast errors by Shafer and Huddleston (1984) show average errors of slightly more than 20 percent for February forecasts in the Pacific Northwest decreasing to between 10 percent and 20 percent for the May forecast date. The variability is a function of the fraction of runoff which results from snowmelt. In an analysis of water supply forecast accuracy, Schaake and Peck (1985) identified three primary sources of error in the forecasts: climate error, model error, and data error. Of these three sources, climate error was the dominant component, particularly early in the forecast season. Thus, improvements in understanding climate variability which result in better long range climate forecasts could be used to decrease the error of water supply forecasts.

This paper describes a study of the relationship between a particular recurring large scale climate phenomenon, the ENSO, and seasonal precipitation and streamflow volume in the Pacific northwestern region of the western United

States. Of particular interest, in this investigation, is the nature and the strength of any relationship and the likelihood that this line of investigation may lead to useful information which could be incorporated into water supply forecasting procedures. First, a brief review of some large scale climate features, including ENSO, is presented along with the current understanding of the relationship of these phenomena to the climate of the western United States. Then, seasonal precipitation and runoff volumes data are analyzed in relation to an index of the ENSO to determine the nature of the relationship. Finally, the results are discussed along with the possibility of incorporating information on short term climate fluctuations such as ENSO into water supply forecasting procedures.

II. LARGE SCALE CLIMATE VARIABILITY

The dependence of streamflow on surface climate, in particular precipitation, is well understood by hydrologists. The processes produced in streamflow have been conceptualized in the hydrologic cycle and have been quantified, particularly over short time intervals, for the purposes of flood prediction and forecasting. However, climatic inputs to hydrologic models have been considered largely random from the point of view of predicting future streamflows. As a result, predictions or forecasts of future climate on time scales of months, seasons, and years have been based principally on the climatology, considering only the observed random variation. Using this approach, predictability results from whatever persistence is observed in the historical record.

Over the past two decades, however, great strides have been made in both describing and understanding the nature of climate variability on large spatial and temporal scales. This improved understanding has come primarily as a result of analyses of data describing the circulation in the upper atmosphere and to a lesser extent, surface pressures. These analyses have identified persistent and recurring modes of variation in the upper air circulation of the Northern Hemisphere and periods of the year over which they are dominant. With regard to the western United States, a circulation pattern over the eastern north Pacific Ocean and North America, called the

Pacific/North America (PNA) pattern emerges as the dominant winter pattern in both the upper atmosphere and at the surface (Wallace and Gutzler, 1981). The PNA is characterized by a strong low pressure center in the northeastern Pacific Ocean, an upper level high pressure centered over western Canada and a deeper than normal low pressure center over the southeastern United States. Surface climate in the western United States has been shown to be related to the strength of the PNA pattern, particularly in the winter season. Redmond and Koch (1988) have shown significant correlation of an index of the PNA with temperature ($r > 0.6$ in the Pacific Northwest) and, to a lesser extent precipitation, ($r > 0.4$ for areas of the Pacific Northwest and desert Southwest) when the data are aggregated over the 6 month period of October through March. Yarnal and Diaz (1986) have also shown a connection between the PNA and temperature and precipitation along the coastal margin of the western United States. Although it is dominant in the northern Hemisphere winter, the PNA is not particularly persistent and is, therefore, not a useful index in predicting subsequent surface climate behavior.

On a global scale, the largest signal in interannual variability of the global climate system is produced by the combined ocean-atmosphere phenomenon, ENSO (Rassumsson and Wallace, 1983). The Southern Oscillation is a circulation pattern in the equatorial Pacific Ocean characterized by high surface pressure centered in the South Pacific near Tahiti and low surface pressure centered over Indonesia and northern Australia. The strength of this pressure gradient is measured as a standardized difference in the surface pressures at Tahiti and Darwin and is called the Southern Oscillation Index (SOI). A positive SOI is associated with a strong gradient, while a negative SOI occurs when the gradient is weaker than normal. This pressure gradient produces a circulation pattern in the plane of the equator which is thought to be responsible for much of the seasonal precipitation in the western Pacific Ocean. As reasonably cool, dry air moves westward it is warmed and moistened by the waters of the western Pacific Ocean and precipitation is produced by condensation of the rising air. The circulation is closed as the dryer air returns eastward in the upper atmosphere. This simplified model of the equatorial circulation is also closely related to the sea surface temperatures (SST) in the equatorial ocean. The circulation is at its strongest when the

SST in the eastern Pacific are cool, while those in the western Pacific are warm. The strength of the Southern Oscillation varies, seasonally, with the cycle of SST which is typified by a warming in the eastern and central pacific, beginning in the fall and reaching its maximum in the northern Hemisphere winter. This warming results in a decrease in the surface winds and a corresponding decrease in the pressure gradient. The phenomena of high SST in the eastern Pacific is called El Niño. Occasionally, the SST increases well above average, as was the case in 1982, and the circulation is strongly affected, resulting in dramatic climatic anomalies on either end of the Southern Oscillation. Hereafter, the term ENSO will be used to describe this condition of anomalously high SST and low pressure gradient in the Southern Oscillation (negative SOI). ENSO events have been observed to occur rather frequently, on the average of once every three to five years, although the strength of the events vary considerably.

Although the phenomena which comprise the ENSO event are principally located in the equatorial ocean, they appear to affect the global climate. Connections with the midlatitudes have been established both through observational studies, using circulation data, (e.g. Horel and Wallace, 1981; Yarnal, 1985) and theoretical computer models (Hoskins and Karoly, 1981). In particular, a strong PNA circulation pattern has been shown to occur more frequently during years when ENSO events occur (Yarnal and Diaz, 1986) thus, providing a direct link to the climate of the western United States. Ropelewski and Halpert (1986), have identified consistent responses, in both temperature and precipitation, in several regions of North America. In particular, increased precipitation was noted in the states bordering the Gulf of Mexico, in the High Plains, and the Great Basin, whereas, decreased precipitation was noted in the Pacific Northwest. It is also interesting to note, that the response in the Pacific Northwest occurred several months after the onset of the ENSO event which was assumed to begin in the summer months. Similar results were reported by Redmond and Koch (1988) in a study confined to the western United States. For divisional precipitation data totalled for the period October through May, correlation coefficients with the SOI were as large as 0.5 in the Pacific Northwest indicating that above normal precipitation was strongly associated with a positive SOI, a condition

opposite to an ENSO event. Conversely, below average precipitation was then associated with ENSO events. The opposite response was noted in the desert Southwest where above normal winter precipitation was found to occur during ENSO events. These correlations were, for SOI, averaged over a 6-month period from June through November, again indicating that ENSO may be a precursor to climate events in the western United States.

At the present time, much statistical evidence exists to suggest global scale relationships in the climate, even though the physical mechanisms producing this behavior are still under investigation. From these studies, it is also clear that certain areas of the western United States are directly affected by short-term climate fluctuations, in particular, ENSO events which may be a precursor to upcoming precipitation, an important factor in water supply forecasting. In the remaining sections of this paper, the nature and significance of the relationship of an index of the ENSO phenomenon to seasonal precipitation and runoff volumes in one region of the western United States, the Pacific Northwest, is investigated.

III. DESCRIPTION OF THE STUDY AREA

The Pacific northwestern region of the United States is defined to be the states of Idaho, Oregon, and Washington, and that portion of Montana which is west of the Continental Divide. The climate of the region varies with distance from the Pacific Ocean and topographic influences. The annual cycle of precipitation is characterized by a distinct winter wet season which reaches a maximum in December and January along the coastal margin due to storms moving inland from the eastern Pacific Ocean. Both the magnitude of the seasonal variation and the amount of annual precipitation decrease with distance from the coast. The amount of precipitation is also strongly dependent on elevation. Orographic effects of the Coast Range and the Cascade Range in Oregon and Washington, and the northern Rocky Mountains in Idaho, as well as isolated mountain ranges in the central part of the region, result in marked variation of precipitation with elevation. In addition to increases in the amount of precipitation with elevation, the form of precipitation also varies. In the higher elevations of all of the mountains, with the exception

of the Coast Range, winter precipitation falls as snow and accumulates in a seasonal snowpack. A general decrease in mean winter temperatures with distance from the coast also contributes to the fraction of winter and spring precipitation which falls as snow. Despite these variations, the entire area has the same principal source of moisture, and might be expected to respond to variation in the circulation patterns in the eastern north Pacific Ocean in a consistent manner.

Runoff is dependent on both the amount and form of precipitation. For the coastal stream, the annual runoff cycle closely follows that of precipitation since there is no seasonal accumulation of snow. Moving eastward, seasonal runoff patterns from streams in the Cascade Range show a dual peak, one in the winter, due to low elevation precipitation, and another in the spring, due to snowmelt. Finally, streams in the eastern part of the region, particularly those in Idaho and Montana, have peak flows in the late spring due almost entirely to snowmelt.

IV. DATA ANALYSIS

To investigate the relationship of ENSO to the seasonal precipitation and runoff volumes in the Pacific Northwest, the null hypothesis that there is no connection is subjected to statistical tests. The basic data used in this study consists of 53 years of divisional, monthly, precipitation for the 30 climate divisions in the Pacific Northwest. These monthly data were aggregated into 3-month totals which preserve the annual cycle. The water year is used as the annual period and the 3-month seasons are fall (October through December), winter (January through March), spring (April through June), and summer (July through September). Most of the precipitation occurs in the fall and winter seasons which have nearly equal contributions to the annual total. Monthly streamflow data were also compiled for several streams in the region to directly assess the relationship of ENSO to seasonal runoff volumes. The monthly data for these streams were aggregated into seasonal runoff data based on the seasons identified and used by the SCS and NWS in their monthly forecasts.

The SOI was used as an index of those conditions in the atmosphere normally associated with ENSO events. As stated earlier, a negative SOI is normally associated with ENSO. The monthly SOI data were also aggregated into 3-month averages for the periods of summer (July through September) and fall (October through December). This represents the active period of ocean warming and associated fluctuation in the SOI. Finally, based on the review of previous work, it was assumed that the surface climate would be related to the averaged SOI in previous seasons. That is, if the fall, winter, and spring, precipitation was related to the SOI, it would most likely be related to those values occurring during the previous summer and fall.

First, correlations of seasonal precipitation and runoff volumes with SOI were calculated and the resulting correlation coefficients tested under the null hypothesis that they were not statistically distinguishable from zero. Then, the sample for each climate division and stream gaging station was split based on the ranking of the SOI index and its division into terciles. The mean and variance of precipitation or runoff volumes were computed for the upper tercile (high values of SOI) and the lower tercile (low values of SOI, ENSO events) and tested for statistically significant differences. Most of the ENSO events, reported by Rasmusson (1984), were contained in the lower tercile of the ranked summer SOI values.

A. Seasonal Precipitation

Correlations between seasonal precipitation and SOI were computed for several different combinations of time periods. In each case, however, the averaging period for SOI was selected to precede the seasonal precipitation so the value of SOI as a useful variable in forecasting could be assessed. For example, fall precipitation was correlated only with summer averaged SOI whereas winter precipitation was correlated individually with summer and fall SOI to determine the strongest relationship. In addition, winter and spring precipitation were correlated with a 6-month averaged SOI over the period July through December. Of these combinations, fall and winter precipitation were most strongly correlated with summer averaged SOI, although some equally high correlations were noted in certain cases for winter precipitation with the 6-

month averaged SOI. Spring precipitation only showed significant correlations with winter averaged SOI. A compilation of the correlation coefficients between seasonal precipitation for each division and SOI are given in table 1. The strength of the correlations is also shown on fig. 1 for the fall and winter seasons. As noted, the fall and winter correlations are with summer SOI, while the spring correlations are with winter SOI. The null hypothesis of no correlations was rejected for a number of divisions, mostly located in the Cascade Mountains of Washington and Oregon, in extreme western Washington and northern and central Idaho.

The strongest correlations were observed for the winter season in the mountainous divisions of Idaho, Oregon, and Washington (fig. 1b). The positive correlation coefficients indicate that above average precipitation is associated with above average SOI. Therefore, ENSO conditions, which are normally coincident with a below average SOI, are associated with below average precipitation. We note that SOI explains approximately 20 percent of the variance in winter season precipitation for several of the divisions in western Washington. Finally, some moderate correlation is also noted for the spring season in southeastern Oregon and southwestern Idaho.

Since a statistically significant correlation between seasonal precipitation and SOI has been established, further analysis is suggested. The Southern Oscillation represents only one of many factors affecting the climate of the midlatitudes, therefore, it is reasonable to assume that the affects would be most pronounced during the extreme phases, the extreme negative phase coinciding with ENSO. Following this reasoning, the sample of seasonal precipitation was split into three terciles based on the ranked SOI. A test difference in means between seasonal precipitation during the two extremes was tested (e.g. Haan, 1977). The results, presented in table 2, are consistent with the results of the correlation analysis. Marked differences are noted in the mean seasonal precipitation between the two extremes of the SOI sample for much of western Washington and Oregon as well as the mountainous divisions of northeastern Oregon and Idaho as is shown in fig. 2a.

TABLE 1

Correlation coefficients between seasonal precipitation and SOI. SOI is averaged over a 3-month period from July through September for correlation with fall and winter precipitation and October through December for spring precipitation.

	DIVISION		SEASON		
STATE	NAME	NUMBER	FALL	WINTER	SPRING
Idaho	Panhandle	1001	0.205	0.265*	0.087
	North Central Prairies	1002	0.290*	0.293*	0.183
	Canyons	1003	0.282*	0.395***	0.170
	Central Mountains	1004	0.157	0.347**	0.169
	Southwest Valleys	1005	0.111	0.005	0.252*
	Southwest Highlands	1006	0.143	0.143	0.185
	Central Plains	1007	0.180	0.115	0.110
	Northeast Valleys	1008	0.177	0.215	0.102
	Upper Snake River Plains	1009	0.134	0.049	0.153
	East Highlands	1010	0.163	0.202	0.173
Montana	West	2401	0.224	0.373*	0.158
Oregon	Coast Area	3501	0.216	0.208	0.159
	Willamette Valley	3502	0.217	0.311*	0.138
	Southwest Valleys	3503	0.22	0.166	0.137
	Northern Cascades	3504	0.305*	0.439***	0.159
	High Plateau	3505	0.177	0.137	0.148
	North Central	3506	0.204	0.163	0.130
	South Central	3507	0.196	0.027	0.219
	Northeast	3508	0.248*	0.276*	0.267*
	Southeast	3509	0.074	0.095	0.363***
Washington	West Olympic Coast	4501	0.308*	0.257*	0.074
	Northeast Olympic San Juan	4502	0.279*	0.396***	0.205
	Puget Sounds Lowlands	4503	0.295*	0.357***	0.131
	East Olympic - Cascade Foothills	4504	0.311*	0.428***	0.110
	Cascade Mountains West	4505	0.278*	0.456***	0.108
	East Slope Cascade	4506	0.259*	0.403***	0.009
	Okanogan - Big Ben	4507	0.112	0.090	0.082
	Central Basin	4508	0.220	0.004	0.024
	Northeast	4509	0.179	0.098	0.189
	Palouse - Blue Mountains	4510	0.241	0.221	0.093

* significant at the 95 percent level
** significant at the 99 percent level
*** significant at the 99.5 percent level

TABLE 2.

Results of the split sample tests on the mean of seasonal precipitation. Shown are the test statistics which are approximately distributed with 51 degrees of freedom.

	DIVISION		SEASON				
STATE	NAME	NUMBER	FALL	WINTER	SPRING	SUMMER	ANNUAL
Idaho	Panhandle	1001	1.183	1.787*	0.679	-0.599	1.701*
	North Central Prairies	1002	1.619	1.932*	0.135	-0.478	1.397
	Canyons	1003	1.488	3.195***	-0.104	-0.752	1.660
	Central Mountains	1004	1.286	3.003***	-0.426	-0.315	2.067*
	Southwest Valleys	1005	1.657	0.112	-1.155	0.177	0.412
	Southwest Highlands	1006	1.638	1.382	-0.250	0.713	1.350
	Central Plains	1007	2.445*	0.697	-0.140	1.001	1.856*
	Northeast Valleys	1008	1.386	1.639	-0.221	1.216	1.694*
	Upper Snake River Plains	1009	2.170*	-0.506	0.016	0.584	1.052
	East Highlands	1010	2.218*	1.376	0.033	0.040	1.475
Montana	West	2401	0.829	2.473**	0.340	-0.194	1.685*
Oregon	Coast Area	3501	1.907*	1.791*	-0.237	-1.291	1.951*
	Willamette Valley	3502	1.817*	2.384*	-0.880	-0.584	2.173*
	Southwest Valleys	3503	1.994*	1.225	-0.266	-1.047	1.725*
	Northern Cascades	3504	2.396*	3.458***	-1.535	-1.045	3.015***
	High Plateau	3505	1.424	1.062	-1.061	0.969	1.348
	North Central	3506	1.535	1.380	0.092	0.102	1.623
	South Central	3507	1.889*	0.181	-0.624	0.347	1.018
	Northeast	3508	1.876*	2.329*	-1.242	-0.434	1.212
	Southeast	3509	1.687*	-0.564	-1.574	0.175	-0.099
Washington	West Olympic Coast	4501	1.610	2.010*	-0.410	-0.948	1.797*
	Northeast Olympic San Juan	4502	1.449	3.033***	0.100	-0.657	2.088*
	Puget Sounds Lowlands	4503	1.697*	2.603**	-0.233	-0.825	1.885*
	East Olympic - Cascade Foothills	4504	1.739*	3.528***	-0.715	-0.759	2.567**
	Cascade Mountains West	4505	1.296	3.571***	-1.151	-0.753	2.396*
	East Slope Cascade	4506	1.331	3.038***	0.951	-0.112	2.663**
	Okanogan - Big Ben	4507	1.198	-0.253	1.198	-0.241	0.991
	Central Basin	4508	1.803	0.256	1.413	-0.118	1.693*
	Northeast	4509	1.236	0.439	0.257	-0.416	0.814
	Palouse - Blue Mountains	4510	1.740	1.823	0.363	-1.146	1.543

* significant at the 95 percent level
** significant at the 99 percent level
*** significant at the 99.5 percent level

For many divisions, the null hypothesis that there is no difference in the two samples is rejected at greater than the 0.5 percent level. These differences in winter precipitation, combined with some smaller differences of the same sign in the fall precipitation, combine to produce statistically significant differences in the mean annual precipitation for several divisions, as shown in fig. 2b. No significant differences are noted for either the spring or summer seasons.

B. Seasonal Runoff Volumes

Since a statistical connection is noted between seasonal precipitation and the SOI, a similar analysis is conducted on seven river basins in the region. These basins were selected since they have minimal regulation and diversion, and the records reflect nearly natural conditions (H.F. Lins, personal communication). Correlation coefficients were calculated between the seasonal runoff volumes for each basin and the summer averaged SOI. In addition, a split sample analysis was conducted. The results, shown in table 3, are similar to those observed for winter precipitation but in many cases, the direct correlation of runoff volumes with SOI is larger than was observed for precipitation. This is particularly true for the Clearwater and Selway Rivers which are located in the Central Mountains climate division of Idaho, as well as for the Wilson River in coastal Oregon and the Skykomish River in western Washington. In several cases, the summer SOI alone explains nearly 25 percent of the variance in the seasonal runoff volumes. With the exception of the John Day River in central Oregon, the split sample tests also show a significant difference in the means at the 5.0 percent level or greater.

V. SUMMARY AND CONCLUSIONS

A brief statistical analysis of the relationship of seasonal precipitation and runoff volumes in the Pacific Northwest to the SOI was presented. The SOI is closely related to the occurrence of the ENSO phenomenon. Statistically significant relationships for both precipitation and streamflow were observed with seasonally averaged SOI occurring as much as one or two seasons earlier.

TABLE 3.

Summary of statistical tests on the seasonal runoff volumes for selected streams in the Pacific Northwest

RIVER BASIN	CLIMATE DIVISION	RUNOFF SEASON	CORRELATION WITH SUMMER SOI	SPLIT SAMPLE STATISTIC
Boise R., ID	Central Mountains	Apr-July	0.284*	1.97*
Clearwater R., ID	Central Mountains	Apr-July	0.489***	2.81**
John Day R., OR	North Central & South Central	Apr-Sep	0.226	1.60
Selway R., ID	Central Mountains	Apr-Sep	0.505***	2.86***
Skykomish R., WA	Cascade Mtns West	Apr-Sep	0.428***	2.76***
Umpqua R., OR	Southwest Valleys	Oct-Sep	0.482***	3.00**
Wilson R., OR	Coast Area	Oct-Sep	0.348**	2.24*

* significant at the 5 percent level
** significant at the 1 percent level
*** significant at the 0.5 percent level

However, these relationships are quite variable in both space and time. For seasonal precipitation, the strongest association was noted in the winter months (January through March), with below average precipitation occurring when the SOI suggests the occurrence of an ENSO event. Similar results were noted for the fall season but were not as significant. The strongest correlations with the SOI and greatest differences in seasonal precipitation during the extreme phases of the SOI were observed in the mountainous divisions. These are the areas where the greatest precipitation occurs as well as the areas of seasonal snow cover. Streamflow was related to the SOI in a similar manner. However, the associations of SOI with runoff volumes were even stronger than those observed for precipitation. This suggests that

processes, in addition to precipitation, for example snow accumulation, may be more significantly affected by the atmospheric conditions accompanying these large scale, short-term climate fluctuations. It is significant to note that as much as 25 percent of the variance in runoff volumes was explained by the summer averaged SOI for one of the river basins.

It is becoming increasingly apparent that improved understanding of large scale climate variability and the interconnections of climate on a global scale will provide much useful information for purposes such as water supply forecasting. In this study, the relationship of both precipitation and streamflow to an index of atmospheric circulation occurring near the equator almost half a year earlier was demonstrated. These results suggest that there is additional information that can be used to condition forecasts of precipitation and streamflow expected to occur in the future, beyond simply the persistence observed in the historical sample. Admittedly, the correlations are not strong and it remains to be shown if reducing the variance of a runoff volume forecast by 10 percent to 25 percent is useful in the operation of a reservoir. It is important to note, however, that this reduction in variance can be achieved at the beginning of the forecast season when there is little additional information.

ACKNOWLEDGMENTS

The work described in this paper was supported, in part, by funds provided by Portland State University under the Research and Publications Grant Program. Discussions with D.M. Johnson on topics related to this study have been very helpful. The computational work was performed by Cecilia Martin. All of this assistance is gratefully acknowledged.

REFERENCES

Haan, C. T., "Statistical Methods in Hydrology," Iowa State University Press, 376 pp., 1977.

Horel, J.D., and Wallace, J.M., "Planetary Scale Atmospheric Phenomena Associated with the Southern Oscillation," Monthly Weather Review, 109:813-829, 1981.

Hoskins, B.J., and Karoly, D.J., "The Steady Linear Response of a Spherical Atmosphere in Thermal and Orographic Forcing," Journal of Atmospheric Science, 38:1179-1196, 1981.

Rassumsson, E.M., and Carpenter, T.H., "Variations in Tropical Sea Surface Temperature and Surface Wind Fields Associated with the Southern Oscillation/El Niño," Monthly Weather Review, 110:354-384, 1982.

Rasmusson, E.M., "El Niño: The Ocean/Atmosphere Connection," Oceanus, 27(2):5-12, 1984.

Redmond, K.T., and Koch, R.W., "Surface Climate Variability in the Western United States and its Relationship to Large Scale Circulation Indices," in review for publication in the AGU Monograph: Interdisciplinary Aspects of Climate Variability in the Eastern Pacific and Western Americas, D.H. Peterson, ed., 1988.

Ropelewski, C.F., and Halpert, M.S., "North American Precipitation and Temperature Patterns Associated with the El Niño/Southern Oscillation (ENSO)," Monthly Weather Review, 114:2352-2362, 1986.

Schaake, J.C., and Peck, E.L., "Analysis of Water Supply Forecast Accuracy," Proceedings of the 53rd Western Snow Conference, pp. 44-53, 1985.

Shafer, B.A., and Huddleston, J.M., "Analysis of Seasonal Volume Streamflow Forecast Errors in the Western U.S.," A Critical Assessment of Forecasting in Western Resources Water Management, American Water Resources Association, pp. 117-126, 1984.

Wallace, J.M., and Gutzler, D.S., "Teleconnections in the Geopotential Height Field during the Northern Hemisphere Winter," Monthly Weather Review, 109:813-829, 1981.

Yarnal, B., "Extratropical Teleconnections with El Niño/Southern Oscillation (ENSO) Events," Prog. Phys. Geogr., 9:315-352, 1986.

Yarnal, B., and Diaz, H.F., "Relationship Between Extremes of the Southern Oscillation and the Winter Climate of the Anglo-American Pacific Coast," Journal of Climatology, 6:197-219, 1986.

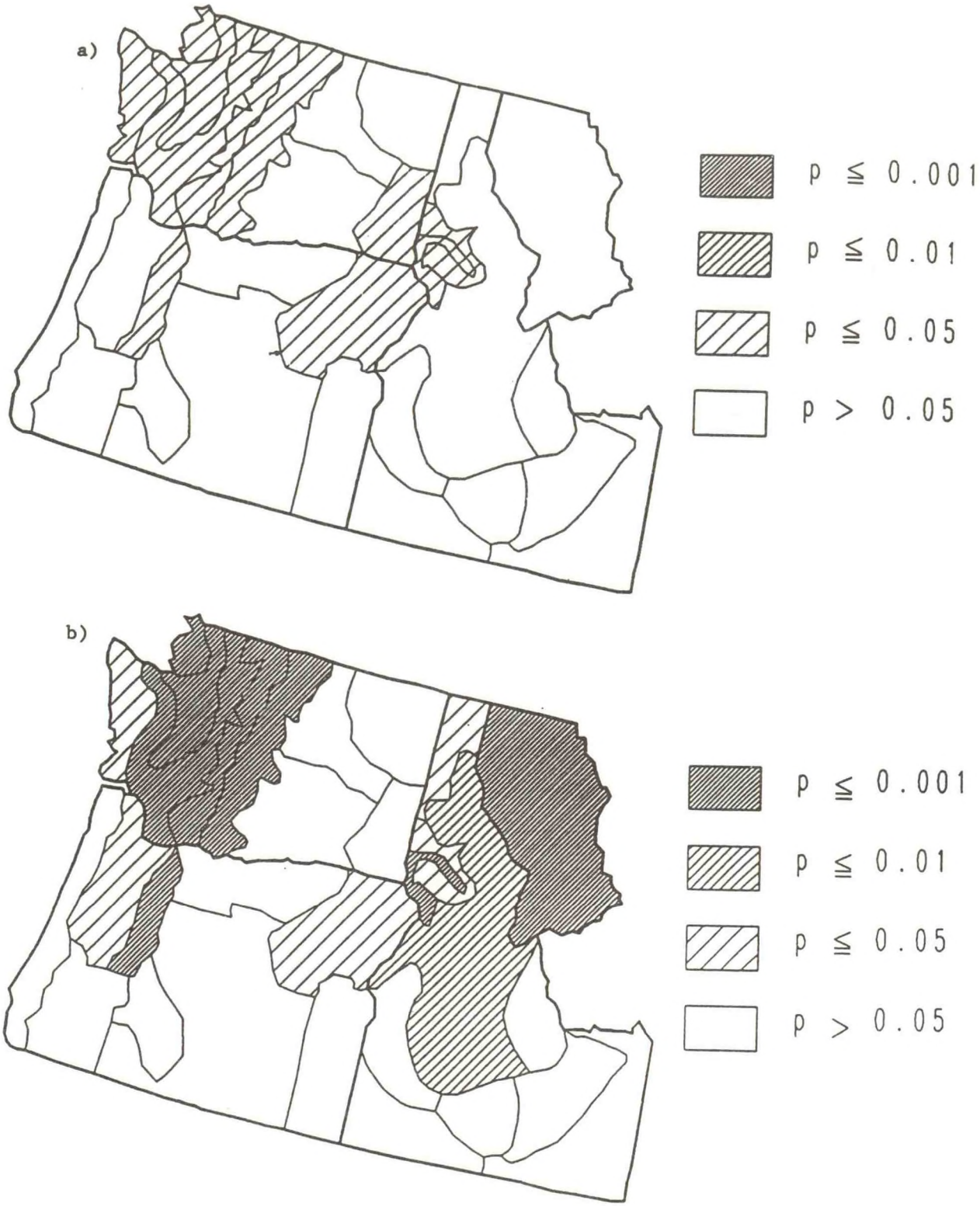

FIGURE 1. Correlation coefficients of (a) fall precipitation and (b) winter precipitation with summer averaged SOI.

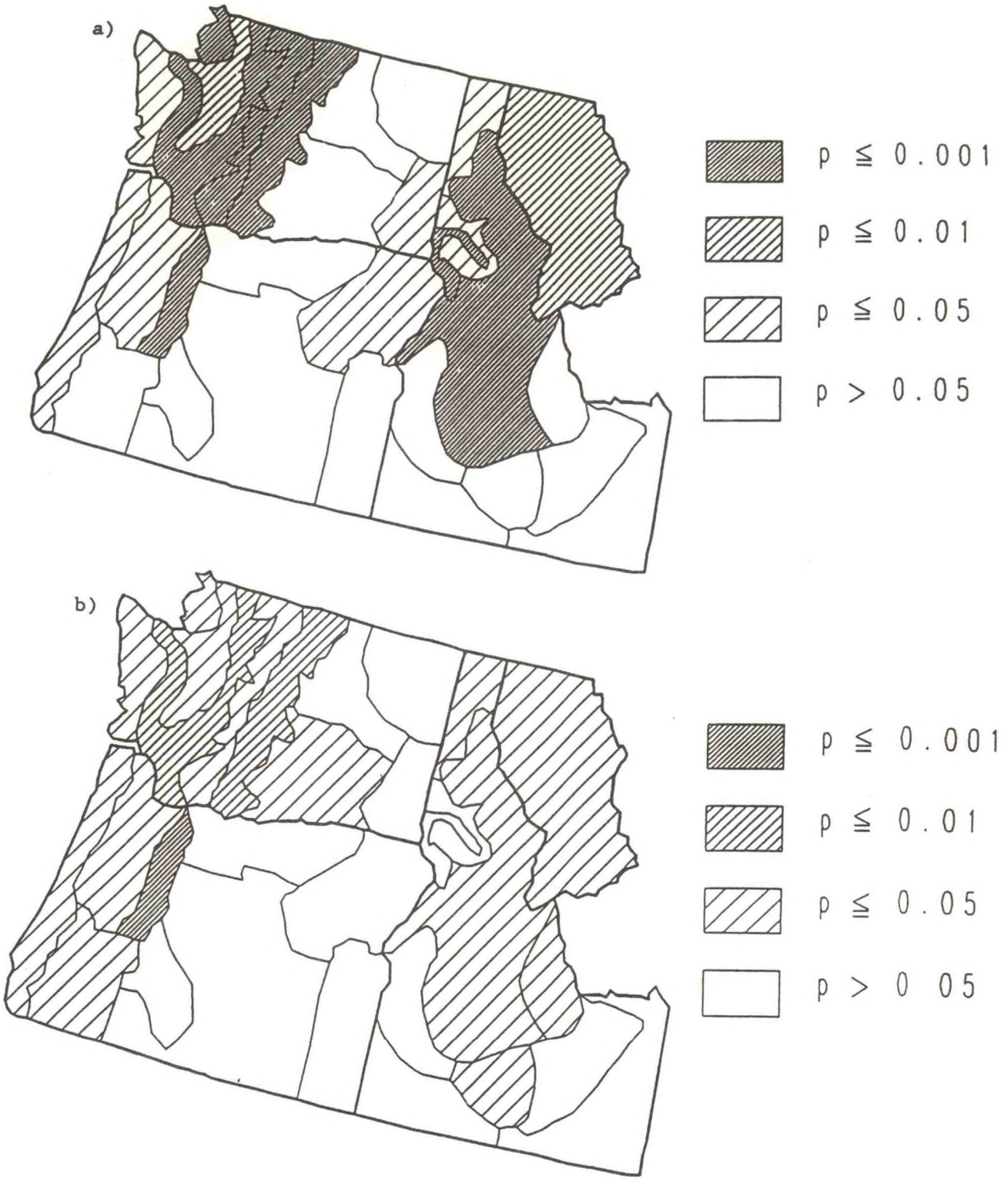

FIGURE 2. Results of the split sample test on the mean of (a) winter and (b) annual precipitation

FLOOD FORECASTING SYSTEM ON MICROCOMPUTER

Zhang Gongsu, Zhu Xingming, Yang Xiaoliu, An Bo, Zhou Senlin
Institute of Water Conservancy and Hydroelectric Power Research (IWHR)
Beijing, China

ABSTRACT. This paper presents a microcomputer based flood forecasting system for using advanced flood forecasting models with subsystems for historical and real-time hydrologic data processing using the principle of a relational data base. The forecasting models were calibrated using computer optimization and manual adjustment. Furthermore, time series analysis techniques were employed for updating the model. The parameters of the model were estimated on-line and off-line by the least square method. Rainfall and water regime could be displayed on color monitor. The complete system, including four subsystems of data processing, model calibration, forecasting calculation, and real-time correction, was developed using macroassembly and FORTRAN language on a microcomputer. Application of the system at the Huang Long hydropower station, Hubei Province is presented as an example.

This system has been applied to nine other catchments in China. It has been shown that the system has performed satisfactorily and has provided both economic and social benefits.

I. INTRODUCTION

China is a country located in middle latitudes with heavy storms causing floods with sharp rises and falls of rivers in mountain areas. In the Hai River and upstream areas of the Huai River, catastrophic floods occurred in 1963 and 1975, respectively, resulting in heavy losses of life and property. In upstream areas of the Han River, two generating units of the Huang Long Tan

hydropower station were out of operation for 2 months, due to the flood of June 1980. In order to control floods and mitigate flood disasters, the automatic hydrologic telemetering and forecasting systems are under construction in major reservoirs and hydropower stations, such as Dan Jian, Lu Shui, Huang Long Tan, and Bai Shan, and important flood control reaches of rivers, such as the Jing Jiang area of the Yangtze River, San Hua area of the Huang River, and the Pu Yang River in Zhejiang Province.

The telemetering and forecasting system consist of data collection and forecasting. The real-time information of rainfall and water stage (or discharge) can be collected, transmitted, and received through the telemetering system developed for the catchment or through the postal and telecommunications service. The flood forecasting component includes hydrologic data processing, model paramter calibration, real-time forecasting, and forecast adjustment. This paper describes the forecasting system.

Flood forecasting and regulation, as a major measure of water conservancy and hydropower projects, plays an important role in construction and operation of the project. It is a necessary measure for water management and the eyes and ears of flood control. Therefore, it has obvious economic and social benefits.

Hydrologic techniques and methods have made rapid progress in recent years. The application of advanced computer techniques and remote sensing techniques from the electronics industry are breakthroughs in information acquisition and forecasting. This has resulted in improved forecast accuracy and lead time.

Advanced techniques from other areas have been used in this paper (e.g. on-line model identification, time series analysis, relational microcomputer data base, etc.). The emphasis is on the expansion of the advanced forecasting models. The four functions of data processing, model parameter calibration, real-time forecasting, and updating procedures have been developed on microcomputers. This complete flood forecasting system is designed and applied to flood control operation of large and medium size reservoirs and hydropower stations.

II. SYSTEM COMPONENTS AND FUNCTIONS

The flood forecasting system and system software was developed on microcomputers. Based on the real-time rainfall information on the catchment, it can forecast the discharge (or water stage) hydrographs of major flood control sections, large and medium size reservoirs, or hydropower stations. It can then promptly provide optimum schemes for flood regulation to assist departments responsible for flood analysis and decision making.

This system consists of hardware, system software, and application software and is operated on a Great Wall 0520, IBM-PC/XT, AT, and compatible computers with DOS (MS, PC, and CC). In order to use the system efficiently, a data base management system was developed. To speed up the operation, the computer system was equipped with MC 8087 or MC 80287. In addition, computer system functions were developed, such as relational data base and program language, a graphics package, Chinese Word Star, and a high-level FORTRAN compiler.

The application software of the system includes the following two parts:

1. design of flood forecasting scheme,
2. on-line real-time flood forecasting.

The operating flow chart is shown in fig. 1.

The major system functions are as follows:

1. Reception (or telegram translation) -- real-time data (rainfall and/or water stage) storage, and rainfall and water regime display by graphs and tables on the computer screen.
2. Original data preprocessing -- classification, verification, modification, and interpolation of miscellaneous hydrologic data.
3. Operation of flood forecasting model to forecast the forthcoming flood (including flood peak, duration, etc.).
4. Updating procedure -- real-time correction according to the real-time observed values; flood forecast dissemination or flood warning issuance.
5. Optimum flood control and regulation scheme -- based on the forecast hydrograph and the flood control rules of the project, the flood control and regulation scheme is optimized to guide operational decision making.

6. Off-line parameter calibration -- the parameter calibration of the flood forecasting model based on the historical hydrologic data.
7. Arrangement of original data -- printout of forecasting procedure and flood regulation schemes.

III. FLOOD FORECASTING METHOD

A. Flood Forecasting Model

In humid and semihumid regions of China, the Xinanjiang Model characterized by three water sources (fig. 1) is widely used. In the computing process, it divides the catchment into different subcatchments and calculates the losses for different layers along the depth. Therefore, it has the advantages of clear conception, reasonable structure, convenient parameter calibration, and high accuracy. This model is the basis of the flood forecasting system.

In order to develop the system functions, the traditional and adaptable API model was employed, and the unit hydrograph was improved. Different unit hydrographs are used for the different effective rainfall intensities on the basis of the Nash Unit Hydrograph and Lab method (fig. 2). The effective rainfall was obtained using the numerical interpolating method from the rainfall-runoff relationship. The software, from data preparation (including separation of multiple peak flood and runoff amount calculation), has been developed in the microcomputer. In addition, the forecasting scheme design, verification of modeling, and real-time forecasting can be operated automatically.

B. Calibration of Model Parameters

Historical hydrologic data are the reflection of rainfall pattern and flood characteristics on a catchment and the basis of determining the parameters of the forecasting model. This system automatically processes the data by computer instead of manually; i.e. the original data, such as rainfall, evaporation, and discharge, can be input, retrieved, modified, inserted, and deleted by using the relational data base management system in the computer. The rainfall data can be simulated and interpolated by using a FORTRAN 77

computer language program. The discharge can be transformed from water stage by using stage-discharge relation. The final objective of data processing is to form the rainfall and runoff data to be used by the programs for model parameter calibration for each subcatchment. At the same time, graphs and tables can be printed out for data management.

A method to combine computer optimization with manual adjustment was adopted for model parameter calibration in the system. The observed rainfall, discharge, and evaporation data are the inputs, and the discharge hydrograph at the control section of the catchment is the output. When the objective function is chosen, the optimization process implies that the parameters of the model are altered successively until the computed and observed outputs agree as much as possible.

In this system, nine parameters of the Xinanjiang Model were classified to three groups according to their effects on the model and physical significances. That is, ratio K of the catchment's evapotranspiration capacity to evaporation from water surfaces; catchment's average storage capacity WM and free water storage capacity SM; and specific yield KSS and KG of surface water and ground water, recession coefficient KKSS and KKG, etc. Different optimization methods and objective functions were used for different groups of parameters in the system controlled by the main program, e.g., 0.618 method and constrained Powell method. This is called the grouping technique of optimization. This technique has the advantage that the parameters and the structure of the model are coordinate. In order to save operating time and make the parameters reasonable, the initial values of the parameters were determined by trial-and-error method. In addition, constrained conditions were used in the optimizing process to avoid the unreasonable hydrologic parameters.

When the parameters are calibrated, that is, the forecasting scheme is determined, the calibrated and verified results, such as flood peaks, volumes, and flood-to-peak times of historical hydrologic events, will be output on the printer to provide the scheme evaluation. Generally speaking, the results obtained by computer optimization are better than those obtained by manual trial and error, but, sometimes there are large errors. In this case, the

adaptability of the model and the representativeness of the hydrologic data in time and space need careful analyzing.

Because storage capacity is limited on the microcomputers, only data for 1 year can be treated at one time. Hence, the synthetic study on the parametric values obtained for each year is required to find out the regularities of the parameters and to improve the forecasting model.

C. Real Time Forecasting

The real-time information of a storm flood event can be transmitted to the front-end processor by a communications system, such as wire, wireless, and satellite communication. This information is then transmitted to the real-time data base after code conversion and coding check. Furthermore, the real-time information of rainfall and water regime can be retrieved and displayed on the computer screen, e.g., color displays of rainfall from each gage station; rise and fall of water elevation; and comparison displays of observed, forecasted, and updated discharge hydrographs.

It is well known that a hydrologic model of a catchment is a way of forecasting runoff from rainfall by means of hydrologic simulation techniques. Because of the measurement errors of the input and output information and the difference between the model structure and the real hydrologic phenomena, errors between forecasted and observed values inevitably occur in real-time forecasting. Eliminating or minimizing the errors is a very important task. Since rainfall information and water regime are collected automatically and transmitted rapidly to the flood forecasting system, the forecast accuracy can be manifestly improved by employing the updating procedure.

The updating technique in the system is essential for improving the adequacy of deterministic models such as the Xin An Jian Model. On this premise, the actual forecast consists of two parts. The major part is the deterministic part computed by the deterministic model; the second part is the updating part. In general, when a deterministic model is used in an actual forecasting situation, it will have an updating procedure that uses the forecast errors already observed in recent forecasts to modify the forecast about to be

made. The updating formula used in the system is an N order of an autoregressive (AR) model obtained by a time series analysis method (on-line or off-line recurrence method) from the error series between computed and observed discharges (or stages). The principle and formulation of this method and calculation can be found in Zhang et al. (1987).

Our forecasting experience indicates that, if the deterministic model is associated with the above-mentioned updating procedure, the results can be improved. In whole flood forecasting systems, the adequacy of the deterministic model is the first consideration, and updating the model is the second.

IV. APPLICATION OF THE SYSTEM

The flood forecasting system is a major part of the automatic telemetering and forecasting system of hydrologic information for Huang Lon Tan Hydropower station in Du He catchment, Hubei province. In the automatic system, there are 24 telemetering raingages, 5 telemetering stage stations, 3 relay stations, 1 data collection center, and 1 forecasting and regulation center. The forecasting and regulation center is located in the hydropower station. All data are automatically transmitted and relayed to the center by UHF radio, as shown in fig. 2.

The catchment area is 11,400km^2 with a river length of 293km and average slope of 15 percent in the upper reach, 3 percent in the middle reach and 1 percent in the lower reach. Most areas in this catchment are covered with forests, bushes, and weeds. Because of the varied topography, complex rainfall patterns, and unrepresentative distribution of the station network resulting from poor transport facilities, the representativeness of hydrologic data in the spatial distribution is inadequate.

Storm flood data during the years 1975 to 1980 have been used for data input, processing, model parameters calibration, and simulation of real-time updating procedure. The data from 1981 to 1984 have been used for verification. The results are shown in table 1.

Table 1 The Parameter Calibrating Results of Xin An Jiang Model with Three Water Sources

(Station: Zhu Shan in Du He catchment, Area: 9051 sq.km.)

occurred date and time	rainfall (mm)	observed runoff (mm)	computed runoff (mm)	observed flood peak (m^3/s)	computed flood peak (m^3/s)	volume error (%)	peak error (%)	time error of flood peak (time interval)
1981 4 17 8- 4 21 2	51.4	39.8	41.5	2930	3097.0	4.3	5.7	0
1981 7 14 8- 7 16 20	34.8	13.4	12.2	1230	1167.7	-8.5	-5.1	-2
1982 7 16 2- 7 19 14	97.6	51.7	56.7	3350	3956.9	9.5	18.1	0
1982 7 20 2- 7 24 17	148.2	124.5	133.2	4680	5136.7	7.0	9.8	0
1982 8 23 14- 8 27 5	50.6	48.3	48.2	2950	3508.6	-0.2	18.9	-1
1982 9 30 14-10 5 14	33.9	36.2	33.9	1760	1559.3	-6.2	-11.4	-1
1983 7 10 2- 7 13 2	41.7	27.6	29.1	2200	2185.3	5.4	-0.7	0
1983 7 21 11- 7 25 2	73.5	51.9	60.4	2830	3863.1	16.3	36.5	-2
1983 8 22 2- 8 24 14	33.3	25.7	28.3	2380	2513.8	10.1	5.6	-1
1983 9 15 11- 9 18 2	62.0	40.8	54.4	4160	5202.6	33.2	25.1	0
1983 9 21 23- 9 25 14	45.1	30.8	36.1	2680	3086.2	17.2	15.2	0
1983 10 4 17-10 9 2	106.2	88.1	91.4	4950	4650.1	3.7	-6.1	0
1983 10 18 2-10 21 14	61.5	52.3	55.5	4090	4242.0	6.1	3.7	-1
1984 6 12 11- 6 16 8	84.7	50.1	35.8	2200	1884.1	-28.5	-14.4	-4
1984 7 6 20- 7 9 5	43.0	33.9	32.5	4060	3281.5	-4.0	-19.2	0
1984 7 23 20- 7 28 17	96.1	60.6	57.9	4900	5308.3	-4.5	8.3	-1
1984 8 5 20- 8 7 23	27.3	13.9	17.5	1450	1801.1	26.3	24.2	1
1984 8 27 17- 8 31 23	71.7	24.1	27.5	1400	1406.9	14.1	0.5	-1
1984 9 9 11- 9 12 23	69.1	31.6	37.2	1490	1781.2	17.9	19.5	4
1984 9 23 23- 9 29 8	98.7	68.9	63.8	2380	2288.9	-7.4	-3.8	0

The system was tested in flood periods in two stages. From June to Sept. of 1987, the performance of the system was examined by using the information from water regime telegram. From May to Sept. of 1988, pilot forecasts of systems were made by using the information from telemetering and telegrams as shown in table 2. Table 2 shows that most computed values are correspondingly smaller than observed values. This is because the rainfall was not estimated and some telemetering information had not been received.

The above-mentioned tests for some medium and small flood events show that the system performs normally, and the expected forecast accuracy is obtained.

This system has been applied to hydropower stations -- e.g., An Sha, Fu Chan Jiang, and Liu Xi He -- and some major flood control river reaches and catchments -- e.g., Pu Yang River and Gui River -- altogether, in nine regions of China. In general, the forecast accuracy is increased in comparison with the original forecasting scheme. In addition, lead time of the forecast is improved, therefore, providing increased economic benefit.

V. CONCLUSION

The flood forecasting model is a major part of the flood forecasting system. Because this system is "on-line" and "real-time", only forecasting models, such as the Xinanjiang Model with three water sources, cannot meet the requirements for forecast services. Hence, it is necessary to improve and expand the models, using the techniques of historical or real-time data input of the forecasting model, automatic calibration of the model parameters, and forecast updating. In the process of system development, we pursued studies of flood forecasting techniques and new techniques of other fields. The purpose is to further improve the techniques and practicability of flood forecasting, so as to satisfy the increasing needs of flood control modernization.

The system software is designed for automatic telemetering and forecasting. If, on the other hand, there is no such automatic system in a catchment, telecommunications information of water regime can be input to the flood forecasting system with the help of telegram translation software or by keyboard entry. When developing the flood forecasting scheme by using

Table 2 The Real-time Forecasting Results for Zhu Shan Station in Du He Catchment

occurred date	observed flood peak (m^3/s)	computed flood peak (m^3/s)	updated flood peak (m^3/s)	computed error (%)	updated error (%)	time error of flood peak (time interval)	remarks
1987 8 28	1744	1650	1755	-5.3	-0.6	0	Telegram information
1987 7 6	4842	3802	4658	-21.5	-3.8	0	
1987 8 25	1757	1590	1693	-9.5	-1.3	-1	Telemetering and
1987 8 28	1110	978	1038	-11.8	-6.5	0	telegram information
1988 5 8	1150	993	1168	-13.0	-1.0	0	Information from central
1988 5 8	1420	1228	1344	-14.0	-5.3	-1	office of flood control & telemetering information
1988 8 20	1400	1155		-17.5		-2	
1988 9 2	584	565		-3.4		0	Telemetering information
1988 9 9	632	638		-0.9		0	
1988 9 13	4000	3090		-22.5		0	

* Table 2 shows that most computed values are correspondingly smaller than observed values. It is because the forthcoming rainfall was not estimated and some telemetering information had not been received.

historical hydrologic data, users can directly run relevant blocks by a menu-type program. According to relevant literature, computer generations currently tend towards both large scale and microscale. In a sense, a microcomputer is close to minicomputer with moderate storage. In addition, man-machine interaction systems in Chinese and western languages, data base management systems, and some high-level program language compilers are loaded in the computer. It has statistical, tabulation, and drawing functions. Its maintenance is very simple and it is inexpensive. Hence, it is predictable that microcomputers will be widely used in water resources and hydrology. Our experiences indicate that, in the process of on-line flood forecasting, microcomputers are manifesting their superiorities each passing day.

REFERENCES

Chen, J.Q., and Zhang, G.S., "Storm Flood Computation for Small Catchments," Water Conservancy and Electric Power, Beijing, China, 1984.

Zhang, G.S. et al., "Real-Time Correction to the Deterministic Flood Forecasting Model," Hydrology, No. 1, Beijing, China, 1987.

Zhang, G.S. et al., "Preliminary Practice of Rainfall and Flood Data Processing on the Microcomputer," Hydrology, No. 1, Beijing, China, 1988.

Zhao, R.J., "Hydrologic Modelling on Catchment," Water Conservancy and Electric Power, Beijing, China, 1984.

Zhu, X.M. et al., "Study on the Method of the Hydrologic Model Parameter Optimization Fitting," Collected Research Papers, No. 28, Institute of Water Conservancy and Hydroelectric Power Research (IWHR), Beijing, China, 1988.

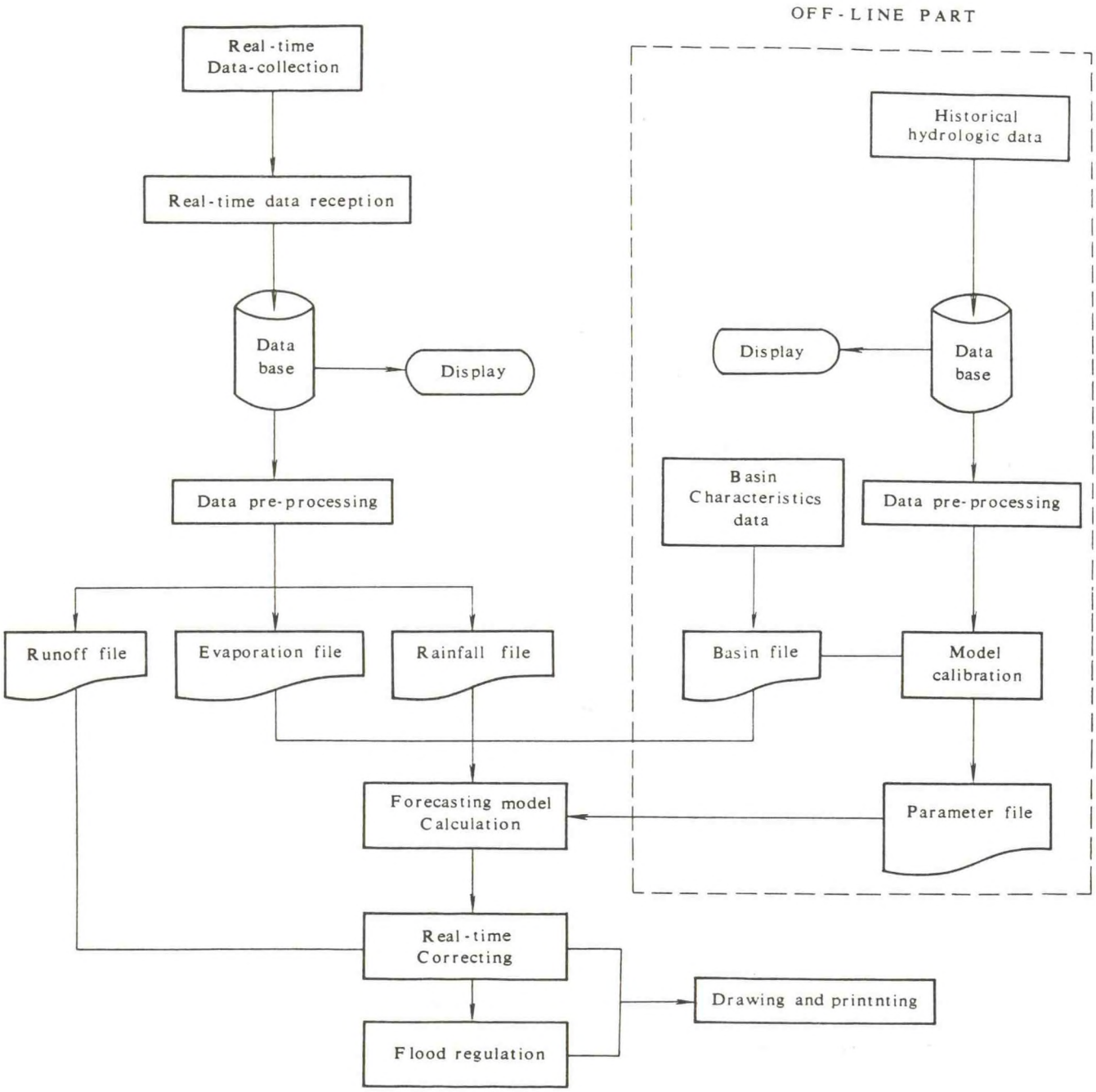

Figure 1 Flow-chart of Flood Forecasting System

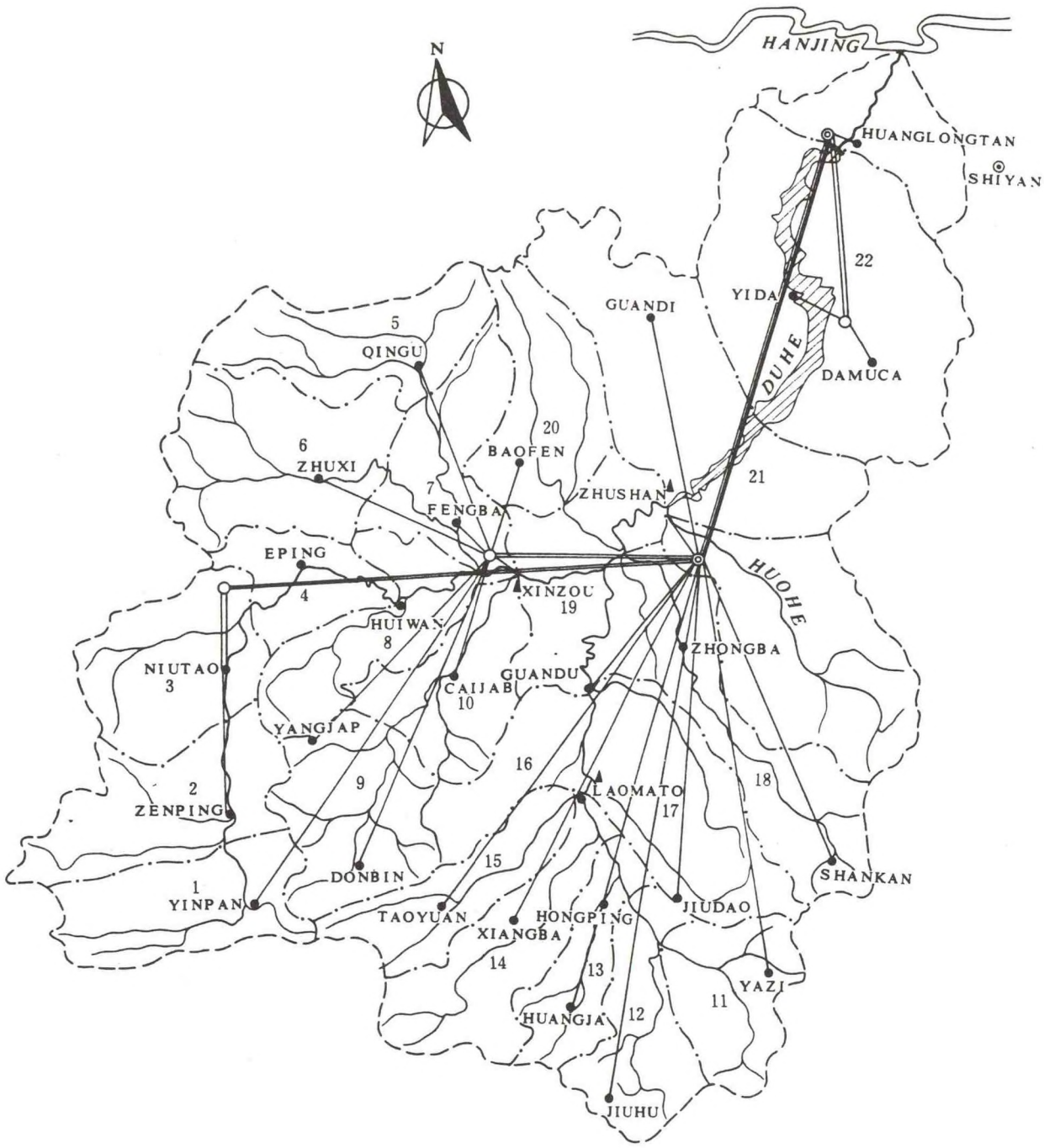

● Telemetering raingauge ○ Relay station

▲ Telemetering stage station ◎ Data collection center

Figure2 The Sketch Map of the Automatic Telemetering System of Hydrologic Information for Huang Long Tan Hydropower Station

AUTOMATED DATA ACQUISITION TECHNIQUES FOR FORECASTING PACIFIC NORTHWEST RIVERS

Phillip A. Pasteris
Northwest River Forecast Center, NWS
Portland, OR 97209

Robert K. Hartman
West National Technical Center, SCS
Portland, OR 97209

ABSTRACT. The 1200-mile Columbia River is one of the world's most managed rivers. A critical balance of many elements (power generation, fish passage, flood control, etc.) hinge on real-time forecasts of seasonal volumes and the resulting runoff. Forecasts require extensive data, most of it received and processed automatically from a wide variety of sources (radio, telephone, satellite, and meteor burst). A network of minicomputers throughout the Pacific Northwest gather this information and transmit it to a regional data base named the Columbia River Operational Hydromet Management System (CROHMS). CROHMS contains both observed and forecast data in coded, plain language, and graphical formats which provide users with a real-time portrait of Columbia Basin water management activities.

The National Weather Service (NWS) River Forecast Center (RFC), as part of an interagency agreement, uses CROHMS to produce real-time river forecasts for efficient water management. The CROHMS computer facilitates the interactive updating of model initial conditions and reservoir regulation by several agencies. After proper review and coordination, forecasts are made available to cooperating agencies.

This paper focuses on the evolution of data acquisition techniques in the Pacific Northwest and their impact on forecast operations.

I. INTRODUCTION

Recent breakdowns in data collection systems technology make vast quantities of real-time hydrometeorological information available to aid in forecasting and water management. Many of these systems are "turn-key" and fulfill the unique needs of an individual agency. These agencies are, more often than not, part of a large "water management mosaic" whose charge is the efficient operation of an entire river system. The Columbia River is such a system.

Management of this system requires extensive data, most of it received and processed automatically from a wide variety of sources. Access to this pool of data is provided through the use of the Columbia River Operational Hydromet Management System (CROHMS) data base.

The existence of CROHMS is largely due to agency agreements to standardize the identification and transmission of data from their unique data collection systems to CROHMS (Speers, 1980).

The purpose of this paper is to document the National Weather Service's (NWS) role in the evolution of automated data collection in the Pacific Northwest, including identification, transmission, and use of the hydromet data in an interagency data base for forecasting and management of the Columbia River.

II. THE WEATHER SERVICE ROLE IN DATA COLLECTION AND FORECASTING

A. The Historic Need for River Forecasts

The backbone of water management is the real-time accounting of the hydrologic cycle components; precipitation (basically rain and snow) and runoff (streamflow). The NWS is a lead agency in the collection of precipitation data through its National Climate program. The Soil Conservation Service (SCS) measures snow water equivalent by monitoring a large network of snowcourses. The U.S. Geological Survey (USGS) maintains a nationwide network to measure streamflow.

In the beginning, these networks independently recorded data on site. Agency personnel periodically retrieved the information and transmitted it by

mail to an archive center. All the data required for effective water management was available but segregated and unavailable in real time.

During the 1930's and 1940's, rapid increase in population, expansion of cities toward the flood plain, development of hydroelectric power, and flooding produced by extremes in weather led Congress in 1948 to designate NWS as the agency with sole authority to issue flood forecasts (NOAA, 1976).

Issuance of timely flood forecasts required "automation" of many network sensors.

B. Early Methods of Automated Data Collection in the Pacific Northwest

Early equipment used to automate river and rainfall data included: telemarks, which provide instantaneous basic decimal encoding and telemetry for audible reporting of water level and precipitation, and binary digital transfers (BDT) which, when used with an analog digital recorder (ADR), provide a means to electronically store and transmit audible water level and precipitation information. These audible "beeps" were transmitted over phone lines, "counted" by the person dialing the gage, transcribed to any number of convenient formats, and transmitted by teletype to the Northwest River Forecast Center (NWRFC).

Snow water equivalent data would be manually measured with a snow tube, phoned to the local NWS office, and then be relayed by teletype to NWRFC.

When a transmission was received by NWRFC, it was then transcribed and encoded for use in the computer forecast model. The resulting forecasts were then transmitted to NWS offices via teletype for public dissemination. The entire process is shown in fig. 1.

Decoding, transcripting, and encoding the data were the most time-consuming parts of this process. It took the application of minicomputer technology to significantly reduce data acquisition and dissemination time requirements at NWS offices.

C. The Role of the Minicomputer in Data Collection

Within the Columbia Basin, the NWS operates five minicomputers for automated data collection. They are located in Portland and Heppner, Oregon; Seattle, Washington; Boise, Idaho; and Great Falls, Montana. These minicomputers collectively data base approximately 350 sensors and have significantly reduced the time involved in data acquisition and transmission.

The fundamental advantages of minicomputer use in data collection are as follows:

- Ability to interrogate gages quickly and repetitively,
- Concurrent collection of dissimilar data and sensor types,
- On-site data base storage and display of up to 200 stations,
- Ability to receive and transmit data from other computers,
- Alarm/Alert "bell and whistle" message generation when user specified criteria are exceeded.

The minicomputer can more accurately interpret a wide variety of sensor types and transmission formats. Some of these include:

- Audio BDT and Telemark phone gages,
- Devise for Automatic Remote Data Collection (DARDC), Limited Automated Remote Collector (LARC) "ASCII" phone gages,
- "EVENT" radio gages,
- Standard Hydrologic Exchange Format (SHEF) encoded Geostationary Operational Environmental Satellite (GOES) data transmitted over a dedicated telephone line.

In the operational environment, the minicomputer would auto-dial river and rain gages via telephone at any user-specified interval. Also, as required, ad hoc polling of a gage(s) could be initiated manually. Concurrently, the minicomputer would monitor designated channels for "random" data transmissions.

Random transmissions include radio signals from any "EVENT" type radio gages. "EVENT" type radio signals are generated whenever specific criteria (tip of a tipping bucket, user-specified rise of fall in a river) are exceeded. The station identifier and data value are then transmitted by radio, received at the minicomputer site, decoded, and filed in the local data base.

The concept of real-time, random, event reporting is part of the NWS-supported Automated Local Evaluation in Real-Time (ALERT) (NOAA, 1981), which enables analysis on-site by local communities to allow rapid response in flash flood areas.

Another type of random transmission is GOES satellite data which requires computer-to-computer communications. Currently, a USGS down-link computer in Tacoma, Washington, transmits Mt. St. Helens GOES data to the minicomputer located at the Weather Service Forecast Office (WSFO) in Seattle, Washington. The Seattle minicomputer decodes and combines this information with radio and phone data into a comprehensive picture of water information in the State of Washington. A typical local display of this information is shown in fig. 2.

It can be seen that a minicomputer data base can aid in the display of a wide variety of sensors and stations to present a "snapshot" of water information over a large area. Should a user specified criteria be exceeded at any sensor, an alarm/alert "bell and whistle" message would be generated of the type shown in fig. 3.

Appropriate action will be taken which may include issuance of flash flood warnings.

D. Transmission of Data from Minicomputers to the NWRFC and CROHMS

Minicomputer data can be transmitted to the NWRFC in two methods. These methods are:

1. Transmission of a visually recognizable format over NWS Automation of Field Operations and Services (AFOS) data circuits. AFOS is a nationwide network of minicomputers and telecommunication equipment installed at approximately 200 NWS sites in the continental United States as shown in fig. 4.

2. Telephone polling by the NWRFC Gateway computer, which maintains a large data base and has the ability to dial and retrieve data from a wide variety of computers. These include the NWS minicomputers and the SCS snowpack telemetry (SNOTEL) computer. The SCS SNOTEL computer receives remote reports of snowpack conditions from nearly 600 stations throughout the western United States. The information is relayed from the remote site using meteor burst technology to two base stations computers, then transferred to the main computer in Portland, Oregon.

In both cases, the data ends up in CROHMS Automated Front End (CAFE) and ultimately the CROHMS mainframe data base. Figure 5 is a complete schematic of NWRFC involvement in CROHMS data collection and transmission.

Access to the CAFE by nongovernmental agencies is controlled by the Corps of Engineers (COE) North Pacific Division. The CAFE can be likened to a very large "in-basket" having preallocated slots for each agency's data. At least once per hour, the CROHMS mainframe computer scans CAFE for new data. When new data is detected, a computer program "posts" the information to the CROHMS data base.

A complete diagram of all agencies transmitting data to CROHMS is shown in fig. 6.

Hydrometeorological information is now available for the generation of reports in tabular (fig. 7) or graphic (fig. 8) formats or as input to any number of forecast models.

NWRFC transfers data directly from CROHMS to the Streamflow Synthesis and Reservoir Regulation (SSARR) model to generate river forecasts. The SSARR model is run interactively on the AMDAHL computer and the resultant forecasts are transmitted to AFOS. Figure 9 is a SHEF coded forecast.

III. IDENTIFICATION AND TRANSMISSION OF HYDROLOGIC DATA

A key element to retrieval of data and forecast generation using CROHMS, or any other data base, is data identification. Without clearly defined rules for data identification, a data base will become nonfunctional and ultimately abandoned.

The NWS, in cooperation with the COE North Pacific Division and several other water management agencies, have developed SHEF to meet both external (transmission) and internal (data base) identification requirements in a thorough manner with application for a broad spectrum of observational data, processed data, and forecast products. The code has received broad acceptance in the water information and management community.

A. Historical Development

The SHEF code has been built to a great extent on the foundation of 20 years of experience with the Columbia Basin Teletype (CBTT) code (U.S. Army, 1976) and, to a lesser degree, on the U.S. Weather Bureau Code (U.S. Department of Commerce, 1961). In efforts to design a multiple-use data system for CROHMS, many requirements of data base structure and data descriptions became evident (Bissell and Davis, 1980). A fair level of sophistication is required to handle data which may be telemetered or manually observed, screened, or unverified, forecasted, flagged for particular purposes, evenly or randomly spaced in time, in English or Standard International (SI) units, in local or Greenwich time, and so on.

The initial CROHMS data base design to meet many of these needs identified by the NWS and the COE was implemented in 1976. Since that time, the need for further refinements has been seen. Concurrent design of a new data base structure and design of a corresponding external data transmission code were initiated in November 1980 by the NWS and COE for applications in the Pacific Northwest.

In November 1981, and January 1982, national meetings of NWS personnel resulted in an endorsement of SHEF for use on AFOS. A working document of the code was prepared in early 1982 and finalized on November 18, 1982 (Pasteris

1982). Decoding software in FORTRAN and a general description of the decoding function and philosophy are published by Bonnin (1983) and by Bonnin and Cox (1983). Several papers have been written by Bissell (1983, 1984) which describe SHEF and its functional capabilities which are now highlighted.

B. SHEFs Functional Capabilities

1. The most fundamental feature of SHEF is that it is readable by both man and machine.
2. Observational, forecast, and processed data can be transmitted within the same descriptive framework.
3. A wide variety of hydrometeorological parameters are supported which encompass the needs of any agency dealing with operational hydromet data. Parameters can run the gamut from common river and rainfall reports to more exotic items like river ice conditions, fish counts, power generation, and lightning strikes.
4. Station identifiers, up to eight characters, are used to represent stations. Furthermore, reports from nonstandard ("stranger") stations may be located within one-tenth of one degree latitude and longitude.
5. Observations can be expressed in either Greenwich Mean Time (GMT), the default, or local time.
6. SI or English units may be used.
7. A "data descriptor" may be attached to an individual value to show, for example, "estimated" or to flag "suspect" data.
8. A variety of transmission format structures are available to allow the most efficient transfer of different data groups.

C. Structure of Parameter Codes

The parameter code is a string of characters, up to seven, which defines the kind of data represented. In most common applications, two or three characters fully define the kind of data being transmitted, with unspecified data characteristics established by default. The full seven-character parameter code "PEDTSEP" contains six descriptors as follows:

1. PE - Physical Element (two characters). Examples include: (HG) river stage, (QR) discharge, and TA (air temperature).
2. D = Duration code (one character). Examples include: (I) instantaneous, (Q) six-hourly, and (D) daily.
3. T = Type code (one character). Examples include: (R) observed, (F) forecasted, and (P) processed.
4. S = Source code (one character) which further defines the type code. Examples include: (R) land radio, (V) visual, and (G) GOES.
5. E = Extremum code (one character). Examples include: (X) max of day, and (M) min of week.
6. P = Probability code (one character). Examples include: (F) exceedance probability of 0.05 or (T) 0.95.

D. SHEF Formats

The SHEF Version I uses three specifically defined data formats. These are the ".A," ".B," and ".E" (read as "dotA," etc.) formats, named after the first two characters in the message.

1. The ".A" Format: The ".A" format is the most flexible of the SHEF formats. It efficiently transmits data from a single station having multiple parameters and/or unevenly spaced times. An example of a ".A" message with explanatory notes is given in fig. 10.
2. The ".B" Format: The ".B" format efficiently transmits data from a group of stations having the same (or nearly the same) parameters and observation times. A "header" line specifies the parameters and the order in which data appears in subsequent lines of text. The header line has complete flexibility in observation times, time zones, units, order of parameters, and so on, and is fully specified by the user. An example of a ".B" format is given in fig. 11.
3. The ".E" Format: The ".E" format is similar to the ".A" format but allows more efficient transmission of strings of evenly spaced data. Examples would be a time series containing 6-hourly forecasts or

observed data having a 15-minute time spacing between data values transmitted every 3 hours. An example of a ".B" format is given in fig. 12.

E. SHEF Coded Data Transmission Examples

SHEF was implemented by the NWS in 1984. A typical SHEF message transmitted by the Weather Service Office (WSO) in Spokane, Washington is shown in fig. 13.

The message makes liberal use of blanks and comment fields to enhance human readability while allowing computer decoding.

SHEF messages are also easily created by a computer. Figure 14 shows a ".E" format SHEF message containing Mt. St. Helens GOES data encoded by the USGS Tacoma downlink computer. The message contains stage and precipitation information spaced at 15-minute intervals.

IV. SUMMARY

It can be readily seen that the operational use of minicomputers for acquisition and transmission of hydrometeorological data to a central data base, such as CROHMS, is essential and desirable to ensure timely forecasts and efficient water management.

It is also widely known that we have only scratched the surface of computer assisted hydrologic data acquisition and transmission. The tools exist (SHEF, ALERT, SNOTEL, GOES, etc.) to further expand this vital link; let us use them wisely.

REFERENCES

Bissell, Vernon C., "SHEF: What and Why," Fifth Conference on Hydrometeorology, American Meteorological Society, Boston, Massachusetts, 1983.

Bissell, Vernon C., "Standard Hydrologic Exchange Format (SHEF) for Automated Data Transmission," ASCE Hydraulics Division Specialty Conference, Coeur D'Alene, Idaho, August 14-17, 1984.

Bissell, V. C., and Davis, E. M., "Hydromet Data Base for Forecasting Operations," Preprints, ASCE, New York, New York, 27 pp, 1980.

Bonnin, Geoffrey M., "The Posting of SHEF Data to the RFC Gateway Database," NOAA Tech Memo NWS CR-68, U.S. Dept. of Commerce, Kansas City, Missouri, 1983.

Bonnin, G. M. and Cox, R. S., "An Explanation of the Standard Hydrologic Exchange Format (SHEF) and its Implementation in the Central Region," NOAA Tech Memo NWS CR-67, U.S. Dept. of Commerce, Kansas City, Missouri, 1983.

NOAA, Hydrologic Services Division, "ALERT, A Cooperative Flood Warning System for Your Community," U.S. Dept of Commerce, Salt Lake City, Utah, 27 pp, 1981.

Pasteris, Phillip A., "Standard Hydrologic Exchange Format (SHEF), Version I," NOAA Tech Memo NWS WR-180, U.S. Dept. of Commerce, Salt Lake City, Utah, 1982.

Speers, Douglas D., "Columbia River Operational Hydromet Management System, Case Studies of Applied Advanced Data Collection and Management," Aerospace Division, ASCE Task Committee Publication, New York, New York, pp. 337-345, 1980.

North Pacific Division, "CBTT Users Manual," U.S. Army Corps of Engineers, Portland, Oregon, 150 pp, 1976.

Weather Bureau, "River Data Code," U.S. Dept. of Commerce, Washington, D.C., 22 pp, 1961.

National Weather Service, "Weekly Weather and Crop Summary Messages and Associated Reports," WSOM Issuance F-11, U.S. Dept. of Commerce, Silver Spring, Maryland, 1983.

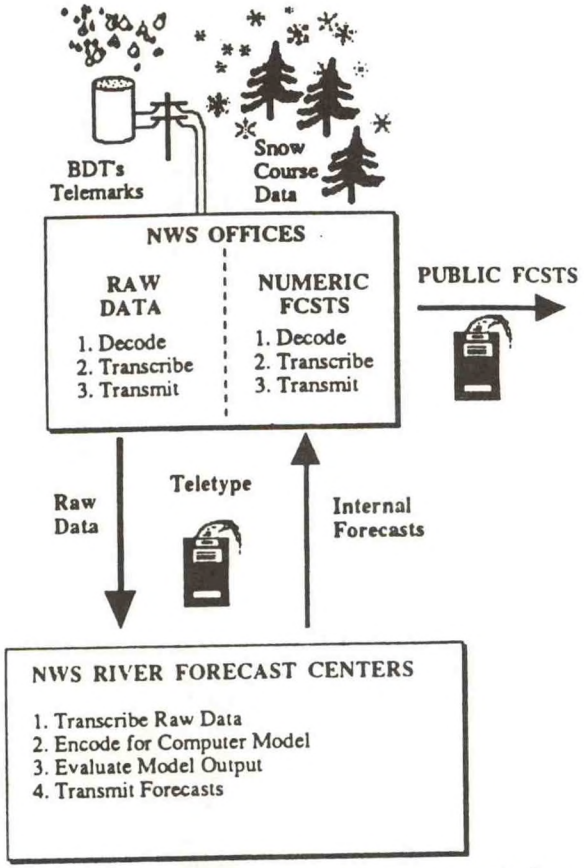

Fig 1. Traditional Data Acquistion, Transmission and Forecast Dissemination

```
NATIONAL WEATHER SERVICE HYDROLOGIC DATA
COLLECTION SYSTEM WSFO SEATTLE, WA
[GROUP #15]  6/8/84 1348Z

STATION #      1       51       58       20
STATION ID   WNMW     CASW      MER     GLAW
PARAMETER    PCIRR    HGIRR     HGIRF    PCIRP
SINCE 1300    0.00    13.60    238.24    0.00
6/8 12-13     0.04    13.52    238.30    0.00
6/8 11-12     0.00    13.48    238.34    1.60
6/8 10-11     0.04    13.40    238.30    0.00
6/8  9-10     0.00    13.32    238.30    0.00
6/8  8-9      0.00    13.28    238.34    0.00
6/8  7-8      0.12    13.20    238.46    0.00
6/8  6-7      0.08    13.21    238.58    0.00
6/8  6-12     0.24    13.60    238.34    1.60
6/8 00-06     0.12    13.24    238.30    1.50
6/7 18-00     0.28    13.24    238.30    1.30
6/7 12-18     0.12    13.24    238.30    1.00
```

Fig. 2. Comprehensive "Snapshot" of Water Information on Seattle Weather Service Minicomputer.

```
ZCZC SEARRASEA
??LOC

ALERT
CRITERION EXCEEDED AT: STN #104
(STAGE)  SNOQUALMIE R NR CARNATION

CURRENT READING: 49.07 AT 21:09 ZULU

SYSTEM DATA: 6/8/84 TIME: 21:10:24

ALARM STAGE=    54.00
ALERT STAGE=    49.00

PLEASE CONSULT YOUR EVENT TERMINAL
MESSAGE SOURCE: WSFO SEATTLE NOVA

NNNN
```

Fig. 3. "Bell and Whistle" message generated by Seattle Weather Service Minicomputer.

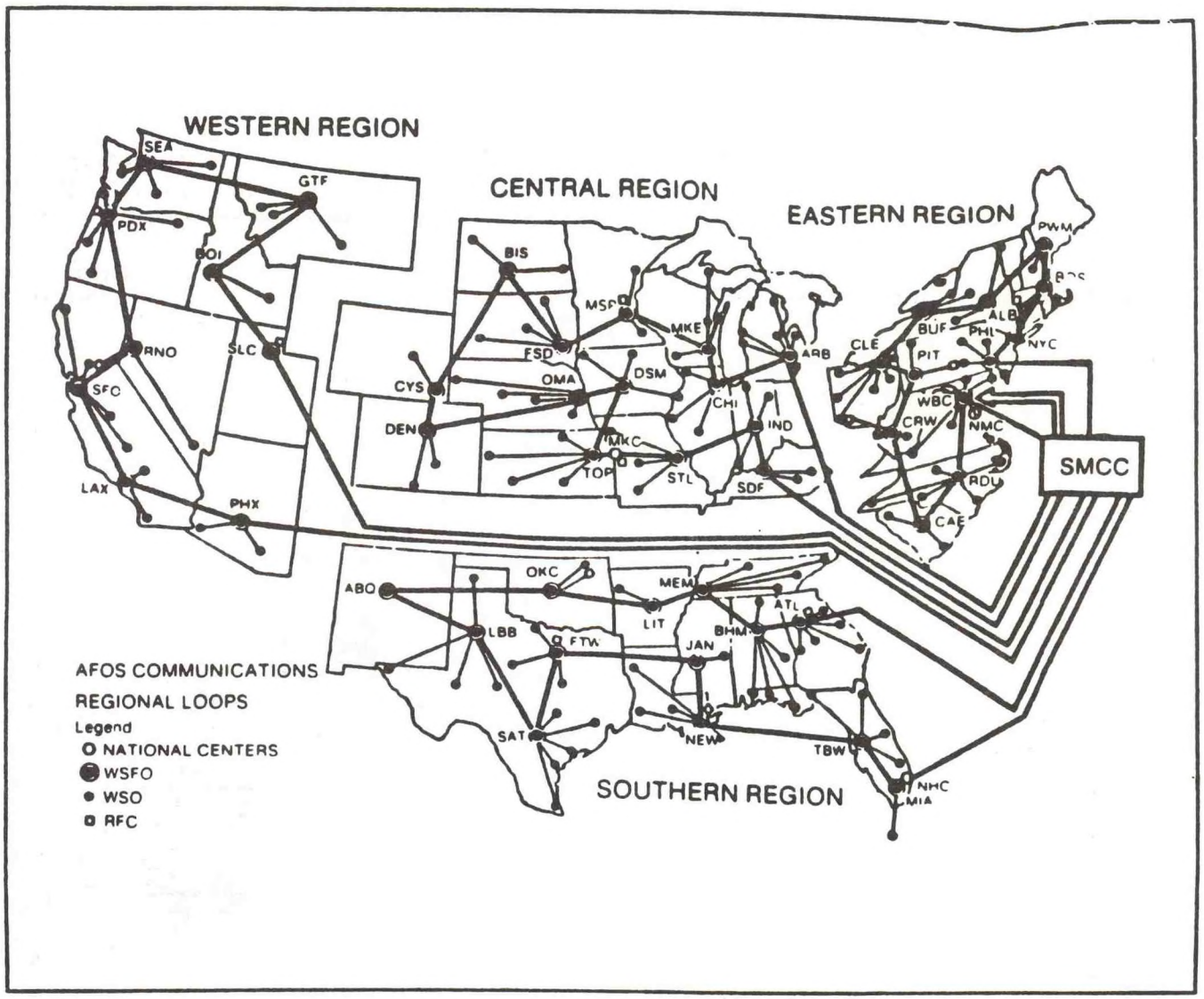

Fig. 4. AFOS Data Distribution Network

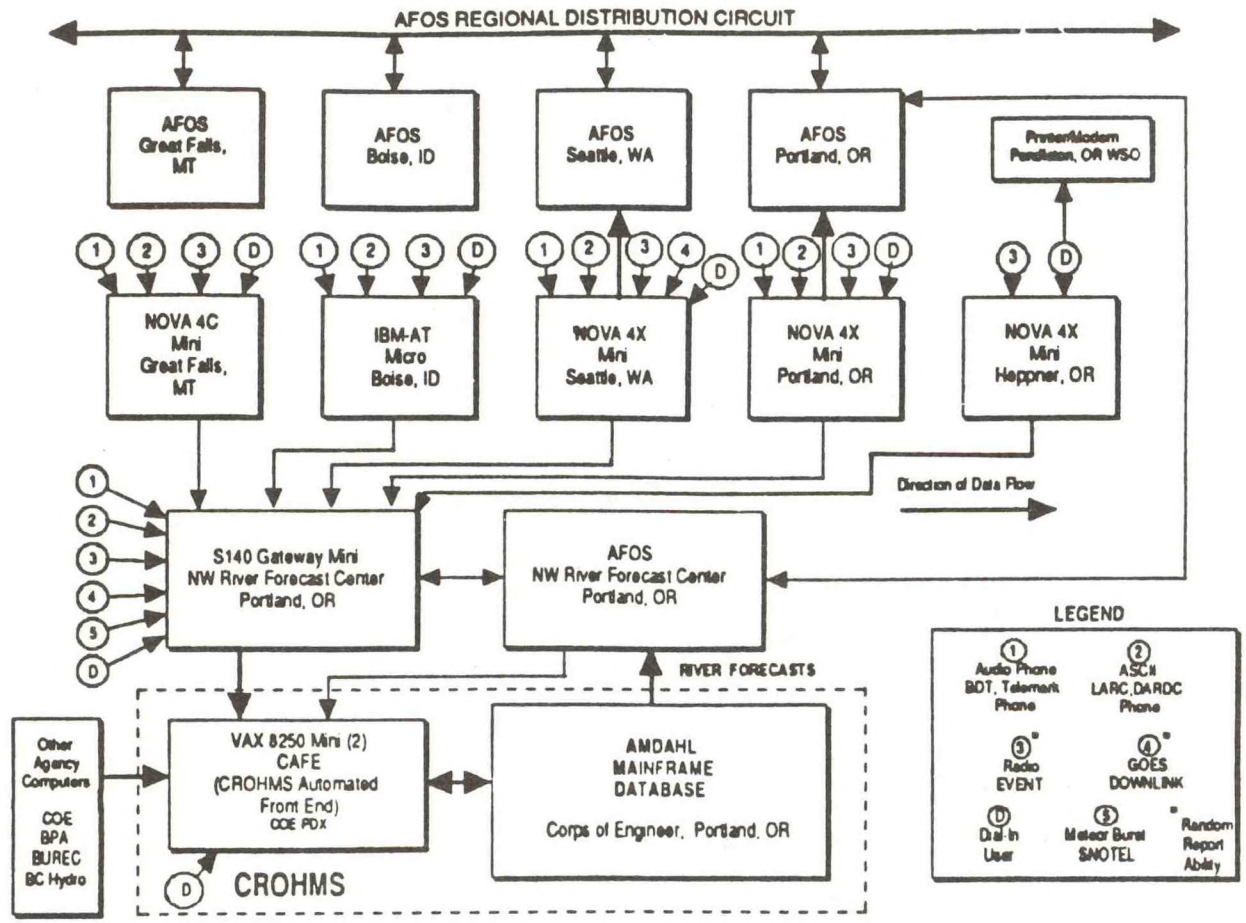

Fig. 5. Schematic of NWRFC & NWS Involvement in CROHMS Data Collection and Transmission.

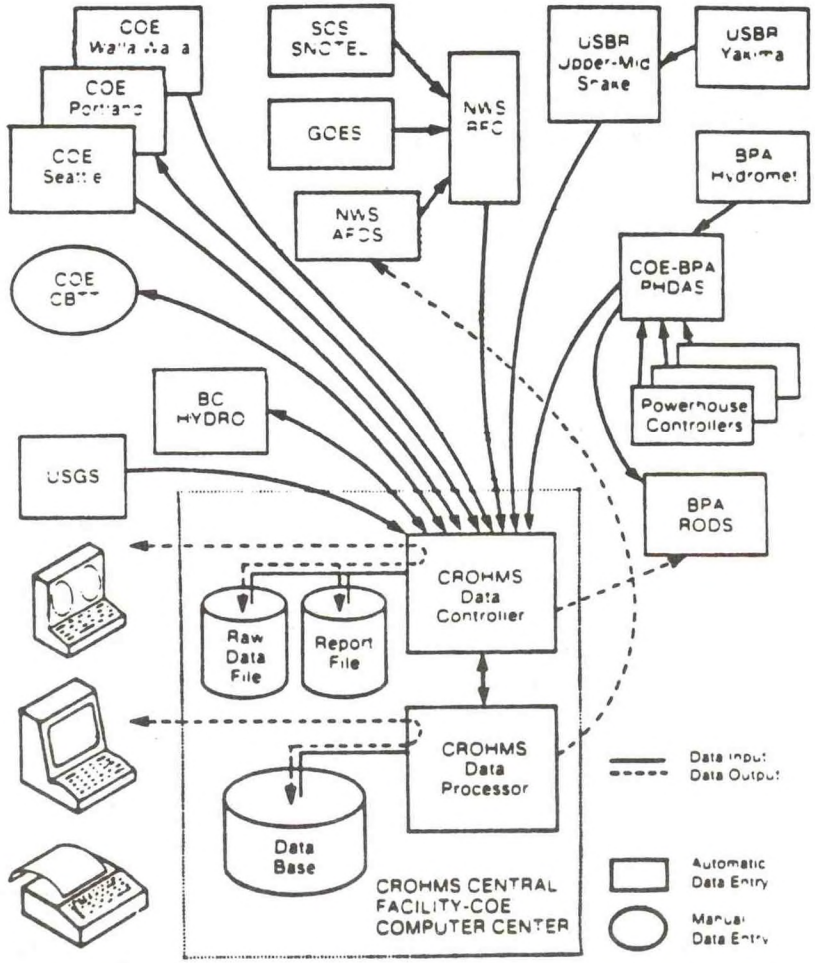

Fig. 6. CROHMS Data Collection System. NWRFC Portion is Shaded (COE-NPD, 1982)

```
PDXRRMOR1
TTAA00 KPDR 041342

:NORTHWEST RIVER FORECAST CENTER  OREGON RIVER UPDATE
:04 MAR 1989  0400  PACIFIC LOCAL TIME
.B PDR 0304 P DH0400/HG/DRH-6/HG/DRH-12/HG/DRH-18/HG/DRH-24/HG
:                  GAGE HEIGHTS
:              HRS   HRS   HRS   HRS   HRS
:              AGO   AGO   AGO   AGO   AGO       FLOOD
:ID     TIME    0    -6    -12   -18   -24        STAGE   NAME
:...SOUTHERN WILLAMETTE AND TRIBUTARIES
PHIO3   DH0200/ 6.73/ 6.66/ 6.70/ 6.79/ 6.89     : 20.0 MARYS R. NR PHILOMATH
CORO3   DH0327/ 2.42/ 2.50/ 2.57/ 2.58/ 2.59     : 20.0 WILLAMETTE @ CORVALLIS
ALBO3   DH0356/ 5.32/ 5.45/ 5.55/ 5.61/ 5.65     : 25.0 WILLAMETTE @ ALBANY
:...NORTHERN WILLAMETTE AND TRIBUTARIES
SUVO3   DH0400/ 8.62/ 8.74/ 8.89/ 9.08/ 9.30     : 27.0 LUCKIAMUTE AT SUVER
SLMO3   DH0400/ 0.00/ 0.00/ 0.00/ 5.55/ 5.57     : 28.0 WILLAMETTE R AT SALEM
WHIO3   DH0400/ +   /10.12/10.36/10.66/10.92     : 38.0 S YAMHILL NR WHITESON
:...NORTH AND CENTRAL COAST
FSSO3   DH0300/ 4.62/ +   / 4.72/ 4.77/ 4.83     : 13.0 NEHALEM R NR FOSS
TLMO3   DH0300/ 4.45/ 4.48/ 4.54/ 4.57/ 4.63     : 11.0 WILSON R. NR TILLAMOOK
BEAO3   DH0315/ 4.51/ 4.53/ 4.55/ 4.57/ 4.61     : 18.0 NESTUCCA NR BEAVER
MPLO3   DH0303/ 6.22/ 6.28/ 6.32/ 6.35/ 6.38     : 18.0 SIUSLAW R NR MAPLETON
:...COLUMBIA RIVER TRIBUTARIES
GIBO3   DH0306/ 3.05/ 3.07/ 3.08/ 3.09/ 3.11     :      UMATILLA R. NR GIBBON
SNDO3   DH0200/ 9.09/ 9.09/ 9.13/ 9.19/ 9.25     :      SANDY R. NR BULL RUN
.END
```

Fig 7. SHEF Coded Tabular Report Generated From the CROHMS Database and Transmitted to AFOS.

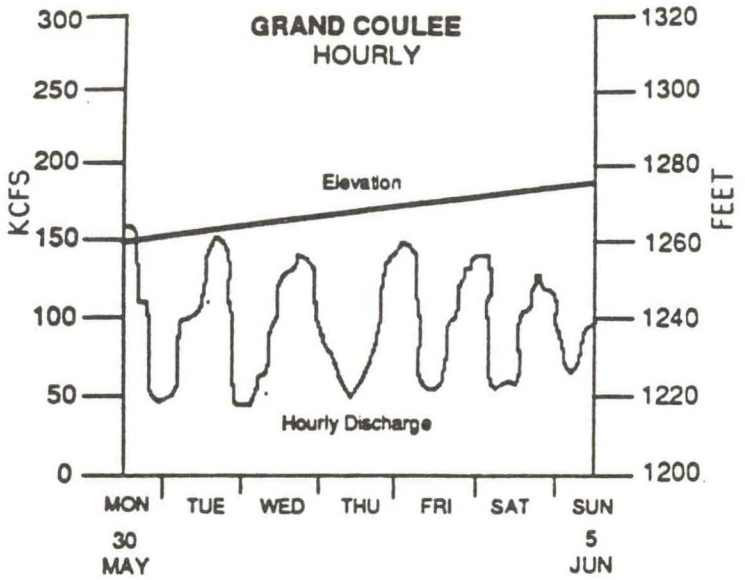

Fig. 8. Graphical Report Generated From the CROHMS Database.

```
PDXRRMOR1
TTAA00 KPDR 041342

:RIVER FORECAST SUMMARY
:PEND OREILLE RIVER ABV NEWPORT
:NW RIVER FORECAST CENTER
:PORTLAND,OR

.B PDR 0406 P DH04/HG/DRD+1/HG/
.B1 DRD+2/HG/DRD+3/HG

:START TIME = 0400 4 JUNE 1984
:           DATE
:STN      04   05   06   07
:WGCM8: 5.1  4.9  5.9  6.5  :FS 11
:CFMM8: 7.7  7.6  8.5  9.0  :FS 13
:ABOM8: 6.7  6.5  8.0 10.5  :FS  8
:BONM8: 5.6  5.5  7.5  9.0  :FS 11
:SRGM8:11.9 11.7 12.2 13.5  :FS 19
.END

:THESE FORECASTS REFLECT THE EXPECTED
:HYDROLOGIC AND METEORLOGIC CONDITIONS
:AS WELL AS THE EFFECTS OF ASSUMED
:RESERVOIR REGULATION AND ARE SUBJECT
:TO CHANGE ON A DAY-TO-DAY BASIS.
```

Figure 9. River Forecasts Coded in SHEF.

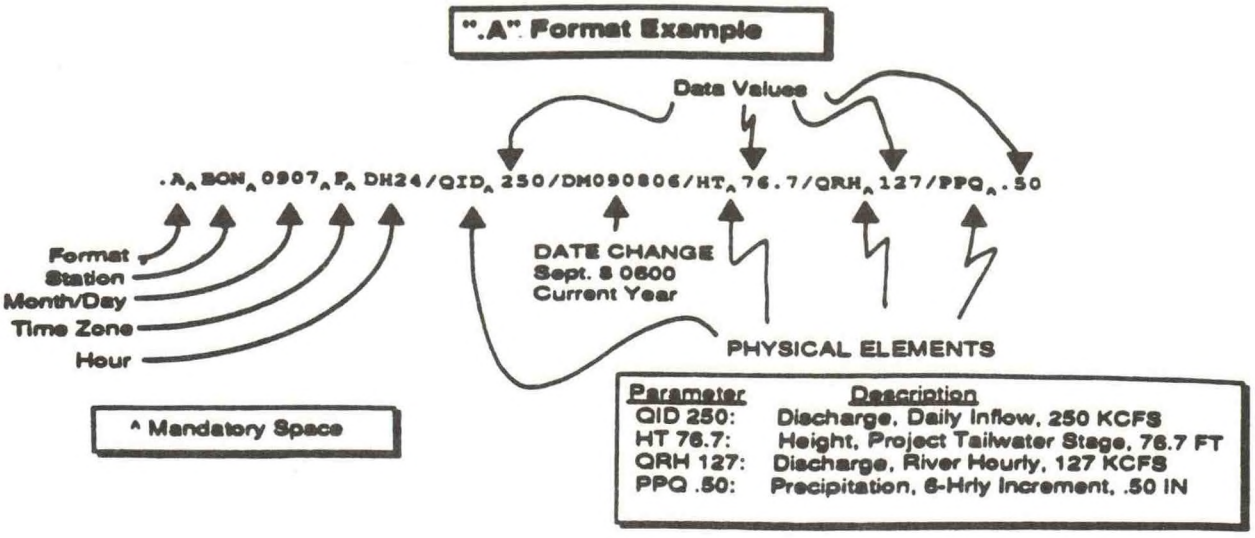

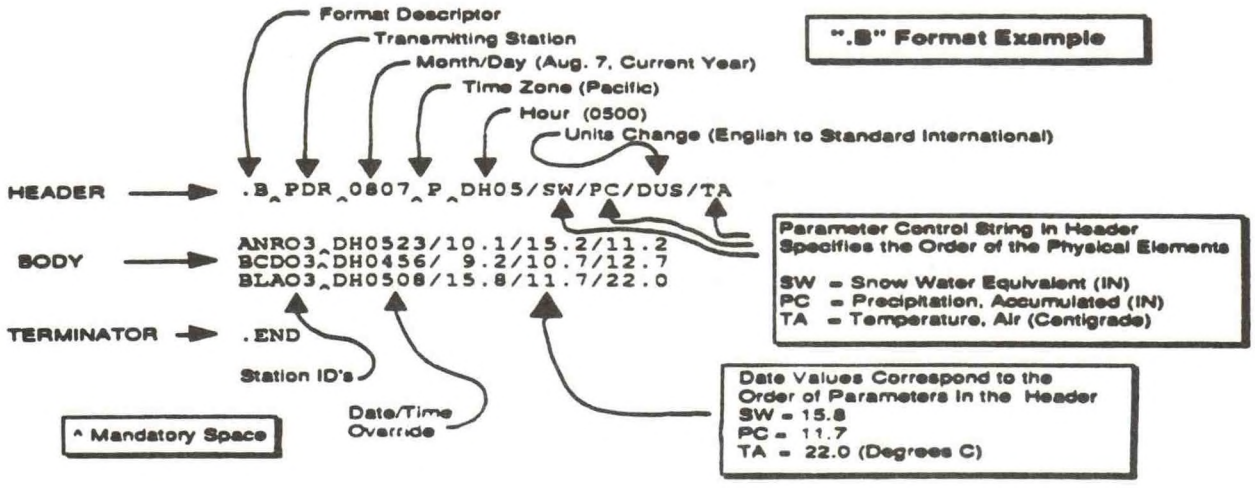

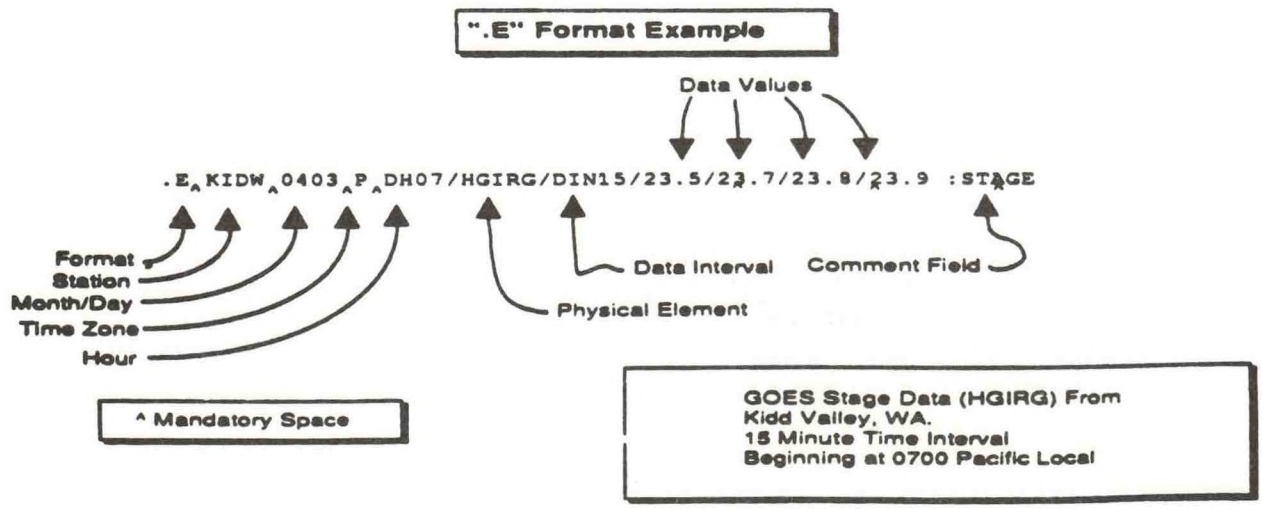

Figs. 10, 11, and 12. SHEF data formats

```
SEARR1GEG
TTAA00 KGEG 241652
NATIONAL WEATHER SERVICE, SPOKANE, WA

.B GEG 0324 P DH08/HG  :TODAYS DATE
SPOW1 21.7             :SPOKANE @ SPOKANE
HAGW1  3.9             :HANGMAN @ SPOKANE
CTLI1 36.4             :CATALDO
.END

.B GEG 0324 P DH08/TX/TX/PP    :TODAY
CAB    50/28/0.02      :CABINET GORGE DAM
WWPI1  46/25/0.15      :WALLACE WOODLAND
KLGI1  54/24/0.36      :KELLOGG
.END

.B GEG 0323 P DH24/HG/QRD: YDA'S DATE
LLK   1535.65/12.243   :SPOKANE @ LONG LK
SPOW1        / 9.993   :SPOKANE @ SPOKANE
NOX   2323.12/ 9.531   :CLARK FK @ NOXOM
CAB   2174.60/ 9.377   :CABINET GORGE DAM
COEI1 2125.95/ 9.390   :COEUR D'ALENE LK
.END
```

Fig. 13. .B Format SHEF Messages Containing a Variety of Hydromet Data.

```
.E KIDW 0403 P DH07/HGIRG/DIN15/
.E1 23.5/ 23.7/ 23.8/ 23.9/ :STAGE

.E KIDW 0403 P DH07/PCIRG/DIN15/
.E1 38.4/ 38.6/ 38.6/ 39.0 :PRECIP
```

Fig. 14. SHEF .E Message Containing Mt. St. Helens GOES Data.

IMPROVED FLOOD FORECASTING SYSTEM FOR THE SUSQUEHANNA RIVER BASIN

Eugene A. Stallings
Office of Hydrology
National Weather Service
Silver Spring, MD

I. INTRODUCTION

The past year has been an extremely quiet time as few large floods have occurred. Flooding was reported at several locations in California and some major flooding occurred in Arkansas and Puerto Rico. FY 1988 marked a stark contrast to the previous year which will be described in detail later on. The drought over large portions of the United States has been the focus of the media's attention. Pictures of shriveled-up corn fields and stalled barges on the Ohio River and the Mississippi River were common place. Whether the drought still exists is an issue which presently has no clear-cut answer. However, heavy snowstorms in late 1988 and early 1989 throughout the far West and the upper Midwest may bring about a return to more normal conditions. In any event, floods will occur in every state in the future whether they are snowmelt runoff events in North Dakota or a flash flood event in Maryland.

Total flood damages sustained during FY 1986 were over $5.5 billion, much above the 10-year moving average (1976-1985) of $3.2 billion and the highest amount incurred since flood records began over 50 years ago. There were an estimated 207 flood fatalities in FY 1986, which approximates the national average. The Susquehanna River basin which extends over parts of New York, Pennsylvania and Maryland has a drainage area of approximately 27,500 square miles. This drainage is slightly less than 1 percent of the total land area of the continental United States but contributes almost ten percent of the national average annual flood damages. Hurricane Agnes in June 1972 was particularly devastating as about $2.3 billion in flood damages occurred and 27 lives were lost in the Susquehanna River basin. Apprpoximately 3 years later, Hurricane Eloise also struck the mid-Atlantic states with fury, and flood damages approached $300 million in New York, Pennsylvania, and Maryland.

II. BACKGROUND

Although the National Weather Service (NWS) has been providing flood forecasting services in the Susquehanna River basin and there are numerous dams and local flood protection projects located throughout the basin, floods continue to cause much damage and an alarming loss of life. The public demand for improvements in flood warnings, river forecasts, flash flood guidance, and other hydrologic services prompted the Susquehanna River Basin Commission (SRBC) to sponsor a flood forecasting system. The Commission is the single Federal-Interstate water resources agency with basin-wide authority and, working closely with the Corps of Engineers, U.S. Geological Survey (USGS) and the NWS developed a plan for improved flood forecasting. Subsequently, water resources agencies in Pennsylvania and New York expressed an interest in the project and attended the numerous coordination meetings. There have been several changes to the original plan occasioned by changing technology and increased knowledge concerning equipment types and locations.

III. PURPOSE AND SCOPE

The program of improvements to the flood forecasting system for the Susquehanna River basin provides equipment and personnel needed to improve the accuracy and timeliness of forecasts to minimize flood damages. When completed, the plan will have the capability to disseminate forecasts within an hour after receipt of data and to update forecasts at approximately 4-hour intervals. The effective flood forecast and warning program requires four basic elements.

1. Real-time hydrologic data including rainfall, river stages, temperature, snow and water equivalent data. (Real-time is defined as having current data for producing accurate and timely forecasts and warnings).

2. Hydrologic forecasting capability including adequate computer facilities, reliable computer forecasting models, an adequate numbers of trained hydrologists.

3. Data dissemination capability. Distribution of the forecasts and warnings to the public in sufficient time to act is essential so that flood damages are reduced and lives are saved.

4. Adequate community preparedness. An aggressive community response capability is essential so that timely flood forecasts and warnings can be effective.

IV. SYSTEM MODULES

The improved forecasting system for the Susquehanna River basin consists of five modules: computer system, data collection network, increased staff, radar component, and National Oceanic and Atmospheric Administration (NOAA) Weather Radios. Details on each of the modules will be described in subsequent sections of this paper. Each of the modules will, by itself, enhance the flood forecasting capability of the NWS for the Susquehanna River, by working in concert with each other, the modules will produce a flood forecasting system that will be a model for any river basin in the Nation. In the first year, FY 1986, the computer was procured, plans to upgrade rainfall and stream gages were finalized, the NOAA Weather Radios were sited, and some initial staff augmentation was accomplished. In 1987, the remaining gages were scheduled to be procured, but problems with real estate, property arrangements, and rising equipment costs delayed operation of all rainfall and stream gages and the data collection network will not be completely operational until mid-1989. The remaining staffing action at Williamsport and Harrisburg was completed in FY 1987 while plans went underway for the RADAP/RADAR. One of the principal benefits of the Susquehanna enhancement project is the 24-hour operation mode of the NWS offices at Williamsport and Harrisburg.

V. COMPUTER MODULE

Improved hydrologic forecasting capability requires an increased computer capability for the Middle Atlantic River Forecast Center (MARFC) at Harrisburg, Pennsylvania. When the plan was conceived, the NWS utilized a

PRIME 750 in its Headquarters office. Similar models were planned for both the Alaska and Kansas City Forecast Centers. Considering the capacity of PRIME 750, the original Susquehanna River basin improved flood forecasting plan required two computers. The second computer would provide additional power and serve as a backup during failures. The PRIME company marketed a PRIME 9755 (II) computer which has over six times the power of the PRIME 750. The single PRIME will be the principal driving mechanism to develop improved flood forecasts in the Susquehanna River basin. There is no question that the PRIME 9755 (II) will do the job and do it well. The only other reason for having two computers would be to provide backup capability to the improved flood forecasting system at Harrisburg.

Basically, there are two types of failures--site and system. Site failures occur more infrequently but outages are measured in days while system failures are measured in hours. For example, the incident at Three Mile Island is a classic example of a site failure. Simply stated, the flood forecast cannot be made because the forecasters cannot get to work. Fires, total communication outages, and bomb threats are other examples of site failure. Based on site failures alone, having a backup computer at the same location as the principal computer makes little sense. The NWS readily acknowledges the need for a backup computer. The river forecast must be made and must be accomplished in a timely manner and even hours of downtime from a system failure are not acceptable. The first backup computer for the Susquehanna River basin is located at the NWS Central Computer Facility in Suitland, Maryland. The second backup will be at one of our river forecast centers with a similar PRIME computer system. This will be determined at a later date.

The staff in the River Forecast Center (RFC) at Harrisburg is quite competent and professionally very sound, but the improved forecasting program is most unique and extremely sophisticated. The capability of the PRIME computer is almost beyond comprehension because of the enormous in-roads in advanced technology. The Harrisburg staff must have strong technical support in software development and implementation from the Hydrologic Research Laboratory and the Hydrologic Operations Division in Washington and the Prototype Real-Time Operational Test, Evaluation and User Simulation (PROTEUS)

Project Office in Kansas City. AWIPS-90, the Advanced Weather Interactive Processing System for the 1990's, is the keystone of the NWS modernization and restructuring planned for the next decade. The AWIPS program is designed to enhance the NWS capability to provide accurate and timely weather and hydrological services to the Nation through the effective application of modern, proven techniques and technology. In support of AWIPS-90, PROTEUS will demonstrate, test, and evaluate the unique features of hydrologic forecasting and requirements for hydrologic operations that are to be satisfied by the AWIPS system. Techniques will be demonstrated which will serve the hydrologic functions of two NWS field offices of the AWIPS era; i.e., Weather Forecast Offices (WFOs) and RFCs. PROTEUS will reside in an operational environment and will focus on advanced interactive forecasting techniques and data handling procedures required for the high resolution spatial and temporal data milieu of the AWIPS era. PROTEUS will also develop and recommend an optimum evolutionary path for the transition from current NWS hydrologic operations to the next generation system.

Presently, the MARFC uses several methods to collect data. The methods range from observers to telemarks to sophisticated satellite data collection platforms (DCPs). The reliance on observers to collect data, especially rainfall data, means certain data may not be available when needed, due in part to failure of the telephone lines or because certain observers must be called by the MARFC. Similarly, data from the Device for Automatic Remote Data Collection and telemark stations may not be available due to the failure of the telephone lines or to the failure of the power source at the site. In contrast, the DCP has its own uninterruptible power supply (solar panels) at the gage site and transmits data via the Geostationary Operational Environmental Satellite (GOES). The data collection network has been improved in two ways. First, substantially more stream gages and rain gages were installed. The data from these additional sites minimize the existing uncertainty in estimating runoff from large ungaged areas. The additional rain gages provide more accurate information regarding areal distribution of rainfall. Secondly, data transmission from the gage to the MARFC is being improved. Normally the DCP will transmit data at a scheduled time every 3 or 4 hours. During extreme hydrological conditions, it can be programmed to

transmit data more frequently (random reporting type). This assures that when flooding is occurring current data are available at approximately hourly intervals. Also the data transmission activity does not have to be initiated by people but occurs automatically at the remote data collection site. A significant reduction in the amount of time spent acquiring data is expected as a result of improved data transmission capability. Naturally, any time savings can be converted into dollars saved through flood damages averted and, most importantly, a potential reduction in flood-related deaths.

The present data collection network will include 31 new stream gaging stations, 87 new rain gages, and 88 new DCPs. The data from the DCP are received from the satellite by a direct readout ground station at Wallops Island, Virginia. Then the data are received at Wallops Island and transmitted over dedicated land lines first to the NOAA computer at Suitland, Maryland, then to the MARFC at Harrisburg.

It should be emphasized that the proposed improved flood forecasting plan takes advantage of all existing gage sites to the extent possible. In general, rain gages are equipped with heaters and/or temperature sensors to assure winter operation. Many sensors are collocated so that they use only one DCP. The final data collection network will probably have some minor changes because of property easements and physical limitations. In order to have the most effective data collection system, the various Federal agencies are working together with both the state water resources agencies and the independent SRBC.

The third module in the Susquehanna River basin project involves the human element. The first module provides a sophisticated powerful PRIME computer that can only produce improved hydrologic forecasting with complex software and competent forecasters. Similarly, the enhanced data collection network will produce more data and at more frequent intervals. But a powerful computer and an enhanced data base can only produce improved hydrologic forecasting capability for the Susquehanna River basin if there are competent experienced staff at MARFC ready to prepare timely forecasts. Seven people comprised the staff at MARFC prior to the proposed flood forecasting improvement system. During normal conditions, the MARFC issues flood

forecasts for not only the Susquehanna basin but also for the Potomac, Rappahannock, James, and Appomatox basins to the south. The normal hours of operation are from 6 a.m. to 10 p.m., 7 days a week. Naturally, during flood emergencies, the MARFC operates around the clock every day until the flood waters abate and normal conditions can be resumed.

Under the enhanced plan, the staff at the MARFC increased as four new professional hydrologists were hired. In late FY 86, action was taken to initiate the paperwork needed to assure that in-house training would be available with both the computer software and a moderate knowledge of the individuality of the Susquehanna River basin. The full complement is on board at the MARFC, and forecasts are now available 7 days a week and 24 hours a day. The staffing increase by itself will effect a slight reduction in flood damages annually experienced in the basin.

Naturally, the benefits of the increased staff at the MARFC in conjunction with the Susquehanna River basin, with 24-hours a day capability, also greatly assist other basins. For example, the residents of the Passaic-Raritan and Delaware basins will receive more timely forecasts. We are presently re-evaluating the benefits of providing increased lead time for other basins. The fourth module is the radar module. The First-Year Plan for the flood forecasting system improvement program proposed a WSR 74-S network radar in the vicinity of Williamsport, Pennsylvania, to fill a gap between the existing radars. A RADAP II and ICRAD were also included in addition to three meteorologist technicians who were hired as result of the Susquehanna Initiative. The additional staff now allows Williamsport to be operational 24 hours a day, 7 days a week. At first glance, this appears to be a most appropriate component to providing improved flood forecasting services for the entire Susquehanna River basin. Unfortunately, the Susquehanna River Basin project did not consider the Modernization and Restructuring Plan for the NWS. One major component of the NWS modernization plan is to provide more sophisticated radar throughout the U.S., beginning in the early 1990's. The radar system for the future NWS is called the Next Generation Weather Radar (NEXRAD).

It is not desirable to provide a WSR 74-S radar at Williamsport in FY 1989 and to discard this unit when NEXRAD is fully implemented. The NWS installed a RADAP II ICRAD at Harrisburg, Pennsylvania, and at Binghamton, New York, and an ICRAD at Williamsport. This option has substantial cost savings and enhances the hydrometeorological program at the Weather Service Office at Williamsport at the earliest possible date. Also it avoids installing a complete radar system which could be replaced by NEXRAD slightly over 2 years after it is installed. NEXRAD will greatly enhance the coverage in the Susquehanna River basin. At the present time, the NWS is investigating the possibility of moving the location of the existing radar site at Harrisburg River basin over the entire West Branch, in the vicinity of Williamsport. We are also pursuing the possibility of moving up the NEXRAD installation dates for the Harrisburg and Binghamton radars. As discussed earlier, the Susquehanna River basin project is a changing plan since technology is constantly evolving. When completed, the flood forecasting project will be a model for the rest of the Nation.

The NOAA Weather Radio is the fifth and final module that comprises the flood forecasting improvement plan for the Susquehanna River basin. The NOAA Weather Radio is the most direct means to communicate with the general public. The current stations do not reach all areas of the Susquehanna River basin. Two sites were added at Wellsboro and Towanda, Pennsylvania, to provide expanded basin coverage.

The "Voice of the National Weather Service" provides continuous broadcasts of the latest weather information directly from NWS offices. Taped weather messages are repeated every 4 to 6 minutes and are routinely revised every 1 to 3 hours, or more frequently if needed. Most of the stations operate 24 hours daily. The broadcasts are tailored to weather information needs of people within the receiving area. During severe weather, NWS forecasters can interrupt the routine weather broadcasts and substitute special warning messages. The forecasters can also activate specially designed warning receivers. Such receivers either sound an alarm indicating that an emergency exists (alerting the listener to turn the receiver up to an audible volume) or, when operating in a mute mode, are automatically turned on so that the

warning message is heard. "Warning alarm" receivers are especially valuable for schools, hospitals, public-safety agencies, and news media offices.

NOAA Weather Radio broadcasts can usually be heard as far as 40 miles from the antenna site; sometimes more. Local radio and TV stations can copy and re-broadcast the material even though land lines in the area may be disrupted. Except for a few part-time stations, NOAA VHF radio weather transmissions are broadcast 24 hours a day on one of seven high-band frequencies, ranging from 162.400 - 162.550 megahertz (MHz). The taped messages are amended as needed to match the changing weather.

VI. MODEL FOR THE COUNTRY

A massive initiative like the Susquehanna River basin project does not just happen without the backing of the Regional and Headquarters offices of the action agency. An extensive software system is needed to provide the required capability for the innovative flood forecasting improvement system. Initial software must be available when the computer is "plugged in," and this software must be continuously upgraded and maintained to assure a quality product. The NWS Office of Hydrology committed resources to assist with the software implementation and maintenance.

In addition to the technical components associated with the Susquehanna River basin flood forecasting program, there are "people" considerations. The plan to improve flood forecasting is very complicated and is on the "cutting edge of technology."

The final system requires a massive interactive capability and will be different from the forecasting configurations of any other WSFO. This system will not work without "people." The people are not only NWS hydrologists and river forecasters but USGS staff, SRBC members and volunteer concerned citizens in Williamsport and Harrisburg and other locations in the Susquehanna River basin. Working together is the major element in successful implementation and maintenance of this complex forecasting system. When completed, the Susquehanna River basin project will be a model for the rest of the country.

Although no funds have been made available yet, a preliminary feasibility study to improve flood forecasting procedures for portions of the Ohio River basin has been prepared. The proposal has not been studied in detail but the plan contains many of the same components as the Susquehanna proposal. With emphasis on tax reform and tight budgets, the future "success" envisioned by the improved flood forecasting system for the Susquehanna River basin will not go unnoticed by the general public. The NWS has an improved system projected in the near future for the Arkansas River basin to complement the PROTEUS pre-prototype package described earlier in the paper.

VII. SUMMARY

Preliminary studies indicate that improved flood warning, coupled with various preparedness measures, can reduce damages 10 to 15 percent. Assuming that the program proposed here will increase forecast lead times by 6 to 10 hours thereby achieving about a 15 percent reduction in average annual flood damages, the damage reduction associated with the plan would amount to $12.375 million per year. Over a 20-year period, the additional savings would exceed the projected cost of the program by a ratio of 8.6 to 1.

The magnitude of the benefits from improved computer facilities at the MARFC has not been estimated. However, it should be noted that such benefits will impact far beyond the boundaries of the Susquehanna River basin. The MARFC also provides river forecasting services to the Passaic-Raritan and Delaware basins to the east and to the Potomac, Rappahannock, James, and Appomatox basins to the south.

The Susquehanna River basin flood forecasting project will be most effective because people of the basin have been providing substantial self-help efforts for a number of years. Of 745 flood-prone municipalities in the basin having some type of flood warning system, 532 receive help from 50 self-help flood forecasting and warning systems. It is estimated that over $200,000 has been spent by non-Federal entities on equipment (communications, computers, etc.) to set up the self-help systems. The value of time contributed by county and municipal employees and volunteers for all flood damage mitigation efforts in the basin is estimated to be in excess of $2 million annually. Finally, the

cost of flood damage reduction efforts undertaken by 100 or more local businesses and industries in the basin is estimated to be approximately $20,000 per establishment for each event.

The improved plan will pay for itself in a relatively short time. Flood damages will be reduced because of the additional lead time and better forecasts. But, most important is the strong possibility that better and more accurate forecasts could reduce the lives lost during flood-related events.

THE SIMULATION OF THE CATCHMENT RUNOFF PRODUCTION COMPUTATION

Wen Kang
Li Diejuan
Jin Guanshen
Li Qi

Nanjing Research Institute of Hydrology
and Water Resources

ABSTRACT. In this paper, the suitability of an Antecedent Precipitation Index (API) model to account for the soil moisture content is discussed and a general catchment runoff production model, called Nanjing Research Institute of Hydrology Model, is established and tested with data from several catchments of different sizes. In our judgment, these results show the model to be an effective simulation tool.

For computation of runoff at a point, the hydraulic method is adopted to describe the moisture flow in both nonsaturated and saturated soil. When the rate of water supply or rainfall intensity, i, is greater than the loss rate, f, ($i > f$), then surface runoff occurs. Generally, however, basin runoff is much more complex than that for a single point; the point loss rate cannot be used to compute the basin runoff.

The general model presented here is subdivided into two parts, a one-layer model and a two-layer model. Suppose that there exists an average loss rate curve for a basin. The average loss rate, f_t, in any time interval consists of infinitely many different random point loss rates. Thus, there exists a stochastic areal distribution of point loss rates within a basin. A one-layer model can be developed by combining the average loss rate curve and the areal

distribution curve of the loss rates. The two-layer model consists of three parts: surface runoff, subsurface flow of the upper zone, and subsurface flow of the lower zone. Surface runoff occurs when rainfall intensity exceeds the infiltration rate. Subsurface flow in the upper zone occurs whenever infiltration rate to the upper zone exceeds the percolation rates to the lower zone. Subsurface flow to the lower zone is assumed as a function of the percolation rates to the lower zone.

Our model was tested with hydrological data from several catchments in the arid, semiarid, and humid regions. There were 26 catchments with 516 flood events for the one-layer model and 20 catchments with 380 flood events for the two-layer model. Model simulations compared very satisfactorily with respect to the observed runoff.

I. INTRODUCTION

An international project on the intercomparison of conceptual models used in operational hydrologic forecasting was initiated in 1968 and completed in 1974 by the World Meteorological Organization (WMO). Based on conclusions and recommendations made there; further findings presented at the International Symposium on Rainfall-Runoff Modeling held in 1981 at Mississippi State University; and our own experiences, we propose the following as a basis for our work:

1. Hydrologic models require greater complexity to correctly simulate arid and semiarid regions than to simulate humid regions. Therefore, models for these areas are more difficult to develop.

2. A model framework need not be very complicated. The number of model parameters should be as limited as possible. A parameter is just a part of the model itself; it need not put undue stress on the physical significance of parameters.

3. Limited models should be calibrated to the total hydrograph measured at the basin outlet. This hydrograph can be simulated with a reasonable level of confidence by current hydrologic simulation techniques. However, the simulation of specific runoff components is very difficult to test with the existing hydrologic data.

II. THE SIMULATION OF THE SOIL MOISTURE WITHIN A BASIN

The soil moisture within a basin is the dominant factor affecting the basin loss rate and runoff. Generally, under the condition that the soil is relatively spatially uniform, the withdrawal of the soil moisture may be assumed to decrease exponentially with time, **t**, or

$$\theta_t = \theta_o K_e^t \tag{1}$$

where θ_t is the soil moisture content at any time **t** after the initial soil moisture content θ_o. K_e is the recession constant less than the unity.

The analysis of the experimental data of the soil moisture content in Tuanshan Gully plot of Zizhou Experiment Station of North Shanxi Province demonstrated that the recession constant K_e varied with the soil depth and the initial soil moisture content. As shown in fig. 1 for the same initial soil moisture content, the thicker the soil depth, the bigger the value of K_e. Likewise, for the same soil depth, the bigger the initial soil moisture content, the smaller the value of K_e. K_e is the recession coefficient in the traditional antecedent precipitation index, P_a

$$P_a = \sum_1^n P_t K_e^t \tag{2}$$

where $\mathbf{P_t}$ is the amount of precipitation which occurs **t** days prior to the studied storm and **n** is the number of days to be counted.

Now since K_e is related to the soil depth, the basin soil depth should be characterized in the hydrologic simulation. Based on the analysis of the soil moisture profile data recorded at the experimental station, it can be roughly seen that after each storm the wetting front will reach a relatively stable position, called influence soil depth, which is about 30 cm and 40 cm from the ground surface for Tuanshan Gully plot and Qiui Experimental Station,

respectively. The influence soil depth may be used as the soil thickness for computing the value of K_e. Combined with the initial soil moisture content θ_o, the recession constant K_e would be easily obtained. Obviously, the value of K_e determined in this way only expresses the recession coefficient at that experimental plot, but not the value of the entire basin. In fact, the recession coefficient K_e of the entire basin cannot be computed from existing plot measurements because the complexity of the underlying surface of the basin differs from that of our plot; hence, the recession coefficient determined by the experimental data can only be considered as the initial estimate of the parameter for the runoff production model. However, this estimate has been found to give an excellent fit to the observed runoff. Based on the test of 10 flood events of Tuanshan Gully plot, the optimized value of K_e is 0.92, which results in a validity of 100 percent (all differences between the simulated and observed runoff were less than the criteria given in the final paragraph). Moreover, the three-layer soil storage computation model proposed by Prof. Zhao (1975) has been used to compute the basin soil moisture content for the intercomparison. For example, the intercomparison of the basin soil moisture content computed by the two methods mentioned above, with 25 flood events for Jieting Station, Zhejiang Province, shows that the relative deviations between them have not exceeded $\pm$ 14 percent on the average. Therefore, the Antecedent Precipitation Index (API) P_a was adopted for simplicity.

III. THE SIMULATION OF THE LOSS PROCESS WITHIN A BASIN

Infiltration is the dominant factor in the basin losses. The algebraic expressions which have been widely used for the reduction in basin loss over time are those developed by Horton and Philip (not referenced). In terms of the value on an areal average:

$$\text{Horton Type } \bar{f}_t = \bar{f}_c + (\bar{f}_o - \bar{f}_c - d^{-kt} \tag{3}$$

$$\text{Philip Type } \bar{f}_t = \frac{A}{2} t^{-1/2} + B \tag{4}$$

where $\bar{f}_t$ is the basin loss rate at any time t, mm/hr or mm/min, $\bar{f}_o$ is the maximum basin loss rate, mm/hr or mm/min, $\bar{f}_c$ and B are the constant rates as the underlying surface becomes saturated, **e** is the napierian base, **k** is the

loss reduction coefficient, t is the time counted from the beginning of the rainfall, and **A** is an empirical constant under the dry condition.

Owing to the variation of geography, soil type, moisture content, and the vegetative cover within a basin, the loss rates vary significantly from point to point at the same instant. While the areal average loss rate $\overline{f}_t$ at any time consists of infinitely many different random point loss rates, there exists a stochastic areal distribution of point loss rates within a basin. If only the areal average loss rate $\overline{f}_t$ is used, it, in turn, develops a uniform loss rate on which the simulation runoff is based. Consequently, the concept of areal variation in loss rates shown by plotting a cumulative frequency distribution of loss rate proposed by Crawford and Linsley (1966) was adopted. This curve is the assumed result from a large number of simultaneous infiltrometer measurements, plotted to show the percentage of watershed area with an infiltration capacity of less than or equal to the measured values, as shown in fig. 2. In this figure, α denotes the percentage of the area with an infiltration capacity less than or equal to the indicated value and f'_m denotes the maximum value of the infiltration capacity of the basin. The area between the curve and the abscissa in fig. 2 represents the average infiltration capacity of the entire basin, $\overline{f}_{\Delta t}$, in any time interval Δt.

A determination of how to formulate the mathematical model of the loss rate areal distribution has not yet been theoretically resolved due to its randomness. We favor the optimization technique, i.e., selecting an expression which is calibrated to give the best fit to observed runoff amounts for a set of flood events. The expression proposed by Crawford and Linsley (1966) was assumed to be linear from zero to a maximum value. We adopted two kinds of expression as follows:

1. A two-term arithmetic series of power n

$$\alpha = 1 - (1 - f/f'_m)^n \tag{5}$$

2. An exponential curve

$$\alpha = 1 - e^{-\beta f} \tag{6}$$

where f'_m is the maximum loss rate within a basin, n is the exponent of the variable term in the series, and β is a constant.

Generally, there are two different area distribution forms with time of the loss rate, i.e., the distribution within the entire basin and the distribution within the partial basin. The first one assumes that the increasing of moisture content leads to a decreasing rate of every point loss within a basin, which will also be true for the basin average loss rate, so the areal distribution curve is time dependent and will vary with time as shown in fig. 3. The other one assumes that as the moisture content increases, a part of the basin would lose its ability to absorb water so that the successive average loss rates can be distributed only on the remaining basin area as shown in fig. 4.

IV. WATERSHED RUNOFF MODEL

Combining the loss rate curve with the areal distribution of the loss rate leads to the runoff model, called Nanjing Research Institute of Hydrology Model (1982), which is subdivided into two parts; the one-layer model and the two-layer model. The key viewpoint of our model is the assumption that whenever the water supply rate i_t (e.g., rainfall, the infiltrating water to the lower soil zone, etc.) is greater than the loss rate f_t ($i_t > f_t$), runoff occurs. Whether the base flow is separated from the total runoff or not depends on whether the computed runoff desired is the total runoff or runoff only from the current storm. The total runoff corresponds to the assumption that the stable loss rate is equal to zero.

Figure 5 shows the formation of the runoff yield amount for the one layer model. In fig. 5, the ordinate denotes the loss rate, **f**, and the horizontal line denotes the areal average rainfall intensity, $\bar{i}$, at any time **t** during a storm period. Note that the distribution curve is time dependent. Loss rates for that partial area of the basin with $\alpha \leq \alpha_i$ are all less than the rainfall intensity, $\bar{i}$. The region that is shaded with solid lines represents the runoff yield intensity, **r**. Obviously, this diagram reflects the influence of the rainfall intensity on the runoff yield. For example, under the condition that the Horton type loss rate formula and the parabola of n-th order of areal distribution were adopted, the runoff yield intensity, **r**, in time interval for the distribution within the entire basin can be computed from:

$$r = \int_0^{\bar{i}} \alpha \, d_f$$

$$= \bar{i} - \bar{f}_{\Delta t} \left[1 - \left(1 - \frac{\bar{i}}{(1+n)\,\bar{f}_{\Delta t}} \right)^{1+n} \right] \tag{7}$$

where $\bar{i}$ and $\bar{f}_{\Delta t}$ are the average rainfall intensity and the average loss rate in time interval Δt respectively. Remembering that the loss rate amount $F_{\Delta t}$ in time interval Δt comes from:

$$F_{\Delta t} = \int_t^{t+\Delta t} \left[\bar{f}_c + (\bar{f}_o - \bar{f}_c)\, e^{-kt} \right] dt$$

$$= \frac{(1-e^{-k\Delta t})}{k} (\bar{f}_o - kP_a) + \bar{f}_c \Delta t \left[1 - \frac{(1-e^{-k\Delta t})}{\Delta t \cdot k} \frac{(\bar{f}_o - kP_a)}{\bar{f}_o} \right] \tag{8}$$

so that the average loss rate in time interval is given by

$$\bar{f}_{\Delta t} = \frac{(1-e^{-k\Delta t})}{\Delta t \cdot k} (\bar{f}_o - kPa) + \bar{f}_c \left[1 - \frac{(1-e^{-k\Delta t})}{\Delta t \cdot k} \frac{(\bar{f}_o - kPa)}{\bar{f}_o} \right] \tag{9}$$

and finally, from eq. 7, the runoff yield amount in time interval under the condition of distribution within the entire basin is given by

$$R = r \cdot \Delta t$$

$$= p = \Delta t\, \bar{f}_{\Delta t} \left[1 - \left(1 - \frac{P}{(1+n)\,\Delta t\, \bar{f}_{\Delta t}} \right)^{1+n} \right] \tag{10}$$

where **P** is the rainfall amount in time interval Δt, and P_a is the antecedent precipitation.

In addition to those, the runoff amount in time interval under the condition of distribution within partial basin is given by

$$R = P - \frac{(1-e^{-k\Delta t})}{k} (\bar{f}_o - kP_a) \left\{ 1 - \left[1 - \frac{P}{(1+n)\,\frac{(1-e^{-k\Delta t})}{k}\,\bar{f}_o - s_o} \right]^{1+n} \right\} \tag{11}$$

where $S_o = (1+n)\,\frac{(1-e^{-k\Delta t})}{k}\,\bar{f}_o \left[1 - \left(1 - \frac{k\,P_a}{\bar{f}_o} \right) \frac{1}{1+n} \right]$ is the ordinate corresponding to P_a. Now if $k\Delta t \geq 4$, then $e^{-k\Delta t} \approx 0$, and hence eq. 11 reduces to

$$R = P - \frac{(\bar{f}_o - kP_a)}{k}\left[1 - \left(1 - \frac{P}{(1+n)\frac{\bar{f}_o}{k} - S_o}\right)^{1+n}\right] \tag{12}$$

and $$S_o = (1+n)\frac{\bar{f}_o}{k}\left[1 - \left(1 - \frac{kP_a}{\bar{f}_o}\right)\frac{1}{1+n}\right]$$

Remembering $Im = \frac{\bar{f}_o}{k}$, then

$$R = P - (Im - P_a)\left\{1 - \left[1 - \frac{P}{(1+n)\ Im - S_o}\right]^{1+n}\right\} \tag{13}$$

$$\text{and } S_o = (1+n)\ Im\left[1 - \left(1 - \frac{P}{Im}\right)\frac{1}{1+n}\right] \tag{14}$$

where Im is the maximum storage capacity of the basin.

The runoff production model consists of many kinds of expressions due to the combination of different loss rate curves and the areal distribution curves of loss rate.

In regions rich in ground water, we proposed a two-layer model which consists of three parts: the surface flow R_1, the subsurface flow of the upper zone R_2, and the subsurface flow of the lower zone R_3. The surface flow occurs when rainfall intensity exceeds the infiltration rate. The subsurface flow of the upper zone is proceeded whenever the infiltration rate to the upper zone exceeds the percolation rate to the lower zone. The subsurface flow of the lower zone is assumed as a part of the percolation rate to the lower zone.

$$R_1 = \bar{i}\Delta t - \bar{f}_1\Delta t\left[1 - \left(1 - \frac{\bar{i}\Delta t}{(1+n_1)\Delta t \cdot \bar{f}_1}\right)\right]^{1+n_1} \tag{15}$$

$$R_2 = \bar{i}_1\Delta t - \bar{f}_2\Delta t\left[1 - \left(1 - \frac{\bar{i}_1\Delta t}{(1+n_2)\Delta t \cdot \bar{f}_2}\right)\right]^{1+n_2} \tag{16}$$

$$R_3 = \eta\bar{i}_2\Delta t \tag{17}$$

where $\bar{i}$ denotes the average rainfall intensity, $\bar{i}_1$ is the water supply rate to the upper zone given by

$$\bar{i}_1 = f_{c1} - \frac{f_{c1}}{\Delta t' \cdot k_1} e^{-k_1 t} (1 - e^{-k_1 \Delta t'}) \quad (18)$$

$\bar{i}_2$ is the water supply rate to the lower zone given by

$$\bar{i}_2 = f_{c2} - \frac{f_{c2}}{\Delta t'' k_2} e^{-k_2 t} (1 - e^{-k_2 \Delta t''}) \quad (19)$$

and η is the runoff coefficient of the lower zone.

The two-layer model framework is shown in fig. 6.

V. THE APPLICATION OF THE RUNOFF PRODUCTION MODEL.

A. The Determination of Model Parameters

There are four parameters, f_o, f_c, k, and n; for the one-layer model and nine parameters; f_o, f_{o2}, k_1, k_2, f_{c1}, f_{c2}, n_1, n_2, and η, for the two-layer model.

Under the condition of the one-layer model, f_c has been set to a constant value of zero owing to the total runoff being used. Based on our experiences, the maximum storage capacity Im could be given easily and remembering that $Im = f_o/k$, once the value of k is obtained, f_o is then determined. Parameters k and n could be obtained in optimization searches after an apparent optimum had been reached by fixing one of the parameters, k and n, by allowing the other one to change. Generally, Im varied from 100 to 200 mm, k varied from 0.5 to 1.0, and n is about 2.

Under the condition of the two-layer model, the apparent optimum technique is also used. Generally, the maximum upper zone storage capacity and the maximum lower zone storage capacity are about 70 and 30 percent of Im respectively. As a simple approximation, suppose that n_1 is about the same value as n_2 and that both are about equal to 2. In our tests, k_1 and k_2 varied from 0.5 to 1.0; f_{c1} varied from 1 to 5 $^{mm}/hr$, and f_{c2} varied from 0.5 to 2 $^{mm}/hr$; η varied from 0.02 to 0.05.

The best values of the parameter subset are determined for the flood events to be used in calibration period by minimizing an error function, or so called objective function (OF)

$$OF = \sum_{i=1}^{L} (R_{oi} - R_{ci})^2 \qquad (20)$$

where R_{oi} and R_{ci} are the observed and calculated runoff amount for the i-th flood event, and L is the number of flood events in the calibration period.

B. Example

A basin having the Horton-type loss rate with f_o=50 mm/hr, f_c=0, k=0.5 ^{1}/hr, Δt=1 hr, and the areal distribution curve like the parabola of the n-th order with n=0.3 had two successive 2-h periods of effective rainfall of 20 and 30 mm respectively. P_a=20 mm. Using the one-layer runoff production model, we proposed estimates for the runoff amounts.

$$R = P - \frac{(1-e^{-k\Delta t})}{k}(f_o - kP_a)\left[1 - \left(1 - \frac{P}{(1+n)\frac{(1-e^{-k\Delta t})}{k}(f_o - kP_a)}\right)^{1+n}\right] \qquad (21)$$

For the first time interval:

(1) $$\frac{(1-e^{-k\Delta t})}{k}(f_o - kP_a) = \frac{1-e^{-0.5}}{0.5}(50-0.5\text{x}20) = 0.786\text{x}40 = 31.44$$

(2) $$(1+n)\frac{(1-e^{-k\Delta t})}{k}(f_o - kP_a) = 1.3\text{x}(1) = 1.3\text{x}31.44 = 40.87$$

(3) $$\frac{P}{(1+n)\frac{(1-e^{-k\Delta t})}{k}(f_o - kP_a)} = \frac{20}{(2)} = \frac{20}{40.87} = 0.489$$

(4) $$R_1 = 20-(1)\text{x}[1-(1-(3))^{1.3}] = 20-(1)\text{x}(1-0.418) = 1.9 \text{ mm}$$

For the second time interval:

(1) Determine the antecedent moisture condition. From the runoff of 1.7 mm in the first time interval, we found that the corresponding loss amount is 20-1.7 = 18.3 mm, and then P_a is 20+18.3 = 38.3 mm.

(2) $$\frac{(1-e^{-k\Delta t})}{k}(f_o - kP_a) = 0.786(50-0.5\text{x}38.3) = 24.2$$

(3) $$(1+n)\frac{(1-3^{-k\Delta t})}{k}(f_o - kP_a) = 1.3\text{x}24.2 = 34.46$$

(4) $$\frac{P}{(1+n)\frac{(1-e^{-k\Delta t})}{k}(f_o - kP_a)} = \frac{30}{(3)} = 0.954$$

(5) $$R_2 = 30-24.2\left[1-(1-0.954)^{1.3}\right] = 30-24.2\times0.98 = 6.3 \text{ mm}$$

C. Results and Conclusions

To make clear the applicability of our model (NRIH) in regions with different hydrological behavior, the model was tested with hydrological data from a number of catchments in arid, semiarid, and humid regions; 26 catchments with 516 flood events for the one-layer model, and 20 catchments with 380 flood events for the two-layer model. Some parameters in the model were optimized. An estimate of the optimum values was obtained using the technique to minimize the relative differences between the computed and the observed runoff yield for each event of a basin. A criterion of validity of a relative difference less than or equal to 20 percent or an absolute difference less than 3 mm was used in this paper. These criteria for validity were met for more than 80 percent of all tested basins. It seems to work quite satisfactorily with respect to the runoff yield computation. We believe that our model can be widely used for catchments in both humid or arid-semiarid regions.

REFERENCES

Crawford, N.H., and Linsley, R.K., "Digital Simulation in Hydrology: Stanford Watershed Model IV," Technical Report No. 39, Department of Civil Engineering, Stanford University, 1966.

East China College of Hydraulic Engineering, "Flood Forecasting Method for Humid Regions of China," Technical Report, Interregional Seminar on Flood Forecasting held by WMO and UNDP, 1977.

Wen, Kang; Li, Diejuan; Guanshen, Jin; and Li, Qi, "A Mathematical Model for Computation of Watershed Runoff Production," Journal of Hydraulic Engineering, No. 8, Beijing, 1982.

Secretariat of the World Meteorological Organization, "Intercomparison of Conceptual Models used in Operational Hydrological Forecasting," Operational Hydrology, Report No. 7, 1975.

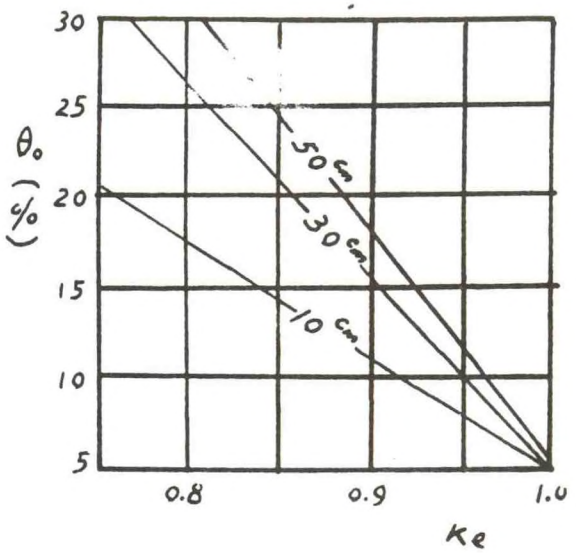

Figure 1. The relationship between K_e and θ_o.

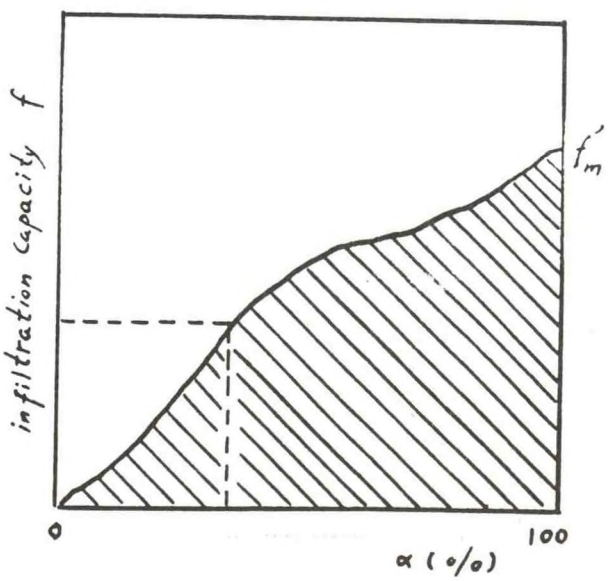

Figure 2. Cumulative frequency distribution of loss rate

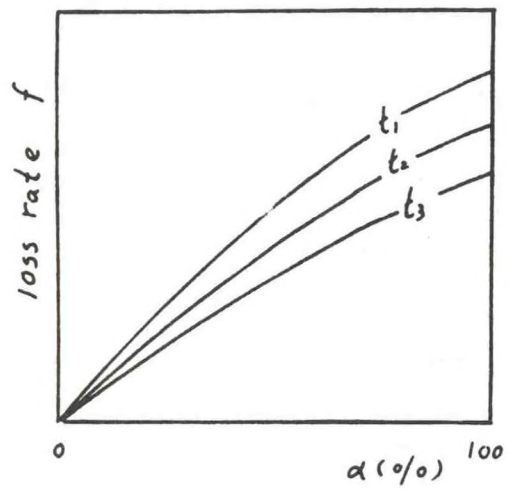

Figure 3. The distribution within the entire basin

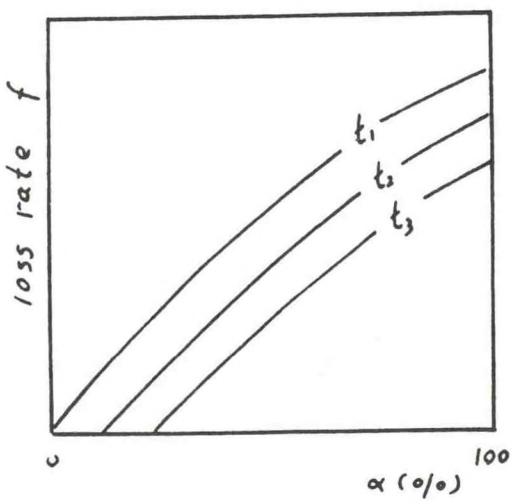

Figure 4. The distribution within the partial basin

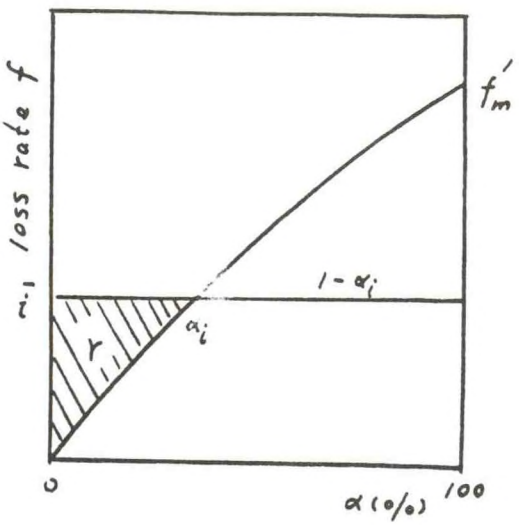

Figure 5. The formation of the runoff yield amount for one layer model

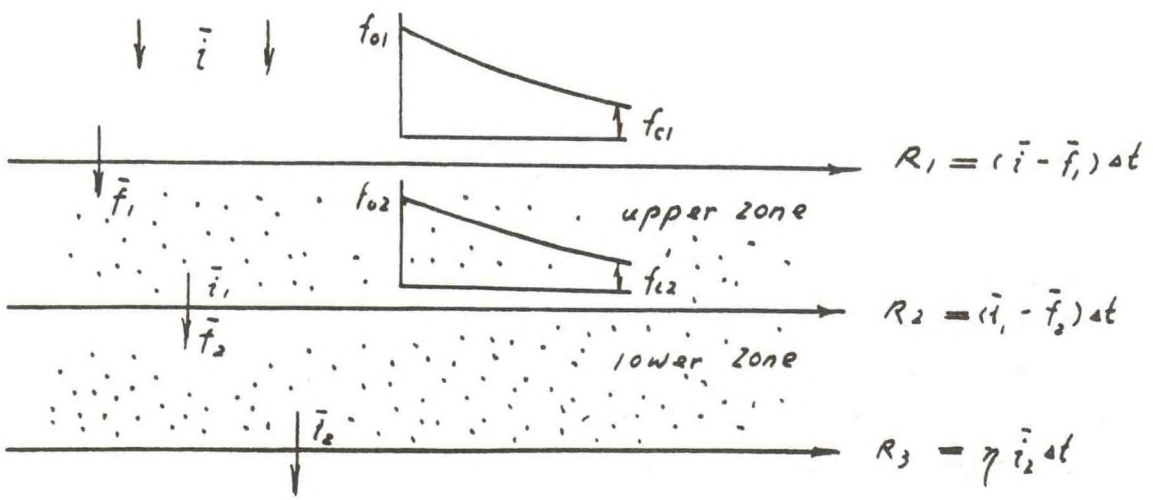

Figure 6. The framework of the two layer model

USE OR MISUSE OF QPF

Charles E. Orwig and Phillip A. Peck
National Weather Service
Portland, OR

I. INTRODUCTION

Quantitative Precipitation Forecasts (QPF) have been used by the Northwest River Forecast Center (NWRFC) for many years. QPF is one of the key inputs into the decision-making process for water management in the Columbia River basin. Often, the information provided by the skill in QPF is utilized in making decisions which have large monetary consequences or that deal in the protection of life and property. The balance of this paper investigates the current preparation and use of the QPF products in water management and flood forecasting.

II. REQUIRED QPF GUIDANCE FOR HYDROLOGY

What kind of QPF information does the operational hydrologist need from the meteorologist? The distribution of precipitation both in time and space is a required input to any hydrologic model. Figure 1 illustrates the variance in rainfall amounts at a valley and a mountain station with two different meteorological patterns (Schermerhorn, 1967). Hydrologic models require the distribution of precipitation with elevation as well as the spatial distribution of precipitation throughout a forecast area.

Another very important input to any hydrologic model is the time distribution of precipitation. Figure 2 schematically illustrates the difference in the resulting hydrographs when 1 inch of precipitation occurs in a 24-hour period and in a 6-hour period. In the first case, the streamflow rise would cause only minor inconvenience to local residents, while the more intense rainfall would produce a flood of serious proportions. Predicting the amount and distribution in time and space of rainfall is a difficult task, but any skill in QPF forecasting must be utilized in the decision-making process in water management and flood forecasting.

III. METEOROLOGY OF HEAVY RAIN EVENTS

Forecasting heavy precipitation for specific points in western Washington and western Oregon focuses on four primary factors:

(1) Use of percent of normal precipitation data,

(2) Application of numerical and subjective QPF guidance from the National Meteorological Center (NMC),

(3) Application of synoptic experience and satellite information, and

(4) Timewise distribution of precipitation amounts.

The use of percent of normal incorporates and simplifies: (1) the variation of rainfall patterns due to the effect of topography, (2) representation of basin boundaries, (3) transmission of detailed forecasts, and (4) presentation of a meteorologically consistent precipitation forecast package. Expressing precipitation amounts in terms of percent of normal replaced the use of rainy-day ratios in 1976. However, the hallmark work of Weaver and Denney (1964), Weaver (1966), and their rainy-day ratio approach to evaluating storm magnitude is still applicable. The percent of normal technique aids the forecast procedure and provides easy input to computerized operations of the RFC.

The application of computer-derived QPF and the massaged guidance from the QPF Section of NMC is, of course, a part of the solution to heavy precipitation forecasting. Accuracy seems to have improved as better modeling and increased computer power have evolved. These QPF products are given a wide range of use -- from being adhered to very closely, to having, at times, little contribution. Reliance is dependent upon how well the computer products appear to coincide with actual developments over the eastern Pacific Ocean and the West Coast. The most consistently-used computer input to the local QPF package is the forecast freezing level values derived from the thickness field. Precipitation with high freezing levels has a drastic effect on large mountain snowpack. Resultant combinations of rain and snowmelt rapidly increases streamflow. Height of the freezing level is forecast by 6-hour increments through 48 hours, which covers the basic QPF period.

Early awareness of heavy precipitation events and accurate forecasting of amounts rely very much on pattern recognition. A study of classic examples of heavy rainfall situations in the Pacific Northwest begins with the storms of

December 20-23, 1964, and January 17-19, 1953, (Hughes & Roe, 1953). Examination of these and other storms (fig. 3) yield striking synoptic similarities with primary interest in the surface isobaric pattern. In each storm, an intense surface pressure gradient evolved with isobars having a general east-west orientation creating a strong west-to-southwest low level flow. As this pattern moves inland, the topography of the coastal and Cascade Mountain barriers exerts its important influence. Two fundamental rain-producing processes are present in this synoptic pattern (U.S. Dept. of Commerce, 1966): (1) orographic precipitation due to mechanical lifting of air by sloping terrain; and (2) convergence precipitation due to high or increasing surface pressure gradients and cyclonic inflow. By and large, the degree of normality of the flow to the mountains and the strength of the flow are the main factors controlling the rate of orographic precipitation. In most instances, heaviest precipitation occurs where the gradient is greatest, ahead of the frontal boundary (fig. 4 and 5).

Two other features which must be assessed are the symmetry of the system and moisture surges based on satellite information. The surface isobar pattern should be asymmetrical with weak flow north of the frontal boundary (fig. 6 and 7). Satellite pictures help to estimate the strength and timing of short waves imbedded in the upper cyclonic flow and the overall potential moistness and source of the air mass.

The application of four basic rules of thumb summarizes the characteristics of heavy precipitation events and their duration.

(1) The longer the fetch of southwesterly flow, the larger the amounts of precipitation.
(2) The tighter the surface pressure gradients, the larger the amounts of precipitation.
(3) The slower the southward movement of the frontal boundary, the larger the amounts of precipitation.
(4) Precipitation diminishes sharply in the north of the front, provided no wave action develops on the front.

Intensity of precipitation is expressed in terms of 6-hour amounts as a percentage of the total 24-hour amount. The importance of the timewise distribution of precipitation amounts parallels that of forecasting the amounts themselves. This parameter determines the shape or peak of the forecast hydrograph. As Kuehl's (1981) analysis indicates, the bulk of precipitation from a storm is often confined to a 12-hour period. Therefore, the usefulness of a QPF is highly dependent on the realistic distribution of amounts.

IV. APPLICATION OF QPF FORECASTS IN WATER MANAGEMENT

The QPFs that are produced by the Weather Service Forecast Offices (WSFO) at Portland, Seattle, Boise, and Great Falls are input directly to the hydrologic forecast model at the NWRFC.

The 24-hour expected precipitation is forecast in percent of normal and annual precipitation and is distributed into 6-hour time blocks. As mentioned previously, both the amount of precipitation and its time distribution are an integral part of the streamflow forecasting efforts.

To illustrate the operational use of the QPF, two examples have been selected from two recent winter-storm events. Figure 8 shows the application of the QPF during the December 1980 storm in the Willamette Valley of Oregon. Several events are worth noting. On December 24, the initial QPF was input, producing streamflow rises to near bankfull conditions by the end of the 3-day forecast period. Based upon this, plans were set in motion to reduce the outflows from the Willamette flood control reservoirs when bankfull conditions were expected to be exceeded. As the day transpired, rainfall rates began to exceed the QPF expectations, and a revised QPF, issued by meteorologists at WSFO Portland was input to the streamflow model, producing a rapid streamflow rise to within 4 feet of flood stage at the Salem gage by the third day of the forecast (Orwig & Fodrea, 1981).

This revised forecast set many different organizations into action. The Corps of Engineers (COE) Reservoir Control Center passed the word for their flood control projects to reduce their outflows to flood control minimums. The state hydrologists issued the streamflow forecast to the County Warning

Center where appropriate actions were begun. All riparian residents had the opportunity to react to the flood statement. Common reactions were: a farmer moving livestock from a low-lying field; a ferryboat operator curtailing services; and the U.S. Forest Service offices sending personnel into the field to try to keep the culverts flowing under mountain roads to prevent road washout and eventual costly road rebuilding.

Another example of the importance of a QPF forecast is shown in fig. 9. In this case, the early QPF forecast for the north fork of the Umpqua River indicated rainfall amounts that would send the stream to a little above bankfull conditions. This did not cause the County Warning Center to take any action since the forecast streamflow rise would produce little, if any, damage. Later that evening the lead meteorologist at WSFO Portland updated the QPF, indicating 12 hours of very heavy rainfall (1 to 2 inches in each 6-hour period). The hydrologic model output from this revised QPF indicated a rapid rise to damage level. The updated warnings were issued early in the morning of December 6, causing the County Warning Center to sound the alarm and begin evacuating people from flood-prone spots along the North Umpqua. The timely and accurate revision of QPF allowed the accurate streamflow forecast to be made, preventing potential loss of life and property. The QPF can be equally important in situations that do not endanger life or property.

Referring back to the Willamette River forecast in fig. 8, after the flood rise, a concerted effort was made to evacuate the storage in the COE flood control reservoirs in preparation for the next storm. If the meteorological guidance indicated new storm development in the near future, water would have to be spilled at the reservoirs. On the other hand, if a dry period was in store, the stored water could be released at a more leisurely pace, perhaps by passing all the water through the power turbines, making full use of the energy.

In another very recent example, the value of a good QPF was again demonstrated. During February 1982, a warm, wet meteorological pattern developed over a major portion of the Columbia Basin. Early in the storm event, rainfall and snowmelt caused streamflow rises on most Lower Snake and

mid-Columbia tributaries. On February 19th, the Portland and Boise WSFO's issued QPF forecasts that indicated 2 wet days were forthcoming with daily amounts in excess of .50 inch expected in eastern Oregon and Idaho. Actual amounts over the 2-day period exceeded 2 inches for some of the wetter locations. The resulting streamflow forecasts indicated that rapid upstream rises on the Snake and Lower Columbia would cause flooding in the Lower Columbia at Portland as the water passed downstream. As a result, outflows were immediately reduced at the Dworshak, Grand Coulee, and Brownlee dams to reduce the downstream flooding. Thus, the early warning based on QPF input was a valuable input to the water management efforts.

V. FUTURE APPLICATIONS OF QPF FORECASTING

While QPF is still largely subjective, the means to more objective preparation and refinement of these forecasts seems to be at hand. Some of the important variables which lend themselves to calculation, correlate well with heavy precipitation events. Obviously any improvement in QPF is directly applicable to streamflow modeling, and therefore of great importance in the water management process.

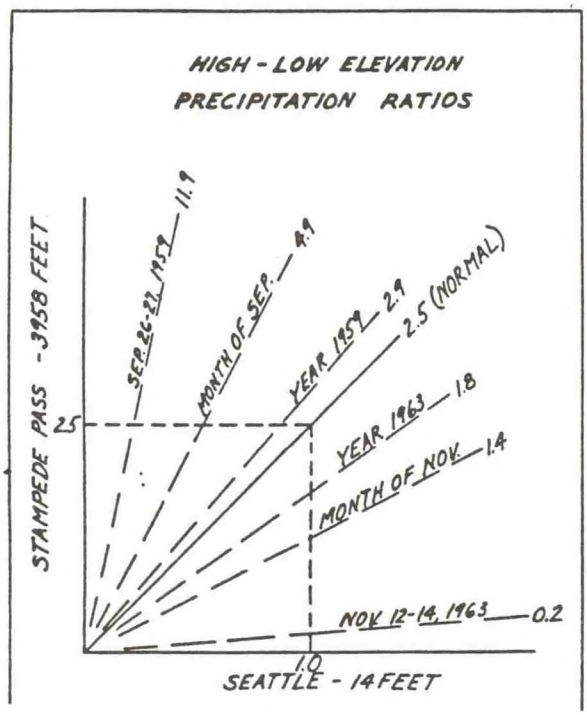

Figure 1. Rainfall Amounts at a Valley and a Mountain Station with two Different Meteorological Patterns

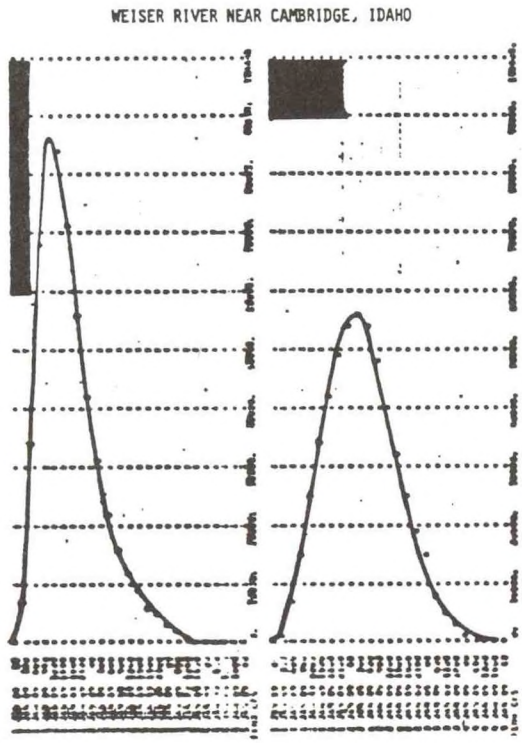

Figure 2. Resulting Hydrographs from Rainfall of Different Intensities

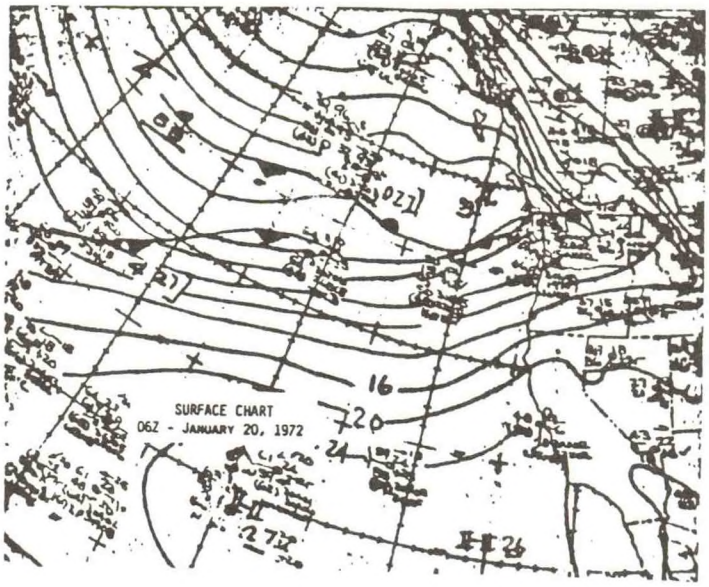

Figure 3. Synoptic Pattern Conducive to Heavy Rainfall in Western Oregon and Washington

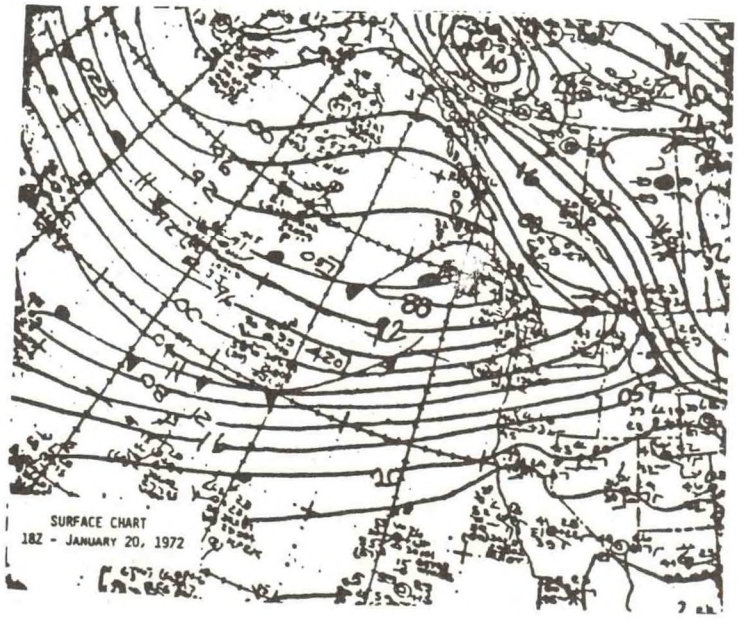

Figure 4. Example of Tight Gradient Ahead of Front Conducive to Heavy Rain.

AST	4 PM JAN 19 4 PM JAN 20	1.93	SEA	4 PM JAN 19 4 PM JAN 20	1.98
ONP	10 PM JAN 19 10 PM JAN 20	3.18	OLM	4 PM JAN 19 4 PM JAN 20	3.35
OTH	10 PM JAN 19 10 PM JAN 20	2.17	PDX	10 PM JAN 19 10 PM JAN 20	2.32
4BK	4 AM JAN 20 4 AM JAN 21	3.48	EUG	4 AM JAN 20 4 AM JAN 21	3.95

Figure 5. Actual 24-hour Precipitation Amounts (in inches) from a Heavy Rainfall Pattern in January 1972

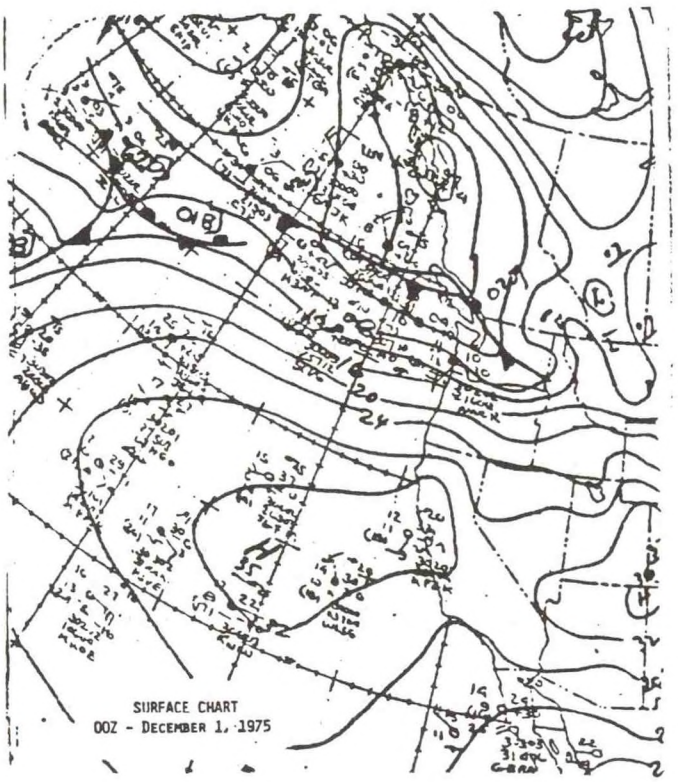

Figure 6. Example of Asymmetrical Surface Flow Pattern Related to Heavy Rain Events

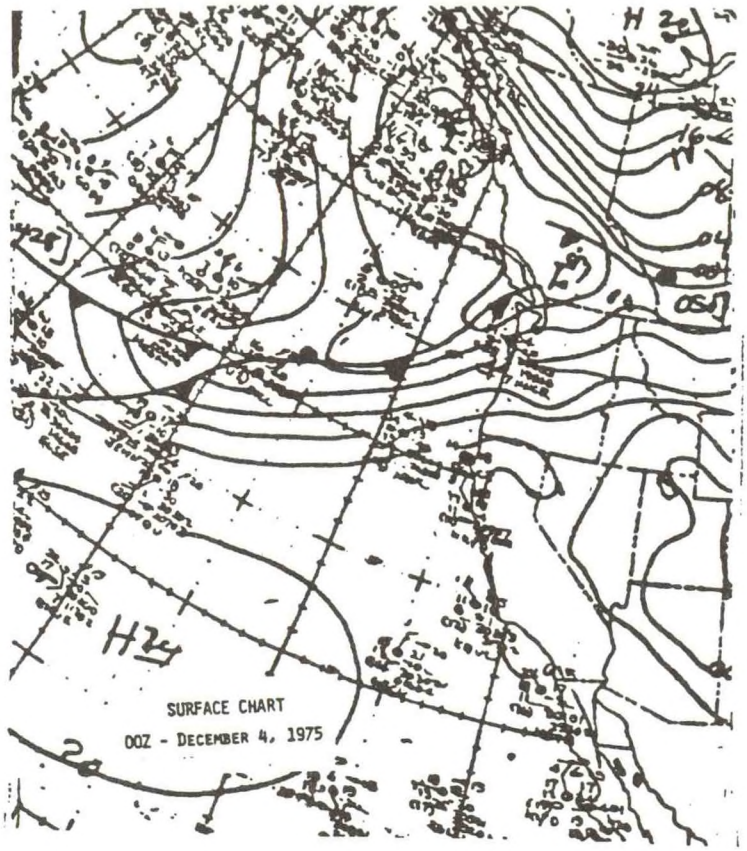

Figure 7. Example of Asymmetrical Surface Flow Pattern Related to Heavy Rain Events

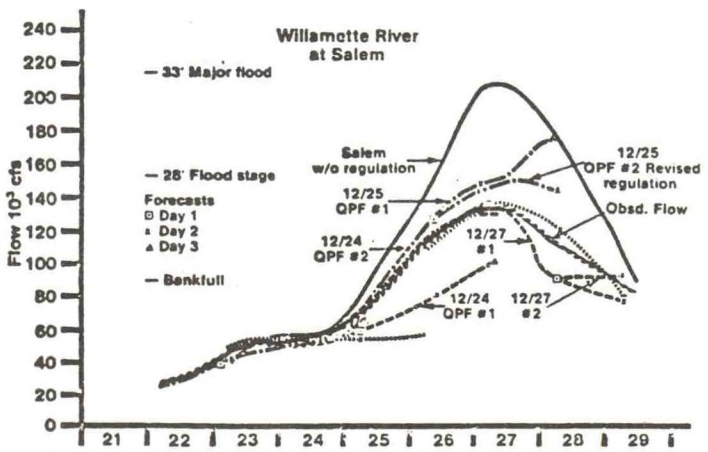

Figure 8. Detailed Hydrograph for Willamette River at Salem during December, 1980 Flood

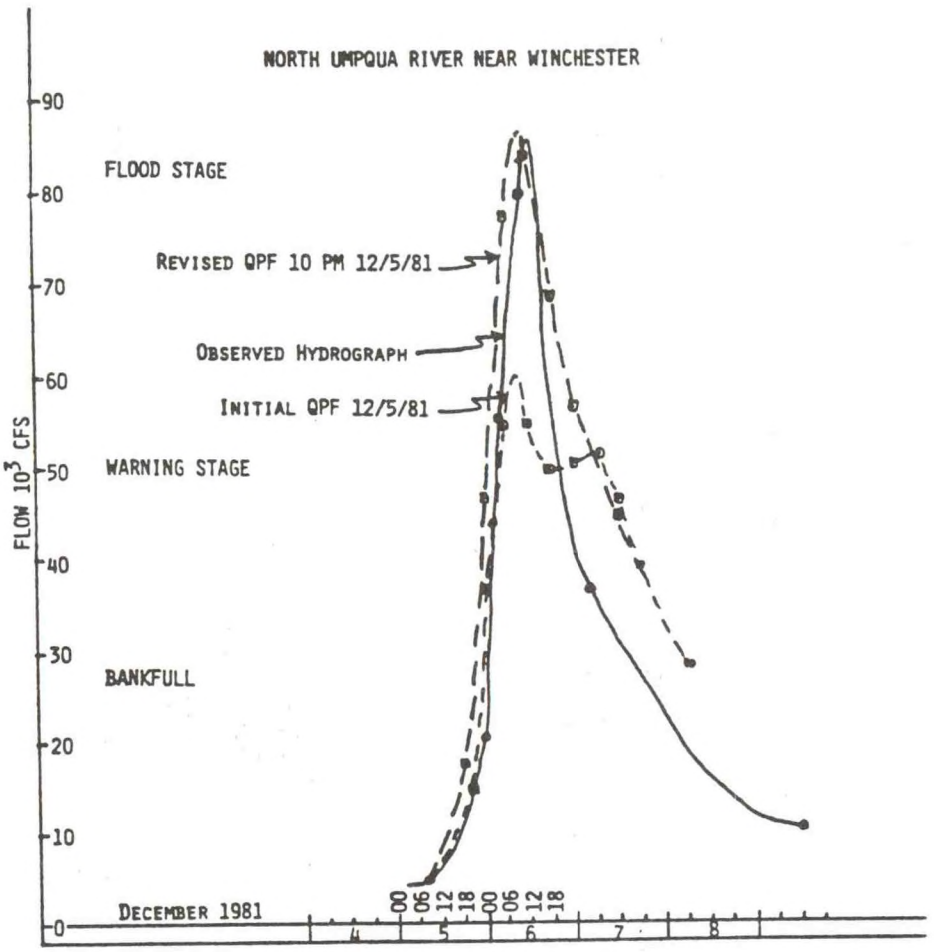

Figure 9. Example of Flood Hydrograph on North Fork Umpqua River from Updated QPF

REFERENCES

Hughes, Grover D., and Roe, Charlotte L. , "Heavy Rainfall During Mid-January Along the Pacific Coast." Monthly Weather Review, (1953).

Kuehl, Donald W., "Climatology of 24-hour Distribution of QPF." Unpublished Weather Service Manuscript, (1981).

Orwig, C.E., and Fodrea, D.J., "Real-Time Operations in the Willamette River System Using the SSARR Model with Meteorological Uncertainty," Proceedings of the International Symposium on Real-Time Operations of Hydrosystems, Waterloo, Ontario, pp. 369-388, June 1981.

Schermerhorn, V.P., "Relations Between Topography and Annual Precipitation in Western Oregon and Washington," Water Resources Research, vol. 3, no. 3, pp. 707-711, (1967).

U.S. Dept. of Commerce, "Probable Maximum Precipitation, Northwest States," Hydrometeorological Report No. 43, 1966.

Weaver, Robert L., "Normalized Daily Precipitation in Washington and Oregon West of the Cascade Divide." Unpublished Weather Bureau Manuscript, (1966).

Weaver, Robert L., and Denney, William, "Normalized Quantitative Precipitation Forecasting in California." Unpublished Weather Bureau Manuscript, Office of Hydrology, (1964).

A COMPARATIVE STUDY ON HYDROLOGICAL FORECASTING MODELS

Zhao Ren-jun
Hohai University

ABSTRACT. Many conceptual models used for hydrologic forecasting obtain high accuracy and the simulated main results, such as, evapotranspiration, runoff production, runoff separation, and runoff concentration also agree closely. Here are the common reasons: the evapotranspiration model is based on potential evapotranspiration and soil layer is divided into sub-layers; and the runoff separation is realized by linear reservoir operation and the runoff concentration is that of the river system. These can be explained by hydrological rules. But for every model there exists the serious problem of dependence of parameter values. Solutions are not unique. The dependence results from the parallel structure of runoff separation, not from the identification condition by hydrographs. While the parameter values of runoff concentration change in an ordinary range, no influence will be produced on the solution of parameter values of runoff separation. The problem of dependence of parameter values can be solved by structural constraints. We should consider the model as a scientific hypothesis of hydrological rule.

Conceptual forecasting models developed rapidly in the 60's and 70's, but have advanced slowly in the recent decade. Few new ideas have appeared. The main point of the discussion is the nature of conceptual models. Is it an expression of hydrological rule or only a useful tool? In this paper, I will try to find the general characteristics of three forecasting models and provide general discussion on each model.

The World Meteorological Organization (WMO) organized a comparison of forecasting models in 1974. Criterion of the comparison is the forecasting error. One of the principle results is in humid regions almost any conceptual model may gain high accuracy. Our experience proves this concept. But does high accuracy mean that the model expresses hydrological rules very well? Accuracy is high but parameter values are unstable or even unreasonable. However, can we assume that they have definite physical meanings? These questions are very critical.

I. INSPIRATION FROM THE FACT THAT ALMOST ALL CONCEPTUAL MODELS OBTAIN HIGH ACCURACY

Much practical experience proves that models have good efficiency, there must be some underlying fundamental physical causes. Success by coincidence is not always possible. If we do not understand it now, we will in the future. There are foregoing examples in hydrology. Many empirical flood routing methods obtained high accuracy. Through investigation, we conclude that they are based on the same theory, they may obtain the same accuracy and their parameters are theoretically exchangeable. The conceptual model is in the situation of empiricism, but they will be unified, in essence, on the basis of the hydrological rule.

I have studied seven basins in humid regions of China by daily model using the Xinanjiang (XIN), Sacramento (SAC), and tank (TANK) model. The results are shown in table 1.

Inputs are daily rainfall and pan evaporation. Daily evaporation times K becomes potential evapotranspiration. Outputs are hydrographs at the basin outlet. For the runoff concentration, I use the same program for every model and for the evapotranspiration, runoff production, and runoff separation, I

use the programs individually. So the comparison of event model is unnecessary. Objective function is taken as:

$$OB = \sum_{I=1}^{m} ABS(LOG[M(I)/Q(I)])/ \sum_{I=1}^{m} LOG[M(I)], \quad M(I) > 1$$

in which M(I) and Q(I) are measured and simulated discharges. From table 1, the following is observed:

As XIN has three components and SAC and TANK have four components, to account for this difference a conversion is necessary for SAC and TANK. For SAC, the primary groundwater is considered as RG and the secondary groundwater and interflow is combined as RI. For TANK, the outflow of the second tank is considered as RI and that of the third and fourth tanks are combined as RG. The conversion is conventional and the error introduced may be large.

We may find that the above consistencies emerge from the model structure. In fact, the main structure of the three models is very similar. They are:

1. The evapotranspiration model is founded on potential evapotranspiration and soil layer is divided into sub-layers. Evapotranspiration decreases by layer. The function of decreasing is different for every model but the difference is quite small.

2. The structure of runoff production is the storage type. XIN uses the concept of runoff production at natural storage. TANK has no infiltration function but storage function. SAC is a generalized model bearing two types of runoff production, but in humid regions the infiltration excess part does not influence the result.

3. The structure of runoff separation is essentially the same. Surface runoff is produced only if the free water storage of the surface soil is fulfilled. Groundwater runoff and interflow are derived from the free water storage and the free water storage is simulated by linear reservoir. So for all the models, runoff separation is determined by two conditions: 1) the level of storage excess, i.e., the free water capacity of the surface soil; and 2) the proportion of divergence from every linear reservoir. The linear reservoir diverts its storage by parallel outlets and the proportion of divergence is equal to the ratio of outflow constants.

Table 1. Simulated Results of XIN, SAC, TANK

XIN / SAC / TANK	OB	K	RS	RI	RG
	0.170	0.68	0.595	0.307	0.098
Misai	0.147	0.68	0.535	0.369	0.096
	0.165	0.65	0.593	0.299	0.108
	0.157	0.85	0.485	0.389	0.126
Shanbou	0.161	0.85	0.451	0.438	0.111
	0.164	0.82	0.552	0.329	0.119
	0.136	0.53	0.476	0.300	0.224
Fengshi	0.154	0.53	0.375	0.448	0.177
	0.150	0.51	0.469	0.304	0.227
	0.075	0.39	0.311	0.266	0.423
Nanqi	0.081	0.39	0.215	0.420	0.365
	0.071	0.39	0.310	0.254	0.436
	0.066	0.92	0.229	0.275	0.496
Renhua	0.076	0.95	0.227	0.362	0.411
	0.080	0.95	0.222	0.230	0.550
	0.104	0.75	0.232	0.439	0.329
Dutou	0.098	0.75	0.322	0.354	0.324
	0.112	0.75	0.431	0.282	0.287
	0.120	1.2	0.231	0.275	0.494
Yifeng	0.130	1.2	0.234	0.393	0.373
	0.162	1.1	0.251	0.246	0.503

1. For any basin, accuracy OB of the three models is almost the same.
2. For any basin, the coefficient of evapotranspiration K agrees closely.
3. For any basin, the result of runoff separation of the three models (proportion of surface runoff, interflow, and groundwater runoff RS, RI, and RG) is approximately the same.

4. The character of runoff concentration is the same. For the three models, through runoff separation, we get the total inflow into the river system and runoff concentration is that of the river storage. River flow is easy to simulate and may be isolated from the other parts of the model.

The above mentioned common structures have achieved successful results and have been explained by physical meanings which are based on hydraulics, fluid mechanics of seepage flow and turbulent flow, and hill slope hydrology. These explanations given by the authors of models are not duplicated in this paper. But the theoretical base of modeling is still weak, especially in the field of experiment.

II. THE PUZZLE OF DEPENDENCE OF PARAMETERS

I have analyzed the parameters of XIN, dividing them into four classes: 1) evapotranspiration, objective is to minimize the error of total runoff; 2) runoff production, objective is to minimize the error of runoff flood events; 3) runoff separation; and 4) runoff concentration. (Parameters belonging to these first two classes are comparatively independent.) The last two parameters have distinguishable physical meanings, class three being determined by rock and soil conditions and class four river system conditions, but they can not be distinguished by identification, as they share a common objective to minimize the error of the hydrograph. As a result the parameters of runoff separation become quite dependent, generally leading to non-unique solutions.

Usually, blame is put on the method of separation of the hydrograph. It is said that any problem on runoff separation can not be solved since there are no measured data on runoff components. But my experience reveals that the parameter dependence of runoff separation emerges from the parallel structure of linear reservoir, not from the condition of identification.

Among the basins that I have studied, I chose the Fonghuangshan to illustrate the problem using a daily model of XIN. Notations are: SM, free water capacity of the surface soil layer; mm; KG, KI, outflow constant of the free water storage to groundwater and interflow storage; EX, exponent of the

free water capacity curve; and CS, CI, CG, recession constant of river storage, interflow storage and groundwater storage.

Let EX=1.5, KG + KI = 0.7, then parameters of runoff separation are reduced to SM and KG, and that of runoff concentration are CS, CI, and CG. Using an objective optimization method to examine how much influence will be produced on the solution of parameters of runoff separation while parameters of runoff concentration varies in an ordinary range. The result is shown in tables 2, 3, and 4. Figures in it are Objective Function (OB).

Table 2. Influence of CG on Solution of Parameters of Runoff Separation.

CG =	0.992	0.994	0.996	0.998
	KG=0.25		KI-0.45	
SM=10	0.116	0.103	0.096	0.095
15	0.093	0.083	0.081	0.090
20	0.085	0.078	0.081	0.092
	KG=0.030		KI=0.040	
SM=10	0.095	0.085	0.083	0.090
15	0.079	0.074	0.078	0.090
20	0.078	0.077	0.083	0.094
	KG=0.35		KI=0.35	
SM=10	0.082	0.076	0.079	0.090
15	0.075	0.075	0.081	0.092
20	0.082	0.085	0.091	0.100

From table 2, we see while CG varies in an ordinary range 0.992-0.998, the solution SM and KG is stable, SM=15, KG=0.3 or 0.35, the optimum value of CG is 0.994. From table 3, we see while CI varies in an ordinary range 0.4-0.8, the solution of SM and KG is stable, SM=15, KG=0.3, or 0.35, the optimum value of CI is 0.8. From table 4, we see while CS varies in an ordinary range 0.1-0.3, the solution of SM and KG is stable, SM=15, KG=0.3, or 0.35, the optimum value of CS is 0.1. As a whole, the parameter of runoff concentration gives no influence to the solution of parameter of runoff separation.

Table 3. Influence of CI on Solution of Parameters of Runoff Separation

CI=	0.4	0.6	0.8
	KG=0.25		KI=0.45
SM=10	0.127	0.119	0.103
15	0.101	0.094	0.083
20	0.090	0.085	0.078
	KG=0.30		KI=0.40
SM=10	0.105	0.098	0.085
15	0.086	0.081	0.074
20	0.083	0.079	0.077
	KG=0.35		KI=0.35
SM=10	0.091	0.086	0.076
15	0.083	0.079	0.075
20	0.085	0.084	0.085

Table 4. Influence of CS on Solution of Parameters of Runoff Separation

CS=	0.1	0.2	0.3
	KG=0.25		KI=0.45
SM=10	0.102	0.103	0.104
15	0.081	0.083	0.104
20	0.076	0.078	0.081
	KG=0.30		KI=0.40
SM=10	0.084	0.085	0.086
15	0.072	0.074	0.076
20	0.075	0.077	0.080
	KG=0.35		KI=0.35
SM=10	0.075	0.076	0.077
15	0.073	0.075	0.078
20	0.082	0.085	0.087

This implies that surface, interflow and groundwater runoff produce quite different hydrographs because of large differences in velocity of flow. CS of surface runoff in 0.1-0.3, corresponding to a recession of half a day, forming a sharp hydrograph of floods. CG of groundwater runoff is 0.992-0.998, corresponding to a recession of 200 days, forming a flat hydrograph of low water. CI of interflow is 0.4-0.8, corresponding to a recession of 2 days, forming decreasing limb of flood tails. The three kinds of hydrographs are located at different portions of a continuous hydrograph, so we can distinguish them by means of an objective function derived from a continuous hydrograph. The hydrographs give basic information for separation of runoff into three components, and runoff separation is capable of identification.

The dependence of parameter of runoff separation emerges from the structure of linear reservoir. Analysis for the three models is as follows:

XIN. Figure 1. If KG + KI remains constant, the RS will be decreasing as SM increases. But if KG + KI decreases simultaneously, RS would remain. In addition, if KG/KI does not change, RI and RG would not change. An example of Misai basin is given in table 5. It shows, while SM increases and KG + KI decreases and KG/KI remain unchanged, the accuracy OB would be the same and the result of runoff separation is also the same. This results from the structure of the linear reservoir which has a threshold and two parallel outlets.

SAC. Figure 2. Notations are: UZFWM, upper zone free water capacity; UZK, outflow constant of upper zone free water storage; LZFPM, lower zone primary free water capacity; LZFSM, lower zone secondary free water capacity; LZPK, outflow constant of primary free water storage; LZSK, outflow constant of secondary free water storage; and PBASE, constant infiltration rate. PBASE=LZFPM*LZPK+LZFSM*LZSK. The structure of the upper layer is the same as XIN. In addition, let PBASE be constant, UZFWM and UZK are also constant, then surface runoff and interflow will be unchanged. If LZFPM*LZPK and LZFSM*LZSK are also constants, the primary and secondary groundwater flow will be unchanged. Under such a condition, the same accuracy and same runoff

Table 5. Dependence of Runoff Separation Parameters of XIN

SM	KG+KI	KG/KI	OB	RS	RI	RG
12	0.7		0.174	0.55	0.34	0.11
20	0.5	0.32	0.171	0.51	0.37	0.12
30	0.2		0.170	0.59	0.31	0.10
40	0.2		0.172	0.52	0.36	0.12

separation results will be obtained. An example of Nanqi basin is shown in table 6. In which UZFPM=30, UZK=0.5, LZFPM*LZPK=1.44, LZFSM*LZSK=3.24. We see in table 6 that LZFPM and LZFSM varying in a large extent will not effect the accuracy of OB and the runoff separation result will not be changed. This results from the structure of PBASE which has two pairs of parameters arranged in parallel.

Table 6. Dependence of Runoff Separation Parameters of SAC

LZFSM / LZFSM	180	220	260	300
90	0.102	0.096	0.093	0.091
130	0.094	0.091	0.090	0.090
170	0.091	0.090	0.089	0.089
210	0.091	0.091	0.091	0.092

TANK. Figure 3. Let the parameters of tank 1, 3, 4 remain constant, the outflow constants of the second tank B1 and B0 change by proportion, or, the parameters of tank 1, 2, 4 remain and C1 and C0 of the third tank change by proportion, then the result of runoff separation will be unchanged. An example is the Fengshi basin shown in table 7. Provided that the result of

Table 7. Dependence of Runoff Separation Parameters of TANK

H1	H2	A0	B1	B0	C1	C0	D1	OB
0.3	0.3	0.12	0.08	0.02	0.01	0.01	0.001	0.156
0.3	0.3	0.12	0.08	0.01	0.01	0.01	0.001	0.161
0.2	0.2	0.1	0.08	0.02	0.01	0.01	0.001	0.163
0.2	0.2	0.1	0.04	0.01	0.01	0.01	0.001	0.161
0.2	0.2	0.1	0.08	0.02	0.02	0.02	0.001	0.165

runoff separation is unchanged, many groups of parameters may obtain the same accuracy. This results from the structure of the linear reservoir which has two parallel outlets. Similarly, if the parameters of the first tank decrease simultaneously, the accuracy would remain unchanged.

In short, the dependence of parameters of runoff separation emerges from the model structure. Provided the result of runoff separation remains unchanged, whatever parameter values may give the same accuracy. In other words, the optimum solution of parameters may be miscellaneous but their result of runoff separation is the same. As shown in table 1, the result of runoff separation of different models at the optimum condition is also the same, which is an interesting unity with underlying hydrological rules.

As the cause of dependence of parameters is known, we can solve the problem by constraint. For example, for XIN, we may put KG+KI=constant. This is a constant derived from model structure, a structural constraint. For the purpose of identification, it is better than constraints given to the parameter values or computational results.

III. TO RAISE THE SCIENTIFIC LEVEL OF FORECASTING MODELS

Different models and different groups of parameter values of a model can obtain the same accuracy and the same results, therefore, using accuracy as the only criterion for model comparison is inadequate. A model may be

considered as a scientific hypothesis of hydrological rule of a basin and should be examined by any possible means. Besides accuracy, the final criterion of the examination is whether it expresses hydrological rule. A model, being a scientific hypothesis, becomes an instrument to investigate hydrological rule and will simulate the progress of scientific hydrology.

In the field of forecasting, there is often a tendency of only looking at accuracy, ignoring hydrological basis. In the past, the subject of forecasting was large floods, where hydrological principals are comparatively simple. For example, when the total basin is at full storage, the accumulated error of evapotranspiration computation is eliminated. The main component of runoff is surface runoff, and the error of runoff separation introduces small effect. Runoff concentration is very close to a linear system, high accuracy can be obtained. But now more should be forecasted as water project management requires added analysis. Besides large floods, there are medium and small floods, low water and underground water to be forecasted. More complicated schemes should be considered. To examine a model, a simple criterion of accuracy is not sufficient. A final criterion relating to hyrological rule is necessary. In addition, for districts lacking in hydrological data or heavily influenced by men's activities, we have to give forecasts now, so the problem of regional rule of model structure and model parameters is brought forward. Regional rule is a good means to verify whether the model expresses hydrological rule of the basin. Investigations should be strengthened. We are obliged to raise the scientific level of forecasting models in order to serve forecasting work better in the future.

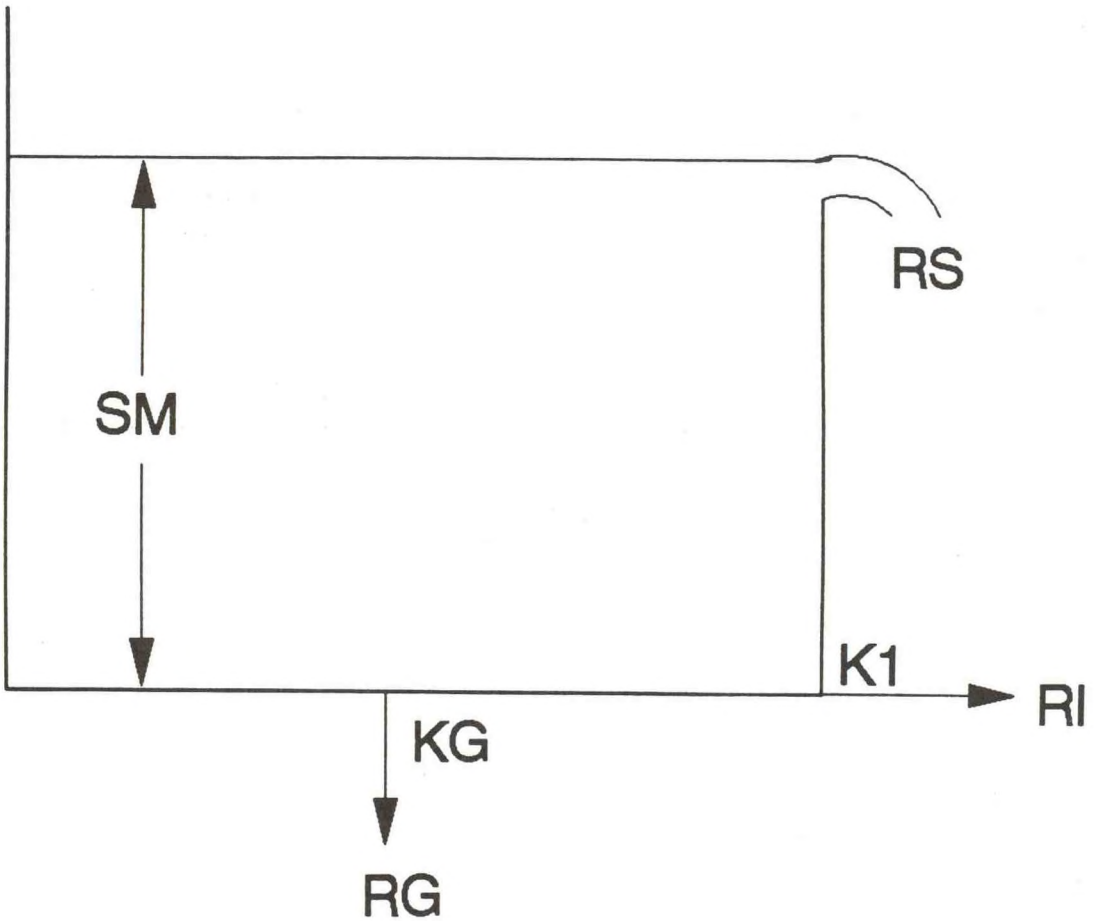

Figure 1. Structure of runoff separation of XIN

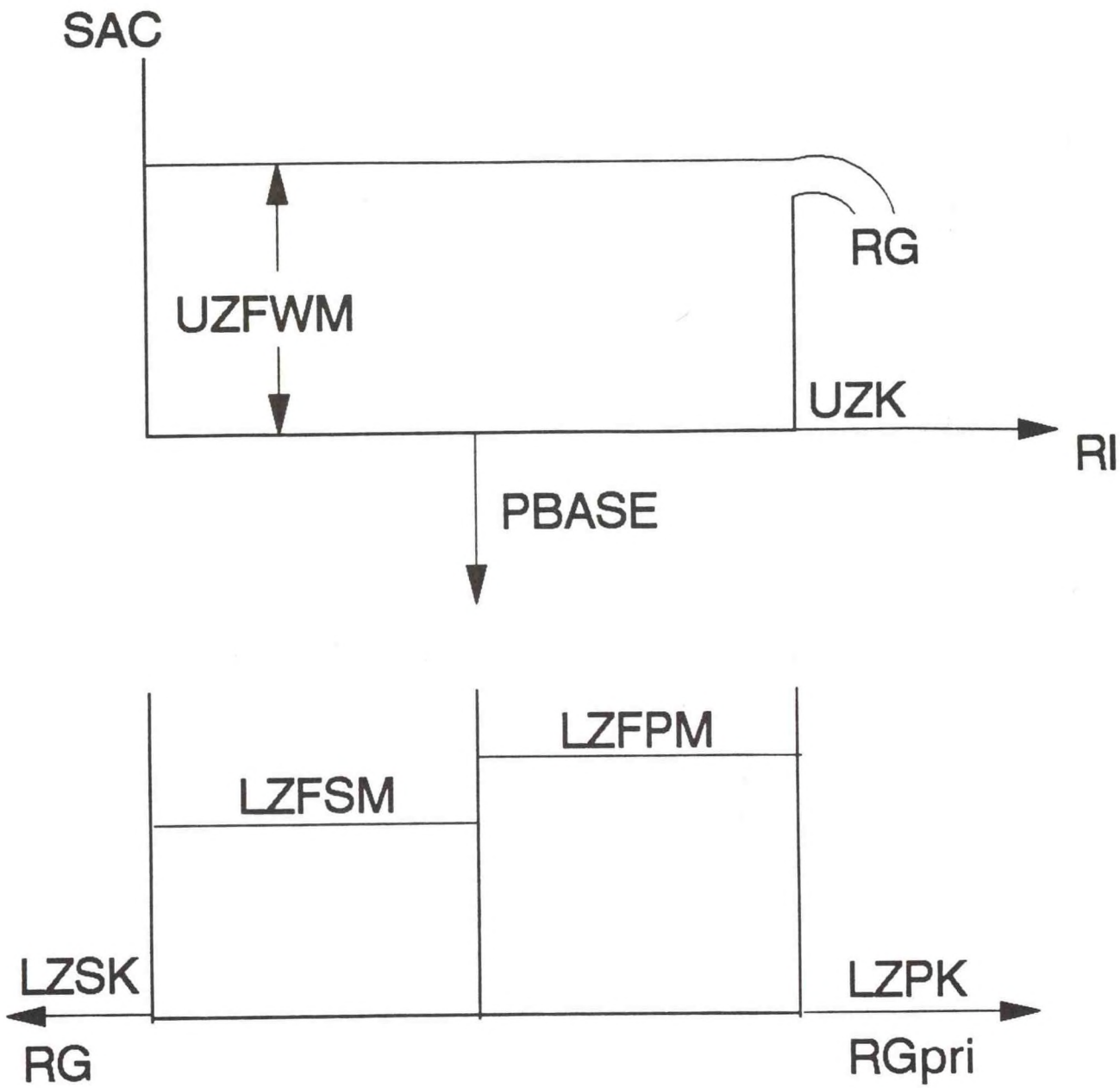

Figure 2. Structure of runoff separation of SAC

ZPERC = 0

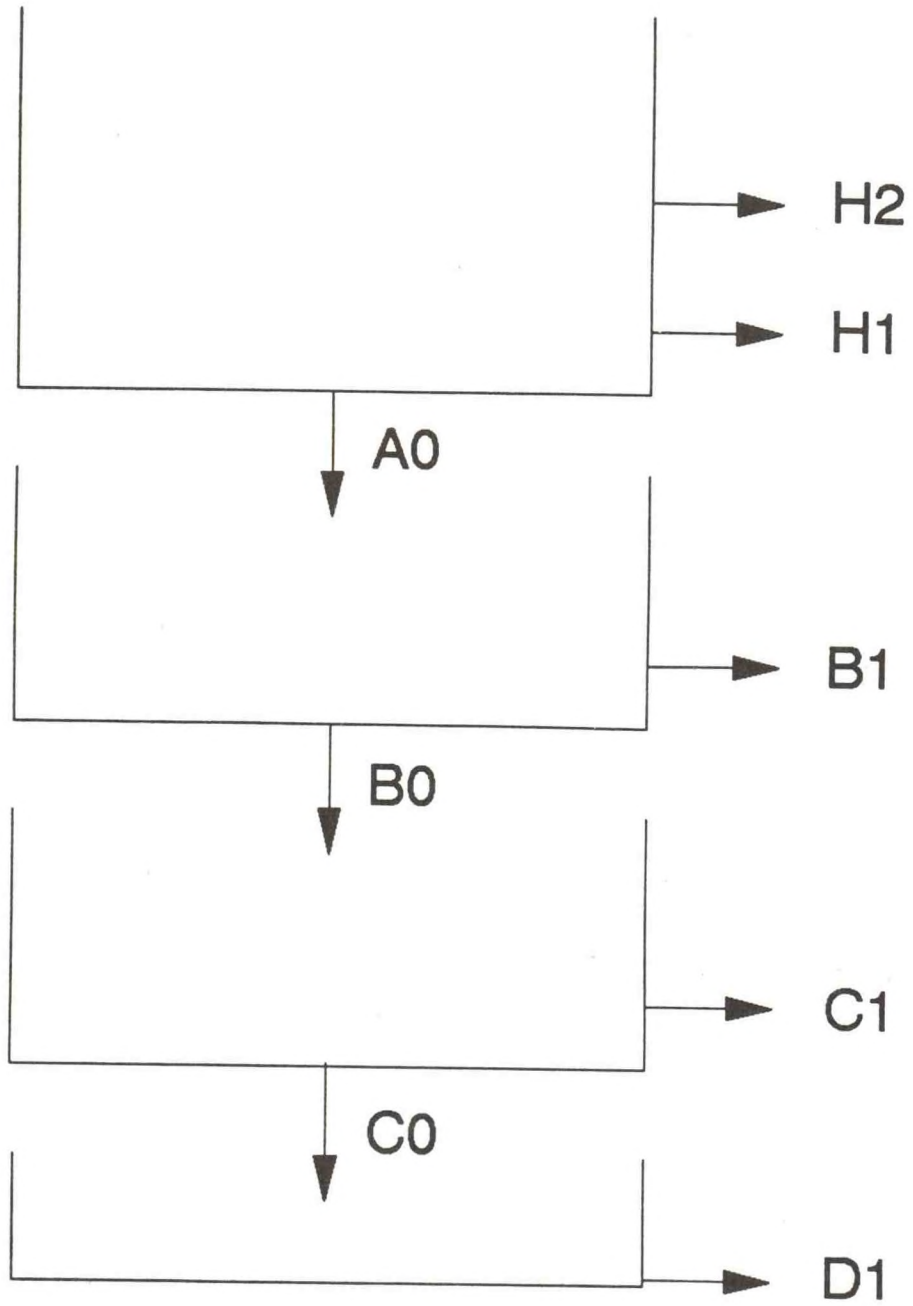

Figure 3. Structure of runoff separation of TANK

FLUVIAL-12
MATHEMATICAL MODEL FOR ERODIBLE CHANNELS

Howard H. Chang
San Diego State University
San Diego, California 92182

I. INTRODUCTION

Alluvial rivers are self-regulatory in that they adjust their characteristics in response to any change in the environment. These environmental changes may occur naturally, as in the case of climatic variation or changes in vegetative cover, or may be a result of such human activities as damming, river training, diversion, sand and gravel mining, channelization, bank protection, and bridge and highway construction. Such changes distort the natural quasi-equilibrium of a river. In the process of restoring the equilibrium, the river will adjust to the new conditions by changing its slope, roughness, bed-material size, cross-sectional shape, or meandering pattern. Within the existing constraints, any one or a combination of these characteristics may adjust as the river seeks to maintain the balance between its ability to transport and the load provided.

River channel behavior often needs to be studied for its natural state and responses to the aforementioned human activities. Studies of river hydraulics, sediment transport, and river channel changes may be through physical modeling or mathematical modeling, or both. Physical modeling has been relied upon, traditionally, to obtain the essential design information. It often involves large expenditure and is time consuming in model construction and experimentation. What limits the accuracy of physical modeling is the scale distortion which is almost unavoidable whenever it involves sedimentation.

Mathematical modeling of erodible channels has been advanced with the progress in the physics of fluvial processes and computer techniques. An evaluation of existing models was made by the National Academy of Sciences (1983). Recommendations in this report have been beneficial for subsequent model development. Since the actual size of a river is employed in mathematical modeling, there is no scale distortion. The applicability and

accuracy of a model depend on the physical foundation and numerical techniques employed.

The traditional regime analyses of rivers are limited to regime rivers and their long-term adjustments in equilibrium. The hydraulic geometry, flow, and sediment transport processes exhibited in the process of adjustments are outside the scope of regime approach, but they are included in the mathematical modeling. This manual addresses the more rapid process-response or the transient behavior of alluvial rivers. The subject is on unsteady flow and sediment transport in river channels with a changing boundary under given physical constraints. In the following, the physical foundation and numerical techniques for the transient process-response of the FLUVIAL model are described. The input/output instructions are provided. Applications of the FLUVIAL model are illustrated by examples given in the appendices.

II. PHYSICAL FOUNDATION OF FLUVIAL PROCESS-RESPONSE

Mathematical modeling of river channel changes requires adequate and sufficient physical relationships for the FLUVIAL processes. While the processes are governed by the principles of continuity, flow resistance, sediment transport, and bank stability, such relations are insufficient to explain the time and spatial variations of channel width in an alluvial river. Generally, width adjustment occurs concurrently with changes in river bed profile, slope, channel pattern, roughness, etc. These changes are closely interrelated; they are delicately adjusted to establish or to maintain the dynamic state of equilibrium. While any factor imposed upon the river is usually absorbed by a combination of the above responses, the extend of each type of response is inversely related to the resistance to change.

The dynamic equilibrium is the direction toward which each river channel evolves. The transient behavior of an alluvial river undergoing changes must reflect its constant adjustment toward dynamic equilibrium, although, under the changing discharge, the true equilibrium may never be attained. For a short river reach of uniform discharge, the conditions for dynamic equilibrium are: (1) equal sediment discharge along the channel, and (2) uniformity in power expenditure γQS, where γ is the unit weight of the water-sediment

mixture, Q is the discharge, and S is the energy gradient. If the energy gradient is approximated by the water-surface slope, then uniform power expenditure or energy gradient is equivalent to the linear (straight-line) water-surface profile along the channel. A river channel undergoing changes usually does not have a linear water-surface profile or uniform sediment discharge, but river channel adjustments are such that the nonuniformities in water-surface profile and sediment discharge are effectively reduced. The rate of adjustment is limited by the rate of sediment movement and subject to the rigid constraints such as the grade-control structures, bank protection, abutments, bedrock, etc.

The energy gradient at a river cross section varies wildly. This variable is usually included in a hydraulic computation such as that of a HEC-2 study. The output of any HEC-2 study, even for a fairly uniform river channel, usually exhibits nonuniformity in energy gradients along the channel. This variation is much more pronounced in disturbed rivers. A mathematical modeler realizes that a river channel will change in order to attain streamwise uniformity in sediment load. It is equally important to perceive that it will also adjust toward equal energy gradient along the channel. Because sediment discharge is a direct function of γQS, channel adjustment in the direction of equal power expenditure also favors the uniformity in sediment discharge. The sediment discharge in the reach will match the inflow rate when the equilibrium is reached.

III. CHANNEL WIDTH ADJUSTMENTS DURING SCOUR AND FILL

An adjustment of the stream channel in the direction of equal power expenditure, or straight water-surface profile, provides the physical basis for the modeling of channel width changes. However, this adjustment does not necessarily mean movement toward uniformity in channel width. For one thing, the power expenditure is also affected by channel roughness and channel-bed elevation, in addition to the width. But, more importantly, the adjustment toward uniformity in power expenditure is frequently accomplished by significant streamwise variation in width. Such spatial width variation

generally occurs concurrently with streambed scour or fill to be illustrated by the following examples.

The transient behavior can be more clearly demonstrated by more dramatic river channel changes in the short term. Field examples of this nature are selected herein to illustrate how the significant spatial variation in width is related to the adjustment of the river channel toward uniform power expenditure. This example will also show why the regime approach may not be employed to simulate river channel changes.

An example is a short reach of the San Diego River at Lakeside, California, on February 25, 1981, during the initial stage of a storm. The estimated discharge of 600 cfs persisted for several subsequent days. Prior to the storm, this sandy streambed was graded, due to sand mining, to a wavy profile. During the initial period of flow, the water-surface profile was not straight because its gradient was steeper over higher streambed areas than over lower areas. Gradually, these higher streambed areas were scoured while lower places were filled. Small widths formed with streambed scour, whereas large widths developed with fill. The width development, in this case, was rapid in occurrence in the sandy material, its significant streamwise variation was depicted by the natural streamlines visible on the water surface. This pattern of significant spatial variation in width actually represents the adjustment of the stream toward equal energy gradient as explained in the following.

The streambed area undergoing scour had a steeper energy gradient (or water-surface slope) than its adjacent areas. Formation of a more narrow and deeper channel was effective to reduce the energy gradient due to decreased boundary resistance and lowered streambed elevation. In addition, the cross section developed a somewhat circular shape which conserved power for being closer to the best hydraulic section. On the other hand, the streambed area, undergoing fill, had a lower streambed elevation and a flatter energy gradient. Channel widening at this area was effective to steepen its energy gradient due to the increasing boundary resistance and rising streambed elevation. In summary, these adjustments in channel width effectively reduced the spatial variation

in power expenditure or nonlinearity in water-surface profile. Because sediment discharge is a direct function of stream power γQS, channel adjustment in the direction of equal power expenditure also favors the equilibrium, or uniformity, in sediment discharge.

The significant spatial width variation was temporary. The small width lasted while streambed scour continued and the large width persisted with sustained fill. At a later stage when scour and fill ceased, the energy gradient or water-surface slope, associated with the small width, became flatter than that for the large width. The new profile of energy gradient or water surface became a reversal of the initial profile. Then, the small width started to grow wider while the large width began to slide back into the channel, resulting in a more uniform width along the channel.

The above example illustrates that a regime relationship for channel width may not be used in simulating transient river channel changes. Under the regime relationship, the width is a direct function of the discharge, i.e., $B \propto Q^{0.5}$; but under transient changes, the channel can have very different widths even though the discharge is essentially uniform along the channel.

The characteristic changes in channel width during channel-bed scour and fill were also observed by Andrews (1982) on the East Form River in Wyoming. This river was in its natural state, undisturbed by human activities. River channel changes were induced by the variation in discharge.

In 1906, the Associated Press (AP) filed a well-written report which seemed to end one of the world's most spectacular stories. In the story, the AP reported that the Colorado River flooded; the water moved from the All American Canal to the New River and poured down to the Salton Sea. The sea rose 7 inches per day. The water became a cascade and its force cut back the banks. Soon the bank was receding faster and faster, moving upstream into the valley at a pace of 4,000 feet a day and widening the New River channel to a gorge of more than 1,000 feet. This example also illustrates the dramatic widening of river channel associated with a rising bed elevation.

A field study by the U.S. Bureau of Reclamation (1963) upstream of Milburn Diversion Dam on the Middle Loup River, central Nebraska, also exemplifies the aggradation of a channel and associated channel widening.

> The construction of Milburn Diversion Dam was completed in May 1956 ... By May 1957, 2 months after the reservoir was impounded for the first irrigation season, the channel had aggraded an average of 1.6 feet, with a rise in the channel thalweg elevation to 2.2 feet; and by October of the same year, the total rise in the streambed averaged 2.2 feet. The cross section obtained in December 1957 showed a continued rise in the thalweg elevation. During the same period, the width of the channel had increased by 70 feet, from 475 feet in 1951, to 545 feet in 1957. One-third of this increase occurred during the June 1956 - December 1957 period.

For these two case histories, both alluvial rivers entered reservoirs with a rising base level. The transient changes are characterized by rising channel bed and increasing channel width. Although measurements of the discharge and other parameters are not available, it is possible to describe, at least in trend, the nature of power transformation in the river channel.

At the river mouth, the base level was controlled in the reservoir. The rising base level first caused a lower velocity and energy gradient in the river channel near the mouth in relation to its upstream reach. In response to this change, channel adjustments, through widening and aggradation near the mouth, provided greater flow resistance and power expenditure at this location partly due to the increased boundary resistance. This process resulted in a more uniform power expenditure per unit channel length along the river.

A lowering base level, on the other hand, would result in a higher energy gradient in the river channel near the mouth. The higher energy gradient could be reduced through the development of a more narrow and deeper channel at this location. This process would also result in a more uniform power

expenditure along the channel. Such morphological features for deltas are also applicable to alluvial fans and hill slopes.

IV. ANALYTICAL BASIS OF THE FLUVIAL MODEL

The FLUVIAL model, with different versions, has been developed for water and sediment routing in rivers while simulating river channel changes. River channel changes simulated by the model include channel-bed scour and fill (or aggradation and degradation), width variation, and changes caused by curvature effects. Because changes in channel width and channel-bed profile are closely interrelated, modeling of erodible channels must include both changes. The analytical background of the FLUVIAL model is described in the following.

The FLUVIAL model has the following five major components: (1) water routine, (2) sediment routing, (3) changes in channel width, (4) changes in channel-bed profile, and (5) changes in geometry due to curvature effect. These interrelated components are described in the following sections.

This model employs a space-time domain in which the space domain is represented by the discrete cross sections along the channel and the time domain is represented by discrete time increments. Temporal and spatial variations in flow, sediment transport, and channel geometry are computed following an iterative procedure. Water routing, which is coupled with the changing curvature, is assumed to be uncoupled from the sediment processes since sediment movement and changes in channel geometry are slow in comparison to the flow hydraulics. A flow chart showing major steps of the computation is given in fig. 1.

V. WATER ROUTING

Water routing provides temporal and spatial variations of the stage, discharge, energy gradient, and other hydraulic parameters in the channel. The water routing component has the following major features: (1) numerical solution of the continuity and momentum equation for longitudinal flow, (2) evaluation of flow resistance due to longitudinal and transverse flows, and

(3) upstream and downstream boundary conditions. The continuity and momentum equations in the longitudinal direction are:

$$\frac{\partial A}{\partial t} + \frac{\partial Q}{\partial s} - q = 0 \qquad (1)$$

$$\frac{1}{A}\frac{\partial Q}{\partial t} + g\frac{\partial H}{\partial s} + \frac{1}{A}\frac{\partial}{\partial s}\left(\frac{Q^2}{A}\right) + gS - \frac{Q}{A^2}q = 0 \qquad (2)$$

where Q is the discharge, A is the cross-sectional area of flow, t is the time, s is the curvilinear coordinate along discharge centerline measured from the upstream entrance, q is lateral inflow rate per unit length, H is the stage of water-surface elevation, and S is the energy gradient. The upstream boundary condition for water routing is the inflow hydrographs and the downstream condition is the stage-discharge relation or the base-level variation. Techniques for numerical solution of eqs. 1 and 2 are described in Chen (1973) and Fread (1971, 1974), among others.

In a curved channel, the total energy gradient, S, in eq. 2 is partitioned into the longitudinal energy gradient, S', and the transverse energy gradient, S", due to secondary currents, i.e.

$$S = S' + S" \qquad (3)$$

The longitudinal energy gradient can be evaluated using any valid flow resistance relationship. If Manning's formula is employed, the roughness coefficient n must be selected by the modeler. However, if a formula for alluvial bed roughness is used, e.g., Brownlie's formula (1983), the roughness coefficient is predicted by the formula.

The method for evaluating the transverse energy gradient by Chang (1983) is used in the model. Because of the streamwise changing curvature, the transverse energy loss varies with the growth and decay of secondary currents along the channel. Analytical relationships pertaining to curved channels are often based upon the mean channel radius, r_c. Under the streamwise changing curvature, the application of such relationships is limited to a fully developed transverse flow for which the curvature is defined. Streamwise

variation of transverse flow, over much of the channel length, is characterized by its growth and decay. In order to describe this spatial variation, the mean flow curvature defined as the flow curvature along the discharge centerline is employed. It is assumed that analytical relationships for developed transverse flows are applicable for developing transverse flows when the mean channel curvature, r_c, is replaced by the mean flow curvature, r_f. Upon entering a bend, the mean flow curvature increases with the growth in transverse circulation. In a bend, the transverse flow becomes fully developed if the flow curvature approaches the channel curvature. In the case of exiting from a bend to the downstream tangent, in which the channel curvature is zero, the flow curvature decreases with the decay of transverse circulation.

The reason that the flow curvature lags behind the channel curvature during circulation growth and decay is attributed to the internal turbulent shear that the flow has to overcome in transforming from parallel flow into the spiral pattern and vice versa. From the dynamic equation for the transverse velocity, an equation governing the streamwise variation in transverse surface velocity, $\tilde{v}$, was derived (Chang, 1984). In finite difference form, the change in $\tilde{v}$ over the distance Δs is given by:

$$\tilde{v}_{i+1} = \left[\tilde{V}_i + F_1(f)\,\frac{U}{r_c}\exp(F_2(f)\Delta s)\,\Delta s\right]\exp\left[-F_2(f)\,\Delta s\right] \qquad (4)$$

where $\tilde{v}$ is the transverse surface velocity along discharge centerline, U is the average velocity of a cross section, i and i+1 are s-coordinate indices, F_1 and F_2 are functions of f (friction factor), and the overbar denotes averaging over the incremental distance between i and i+1. Eq. 4 provides the spatial variation in $\tilde{v}$, from which the mean flow curvature may be obtained using the transverse velocity profile. From the transverse velocity profile by Kikkawa, et al. (1976), the mean flow curvature, r_f, is related to the transverse surface velocity as:

$$r_f = \frac{D_c}{\kappa}\,\frac{U}{\tilde{v}}\left(\frac{10}{3} - \frac{1}{\kappa}\,\frac{5}{9}\sqrt{\frac{f}{2}}\right) \qquad (5)$$

where D_c is the flow depth at discharge centerline (thalweg) and κ is the Karman constant. At each time step, the mean flow curvature at each cross section is obtained using eqs. 4 and 5. Accuracy of computation for the finite difference equation (eq. 4) is maintained if the step size $\Delta s \leq 2D_c$. For this reason, the distance between two adjacent cross sections is divided into smaller increments, if necessary. Flow parameters for these increments are interpolated from values known at adjacent cross sections.

If the temporal terms in eqs. 1 and 2 are ignored, water routing may be simplified by computing water-surface profiles at successive time steps. This option is available in the model. Computation of the water-surface profile at each time step is based upon the standard-step method (see Chow, 1957) using techniques similar to the HEC-2 computer model (1982). For many cases, spatial variation in discharge due to channel storage is small and this technique produces similar results as the unsteady routing.

VI. SEDIMENT ROUTING

The sediment routing component for the FLUVIAL model has the following major features: (1) computation of sediment transport capacity using a suitable formula for the physical conditions, (2) determination of actual sediment discharge by making corrections for sorting and diffusion, (3) upstream conditions for sediment inflow, and (4) numerical solution of the continuity equation for sediment. These features are evaluated at each time step, the results obtained are used in determining the changes in channel configuration.

A. Determination of Sediment Discharge

To treat the time-dependent and nonequilibrium sediment transport, the bed material at each section is divided into several size fractions and the size is represented by the geometric mean for each fraction i.e., five. For each size fraction, sediment transport capacity is first computed by using a sediment transport formula. The FLUVIAL model currently provides the choices of the following five sediment formulas: (1) Engelund-Hansen formula (1967); (2) Yang's unit stream power formula (1973, 1986); (3) Graf's formula (1970);

(4) Ackers-White formula; and (5) Parker, et al. formula for gravel (1982). The actual sediment rate is obtained by considering sediment material of all size fractions already in the flow and the exchange of sediment load with the bed using the method by Borah, et al. (1982). If the stream carries a load in excess of its capacity, it will deposit the excess material on the bed. In the case of erosion, any size fraction available for entrainment at the bed surface will be removed by the flow and added to the sediment already in transport. During sediment removal, the exchange between the flow and the bed is assumed to take place in the active layer at the surface. Thickness of the active layer is based upon the relation defined by Borah, et al. This thickness is not only a function of the material size and composition, but also reflects the flow condition. During degradation, several of these layers may be scoured away, resulting in the coarsening of the bed material and the formation of an armor coat. However, new active layers may be deposited on the bed in the process of aggradation. Materials eroded from the channel banks, excluding that portion in the wash load size range, are included in the accounting. Bed armoring develops if bed shear stress is too low to transport any available size.

The nonequilibrium sediment transport is also affected by diffusion, particularly for finer sediments. Because of diffusion, the deposition or entrainment of sediment is a gradual process and it takes certain travel time or distance to reach the transport capacity for a flow condition. Therefore, the actual sediment discharge at a section depends not only on the transport capacity at the section but also on the supply from upstream and its gradual adjustment toward the flow conditions of the section. In the model, the sediment discharge is corrected for the diffusion effects on deposition and entrainment using the method by Zhang, et al. (1983). The procedures for computing sediment transport rate, sediment sorting, and diffusion are applied to the longitudinal and transverse directions. They are also coupled with bed-profile evolution described later in this section.

Sediment discharge may be limited by availability, as exemplified by the flow over a grade-control structure or bed rock. The very high transport capacity at such a section, associated with the high velocity, is limited by

the supply rate from upstream; that is, the sediment discharge at such a section is under upstream control.

B. Upstream Boundary Conditions for Sediment Inflow

The rate of sediment inflow into the study reach is provided by the upstream boundary condition for sediment. If this rate is known, it may be included as a part of the input and used in the simulation. Unfortunately, sediment rating data are rarely very reliable or simply not available. For such cases, it is assumed that the river channel remains unchanged above the study reach, and the sediment inflow rate is computed at the upstream section at each time step just as they are computed at other cross sections. For this reason, the study reach should extend far enough upstream so that the channel beyond may be considered basically stable. Factors that may induce river channel changes must be included in the study reach.

C. Numerical Solution of Continuity Equation for Sediment

Changes in the cross-sectional area, due to longitudinal and transverse imbalances in sediment discharge, are obtained based upon numerical solution of continuity equations for sediment in the respective directions. First, the continuity equation for sediment in the longitudinal direction is

$$(1 - \lambda) \frac{\partial A_b}{\partial t} + \frac{\partial Q_s}{\partial s} - q_s = 0 \qquad (6)$$

where λ is the porosity of bed material, A_b is the cross-sectional area of channel bed within some arbitrary frame, Q_s is the bed-material discharge, and q_s is the lateral inflow rate of sediment per unit length. According to this equation, the time change of cross-sectional area $\partial A_b/\partial t$ is related to the longitudinal gradient in sediment discharge $\partial Q_s/\partial t$ and lateral sediment inflow q_s. In the absence of q_s, longitudinal imbalance in Q_s is absorbed by channel adjustments toward establishing uniformity in Q_s

The change in cross-sectional area ΔA_b for each section at each time step is obtained through the numerical solution of eq. 6. This area change will be

applied to the bed and banks following correction techniques for channel width and channel-bed profile.

From eq. 6, the correction in cross-sectional area of channel bed for a time increment can be written as:

$$\Delta A_b = - \frac{\Delta t}{1 - \lambda} \left(\frac{\partial Q_s}{\partial s} - q_s \right) \tag{7}$$

At a section i, the lateral sediment inflow may be written as

$$q_{s_i} = \frac{1}{2} \left(q_{s_i}^{j} + q_{s_i}^{j+1} \right) \tag{8}$$

where superscripts j and j+1 are the times at t and t + Δt, respectively. This model employs an upstream difference in s and a centered difference in to for the partial derivative, $\partial Q_s / \partial s$, in eq. 6, i.e.

$$\left(\frac{\partial Q_s}{\partial s} \right)_i = \frac{2}{\Delta s_i + \Delta s_{i-1}} \left(\frac{Q_{s_i}^{j} + Q_{s_i}^{j+1}}{2} - \frac{Q_{s_{i-1}}^{j} + Q_{s_{i-1}}^{j+1}}{2} \right) \tag{9}$$

where Δs_i is the distance between sections i and i+1, and Δs_{i-1} is the distance between i-1 and i. With this upstream difference for $\partial Q_s / \partial s$, the change in bed area at a section i depends on sediment rates at this section and its upstream section i-1; it is independent of the sediment rate at the downstream section. In other words, it is under upstream control. Contrary to this, the stage at a section in subcritical flow depends on the downstream stage and is independent of the upstream stage, i.e., the stage is under downstream control in a subcritical flow.

VII. SIMULATION OF CHANGES IN CHANNEL WIDTH

The change in cross-sectional area ΔA_b obtained in sediment routing represents the correction for a time increment t that needs to be applied to the bed and banks. With ΔA_b being the total correction, it is possible for both the bed and banks to have deposition or erosion; it is also possible to

have deposition along the banks, but erosion in the bed and vice versa. The direction of width adjustment is determined by following the stream power approach and the rate of change is based upon bank erodibility and sediment transport described in the following.

A. Direction of Width Adjustment

For a time step, width corrections at all cross sections are such that the stream power for the reach moves toward uniformity. These corrections are subject to the physical constraint of rigid banks and limited by the amount of sediment removal or deposition along the banks within the time step. A river channel undergoing changes usually has nonuniform spatial distribution in power expenditure of γQS. Usually the spatial variation in Q is small but that in S is pronounced. An adjustment in width reflects the river's adjustment in flow resistance of the river; that is, in power expenditure. A reduction in width at a cross section is usually associated with a decrease in the energy gradient for the section whereas, an increase in width, is accompanied by an increase in the energy gradient. To determine the direction of width change at a section i, the energy gradient at this section, S_i, is compared with the weighted average of its adjacent sections, $\overline{S}_i$. Here:

$$\overline{S}_i = \frac{S_{i+1}\Delta s_i + S_{i-1}\Delta s_{i+1}}{\Delta s_i + \Delta s_{i+1}} \tag{10}$$

If the energy gradient S_i is greater than $\overline{S}_i$, channel width at this section is reduced so as to decrease the energy gradient. On the other hand, if S_i is lower, channel width is increased in order to raise the energy gradient. These changes are subject to the rate of width adjustment and physical constraints.

Width changes in alluvial rivers are characterized by widening during channel-bed aggradation (or fill) and reduction in width at the time of degradation (or scour). Such river channel changes represent the river's adjustments in resistance of the river to seek equal power expenditure along its course. A degrading reach usually has a higher channel-bed elevation and energy gradient than its adjacent sections. Formation of a more narrow and

deeper channel at the degrading reach decreases its energy gradient due to reduced boundary resistance. On the other hand, an aggrading reach is usually lower in channel-bed elevation and the energy gradient. Widening at the aggrading reach increases its energy gradient due to increasing boundary resistance. These adjustments in channel width reduce the spatial variation in the energy gradient and the total power expenditure of the channel.

B. Rate of Width Adjustment

For a time increment, the amount of width change depends on the sediment rate, bank configuration, and bank erodibility. The slope of an erodible bank is limited by the angle of repose of the material. The rate of width change depends on the rate at which sediment material is removed or deposited along the banks. For the same sediment rate, width adjustment at a tall bank is not as rapid as that at a low bank. The rates of width adjustment for cases of width increase and decrease are somewhat different as described below.

An increase in width at a channel section depends on sediment removal along the banks. The maximum rate of widening occurs when sediment inflow from the upstream section does not reach the banks of that section, while bank material at the section is being removed. River banks have different degrees of resistance to erosion; therefore, the rate of sediment removal along a bank needs to be modified by a coefficient. For this purpose, the bank erodibility factor is introduced as an index for the erosion of bank material and the four bank types reflecting the variation in erodibility are classified as follows: (1) nonerodible banks; (2) erosion-resistant banks, characterized by highly cohesive material or substantial vegetation, or both; (3) moderately erodible banks having medium bank cohesion; and (4) easily erodible banks with noncohesive material. Values of bank erodibility factor vary from zero for the first type to one for the last type of bank. The values of 0.2 and 0.5 have been empirically determined for the second and third types, respectively, based upon test and calibration of the model, using field data from rivers in the western United States. However, the bank erodibility factor should still be calibrated whenever data on width changes are available.

A decrease in channel width is accomplished by sediment deposition along the banks or a decrease in stage, or both. For practical reasons, deposition does not exceed the stage in the model. The maximum amount of width reduction at a section occurs when sediment inflow from the upstream section is spread out at this section and the sediment removal from the bank areas at this section is zero.

Within the limit of width adjustment, changes in width are made at all cross sections in the study and reach toward establishing uniformity in power expenditure.

VIII. SIMULATION OF CHANGES IN CHANNEL-BED PROFILE

After the banks are adjusted, the remaining correction for A_b is applied to the bed. Distributions of erosion and deposition, or fill and scour, at a cross section are usually not uniform. Generally speaking, deposition tends to start from the low point and it is more uniformly distributed because it tends to build up the channel bed in nearly horizontal layers. This process of deposition is often accompanied by channel widening. On the other hand, channel-bed erosion tends to be more confined with greater erosion in the thalweg. This process is usually associated with a reduction in width as the banks slip back into the channel. Such characteristic channel adjustments are effective in reducing the streamwise variation in stream power as the river seeks to establish a new equilibrium. In the model, the allocation of scour and fill across a section during each time step is assumed to be a power function of the effective tractive force $\tau_o - \tau_c$, i.e.:

$$\Delta z = \frac{(\tau_o - \tau_c)^n}{\sum_B (\tau_o - \tau_c)^n \, \Delta y} \Delta A_b \qquad (11)$$

where Δz is the local correction in channel-bed elevation, τ_o (given by YDS) is the local tractive force, τ_c is the critical tractive force, n is an exponent, and y is the horizontal coordinate, and B is the channel width. The value of τ_c is zero, in the case of fill.

The n value in eq. 11 is generally between 0 and 1; it affects the pattern of scour-fill allocation. For the schematic cross section shown in fig. 2, a small value of n, i.e. 0.1, would mean a fairly uniform distribution of Δz across the section; a larger value, i.e. 1, will give a less uniform distribution of Δz and the local change will vary with the local tractive force or roughly the depth. The value of n is determined at each time step such that the correction in the channel-bed profile will result in the most rapid movement toward uniformity in power expenditure, or linear water surface profile, along the channel.

Equation 11 may only be used in the absence of channel curvature. The change in bed area at a cross section in a curved reach is:

$$\Delta A_b = \frac{1}{r_f} \int r \, \Delta z \, dr \tag{12}$$

where r_f is the radius of curvature at the discharge centerline or thalweg. Because of the curvature, adjacent cross sections are not parallel and the spacing Δs between them varies across the width. Therefore, the distribution of Δz given in eq. 11 needs to be weighted according to the r-coordinate, with respect to the thalweg radius, r_f/r, i.e.:

$$\Delta z = \frac{(\tau_o - \tau_c)^n / r}{\sum_B (\tau_o - \tau_c)^n / r \, \Delta r} \Delta A_b \tag{13}$$

IX. SIMULATION OF CHANGES DUE TO CURVATURE EFFECT

Simulation of curvature-induced scour and deposition is based upon the flow curvature from which the streamwise variation is given in eq. 4. The major features of transverse sediment transport and changes in bed topography are described below.

Sediment transport, in the presence of transverse flow, has a component in that direction. Sediment movement in the transverse direction contributes to the adjustment of the transverse bed profile. In an unsteady flow, the transverse bed profile varies with time, and it is constantly adjusted toward the equilibrium through scour and deposition. The transverse bed load per

unit channel length q_b' can be related to the streamwise transport q_b. Such a relationship, by Ikeda (1982), can be written in parametric form as

$$\frac{q_b'}{q_b} = F\left(\tan \delta, \frac{\partial z}{\partial r}\right) \tag{14}$$

where δ is the angle of deviation of bottom currents from the streamwise direction. The near-bed transverse velocity is a function of the curvature, and it is computed using the flow curvature.

Equation 14 relates the direction of bed-load movement to the direction of near-bed velocity and transverse bed slope $\partial z/\partial r$. As transverse velocity starts to move sediment away from the concave bank, it creates a transverse bed slope that counters the transverse sediment movement. An equilibrium is reached, i.e., $q_b' = 0$, when the effects of these opposing tendencies are in balance. Transverse bed-profile evolution is related to the variation in the bed-material load. Ikeda and Nishmura (1986) developed a method for estimating transport and diffusion of fine sediments in the transverse direction by vertical integration of suspended load over the depth. Their model for predicting the transverse bed slope is also employed.

Changes in channel-bed elevation at a point due to transverse sediment movement are computed using the transverse continuity equation for sediment:

$$\frac{\partial z}{\partial t} + \frac{1}{1 - \Lambda} \frac{1}{r} \frac{\partial}{\partial r} (r\, q_s') = 0 \tag{15}$$

Written in finite difference form, with a forward difference for q_s', this equation becomes:

$$\Delta z_k = \frac{\Delta t}{1 - \lambda} \frac{2}{r_k} \frac{r_{k+1}\, q'_{s_{k+1}} - r_k\, q'_{s_k}}{r_{k+1} - r_{k-1}} \tag{16}$$

where k is the radial (transverse) coordinate index measured from the center of the radius. Equation 16 provides the changes in channel-bed elevation for a time step due to transverse sediment movement. These transverse changes, as well as the longitudinal changes, are applied to the stream bed at each time

step. Bed-profile evolution is simulated by repeated iteration along successive time steps.

X. TEST AND CALIBRATION OF MATHEMATICAL MODEL

The accuracy of a mathematical model depends on the physical foundation, numerical techniques, and physical relations for momentum, flow resistance, and sediment transport. Test and calibration are important steps to be taken for more effective use of a model. Because of the difference in sensitivity of simulated results to each relation or empirical coefficient, more attention needs to be paid to those that generate sensitive results. Major items that require calibration include the roughness coefficient, sediment transport equation, bank erodibility factor, bed erodibility factor, etc.

To determine the sensitivity of flow, sediment transport and channel changes caused by the variation of each variable, different values of the variable need to be used in simulation runs and the results obtained are compared. Generally speaking, the rate of channel changes is more sensitive to the sediment rate computed from a sediment equation, but the equilibrium channel configuration is less sensitive. For example, the constriction scour at a bridge crossing, or the equilibrium local scour at a bridge pier, is found to be more or less independent of the sediment equation, or sediment size, since both inflow and outflow rates of sediment are affected by about the same proportion. It may also be stated that the rate of widening is sensitive to the bank erodibility factor, but the equilibrium width is not nearly as sensitive.

Field data are generally required for test and calibration of a model. Generally, the channel configuration before and after the changes, flow records and sediment characteristics are required. Data sets with more complete information are also more useful.

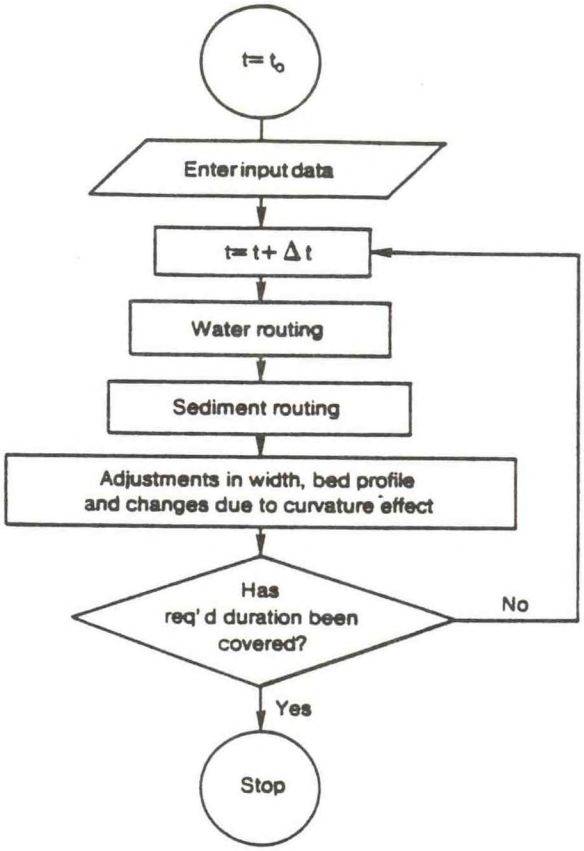

Figure 1. Flow chart showing major steps of computation for FLUVIAL model

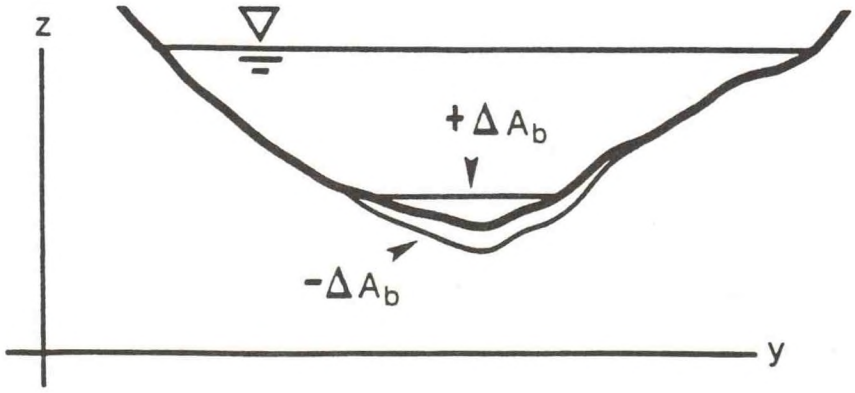

Figure 2. Corrections of bed profile for aggradation and degradation. They are made in such a way the water-surface profile or power expenditure moves toward uniformity

REFERENCES

Ackers, P., and White, W. R., "Sediment Transport: A New Approach and Analysis," Journal of the Hydraulics Division, ASCE, Vol. 99, No. HY11, pp. 2041-2060, November 1973.

Andrews, E. D., "Bank Stability and Channel Width Adjustment, East Fork River, Wyoming," Water Resources Research, Vol. 18, No. 4, pp. 1184-1192, August 1982.

Borah, D. K., Alonso, C. V., and Prasad, S. N., "Routing Graded Sediments in Streams: Formulations," Journal of the Hydraulics Division, ASCE, Vol. 108, No. HY12, pp. 1486-1503, December 1982.

Brownlie, W. R., "Flow Depth in Sand-Bed Channels," Journal of Hydraulic Engineering, ASCE, Vol. 109, No. 7, pp. 959-990, July 1983.

Chang, H. H., "Energy Expenditure in Curved Open Channels," Journal of Hydraulic Engineering, ASCE, Vol. 109, No. 7, July 1983.

Chang, H. H., "Variation of Flow Resistance through Curved Channels," Journal of Hydrologic Engineering, ASCE, Vol. 110, No. 12, pp. 1772-1782, December 1984.

Chang, H. H., "Water and Sediment Routing through Curved Channels," Journal of Hydrologic Engineering, ASCE, Vol. 111, No. 4, pp. 644-658, April 1985.

Chen, Y-H., "Mathematical Modeling of Water and Sediment Routing in Natural Channels," Ph.D. Thesis, Department of Civil Engineering, Colorado State University, Ft. Collins, Colorado, March 1973.

Chow, V. T., Open Channel Hydraulics, McGraw-Hill Book Co., 1957.

Engelund, F., and Hansen, E., "A Monograph on Sediment Transport in Alluvial Streams," Teknisk Vorlag, Copenhagen, Denmark, 1967.

Fread, D. L., "Discussion on Implicit Flood Routing in Natural Channels by M. Amein and C. S. Fang (December 1970)," Journal of the Hydraulics Division, ASCE, Vol. 97, No. HY7, pp. 1156-1159, July 1971.

Fread, D. L., "Numerical Properties of Implicit Four-Point Finite Difference Equations of Unsteady Flow," National Weather Service, NOAA, Technical Memorandum NWS Hydro-18, March 1974.

Graf, W. H., Hydraulics of Sediment Transport, McGraw-Hill Book Co., 1970.

Ikeda, S., "Lateral Bed Load Transport on Side Slopes," Journal of the Hydraulics Division, ASCE, Vol. 108, No. HY11, pp. 1369-1373, November 1982.

Ikeda, S., and Nishimura, T., "Flow and Bed Profile in Meandering Sand-Silt Rivers," Journal of Hydraulic Engineering, ASCE, Vol. 112, No. 7, pp. 562-579, July 1986.

Kikkawa, H., Ikeda, S., and Kitagawa, A., "Flow and Bed Topography in Curved Open Channels," Journal of the Hydraulics Division, ASCE, Vol. 102, No. HY9, pp. 1327-1342, September 1976.

National Academy of Sciences, "An Evaluation of Flood-Level Prediction Using Alluvial River Models," Committee on Hydrodynamic Computer Models for Flood Insurance Studies, Advisory Board on the Built Environment, National Research Council, National Academy Press, Washington, D.C., 1983.

Parker, G., Klingeman, P. C., and McLean, D. G., "Bed Load and Size Distribution in Paged Gravel-Bed Streams," Journal of the Hydraulics Division, ASCE, Vol. 108, No. HY4, pp. 544-571, April 1982.

U. S. Bureau of Reclamation, "Aggradation and Degradation in the Vicinity of Milburn Diversion Dam," Sedimentation Section, 1963.

Yang, C. T., "Unit Stream Power and Sediment Transport," Journal of the Hydraulics Division, ASCE, Vol. 18, No. HY10, pp. 1805-1826, October 1972.

Yang, C. T., "Unit Stream Power Equation for Gravel," Journal of Hydraulic Engineering, ASCE, Vol. 110, No. HY12, pp. 1783-1798, December 1984.

Zhang, Q., Zhang, Z., Yue, J., Duan, Z., and Dai, M., "A Mathematical Model for the Prediction of the Sedimentation Process in Rivers," Proceedings of the 2nd International Symposium on River Sedimentation, Nanjing, China, 1983.

APPLICATION OF THE VARIABLE ISOCHRONE METHOD

Feng Yan
Haihe River Water Conservancy Commission

I. INTRODUCTION

The currently used Sherman unit hydrograph and the Nash instantaneous unit hydrograph are both a lumped model of flow concentration on a catchment and do not account for the effect of spacial distribution of runoff production, though some parameters used can be nonlinearized by being made a variable.

These isochrone methods, which are now commonly used, were proposed by Ross, Turney, Burdoin, Clark, Sokolovski, O'Kelly, Larrieu, and Laurenson, and are all a distributed model of flow concentration. These methods consider the variation of runoff areal distribution but do not reflect the nonlinear effect of the intensity (rate) of runoff production as they are all based on the assumption of a fixed isochrone (FI). Such an effect could be reflected to some extent by choosing a fixed isochrone based on an average intensity of rainfall excess during a rainfall.

It is more difficult for the aforementioned methods to reflect such a complicated process of flow concentration when a given time and spacial distribution of rainfall excess are combined with a particular distribution curve of runoff contributing area. For example, on the Hanjiang river, the curve for the upstream area of the Shiquan water power station has a double peak (fig. 1). The factors such as the local rainfall pattern, the topographical condition, and a large variation in rainfall and runoff contribution area between each time interval further complicate the runoff processes at Shiquan (fig. 2). Even in the span of just one or two time intervals, the flood with either a double peak or a single peak may occur. And the peak of the flood may be either broad or sharp due to the difference in the spacial distribution of runoff. Under such conditions of flow concentration, the isochrones varies with the rate of runoff. The variable isochrone (VI) method is proposed in this paper based on the concept of isochrones varying with the rate of runoff.

II. VARIABLE ISOCHRONE METHOD

A. Basic Formula

On the basis of isochrone principle, the equation of overland flow discharge can be expressed as:

$$Q'(t) = \int_0^t i(\tau)A(t-\tau)d\tau \qquad (1)$$

where: $Q'(t)$ is the overland flow discharge at time t;
$i(\tau)$ is the rainfall excess in time τ; and
$A(t-\tau)$ is the time-area diagram.

Simplifying the integration with two variables, when duration of effective rainfall is less than the flow concentration time of watershed ($t_c < \tau_m$), one has

$$Q_m = \rho\ \theta\ \overline{U}\ B_c\ R \qquad (2)$$

where: Q_m is the peak discharge at the outlet;
ρ is a coefficient of simplification for the two variables integral;
$\rho > 1.0$; θ is the regulating coefficient of nature river network;
$\overline{U}$ is the average wave velocity traveling along the river;
B_c is the average width of maximum flow contributing area corresponding to t_c; and
R is the runoff depth during a rainfall.

The key point of the flow concentration on a catchment is the flood wave routing in the river system. Assuming that the relationship between the surface width of cross sectional area B and the relevant water depth d is: $B = b,d^{\mu}$, the formula for the flood wave velocity can be expressed as:

$$u = v + A(dv/dA) = V + [0.67/(\mu+1)]V = K_b V \qquad (3)$$

where A is the area of the cross section; μ is the geometrical index of the cross sectional area. The average wave velocity along the river during a runoff process is:

$$\overline{U} = K_1 K_b V = K_1 K_b a Q_m^{\alpha} S^{\beta} \qquad (4)$$

where: K_1 is the ratio of the average wave velocity along the river to the wave velocity at cross sections;

a, α, and β are the coefficient and indices for flow concentration; and

S is the average slope along the river reach.

Solving Eqs. (2) and (4) simultaneously, one gets

$$\overline{U} = CR^{\alpha m} = CR^{n} \tag{5}$$

$$Q_m = K_m R^m \tag{6}$$

where C and K_m are synthetic coefficients, and m and n are the nonlinear exponents.

Eq. (5) is the basic formula for the variable isochrone which can be used to rectify the nonlinear average wave velocity along the reach.

The cross-sectional geometry of a river is a dominant factor affecting flood routing. The relationship of geometrical index μ to the other relevant parameters of flow concentration are shown in table 1.

Table 1. Relationship of Cross-Sectional Geometry to the Flow Concentration Parameters

Geometry of river cross-section	μ	$K_b = \frac{\mu+1.67}{\mu+1}$	$\alpha = \frac{0.67}{\mu+1.67}$	$\beta = \frac{0.5(\mu+1)}{\mu+1.67}$	$m = K_b$	$n = \frac{0.67}{\mu+1}$
Rectangle	0	1.67	0.40	0.30	1.67	0.67
Parabola	0.5	1.45	0.31	0.35	1.45	0.45
Triangle	1	1.33	0.25	0.38	1.33	0.33
Anti-Parabola (1)	2	1.22	0.18	0.41	1.22	0.22
Anti-Parabola (2)	4	1.13	0.12	0.44	1.13	0.13

B. Determination of Parameters

The Parameters Were Determined From the Hydrological Data

By plotting the mean section velocity against corresponding peak flood discharge logarithmically ($V = MQ_m^{\alpha}$) , the values of M and α are obtained.

As shown by Eq. (6), the logarithmic relationship between peak discharges and flood volumes is plotted with rainfall duration t_c as a parameter to arrive at values K_m and m.

Based on the data of travel time of flood wave from the upstream section to the downstream section and the wave velocities at both cross sections, the value of K_b can be calculated by using Eq. (7).

$$K_b = L/\bar{v}t_p \tag{7}$$

where: L and t_p are the distance and travel time between the two sections respectively;

$\bar{v}$ is the average velocity for the two cross sections; and

K_1 is about 0.6-0.7 for the medium and small catchments ($t_c > \tau_m$) which increases with the increase in the catchment area.

Finally, the basic equation of variable isochrone can be expressed by Eq. (5)'.

$$\bar{U} = K_1 K_b M K_m^{\alpha} R^{\alpha m} = CR^n \tag{5}'$$

Parameter Estimation in Ungaged Regions

After the relationship between each parameter of flood routing and geometrical index of river section area have been established, the final step is to regionalize the synthetic coefficient K_m.

The regional synthetic coefficient K_m for the upstream of Hanjiang River is:

$$K_m = \Psi A^{\lambda} \tag{8}$$

where: A is the catchment area;

λ is the influencing index with the value of 0.8; and

Ψ is a synthetic coefficient -- 0.055 for fan-shaped broad catchment

(L/B=2), 0.045 for ordinary area (L/B=4), and 0.035 for feather-like narrow area (L/B=8).

For the ungaged catchments, the key point for parameter estimation is to analyze geometrical index μ of a cross section in order to select an average value for the reach or a value at the representative cross section. Other parameters -- K_b, α, β, and n -- can then be estimated by the above formula.

After the selection of roughness coefficient n_1 of the river, and determination of R_1 (hydraulic radius when A=1) based on the cross-sectional data, the value of M can be estimated as follows:

$$M = aS^{\beta} = (1/n_1)^{\frac{\cdots+1}{\mu+1.67}} R_1^{\alpha} S^{\beta} \qquad (9)$$

then the parameter, $\overline{U}$, can be calculated by Eq. (5)'.

C. Application

Application of the Variable Isochrone (VI) Method of a Medium-Sized Basin

Using the flood in August 1965, at Zuolonggou station (1836 km^2) of the Lanhe River as an example:

(a) Based on the relevant data of the Lanhe River, one obtains

$v = 0.25Q_m^{0.37}$, $\mu = 0.32$, $K_b = 1.51$, and $Q_m = 1.85R^{1.3}$. Hence

$\overline{U} = 0.67R^{0.48}$.

(b) The average length of the river reach for the subarea of isochrone 1 can be expressed as follows:

$$l = CR^n \cdot \Delta t$$

when R = 5 mm, Δt = 6 hr, and l = 31.5 KM.

(c) From the curve, which represents the relationship between l and ΣAi, determine the corresponding areas of isochrone. When l = 31.5 km, the area of isochrone is 240,500,720,380 km^2.

(d) The corresponding discharge generated in the areas of isochrone is:

$Q_i = A_i R/\Delta t$

When 1 = 31.5 km, the corresponding discharge is 56,116,167,880 M/S.

(e) Similarly, calculate the runoff from the rainfall excess in the other time intervals (table 2, fig. 3)

Table 2 -- Computed Storm Hydrograph by the Variable Isochrone Method

Time	Rainfall excess in time interval R(mm)					ΣQ_i	Baseflow Q_o	$\Sigma Q_i + Q_o$	Q
t	16, 14-20 5	16, 20-17, 2 6	17, 2-8 23	8-14 13	14-20 1	(m^3/s)	(m^3/s)	(m^3/s)	(m^3/s)
16,17	0					0	50	50	50
23	56	0				56	40	96	90
17, 5	116	78	0			194	30	224	290
11	167	161	873	0		1201	20	1221	1090
17	88	220	1090	331	0	1729	50	1779	1680
23	0	53	0	642	4	699	130	829	930
18, 5		0		132	7	139	210	349	470
11				0	10	10	230	240	400
17					12	12	210	222	260
...	...	...	....	...	..	....	...	....	....

Comparison With the Fixed Isochrone (FI) Method

For the purpose of comparison, computations by the fixed isochrone method for the above examples are presented as follows.

(a) The translation velocity of the fixed isochrone is constant, hence:
$\bar{u} = 0.67(\bar{R})^{0.48} = 0.67(9.6)^{0.48} = 1.98$ m/s.

(b) When $\bar{R} = 9.6$ mm, the average length of the river reach is:
$\bar{l} = \bar{u} \cdot \Delta t = 43$ km.

(c) When $\bar{R} = 9.6$ mm, the areas of the fixed isochrone are 415, 850, and 517 km^2, respectively.

(d) Compute the runoff from the rainfall excess as shown in table 3 and fig. 3.

From fig. 3, the result of the variable isochrone method shows a better agreement with the observed hydrograph than that of the fixed isochrone method.

Table 3 -- Computed Storm Hydrograph by the Fixed Isochrone Method

Time	Area	Rainfall excess in time interval R(mm)					ΣQ_i	Baseflow	$\Sigma Q_i + Q_o$	Q
t	F Km^2	16, 14-20 5	16, 20-17, 2 6	17, 2-8 23	8-14 13	14-20 1	m^3/s	Q_o m^3/s	m^3/s	m^3/s
16,17	0	0					0	50	50	50
23	415	96	0				96	40	136	90
17, 5	850	197	115	0			312	30	342	290
11	571	132	236	442	0		810	20	830	1090
17	0	0	158	906	250	0	1314	50	1364	1680
23			0	607	512	19	1138	130	1268	930
18, 5				0	343	39	382	210	592	470
11					0	26	26	230	256	400
17						0	0	210	210	260

Application of the Variable Isochrone Method to a Large Basin

By analyzing hydrological data of the upstream basin of the Hanjiang River, the equation for calculating a 6-hour variable isochrone results in:

Shiquan Basin (23,370 km^2) $\bar{U} = 0.58R^{0.48}$

From Eq. (5), the isochrones of a given time interval and the different runoff depths can be made from an area distribution curve of flow concentration (or a cumulative curve of the width of runoff contribution versus the length of reach). Thus a group of hydrographs corresponding to each time interval can be estimated. This is convenient for flood hydrograph computation in river forecasting.

Summing the hydrographs corresponding to runoff for each time interval with the time lag and the addition of base flow, a total hydrograph is obtained.

For the convenience of dealing the effect of a large variation in areal distribution of runoff, which often happens during a flood, a set of variable isochrones for each subarea may be derived with respect to the outlet of catchment. It means that the variable isochrones for each subarea is computed with the same basic formula as that for the whole catchment, and all relevant variable isochrones of subareas are derived with respect to the outlet of

catchment. The summation of the hydrograph of each subarea results in the total hydrograph at the outlet. This method has been applied in the upstream catchment of the Hanjiang River with satisfactory results.

III. A FLOOD ROUTING MODEL OF VARIABLE ISOCHRONE (FRVI)

A. Flood Routing Model With the Consideration of Translational and Storage Effects

First, flood water is a substance, the same as any other substance, and has the property of a physical translation field. Any displacement in motion must be related to a certain lag time.

Secondly, flood water is a fluid. Its "lag" property is different from that of a rigid body. It is not only subjected to the effects of translation and displacement, but also to the effects of storage and delay.

In fact, the outflow hydrograph of a river reach is a result of inflow hydrograph modulated by the combination of the two effects. Obviously, the storage-discharge equation of a linear reservoir does not adequately describe the properties of flow routing in a channel. After all, a river is not a reservoir. And the storage-discharge equation will represent the reality only when both effects of flow routing are considered. For simplicity, these two effects are named the effect of "translation and storage."

For the convenience of analysis, the two effects should be distinguished. The effect of flood translation in a unit reach should be simulated by a linear channel reach (Dooge, 1959) while the lag of regulated storage effect by a linear reservoir.

It is not important in which order the linear channel and a linear reservoir are arranged to simulate the unit river reach, because the order would not affect the final results.

Now one considers the continuity equation in which the translation will be considered first and then the storage effect.

The storage volume in a river at any time s(t) is composed of S_t and S_s which correspond to the two effects mentioned above. The storage-discharge equation of a unit river reach may be written as follows:

1. If $t < t_e$, one obtains (fig. 4)

$$S(t) = S_t + S_s = S_1 + S_2 = \int_o^t [I(t) - I(t-\tau)]\, dt + KO(t) \qquad (10)$$

2. If $t > t_e$, one has (fig. 4)

$$S(t) = S_t + S_s = (S_1 - S_3) + (S_2 + S_3) = S_1 + S_2 \qquad (10)$$

where I(t) and O(t) are the inflow and outflow, and K is the duration of translational and storage effect for the unit river reach.

The water balance equation in differential form for the river is:

$$I(t) - O(t) = \frac{ds(t)}{dt} \qquad (11)$$

Assuming -, K for each unit river reach are constant, then one may substitute the outflow of a river reach for the inflow of the next river reach successively to solve equations (10) and (11) simultaneously by applying the Laplace transformation and the Heaviside's displacement rule. One gets:

$$P(t) = \frac{1}{K\Gamma(n)} \left(\frac{t-n\tau}{K}\right)^{n-1} \exp\left(-\frac{t-n\tau}{K}\right) \qquad (12)$$

where n is the number of unit river reaches. Eq. (12) is the instantaneous routing flow model with the translational and storage effects.

When n=1, Eq. (12) becomes Meyer's lag method of flood routing. When $\tau = 0$, Eq. (12) is simply the Kalinin-Milukov instantaneous routing model for a river reach, or the Nash's instantaneous unit hydrograph model. Obviously, the routing method with translational and storage effects is superior to those above mentioned methods in adaptability.

B. Basic Equation

To combine the variable isochrone method and the flood routing model with the translational and storage effects, the basic formula of the variable isochrone should be first converted into a variable time-area diagram of overland flow. The velocity of flow concentration related to time-area diagram of overland flow (i.e., kinematic wave) reflects only the translational effect of rainfall flood propagation instead of the storage effect of the river system. Since the distances of flow concentration for either rainfall flood or kinematic wave are the same, the average wave velocity for a variable time-area diagram of overland flow may be represented by:

$$\overline{U}_o = \left(\frac{Ct_p}{t_o}\right) R^n \tag{13}$$

where t_o and t_p are the time of overland flow displacement and the time of runoff displacement, respectively.

In flow concentration on a catchment, the inflows collected by river reaches from each subarea are from the rainfall excess which contribute in a distributed form. It is necessary to take a concentrated inflow over a subarea at a representative point instead of the distributed inflow. Assuming that all representative points for each subarea and inflow are at the mid points of these corresponding reaches of river, it does not mean that all the subareas are generalized as a rectangle but means that the geometrical centers of them are unbiased. The flood routing model with the translational and storage effects becomes:

$$P(t) = \frac{1}{k\Gamma(n-0.5)} \left(\frac{t-(n-0.5)\tau}{K}\right)^{n-1.5} \exp\left(-\frac{t-(n-0.5)\tau}{K}\right) \tag{14}$$

C. Determination of Parameters and their Applications

In principle, three parameters (τ, k, n) of this model can be derived by using the moment formulas relating these parameters such as by the first moment about the origin as well as the second and third moments about mean of the inflow and the outflow. However, computational errors for the higher order moments are difficult to control due to the inevitable arbitrarity in deriving the rainfall

excess and in separating the base flow. In order to reduce the computational errors, it is necessary to make full use of the relationship between the hydrological characteristic values of the inflow and the outflow instead of the use of higher order moments.

Determination of Parameters.

(a) If both the time lags of peak (t_p) and the rising point (t_o) for the inflow and the outflow can be determined, only the first order moment about the origin is required to derive the other parameters.

$$\begin{cases} n = t_o \, L/t_p \, \bar{U}\Delta t \\ n\tau = t_o \\ nK = (0_1' - 1_1') - t_o \end{cases} \tag{15}$$

where $1_1'$ and $0_1'$ are respectively the first order moments about the origin of the inflow and the outflow.

(b) If only the value of t_p is known, the following formula can be used to determine the other parameters.

$$\begin{cases} K = (0_1' - 1_1') - t_p \\ nK^2 = 0_2 - 1_2 \\ n\tau = (0_1' - 1_1') - nK \end{cases} \tag{16}$$

where 1_2 and 0_2 are the second order moment about mean for the inflow and the outflow, respectively.

Procedures of Application

First, determine the values of t_p and t_o based on the hydrographs from an average rainfall excess and the outflow of a given catchment. Select Δt by using the Eq. (5). Then determine the interval between the two subareas of variable isochrone by:

$$1_o = \left(\frac{C \, t_p \cdot \Delta t}{t_o}\right) R^n \tag{17}$$

Second, calculate the rainfall excess on each subarea which is estimated by dividing the average rainfall excess in each time interval. As the rainfall excess on each subarea for each time interval may differ substantially, it is required to adjust the value 1_o by using Eq. (17) for the rainfall excess on each subarea.

Finally, three parameters of the model for each time interval are determined by the above mentioned equations. With the modified subarea and the rainfall excess on the area known, the runoff hydrograph for each time interval may be estimated and so does the runoff hydrograph for a given rainfall.

Example -- July 1967 Flood of the Hanjiang River

Use the flood in July 1967 at Yangxan station (14,160 km^2) of the Hanjiang River as an example.

Basic formula and parameters. The basic formula for variable isochrone is determined as:

$$\bar{U} = 0.67R^{0.49}$$

The basic formula for variable isochrone of overland flow are:

$$\bar{U}_o = \frac{t_p}{t_o}\bar{U} = \frac{13.5}{10.5}\bar{U} = 0.77R^{0.49}$$
$$m_1 = 0_1^9 - 1_1' = 31.9 - 7.2 = 24.7$$

The results are as follows:

Time Interval	R (mm)	$\bar{U}$ (m^3/s)	$\bar{U}$ (m^3/s)	1_o (km)	τ (hr)	K (hr)	n
8:00-14:00	7	1.56	2.00	43	1.9(2)	2.5(3)	5.5(6)
14:00-20:00	16	2.32	2.96	64	2.9(3)	3.8(4)	3.7(4)

Estimation of basin runoff for the rainfall excess in each time interval.

First, determine the subareas of isochrone of overland flow based on the average rainfall excess in each time interval and then estimate the

precipitation and rainfall excess on each subarea. One obtains the following runoff hydrograph on the basin in each time interval as follows:

8:00-14:00	0	0	4300	200	0	144	(m^3/s)
14:00-20:00	500	2720	6500	1100			

Computation of flow concentration from the runoff hydrograph on the basin in each time interval. The flow concentration may be computed from Eq. (14). Table 4 shows the details of computation.

Table 4 -- Computation of Flow Concentration for the Time Interval 8:00-14:00

Time	0	0	4300		200		0	144		
t	$P_{0.5t}$	$P_{1.5t}$	$P_{2.5t}$	Q_i	$P_{3.5t}$	Q_i	$P_{4.5t}$	$P_{5.5t}$	Q_i	ΣQ_i
3, 9:00	0									0
15:00	0	0								0
21:00	0	0	0	0						0
4, 3:00	0	0	0.451	1940	0	0				1940
9:00	0	0	0.393	1690	0.220	44	0			1734
15:00	0	0	0.121	520	0.447	89	0	0	0	609
21:00		0	0.028	120	0.232	46	0	0.030	4	170
5, 3:00			0.006	26	0.076	15	0	0.257	37	78
9:00			0.001	4	0.019	4	0	0.349	50	58
15:00					0.005	1	0	0.223	32	33
21:00					0.001	0		0.096	14	14
6, 3:00								0.032	5	5
9:00								0.010	1	1
15:00								0.003	0	0
21:00								0.001	0	0

Computation of flow concentration of the basin. The flow concentration of the basin may be computed from Eq. (12) as shown by table 5, and fig. 4.

Table 5. Computation of flood hydrograph for the floods in July, 1967 at Yangxan station of the Haniang river. (m /s)

Time t	ΣQ_i 8:00-14:00	ΣQ_i 14:00-20:00	base flow Q_o	$\sum\Sigma Q_i + Q_o$	Q
3,15:00	0	0	310	310	310
21:00	0	350	250	600	470
4, 3:00	1940	1500	220	3660	3150
9:00	1734	2880	240	4854	4550
15:00	609	2850	260	3720	3150
21:00	170	1700	350	2220	2200
5, 3:00	78	930	450	1458	1650
9:00	58	420	580	1058	1300
15:00	33	200	630	864	1000
21:00	14	80	630	724	850
6, 3:00	5	15	610	630	730
9:00	1	6	590	597	640
15:00		2	530	532	530

D. The Forecast of an Extreme Flood at Ankang of the Hanjiang River in July 1983

A flood with a peak flow of 31000 m^3/s corresponding to a flood with a return period of 200 years occurred at Ankang (38740 km^2) of the Hanjiang river on July 31, 1983. The flood was catastrophic to the city with a heavy loss of property and life.

The Division of Subarea

The drainage area above the Ankang Water Power Plant (35600 km^2) is divided into 15 subareas, based on the spatial distribution of the river system, the state of hydrologic network, and hydraulic projects (fig. 5). The drainage area above Shiguen (23370 km^2) is divided into 9 subareas.

The Computation of Rainfall Excess for Each Subarea

The computation of rainfall excess for each subarea is made by rainfall-runoff coaxial graphical method of correlation, $R = f(P, P_a, t_c)$, in which P_a is the antecedent rainfall index; t_c is the duration of the rainfall excess.

The Computation of Overland Flow for Each Subarea

First, the length of overland flood isochrone corresponding to the average rainfall excess for each time interval may be determined by:

$$1_o = t_p/t_o \Delta t \; cR^n$$

Then, based on the above formula, one may find the corresponding areas of overland flow isochrone on the curve b = f(1) for each time interval. Hence,

$$Q_{o_i} = (A_i R)/\Delta t$$

The Computation of Flood Runoff Hydrograph for Each Subarea

The overland flow hydrograph of each subarea is determined through the successive computation of flow concentration by Eq. (14), then the flood hydrograph at the outlet of each subarea is obtained. The parameters are estimated by Eq. (15).

The Flood Routing of Flood Hydrograph for Each Subarea

Because the Shiquan Water Power Plant is above the Ankang Water Power Plant, the rainfall runoff from subareas No. 1-9 are first concentrated to the Shiguan by Eq. (12), then the storage effect is considered before it is taken as the inflow to the Ankang Water Power Plant. The outflow of the Shiquan and the flood hydrograph for the subareas No. 10-15 after going through the computations of channel flow concentration and addition of the base flow, the flood hydrograph at Ankang Water Power Plant is obtained.

The Result of the Forecast

The peak flow at Ankang Water Power Plant estimated by the above-mentioned method is 29376 m^3/s. The peak flow of the forecast is 30000 m^3/s and the observed value is 28500 m^3/s. This forecast is accurate. (Table 6, Fig. 6).

Table 6. Overland peak flow of subareas and the combined flow at the Ankang Water Power Plant (m^3/s)

Subarea	Catchment area (km^2)	Parameter		Overland Peakflow	Peak flow	Peak flow routed to Ankang	Combined flow at Ankang
		c	m				
1	3092	0.5	0.5	2237	2141	1995	1981
2	3861	0.4	0.58	2200	2150	2139	2104
3	2341	0.45	0.5	2111	2050	1893	1277
4	2143	0.4	0.58	1877	1837	1827	780
5	2720	0.38	0.52	2519	2512	2509	2350
6	1613	0.46	0.6	1102	1072	1038	974
7	2816	0.34	0.61	1512	1502	1489	1400
8	2182	0.42	0.5	3025	2989	2951	2951
9	2403	0.38	0.55	2156	2104	2104	2020
Base flow							300
Shiquan: Inflow							16137
Outflow							15700
1 - 9	23370						14850
10	1412	0.76	0.39	1381	1354	1280	1050
11	1850	0.39	0.57	2910	2840	2801	2463
12	2251	0.9	0.46	5447	5422	5262	5100
13	2651	1.1	0.38	2100	2040	2002	2002
14	1826	0.67	0.48	695	659	627	215
15	2230	0.57	0.62	3433	3196	3196	3196
Base flow							500
Ankang	35600						29376

IV. Conclusions

The variable isochrone method (VI) combines the major advantages of both the lumped and the distributed models of the flood routing in conceptual models. It may be used to consider the effect of nonlinearity as well as the spacial distribution of rainfall simultaneously. The data analysis used in the derivation of model parameters is realizable. The method presented in the paper has a higher simulating accuracy for peak flow and the rising segment of hydrograph. But it is faster in rising and slower in recession.

The flood routing model of variable isochrone (FRVI) combines the variable isochrone and flood routing with the effect of translation and lag, which is a conceptual model in a sense that is partially empirical and partially theoretical. This model can be used to consider simultaneously four basic problems: 1) the nonlinearity of flood routing, 2) the spacial variation of rainfall excess, the distribution curve of runoff contribution area and the regulating effect of river storage, thus the scope of its application is widened and the practical results of its application are satisfactory.

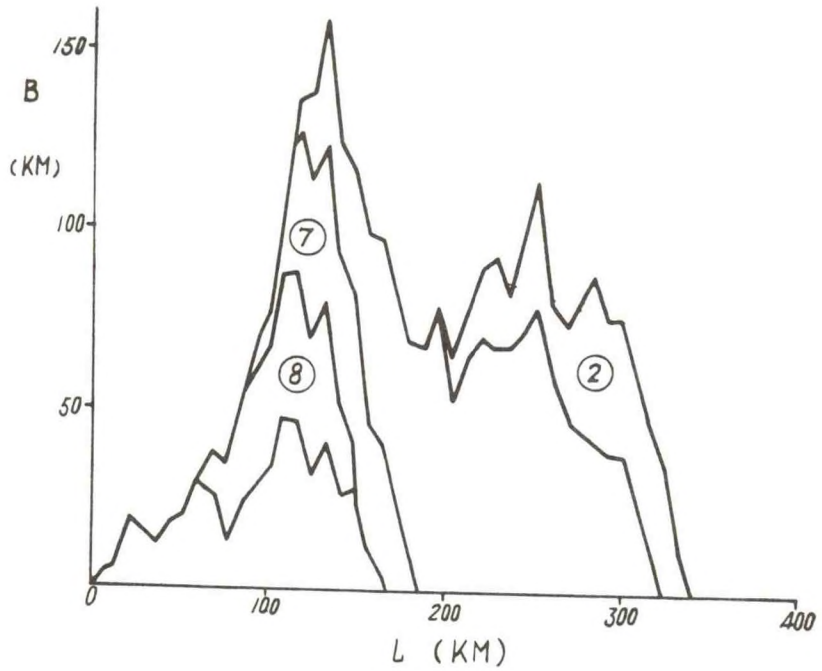

Figure 1. The distribution curve for the upstream area of Shiquan in the Hanjiang River.
Subarea: 2 - Baohe River, 7- Ziwu River, 8 - Muma River

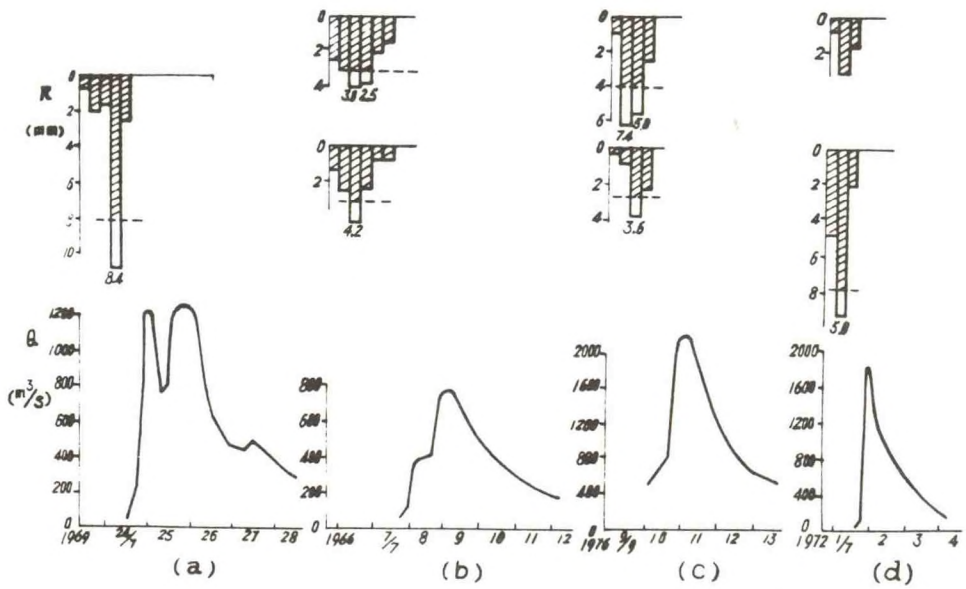

Figure 2. The tape for the watershed routing of storm flood at Shiquan. In fig. (b) - (d), the upper and lower rain chart indicate the rainfall for the upstream and downstream of Yangxian

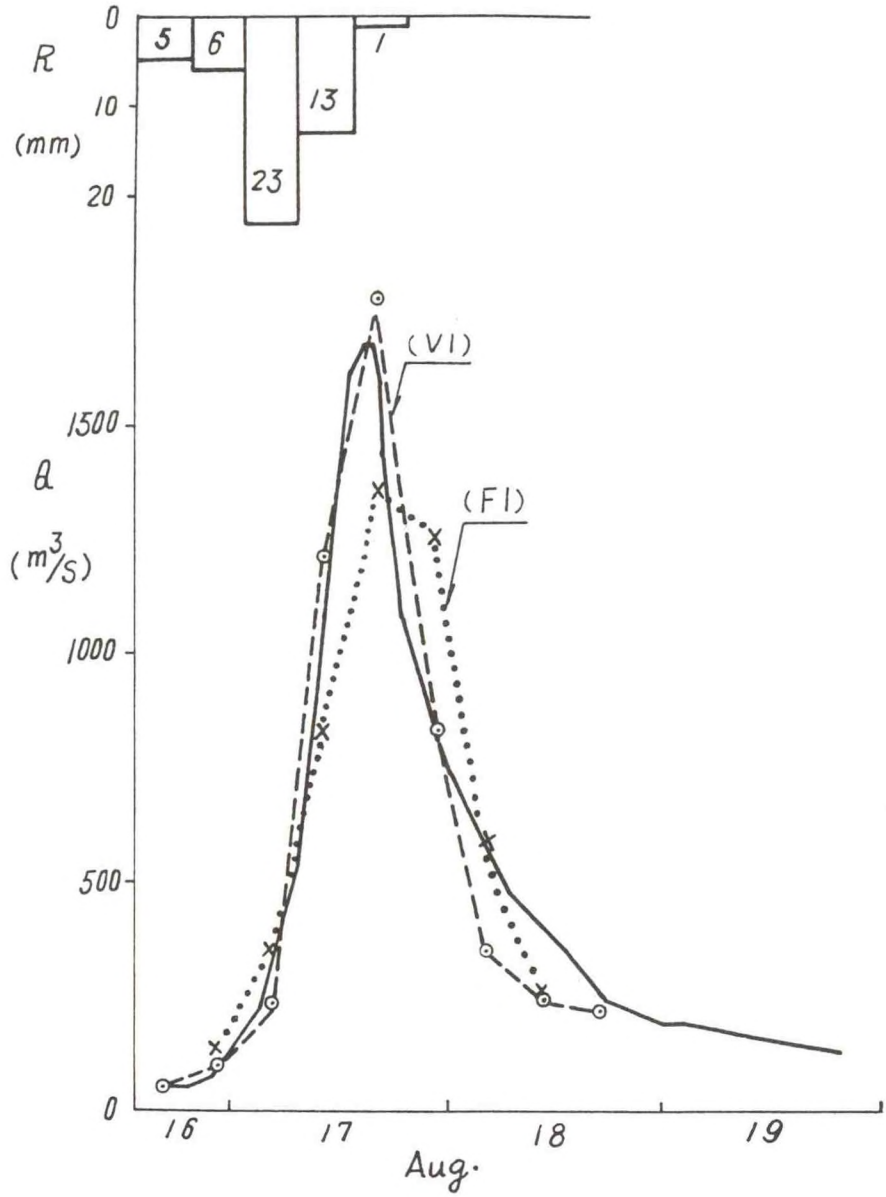

Figure 3. The examined hydrograph for variable isochrone [VI] method and fixed isochrone [FI] method at Zuolonggou station of the Lanhe River

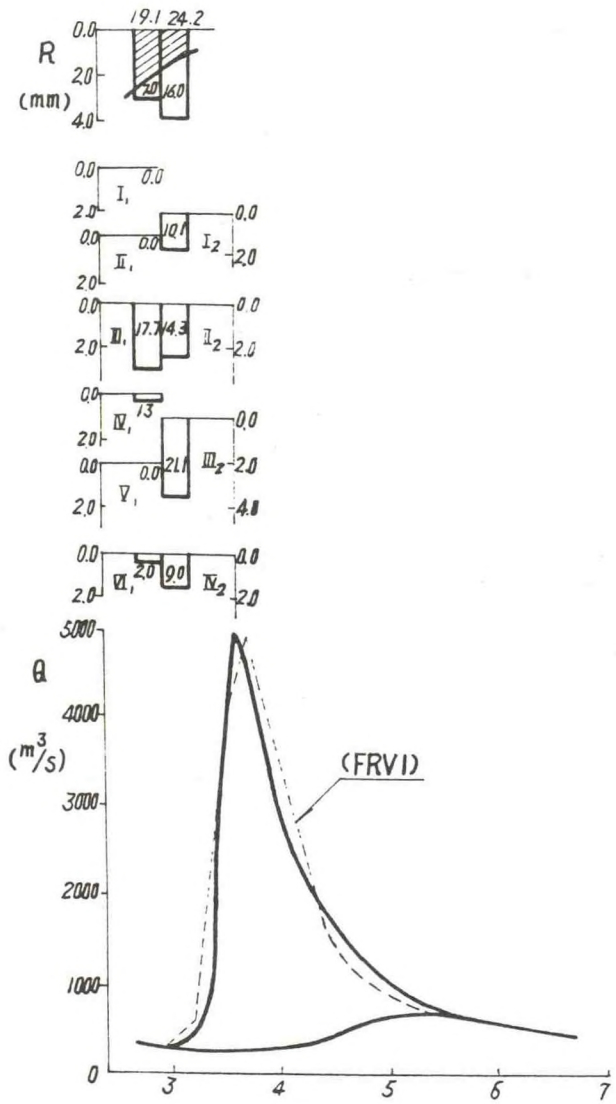

Figure 4. The examined hydrograph for the flood routing model of variable isochrone at Yangxian station in Hanjiang River NOTE: In fig., I_1, II_1, III_1, IV_1, V_1, VI_1, and I_2, II_2, III_2, IV_2 are the number of time-area corresponding to the first and second net rainfall in time interval

Figure 5. The basin configuration and subbasins for the upstream of Ankang Water Power Station in the Hanjiang River

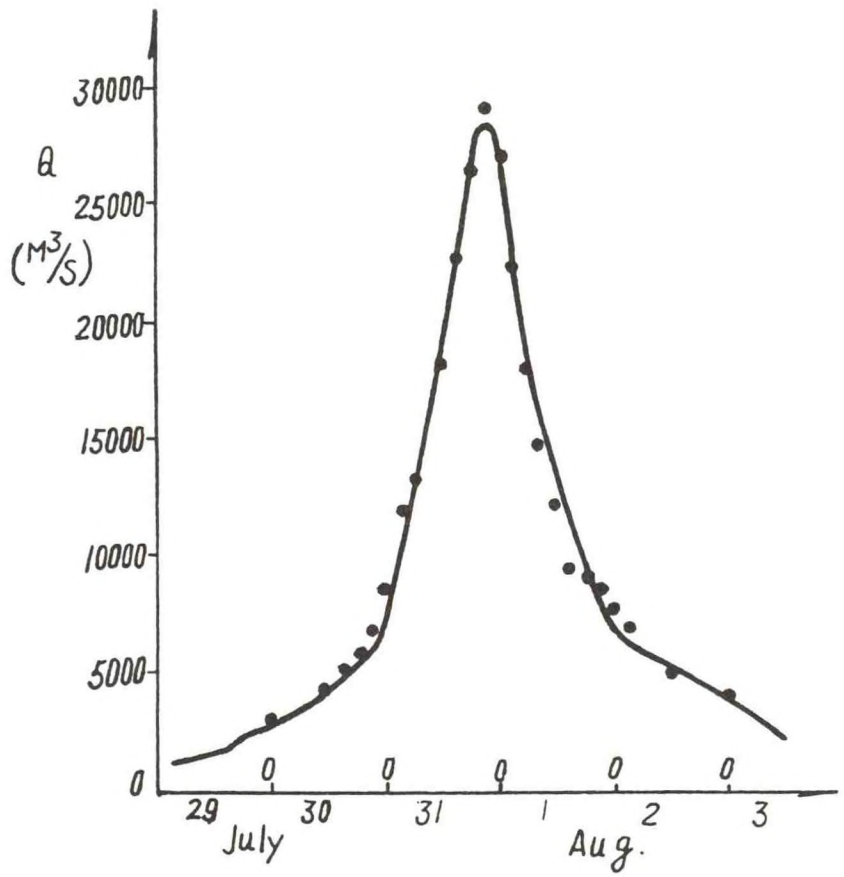

Figure 6. The computational result of storm flood of the "83.7" at Ankang Water Power Station

REFERENCES

[1] Ross, C.N., "The Calculation of Flood Discharge by the Use of Time Contour Plan," Trans. 1E, (Australia) Vol. 2. pp. 85-92, 1921.

[2] Clark, C.O., "Storage and the Unit Hydrograph," Trans. ASCE, Vol. 110, pp. 1419-1446, 1945.

[3] Be^ukahob, M.A., 1948.

[4] Dooge, J.C.I, "A General Theory of the Unit Hydrograph," J. Geophys. Res. Vol. 64, No. 1, pp. 241-256, 1959.

[5] Nash, J.E., "A Unit Hydrograph Study, With Particular Reference to British Catchments," Proc. ICE, Vol. 17, pp. 249-282, 1960.

[6] Remenieras, G. and Jacquet, J., "Comparison de Queiques Methodes de Detemination Dun Hydrogramme de Ruissellement Pluvial," Electricite de France, No. 1, 1962.

[7] Laureson, E.M., "A Catchment Storage Model for Runoff Routing," J. Hydrology, 2, pp. 141-163, 1964.

[8] Feng, Y., "Preliminary Research of Unit Graph and Synthetic Unit Graph," Treatise of Hydrological Computation 3, pp. 131-144, 1965. (In Chinese).

[9] Sauer, V.B., "Unit Response Method of Open Channel Flow Routing," J. Hydraul. Div., ASCE, Vol. 99, No. Hy-1, pp. 179-193, 1973)

[10] Feng, Y., "A Study on the Variable Isochrone Method for Flood Computation," J. Hydraul. Eng., Beijing, No. 4., pp. 1-7, 1981. (In Chinese)

[11] Feng, Y., "On the Lag Channel Mode of Flood Concentration," Treatise of Storm Flood Computation, 1, Nanjing Hydrol. Res. Inst., pp. 261-272, 1981. (In Chinese).

[12] Linsley, R.K., Kohler, M.A., and Paulhus, J.L.H., "Hydrology for Engineers," McGraw-Hill, New York, N.Y., 3rd Ed., 1982.

[13] Feng, Y. and He, C.C., "A Study of the Relationship Between Storm Rainfall and Flood Based on Analysis of the '83.7' Flood at Ankang in the Han River Basin," J. Hydrology, 96, pp. 353-363, 1987.

NUMERICAL FLOOD ROUTING MODELS USED IN NWS

D. L. Fread
National Weather Service
Silver Spring, MD 20910

ABSTRACT. Three numerical dynamic routing models (DWOPER, DAMBRK, SMPDBK) have been developed by the National Weather Service (NWS) to route floods through rivers, reservoirs, and estuaries. The DWOPER model is based on an implicit finite-difference solution of the Saint-Venant one-dimensional equations of unsteady flow, and is suitable for real-time routing of floods through a single waterway (river) or a system of interconnected waterways. The DAMBRK model (also based on the Saint-Venant equations) and the SMPDBK model (a much simplified version of DAMBRK) are used for real-time forecasting of dam-break floods emanating from breached dams along a single river. These models are also extensively used by many federal and state agencies concerned with dam safety and associated emergency evacuation plans. More recently, a new comprehensive flood routing model (FLDWAV) has been undergoing development and testing; it combines the capabilities of the DWOPER and DAMBRK models as well as provides features not contained in either of these models. The FLDWAV model will be placed in operational use in NWS during the next several years. This paper describes the characteristics and capabilities of the four models with emphasis on the new FLDWAV model.

I. INTRODUCTION

The National Weather Service (NWS) hydrology program provides flood and daily river forecasts to the general public. Thirteen River Forecast Centers (RFC) prepare the forecasts for dissemination throughout the United States.

Within NWS flood forecasting procedures such as the National Weather Service River Forecast System (NWSRFS), the runoff generated by rainfall-runoff models is aggregated in fairly large, well-defined channels (rivers), and then transmitted downstream by unsteady flow routing techniques of the hydrologic or storage variety. Although these routing techniques function adequately in many locations, they have serious shortcomings when the unsteady flows are subjected to backwater effects due to reservoirs, tides, or inflows from large tributaries. When effective hydraulic slopes of the rivers are quite mild, the flow inertial effects ignored in the hydrologic techniques become important. Also, highly transient flows resulting from dam breaks which usually greatly exceed the flood-of-record are not treated adequately by the hydrologic routing methods.

To improve the routing capabilities within NWS forecasting procedures, the Hydrologic Research Laboratory (HRL) has developed dynamic routing models suitable for efficient operational use in a wide variety of applications involving the prediction of unsteady flows in rivers, reservoirs, and estuaries.

One of the models, Dyanmic Wave Operational (DWOPER), developed in the early 1970's and enhanced in the early 1980's, is based on an implicit finite-difference solution of the Saint-Venant one-dimensional equations of unsteady flow. The DWOPER model is used for real-time routing of rainfall/snowmelt-generated floods, hurricane-generated storm surges, tidal fluctuations, and reservoir releases to a single reach of river or a system of interconnected rivers, such as the Mississippi, Ohio, Columbia, and several Gulf coast rivers. Also, DWOPER has received considerable use by other Government agencies and private consultants in engineering/design studies of waterways.

Catastrophic flooding emanating from breached dams along a single river is forecast by the dam-break flood forecasting (DAMBRK) model (also based on the Saint-Venant equations) and the simplified DAMBRK (SMPDBK) model (a much simplified version of the DAMBRK model). DAMBRK, developed in 1977, has been adopted for use in the United States by most federal and state agencies concerned with dam safety and associated emergency evacuation plans. Also, DAMBRK is being used in many other countries around the world by governmental

agencies, power companies, and private engineering consultants. Research has been on-going in developing improvements in the DAMBRK model allowing it to have an increasing range of application. The most recent version of DAMBRK became operational in late 1988. DAMBRK can also be used for routing any specified hydrograph through reservoirs, rivers, canals, or estuaries as part of general engineering studies of waterways. SMPDBK, developed in 1982-83, has received considerable use within NWS and by other agencies in the United States when available time and resources are too limited for the use of DAMBRK and the attendant reduction in accuracy is judged acceptable. Another NWS model, Generalized Dam-Breach Erosion Model (BREACH), developed in 1984-85, predicts only the breach hydrograph and the breach size and its time of formation due to overtopping or piping of earthen dams that are man-made or naturally formed due to landslide blockages of streams and rivers. It is intended to aid in the selection of breach parameters for DAMBRK and SMPDBK.

More recently, a new comprehensive flood routing model Flood Wave (FLDWAV) has been undergoing development and testing; it combines the capabilities of DWOPER and DAMBRK as well as provides features not contained in either of these models. The FLDWAV model will be placed in operational use within NWS during the next several years.

A. Scope

Since FLDWAV encompasses the features of both the DWOPER and DAMBRK models, it is presented first herein. Then, the DWOPER and DAMBRK models' departures and exceptions to the FLDWAV model are presented. Finally, descriptions of the SMPDBK and BREACH models are given. All models are written in FORTRAN and suitable for execution on mainframe, mini, or microcomputers; the latter must have 640K storage and a math coprocessor.

II. FLDWAV MODEL

The FLDWAV model is based on an implicit finite-difference solution of the complete one-dimensional Saint-Venant equations of unsteady flow coupled with an assortment of internal boundary conditions for simulating unsteady flows controlled by a wide spectrum of hydraulic structures. The flow may occur in

a single waterway or a system of interconnected waterways in which sinuosity effects are considered. The flow which can range from Newtonian (water) to non-Newtonian (mud/debris, mine tailings) may freely change with time and location from subcritical to supercritical or vice versa, and from free-surface to pressurized flow. Special modelling features include time-dependent dam breaches, levee overtopping and crevasse, time-dependent gate controlled flows, assorted spillway flows, bridge/embankments, tidal flap gates, off-line detention basins and/or pumping basins including individual pump specifications, and floodplain compartments with free/submerged weir flow connecting with the waterway or adjacent compartments. FLDWAV can be automatically calibrated for a single channel or dendritic system of channels; calibration is achieved through an efficient automatic adjustment of the Manning coefficient that varies with location and flow depth. The model has automatic selection of the critical computational time and distance steps. Data input is through either a batch or an interactive mode and output is tabular and graphic. Input/output may be in English or metric units. It is planned that future NWS research and development in river mechanics will be integrated within the FLDWAV model framework. The model can be used by hydrologists/engineers for a wide range of unsteady flow applications, including real-time flood forecasting in a dendritic system of waterways subject to backwater effects; real-time dam-breach flood forecasting or preparation of inundation maps for sunny-day dam-breach piping failures or overtopping failures due to Probable Maximum Flood (PMF) reservoir inflows including the complexities associated with the failure of two or more dams sequentially located along a watercourse; design of waterway improvement structures such as levees, off-channel detention ponds, etc.; floodplain mapping for flood insurance studies; analysis of irrigation systems with gate controlled flows; analysis of storm sewer systems having a combination of free surface and/or pressurized unsteady flows; mud/debris flow inundation mapping; and unsteady flows due to hydropower operations.

A. Governing Equations

The governing equations of the FLDWAV model are: (1) an expanded form of the one-dimensional equations of unsteady flow originally derived by Saint-Venant

(1871); (2) an assortment of internal boundary equations representing flow through one or more hydraulic flow control structures located sequentially along the main-stem river and/or its tributaries (distributaries); and (3) external boundary equations describing known upstream/downstream discharges or water elevations which vary either with time or each other.

The Saint-Venant equations of conservation of mass and momentum may be expressed in an expanded form to account for some effects omitted in their original derivation. These effects are: (1) lateral inflows/outflows, (2) nonuniform velocity distribution across the flow section, (3) expansion/contraction losses, (4) off-channel (dead) storage, (5) flow-path differences between a sinuos channel and its floodplain, (6) surface wind resistance, and (7) internal viscous dissipation of non-Newtonian (mud/debris) flows. The conservation of mass (continuity) equation is:

$$\partial Q/\partial x + \partial s_c(A+A_o)/\partial t - q = 0 \qquad (1)$$

in which Q is discharge (flow); A is wetted active cross-sectional area; A_o is wetted inactive off-channel (dead) storage area associated with topographical embayments or tributaries; s_c and s_m are depth-dependent sinuosity coefficients (DeLong, 1985) that account for channel meander; q is lateral flow (inflow is positive, outflow is negative); t is time; and x is the distance measured along the mean flow-path of the floodplain or along the channel if there is minimal channel meander. The conservation of momentum equation is:

$$\partial(s_m Q)/\partial t + \partial(\beta Q^2/A)/\partial x + gA(\partial h/\partial x + S_f + S_e + S_i) + L + W_f B = 0 \qquad (2)$$

in which g is the gravity acceleration constant; h is the water surface elevation; B is the wetted cross-sectional active topwidth; L is the momentum effect (Strelkoff, 1970) of lateral flows ($L = -qv_x$ for lateral inflow, where v_x is the lateral inflow velocity in the x-direction; $L = -q\,Q/(2A)$ for seepage lateral outflows; $L = -q\,Q/A$ for bulk lateral outflows); W_f is the wind factor (Fread, 1985), i.e., $W_f = C_w|V_r|V_r$ in which C_w is the wind resistance coefficient, and $V_r = Q/A - v_w \cos\omega$, where v_w is the wind velocity and ω is the acute angle between the wind direction and x-axis; S_f is the

boundary friction slope, i.e., $S_f = |Q|Q/K^2$ in which K is the total conveyance determined by summing conveyances of the left/right floodplains and the channel in which the channel conveyance is modified by the factor $(1/\sqrt{s_m})$ and all conveyances are determined automatically from the data input of topwidth/Manning n versus elevation tables for cross sections of the channel and left/right floodplains; S_e is the expansion/contraction slope, i.e., $S_e = k_e/(2g)\ \partial(Q/A)^2/\partial x$ in which k_e is the expansion/contraction loss coefficient; β is the momentum coefficient for nonuniform velocity distribution and is internally computed from the conveyances and areas associated with flow in the channel and left/right floodplains and S_i is the non-Newtonian internal viscous dissipation slope (Fread, 1987), i.e.,

$$S_i = \kappa/\gamma[(b+2)Q/(AD^{b+1}) + (b+2)/(2D^b)\ (\tau_o/\kappa)^b]^{1/b} \qquad (3)$$

in which D=A/B; κ is the apparent fluid viscosity; γ is the fluid's unit weight; τ_o is the initial shear strength of the fluid; and b = 1/m where m is the exponent of a power function that represents the fluid's stress (τ_s)-rate of strain (dv/dy) relation, i.e., $\tau_s = \tau_o + \kappa(dv/dy)^m$ in which v and y are the flow velocity and depth, respectively.

There may be various locations (internal boundaries) along the main-stem river and/or tributaries where the flow is rapidly varied in space and eqs. 1-2 are not applicable, e.g., dams, bridges/road-embankments, waterfalls, short steep rapids, weirs, etc. The following equations are used in lieu of eqs. 1-2 at internal boundaries:

$$Q_i - Q_{i+1} = 0 \qquad (4)$$

$$Q_i = f(h_i,\ h_{i+1},\ \text{properties of control structure}) \qquad (5)$$

in which the subscripts i and i+1 represent sequential cross sections located just upstream and just downstream of the structure, respectively. If the structure is a bridge, then eq. 5 assumes the following form:

$$Q = \sqrt{2g}\ C_b A_b\ (h_i - h_{i+1} + v^2/2g - \Delta h_f)^{1/2} + C_e L_e K_e (h_i - h_e)^{3/2} \qquad (6)$$

in which C_b is the coefficient of flow through the bridge, A_b is the wetted cross-sectional area of the bridge opening, $v = Q/A$, Δh_f is the head loss through the bridge, C_e is the coefficient of discharge for flow over the embankment, L_e is the length of the road embankment, h_e is the elevation of the embankment crest, and K_e is a broad-crested weir submergence correction, i.e., $K_e = 1-23.8[(h_{i+1} - h_e)/(h_i - h_e) - 0.67]^3$. If the flow structure is a dam, then eq. 5 assumes the following form:

$$Q = K_s C_s L_s (h_i - h_s)^{3/2} + \sqrt{2g}\, C_g A_g (h_i - h_g)^{1/2} + K_d C_d L_d (h_i - h_d)^{3/2} + Q_t + Q_{br} = 0 \quad (7)$$

in which K_s, C_s, L_s, h_s are the uncontrolled spillway's submergence correction factor, coefficient of discharge, length of spillway, and crest elevation, respectively; K_d, C_d, L_d, h_d are similar properties of the crest of the dam; C_g, A_g, h_g are the coefficient of discharge, area, and height of opening of a fixed or time-dependent moveable gate spillway; Q_t is a constant or time-dependent turbine discharge; and Q_{br} is the flow through a time-dependent breach of the dam (Fread, 1977) given by the following:

$$Q_{br} = C_v K_b [3.1\, b_i (h_i - h_b)^{3/2} + 2.45\, Z\, (h - h_b)^{5/2}] \quad (8)$$

in which b_i is the known time-dependent bottom width of the breach, h_i is the known time-dependent bottom elevation of the breach, Z is the side slope of the breach (1: vertical to Z: horizontal), C_v is a velocity of approach correction factor, and K_b is a broad-crested weir submergence correction factor similar to K_e in eq. 6. If the structure is a natural rapid or waterfall, then a simple critical flow equation can be used for eq. 5. Also, empirical rating curves of Q versus h may be used in lieu of eq. 5 or in place of any or all of the first three terms in eq. 7.

The flow structure may be a navigational dam with an associated lock where minimal navigational depths are maintained upstream of the dam by a dam tender who operates adjustable gates which control the river flow. In this case, eq. 5 takes the following form:

$$h_i = h_t \tag{9}$$

where h_t is the target pool elevation which the dam tender attempts to maintain via operation of the gates. The target pool elevation may be a constant value, or it may be specified as a function of time and read in as a time series. When the simulated tailwater elevation exceeds a specified tailwater elevation, the flow is computed via eqs. 1-2.

External boundary equations at the upstream or downstream extremities of the waterway must be specified to obtain solutions to the Saint-Venant equations. In fact, in many applications, the unsteady disturbance is introduced to the waterway at one or more of the external boundaries via a specified time series of discharge (a discharge hydrograph) or water elevation as in the case of a lake level or estuarial tidal fluctuation. If the water surface of the most upstream reservoir is assumed to remain level as it varies with time due to the inflows and spillway/breach outflows, then the following upstream boundary equation is used:

$$Q_1 = QI(t) - 0.5\ \overline{S}_a\ 43560.\ \Delta h/\Delta t \tag{10}$$

in which Q_1 is the discharge at the upstream most section (the upstream face of the dam); QI(t) is the specified inflow to the reservoir; $\overline{S}_a$ is the average surface area (acre-ft) of the reservoir during the Δt time interval; and Δh is the change in reservoir elevation during the time step. Equation 10 represents a level-pool routing algorithm in the form of an upstream boundary condition. The use of eq. 10 requires that a table of reservoir surface area versus elevation be specified. At the downstream extremity, or N^{th} cross section, the boundary equation could be eq. 7, an empirical rating of h and Q, or a channel control, loop-rating based on the Manning equation in which S (the dynamic energy slope) is approximated by:

$$S = (h_{N-1} - h_N)/\Delta x - (Q^{t+\Delta t} - Q)/(gA\ \Delta t) - [(Q^2/A)_N - (Q^2/A)_{N-1}]/(gA\ \Delta x) \tag{11}$$

in which Δx represents the reach length between the last two cross sections at the downstream extremity of the waterway.

B. Solution Technique

The Saint-Venant eqs. 1-2 cannot be solved directly; however, they can be solved by finite-difference approximations. The FLDWAV model utilizes a weighted four-point nonlinear implicit finite-difference solution technique as described by (Fread, 1985). Substitution of appropriate simple algebraic approximations for the derivative and nonderivative terms in eqs. 1-2 result in two nonlinear algebraic equations for each Δx reach between specified cross sections which, when combined with the external boundary equations and any necessary internal boundary equations, may be solved by an iterative quadratic solution technique (Newton-Raphson) along with an efficient, compact, quad-diagonal Gaussian elimination matrix solution technique. Initial conditions are also required at $t = 0$ to start the solution technique. These are automatically obtained within FLDWAV via a steady flow backwater solution or they may be specified as data input for unsteady flows occurring at $t = 0$.

A river system consisting of a main-stem river and one or more principal tributaries is efficiently solved using an iterative relaxation method (Fread, 1973) in which the flow at the confluence of the main stem and tributary is treated as the lateral inflow/outflow term (q) in eqs. 1-2. This method solves, during a time step, the unsteady flow equations first for the main stem and then for each tributary of the river system. The tributary flow at the confluence with the main-stem river is treated as a lateral flow q which is first estimated when solving the equations for the main stem. The tributary flow depends on its upstream boundary condition, lateral inflows along its reach, and the water surface elevation at the confluence (downstream boundary for the tributary) which is obtained during the simulation of the main stem. Due to the interdependence of the flows in the main stem and its tributaries, the following iterative or relaxation algorithm is used:

$$q^* = \alpha\, q + (1 - \alpha)\, q^{**} \tag{12}$$

in which α is a weighting factor ($0 < \alpha \leq 1$); q is the computed tributary flow at the confluence; q** is the previous estimate of q; and q* is the new estimate of q. Convergence is attained when q* is sufficiently close to q**. Usually, one or two iterations is sufficient; however, the ~ weighting factor has an important influence on the efficiency of the algorithm. Optimal values of ~ can reduce the irerations by as much as one-half. A priori selection of α is difficult since α varies with each river system. Good first approximations for α are in the range, $0.6 \leq \alpha \leq 0.8$ and the optimal α value may be obtained by trial-and-error. FLDWAV can accommodate any number of 1st order tributaries. Systems with 2nd order tributaries can sometimes be accommodated by reordering the system, i.e., selecting another branch of the system as the main stem.

If the river consists of bifurcations such as islands and/or complex dendritic systems with tributaries connected to tributaries, etc., a network solution technique is used (Fread, 1985), wherein three internal boundary equations conserve mass and momentum at each confluence, i.e.,

$$Q_i^{j+1} + Q_{i'}^{j+1} - Q_{i'+1}^{j+1} - \Delta s/\Delta t^j = 0 \tag{13}$$

$$2g\,(h_i^{j+1} - h_{i'+1}^{j+1}) + (Q^2/A^2)_i^{j+1} - T\,(Q^2/A^2)_{i'+1}^{j+1} = 0 \tag{14}$$

$$2g\,(h_{i'}^{j+1} - h_{i'+1}^{j+1}) + (Q^2/A^2)_{i'}^{j+1} - T\,(Q^2/A^2)_{i'+1}^{j+1} = 0 \tag{15}$$

where:

$$\frac{\Delta s}{\Delta t} = \Delta x_i/(6\Delta t^j)\,\tilde{B}\,(h_i^{j+1} + h_{i'}^{j+1} + h_{i'+1}^{j+1} - h_i^j - h_{i'}^j - h_{i'+1}^j) \tag{16}$$

$$i' = i + m + 1 \tag{17}$$

$$\tilde{B} = B_i^j + B_{i'+1}^j + B_{i'}^j \cos \omega_t \tag{18}$$

$$T = 1 + C_m + C_f \tag{19}$$

$$C_m = (0.1 + 0.83\,Q_{i'}^j/Q_{i'+1}^j)\,(\cdot\cdot_t/90)^\mu \tag{20}$$

$$C_f = 2g\ \Delta x_i\ \bar{n}^2 / [2.21\ (\bar{D}^{4/3})^j] \qquad (21)$$

in which $\bar{D}$ is the average depth in the junction, $\bar{n}$ is the Manning n for the junction, ω_t is the acute angle between the upstream reach and the branch, μ is an exponent assumed to be unity, and m is the total number of Δx reaches located upstream (downstream) along the branching channel. The parameters C_f and C_m are related to friction effects and to the head loss due to mixing as reported by Lin and Soong (1979), respectively. The superscript (j) and the subscript (i) represent the time line and cross section location in the x-t computational plane, respectively.

This method of simulating a network of channels maintains a nonlinear formulation of the entire system, thus retaining the Newton-Raphson iterative equation solver, and yet performs the computations quite efficiently. The matrix is 2N x 2N where N is the total number of cross sections. Since it is not possible to maintain a diagonally banded matrix for the coefficients introduced via eqs. 13-15 in the composition of the coefficient matrix, the number of off-diagonal elements and their consequences can be minimized by using a special Gauss elimination matrix solution technique that operates only on nonzero off-diagonal elements. The number of operations (addition, subtraction, multiplication, division) required to solve the matrix is approximately (102 + 46J)N, where J is the total number of junctions. This is compared to (95N-48) operations for the relaxation algorithm, (38N-19) for a single channel and $(5N^3+8N^2+5N)$ for a standard Gauss elimination method. For example, if N = 100 and J = 5, the network algorithm requires 33,200 operations, while the relaxation method requires 9452 operations (but it is not applicable to networks other than first order dendritic), and the standard Gauss method requires 5,080,500 operations.

C. Subcritical/Supercritical Algorithm

This optional algorithm (Fread, 1985) automatically subdivides the total routing reach into subreaches in which only subcritical (Sub) or supercritical (Sup) flow occurs. The transition locations where the flow changes from Sub

to Sup or vice versa are treated as external boundary conditions. This avoids the application of the Saint-Venant equations to the critical flow transitions. At each time step, the solution commences with the most upstream subreach and proceeds subreach by subreach in the downstream direction. The upstream boundary (UB) and downstream boundary (DB) are automatically selected as follows: (1) when the most upstream subreach is Sub, the UB is the specified discharge hydrograph and the DB is the critical flow equation since the next downstream subreach is Sup; (2) when the most upstream subreach is Sup, the UB is the specified hydrograph and a loop-rating quite similar to that previously described as an external boundary condition, and no DB is required since flow disturbances created downstream of the Sup reach cannot propagate upstream into this subreach; (3) when an inner subreach is Sup, its two UB conditions are the discharge just computed at the DB of the adjacent upstream subreach and the computed critical water surface elevation at the same DB; (4) when an inner subreach is Sub, its UB is the discharge just computed at the most downstream section of the adjacent upstream Sup subreach and the DB is the critical flow equation. Hydraulic jumps are allowed to move either upstream or downstream prior to advancing to another computational time step; this is accomplished by comparing computed sequent elevations (h_s) with computed backwater elevations (h) at each section in the vicinity of the hydraulic jump. The jump is moved section by section upstream until $h_s > h$ or moved downstream until $h > h_s$. The Froude number $\left(Fr = Q/(A\sqrt{gD})\right)$ is used to determine if the flow at a particular section is Sub or Sup, i.e., if $Fr < 1$ the flow is Sub and if $Fr \geq 1$ the flow is Sup. The Sub/Sup algorithm increases the computational requirements by approximately 20 percent.

D. Levee Overtopping

Flows which overtop levees located along either or both sides of a main-stem river and/or its principal tributaries may be simulated within FLDWAV. The overtopping flow is considered lateral outflow (-q) in eqs. 1-2, and is computed as broad-crested weir flow. Three options exist for simulating the interaction of the overtopping flow with the receiving floodplain area. The first option simply ignores the presence of the floodplain and is described later in the subsection on lateral flows. The second option treats the

receiving floodplain as a storage or ponding area having a user-specified storage-elevation relationship. The floodplain water surface elevations are computed via the simple storage (level-pool) routing equation; i.e., inflow - outflow = temporal change in storage. The overtopping broad-crested weir flow is corrected for submergence effects if the floodplain water elevation sufficiently exceeds the levee crest elevation. In fact, the overtopping flow may reverse its direction if the floodplain elevation exceeds the river surface water elevation. The overtopping flow is computed according to the following:

$$q = -C\, K_s\, (h - h_c)^{3/2} \tag{22}$$

where:

$$K_s = 1.0 \qquad \text{if} \qquad h_r \leq 0.67 \tag{23}$$

$$K_s = 1.0 - 27.8\, (\gamma - 0.67)^3 \qquad \text{if} \qquad h_r > 0.67 \tag{24}$$

$$h_r = (h_{fp} - h_c)/(h - h_c) \tag{25}$$

in which C is the discharge coefficient; K_s is the submergence correction factor; h_c is the levee crest elevation; h is the water elevation of river; and h_{fp} is the water elevation of the floodplain. In the third option, the floodplain is treated as a tributary of the river and the Saint-Venant equations are used to determine its flow and water surface elevations; the overtopping levee flow is considered as lateral inflow (q) in eqs. 1-2. In each option the levee may also crevasse (breach) along a user-specified portion of its length.

If the receiving floodplain area is divided into separate compartments by additional levees or road embankments located perpendicular to the river and its levees, the flow transfer from a compartment to an adjacent upstream or downstream compartment is simulated via broad-crested weir flow with submergence correction. Flow reversals (outflows) can occur when dictated by the water surface elevations within adjacent compartments, which are computed by the storage routing equation as in the second option. The compartment elevation (h_{fp}) is obtained iteratively via a table look-up algorithm applied

to the specified table of volume-elevation values. The outflow from a floodplain compartment may also include that from one or more pumps associated with each floodplain compartment. Each pump has a specified discharge-head relation given in tabular form along with start-up and shut-off operation instructions as delineated by specified water surface elevations. The pumps discharge to the river.

E. Automatic Calibration

An option within FLDWAV allows the automatic determination of the Manning n such that the difference between computed water surface elevations (stage hydrographs) and observed hydrographs is minimized. The Manning n can vary with either flow or water elevation and with subreaches separated by water level recorders. The algorithm (Fread and Smith, 1978) for efficiently accomplishing this is applicable to a single multiple-reach river or a main-stem river and its principal tributaries. The algorithm is based on a scheme of decomposing complex river systems of dendritic configuration. Optimum Manning n values are sequentially determined for each reach bounded by gaging stations, commencing with the most upstream reach, and progressing reach by reach in the downstream direction. Tributaries are calibrated before the main-stem river and their flows are added to the main stem as lateral inflows. Discharge is input at the upstream boundary of each river, while observed stages at the downstream gaging station of each reach is used as the downstream boundary condition. Computed stages at the upstream boundary are tested against observed stages at that point. Statistics of bias (Φ_j) and root-mean-square (RMS) error are computed for several (j) ranges of discharge or stage so that the Manning n can be calibrated as a function of discharge or stage. For each range of discharge, an improved estimate of the optimum Manning n (n_j^{k+1}) is obtained via a modified Newton-Raphson iterative algorithm, i.e.,

$$n_j^{k+1} = n_j^k - \frac{\Phi_j^k (n_j^k - n_j^{k-1})}{\Phi_j^k - \Phi_j^{k-1}} \qquad k \geq 2;\ j = 1,2,\ldots J \qquad (26)$$

in which the k superscript denotes the number of iterations and Φ_j is the bias for the j^{th} range. Equation 26 can be applied only for the second and successive iterations; therefore, the first iteration is made using the following algorithm:

$$n_j^{k+1} = n_j^k \, (1.0 - 0.01 \, \Phi_j^k / |\Phi_j^k|) \qquad k = 1; \; j = 1,2,...J \tag{27}$$

in which a small percentage change in n is made in the correct direction as determined by the term $(-\Phi_j^k / |\Phi_j^k|)$. The convergence properties of eq. 26 are quadratic with convergence usually obtained within three to five iterations. Improved n values obtained via eq. 26 are used, and the cycle is repeated until a minimum RMS error for the reach is found. Then, the discharges computed at the downstream boundary using the optimum Manning n are stored internally and then input as the upstream boundary condition for the next downstream reach.

FLDWAV also provides an option to conveniently utilize a methodology (Fread and Lewis, 1988) for determining optimal n values which may for some applications eliminate the need for time-consuming preparation of detailed cross-sectional data. Approximate cross sections represented by separate 2-parameter power functions for the channel and the floodplain are used. Optimized n values can be constrained to fall within user-specified min-max ranges. Also, specific cross-sectional properties at key sections (bridges, natural constrictions, etc.) can be utilized wherever considered appropriate.

F. Dam Breach Parameters

The breach is the opening formed in the dam as it fails. The actual failure mechanics are not well understood for either earthen or concrete dams. In FLDWAV, the breach is assumed to develop over a finite interval of time (τ) and will have a final size determined by a terminal bottom width parameter (b) and various shapes depending on another parameter (Z), the side slope of the breach which depends on the angle of repose of the dam's materials. This parametric representation of the breach follows Fread and Harbaugh (1973) and is utilized in FLDWAV for reasons of simplicity, generality, wide applica-

bility, and the uncertainty in the actual failure mechanism. The model assumes the breach bottom width starts at a point and enlarges at a linear or nonlinear rate over the failure time (τ) until the terminal bottom width (b) is attained and the breach bottom has eroded to the elevation h_{bm}. If τ is less than one minute, the width of the breach bottom starts at a value of b rather than zero. This represents more of a collapse failure than an erosion failure. The bottom elevation of the breach is simulated as a function of time (τ) according to the following:

$$h_b = h_d - (h_d - h_{bm})\left(\frac{t_b}{\tau}\right)^{\rho} \qquad \text{if} \quad 0 < t_b \leq \tau \qquad (28)$$

in which h_{bm} is the final elevation of the breach bottom which is usually, but not necessarily, the bottom of the reservoir or outlet channel bottom, t_b is the time since beginning of breach formation, and ρ is the parameter specifing the degree of nonlinearity, e.g., ρ=1 is a linear formation rate, while ρ=2 is a nonlinear quadratic rate; the range for ρ is $1 \leq \rho \leq 4$; however, the linear rate is usually assumed. The instantaneous bottom width (b_i) of the breach is given by the following:

$$b_i = b(t_b/\tau)^{\rho} \qquad \text{if} \quad 0 < t_b \leq \tau \qquad (29)$$

During the simulation of a dam failure, the actual breach formation commences when the reservoir water surface elevation (h) exceeds a specified value, h_f. This feature permits the simulation of an overtopping of a dam in which the breach does not form until a sufficient amount of water is flowing over the crest of the dam. A piping failure may also be simulated by specifing the initial centerline elevation of the pipe.

Concrete gravity dams tend to have a partial breach as one or more monolith sections formed during the construction of the dam are forced apart and overturned by the escaping water. The time for breach formation is in the range of a few minutes. Concrete arch dams tend to fail completely and are assumed to require only a few minutes for the breach formation. The shape parameter (Z) is usually assumed to be zero for concrete dams.

Earthen dams which exceedingly outnumber all other types of dams do not tend to completely fail, nor do they fail instantaneously. The fully formed breach in earthen dams tends to have an average width ($\bar{b}$) in the range ($h \leq \bar{b} < 5h_d$) where h_d is the height of the dam. The middle portion of this range for $\bar{b}$ is supported by the summary report of Johnson and Illes (1976) and the upper range by the report of Singh and Snorrason (1982). Breach widths for earthen dams are, therefore, usually much less than the total length of the dam as measured across the valley. Also, the breach requires a finite interval of time (τ) for its formation through erosion of the dam materials by the escaping water. Total time of failure (for overtopping) may be in the range of a few minutes to usually less than an hour, depending on the height of the dam, the type of materials used in construction, the extent of compaction of the materials, and the magnitude and duration of the overtopping flow of the escaping water. The time of failure as used in DAMBRK is the duration of time between the first breaching of the upstream face of the dam until the breach is fully formed. For overtopping failures, the beginning of breach formation is after the downstream face of the dam has eroded away and the resulting crevasse has progressed back across the width of the dam crest to reach the upstream face. Piping failures occur when initial breach formation takes place at some point below the top of the dam due to erosion of an internal channel through the dam by the escaping water. Times of failure are usually considerably longer for piping than overtopping failures since the upstream face is slowly being eroded in the very early phase of the piping development. As the erosion proceeds, a larger and larger opening is formed; this is eventually hastened by caving-in of the top portion of the dam. Poorly constructed coal-waste slag piles (dams) which impound water tend to fail within a few minutes, and have average breach widths in the upper range of the earthen dams mentioned above.

Recently, some statistically derived predictors for $\bar{b}$ and τ have been presented in the literature, i.e., MacDonald and Langridge-Monopolis (1984) and Froelich (1987). From Froelich's work, in which he used the properties of 43 breaches of dams ranging in height from 15 to 285 ft with all but 6 between 15 and 100 ft, the following predictive equations can be obtained:

$$\bar{b} = 9.5\ k_o\ (V_r\ h_d)^{0.25} \tag{30}$$

$$\tau = 0.8\ (V_r/h_d^2)^{0.50} \tag{31}$$

in which $\bar{b}$ is average breach width (ft), τ is time of failure (hrs), $k_o = 1.0$ for piping and 1.4 for overtopping, V_r is volume (acre-ft) and h_d is the height (ft) of water over the breach bottom which is usually about the height of the dam. Standard error of estimate for $\bar{b}$ was ±94 ft which is an average error of ±54% of $\bar{b}$, and the standard error of estimate for τ was ±0.9 hrs which is an average error of ±70 percent of τ.

Another means of determining the breach properties is the use of physically based breach erosion models. Recently the author (Fread, 1984, 1987) developed such a model (BREACH) which is described later herein.

G. Landslide-Generated Waves

Reservoirs are sometimes subject to landslides which rush into the reservoir, displacing a portion of the reservoir contents and, thereby, creating a very steep water wave which travels up and down the length of the reservoir (Davidson and McCartney, 1975). This wave may have sufficient amplitude to overtop the dam and precipitate a failure of the dam, or the wave by itself may be large enough to cause catastrophic flooding downstream of the dam without resulting in the failure of the dam as in the case of a concrete dam in Vaiont, Italy in 1963.

The capability to generate waves produced by landslides is provided within FLDWAV. The volume of the landslide mass, its porosity, and the time interval over which the landslide occurs are specified as input to the model. In the model, the landslide mass is deposited during very small computational time steps within the reservoir in layers commencing at the center of the reservoir and extending toward the side of the landslide, and simultaneously the original dimensions of the reservoir are reduced. The time rate of reduction in the reservoir cross-sectional area (Koutitas, 1977) creates the wave during the solution of the unsteady flow, eqs. 1-2, which are applied to the reservoir cross sections.

Wave runup is not considered in the model. For near vertical faces of concrete dams the runup may be neglected; however, for earthen dams the usual angle of the earthfill on the reservoir side will result in a surge that advances up the face of the dam to a height approximately equal to 2.5 times the height of the landslide-generated wave (Morris and Wiggert, 1972).

H. Lateral Flows

Unsteady flows associated with tributaries along the routing reach can be added to the unsteady flow resulting from the dam failure. This is accomplished via the term q in eqs. 1-2. The tributary flow is distributed along a single Δx reach. Within the FLDWAV model, Q(t) is divided by Δx to obtain q(t). Backwater effects of the routed flow on the tributary flow are ignored, and the lateral tributary flow is assumed to enter perpendicular to the routed flow. Outflows are assigned negative values. Outflows which occur as broad-crested weir flow over a levee or natural crest may be simulated within the FLDWAV model, i.e.,

$$q = -C_w (\bar{h} - h_w)^{1.5} \tag{32}$$

in which C_w is the discharge coefficient for broad-crested weir flow ($2.6 \leq C_w \leq 3.2$), $\bar{h}$ is the average of the computed water elevations at sections i and i+1 bounding the Δx reach in which the weir outflow occurs, and h_w is the average crest elevation of the weir along the Δx reach. The crest elevation, discharge coefficient, and location along the river/valley must be specified by the user.

I. Cross Section and Flow Resistance Parameters

In FLDWAV, active cross sections which convey flow may be of irregular as well as regular geometrical shape. Each cross section is read in as tabular values of channel width and elevation, which together constitute a piece-wise linear relationship. Experience has shown that in most instances the cross section may be sufficiently described with eight or less sets of widths and associated elevations. A low-flow, cross-sectional area which can be zero is

used to describe the cross section below the minimum elevation read-in. From this input, the cross-sectional area associated with each of the widths is initially computed within the model. During the solution of the unsteady flow equations, any areas or widths associated with a particular water surface elevation are linearly interpolated from the piece-wise linear relationships.

Dead storage areas, wherein the flow velocity in the x-direction is considered negligible relative to the velocity in the active area of the cross section, is a feature of FLDWAV. Such dead or off-channel storage areas can be used to effectively account for embayments, ravines, or tributaries which connect to the flow channel but do not convey flow and serve only to store the flow. The dead storage cross-sectional properties are described similarly to those of the active cross sections.

The Manning n is used to describe the resistance to flow caused by bed forms, bank vegetation and obstructions, bend effects, and small scale eddy losses. The Manning n can vary considerably with flow elevation, i.e., the n value can be considerably larger for flow inundating the floodplain than flow confined within the channel bank. It can be larger for lesser floodplain depths than for greater flow depths; however, within the channel banks, the n value may decrease with increasing flow depth. The Manning n is defined for each channel reach bounded by gaging stations and is specified as a function of either stage or discharge via a piece-wise linear relation specified as input in tabular form. Linear interpolation is used to obtain n for values of h or Q intermediate to the tabular values. Simulation results are often sensitive to the Manning n. Although in the absence of necessary data (observed stages and discharges), n can be estimated, best results are obtained when n is adjusted to reproduce historical observations of stage and discharge. Such an adjustment process is known as calibration which may be either trial-and-error or an automatic technique described previously.

J. Program Structure

The FLDWAV model is coded in FORTRAN with over 80 subroutines which provide the desired modularity for future expansions to enable the simulation of other hydraulic phenomena. Arrays are coded with a variable dimensioning technique

which utilizes a single, large array as the only array of fixed size. At each execution of the model, the large array is automatically partitioned into individual variable arrays required for a particular hydraulic application. The size of each array is automatically determined by user-specified data which describes the hydraulic application. This program structure allows maximum utilization of storage space since arrays not used during a particular simulation require no storage space.

The FLDWAV model's input/output is in either English or metric units. The input is either batch or interactive. The output form is numerical tabular and/or graphical.

K. Testing and Verification

The FLDWAV model has been tested and verified on several rivers throughout the United States. The applications include the following.

(1) A dendritic river system consisting of 393 miles (629 km) of the Mississippi-Ohio-Cumberland-Tennessee rivers schematically shown in fig. 1. An example of this application is shown in fig. 2, Computed and Simulated Stages for Cairo at Junction of Mississippi and Ohio Rivers.

(2) A 292-mile (469 km) reach of the lower Mississippi which was calibrated for a 1969 flood using records of six gaging stations located throughout the reach. The average RMS error between the computed and observed water levels was 0.25 ft (0.08 m). For the years 1959-71, using the 1969 calibration, it was 0.47 ft (0.15 m) with a maximum average RMS value during test period of 0.91 ft (0.28 m).

(3) A 130-mile (209 km) reach of the tidal affected lower Columbia river including a 25-mile (40 km) tributary reach of the Willamette. The average RMS error for seven gaging stations was 0.21 ft (0.06 m) for stage hydrographs with a diurnal tidal fluctuation of as much as 7 ft (2.13 m).

(4) A dendritic river system consisting of 463 miles (744 km) of the Upper Mississippi-Illinois-Missouri rivers and 9 locks and dams. The average RMS error for 18 water level recording stations was 0.38 ft (0.12 m).

(5) A 60-mile (96 km) reach of the Teton-Snake rivers located downstream of the 262-ft (79.8 m) high Teton dam which failed in 1976 (Ray, et al., 1976) producing a peak discharge in excess of 2 million cfs (56,800 cms). Variations between computed and observed high water marks averaged about 1.5 ft (0.47 m) and differences between computed and observed discharges were less than 5 percent as indicated on the peak discharge profile of fig. 3

(6) A 16-mile (26 km) reach of Buffalo Creek located downstream of a 44-ft (13.4 m) high coal-waste dam which failed in 1972 (Davies, et al., 1975) producing a peak discharge of over 80,000 cfs (2270 cms). Variations between computed and observed high water marks averaged about 1.8 ft (0.55 m) and peak discharges compared within an average of 9 percent variation with observed values as shown in fig. 4.

III. DWOPER MODEL

The DWOPER model (Fread, 1978) is based on the following form of the Saint-Venant equations:

$$\partial Q/\partial x + \partial(A + A_o)/\partial t - q = 0 \qquad (33)$$

$$\partial Q/\partial t + \partial(Q^2/A)/\partial x + gA(\partial h/\partial x + S_f + S_e) + L + W_f B = 0 \qquad (34)$$

in which $S_f = n^2|Q|Q/(2.21\ A^2R^{4/3})$ and all other terms are defined as in eqs. 1-2, the governing equations of the FLDWAV model. The sinuosity coefficients (S_c and S_m) of eqs. 1-2 are not included, and the friction slope (S_f) is defined in terms of the Manning n rather then the total conveyance. Also, the non-Newtonian internal viscous dissipation slope (S_i) of eqs. 1-2 for mud/debris flows is not included. Internal boundary conditions include

bridges and dams; however, neither can be breached as in the FLDWAV model, and dams are represented by a rating curve (head vs. discharge) rather than eq. 7.

The DWOPER model cannot accomodate supercritical flows or mixed subcritical/supercritical flows as can the FLDWAV model. Only the third option of levee overtopping in the FLDWAV model is available in the DWOPER model, i.e., the floodplain beyond the levee is treated as a tributary of the river contained by the levee. Although the DWOPER model provides an automatic calibration option as in the FLDWAV model, it does not have the option of 2-parameter power function representation of cross-sectional geometry as described by Fread and Lewis (1986). The DWOPER model does not have the metric input/output option. The DWOPER model does have the capability of modeling river systems with either the relaxation algorithm or the network algorithm, and DWOPER is programmed with variable dimensioned arrays.

IV. DAMBRK MODEL

The DAMBRK model (Fread, 1977, 1984, 1988) is based on the following form of the Saint-Venant equations.

$$\partial Q/\partial x + \partial\, s_c(A + A_o)/\partial t - q = 0 \tag{35}$$

$$\partial(s_m Q)/\partial t + \partial(Q^2/A)/\partial x + gA(\partial h/\partial x + S_f + S_e + S_i) + L = 0 \tag{36}$$

in which all terms are defined as in eqs. 1-2, the governing equations of the FLDWAV model. Equations 35-36 do not contain the wind factor (W_f) as in the FLDWAV model, and the lateral flow momentum term (L) does not include the effect of lateral inflow velocities that are not perpendicular to the receiving stream, i.e., $L = -qv_x$ is not an available option in the DAMBRK model.

Only a single river can be simulated with the DAMBRK model rather than a system of interconnected rivers which can be modeled by FLDWAV. The DAMBRK model uses eqs. 4-8 for internal boundaries; thus, breached dams or bridge embankments can be simulated. DAMBRK can treat supercritical or mixed subcritical/supercritical flows as does FLDWAV. Only the first option of

levee overtopping in FLDWAV is available in DAMBRK. The multiple floodplain compartments option is available in DAMBRK. Automatic calibration is not an option in DAMBRK. The metric input/output is available as in FLDWAV. DAMBRK is programmed with fixed arrays rather than variable dimensioned arrays as in FLDWAV.

V. SMPDBK MODEL

The SMPDBK model, as described in detail by Wetmore and Fread (1984), is a simple model for predicting the characteristics of the floodwave peak produced by a breached dam. It will, with minimal computational resources (hand-held calculators, microcomputers), determine the peak flow, depth, and time of occurrence at selected locations downstream of a breached dam. SMPDBK first computes the peak outflow at the dam, based on the reservoir size and the temporal and geometrical description of the breach. The computed floodwave and channel properties are used in conjunction with routing curves to determine how the peak flow will be diminished as it moves downstream. Based on this predicted floodwave reduction, the model computes the peak flows at specified downstream points. The model then computes the depth reached by the peak flow based on the channel geometry, slope, and roughness at these downstream points. The model also computes the time required for the peak to reach each forecast point and, if a flood depth is entered for the point, the time at which that depth is reached as well as when the floodwave recedes below that depth, thus providing a time frame for evacuation and fortification on which a preparedness plan may be based. The SMPDBK model neglects backwater effects created by downstream dams or bridge embankments, the presence of which can substantially reduce the model's accuracy. However, its speed and ease of use together with its small computational requirements make it an attractive tool for use in cases where limited time and resources preclude the use of the DAMBRK model. In such instances, forecasters, planners, emergency managers, and consulting engineers responsible for predicting the potential effects of a dam failure may employ the model where backwater effects are not significant.

The SMPDBK model retains the critical deterministic components of the DAMBRK model while eliminating the need for extensive numerical computations. It accomplishes this by approximating the downstream channel/valley as a prism, concerning itself with only the peak flows, stages, and travel times, neglecting the effects of backwater from downstream bridges and dams, and utilizing dimensionless peak-flow routing graphs developed by using the DAMBRK model. The applicability of the SMPDBK model is enhanced with its user friendly interactive input and option for minimal data requirements. The peak flow at the dam may be computed with only four readily accessible data values and the downstream channel/valley may be defined with a single average cross section, although prediction accuracy greatly increases with the number of specified cross sections.

A. Breach Outflow

The model uses a single equation to determine the maximum breach outflow and the user is required to supply the values of four variables for this equation. These variables are: 1) the surface area (A_s, acres) of the reservoir; 2) the depth (H, ft) to which the breach cuts (this is usually the same value as the height of the dam plus the depth of overtopping flow); 3) the time (τ , hours) required for breach formation; and 4) the final width (B_r, ft) of the breach. These parameters are substituted into a broad-crested weir flow equation to yield the maximum breach outflow (Q_{bmax}) in cfs, i.e.,

$$Q_{bmax} = Q_o + 3.1\ B_r \left(\frac{C}{\tau + C/\sqrt{H}}\right)^3 \qquad (37)$$

where:

$$C = \frac{23.4\ A_s}{B_r} \qquad (38)$$

and Q_o is the spillway flow and overtopping crest flow which is estimated to occur simultaneously with the peak breach outflow.

Once the maximum outflow at the dam has been computed, the depth of flow produced by this discharge may be determined based on the geometry of the

channel immediately downstream of the dam, the Manning n (roughness coefficient) of the channel and the slope of the downstream channel. This depth is then compared to the depth of water in the reservoir to find whether it is necessary to include a submergence correction factor for tailwater effects on the breach outflow, i.e., to determine if the water downstream is restricting the free flow through the breach. This comparison and (if necessary) correction allows the model to provide the most accurate prediction of maximum breach outflow which properly accounts for the effects of tailwater depth downstream of the dam. The submergence correction factor (K_d) is similar to that in eq. 8 and must be applied iteratively since the outflow produces the tailwater depth which determines the submergence factor which affects the outflow.

B. Peak Flow Routing

The peak discharge is routed to downstream points of interest through the channel/valley which is described by selected cross sections defined by tables of widths and associated elevations. The routing reach from the dam to the point of interest is approximated within SMPDBK as a prismatic channel by defining a single cross section (an average section that incorporates the geometric properties of all intervening sections via a distance weighting technique). This prismatic representation of the channel allows easy calculation of flow area and volume in the downstream channel which is required to accurately predict the amount of peak flow attenuation. The peak flow at the dam computed by eq. 37 is routed downstream using the dimensionless routing curves (see fig. 5). These curves, developed from numerous executions of the NWS DAMBRK model, are grouped into families based on the Froude number associated with the floodwave peak and have as their X-coordinate the ratio of the downstream distance (from the dam to a selected cross section) to a distance parameter (X_c). The Y-coordinate of the curves used in predicting peak downstream flows is the ratio of the peak flow at the selected cross section to the computed peak flow at the dam. The distinguishing characteristic of each member of a family is the ratio (V*) of the volume in the reservoir to the average flow volume in the downstream channel. Thus, it may be seen that to predict the peak flow of the floodwave at a downstream

point, the desired distinguishing characteristic of the curve family and member must be determined. This determination is based on the calculation of the Froude number (F_c) and the volume ration parameter (V*). To specify the distance in dimensionless form, the distance parameter (X_c) in ft is computed as follows:

$$X_c = 6\ VOL/[\bar{A}(1 + 4(0.5)^{m+1})] \qquad (39)$$

in which VOL is the reservoir volume (acre-ft), m is a shape factor for the prismatic routing reach, and $\bar{A}$ is the average cross-sectional area in the routing reach at a depth corresponding to the height of the dam. The volume parameter (V*) is simply $V^* = VOL/(\bar{A}_c X_c)$ in which $\bar{A}_c$ represents the average cross-sectional area in the routing reach at the average maximum depth produced by the routed flow. The Froude number (F_c) is simply $F_c = V_c/(gD_c)^{0.5}$ where V_c and D_c are the average velocity and hydraulic depth, respectively, within the routing reach. Using families of curves similar to fig. 5, the routed peak discharge can be obtained. The corresponding peak depth is computed from the Manning equation using an iterative method since the wetted area and hydraulic radius are nonlinear functions of the unknown depth.

The time of occurrence of the peak flow at a selected cross section is determined by adding the time of failure to the peak travel time from the dam to that cross section. The travel time is computed using the kinematic wave velocity which is a known function of the average flow velocity throughout the routing reach. The times of first flooding and "deflooding" of a particular elevation at the cross section may also be determined within SMPDBK. Further description of the computational procedure for determining these times, as well as the time of peak flow and dimensionless parameters, may be found in Wetmore and Fread (1984).

C. Testing and Verification

The SMPDKB model was compared with the DAMBRK model in several hypothetical applications where backwater effects were negligible. The average difference between the two models was 10-20 percent for predicted flows and travel times

with depth differences of less than about 1 ft (0.3 m). Since the DAMBRK model is considered more accurate, the differences can be considered errors due to the simplifications of SMPDBK. The application of SMPDBK to the Teton dam breach is shown in fig. 3, and its application to the Buffalo Creek "coal waste" dam is shown in fig. 4. In each case, the peak discharge profile computed with the DAMBRK and FLDWAV models, and the observed peak flows are shown for comparison.

Additional testing of SMPDBK was conducted by Westphal and Thompson (1987) who concluded that SMPDBK produced peak discharges differing by an average of 13 percent from DAMBRK for six dams in the state of Missouri; the average difference between the two models for peak depths was about 2 ft (0.6 m).

VI. BREACH MODEL

This model (Fread, 1984, 1987) predicts the outflow hydrograph from a breached dam and the breach size, shape, and time of formation of a breach in earthen/rockfill dams where the breach may be initiated by either piping or overtopping. The dam can be naturally formed by a landslide blockage of a river or man-made with either homogeneous fill or fill with a distinctive central core. The downstream face may be grass covered or bare. The model utilizes the principles of soil mechanics, hydraulics, and sediment transport to simulate the erosion and bank collapse processes which form the breach. Reservoir inflow, storage, and spillway characteristics, along with the geometrical and material properties of the dam (D_{50} size, cohesion, internal friction angle, porosity, and unit weight) are utilized to predict the outflow hydrograph. The essential model components are described as follows.

A. Reservoir Level

Conservation of mass is used to compute the reservoir water surface elevation (H) due to the influence of a specified reservoir inflow hydrograph (Q_i), spillway overflow (Q_{sp}) as determined from a spillway rating table, broad-crested weir flow (Q_o) over the crest of the dam, broad-crested weir flow (Q_b) through the breach, and the reservoir storage characteristics described by a surface area (S_a)-elevation table. Letting ΔH represent the

change in reservoir level during a small time interval (Δt), the conservation of mass requires the following relationship:

$$\Delta H = \frac{0.0826\ \Delta t}{S_a} \left(\bar{Q}_i - \bar{Q}_b - \bar{Q}_{sp} - \bar{Q}_o\right) \tag{40}$$

in which the bar (-) denotes the average value during the Δt time interval. Thus, the reservoir elevation (H) at time (t) can easily be obtained since, $H = H' + \Delta H$, in which H' is the reservoir elevation at time $(t - \Delta t)$. If the breach is formed by piping, a short-tube, orifice flow equation is used instead of a broad-crested weir flow equation, i.e.,

$$Q_b = 3\ A_b(H - h_b)^{0.5} \qquad \text{(broad-crested weir flow)} \tag{41}$$

$$Q_b = A_b\left[2g(H-h_p)/(1 + fL/D)\right]^{0.5} \qquad \text{(orifice flow)} \tag{42}$$

in which A_b is the area of flow over the weir or orifice area, h_b is the elevation of the bottom of the breach at the upstream face of the dam, h_p is the specified center-line elevation of the pipe, f is the Darcy friction factor which is dependent of the D_{50} grain size, L is the length of the pipe, and D is the diameter or width of the pipe.

B. Breach Width

Initially, the breach is considered rectangular with the width (B_0) based on the assumption of optimal channel hydraulic efficiency, $B_0 = B_r\ Y$, in which Y is the critical depth of flow at the entrance to the breach; i.e., $Y = 2/3(H-h_b)$. The factor B_r is set to 2 for overtopping and 1 for piping. The initial rectangular-shaped breach can change to a trapezoidal shape when the sides of the breach collapse due to the breach depth exceeding the limits of a free-standing cut in soil of specified properties of cohesion (C), internal friction angle (ϕ), unit weight (γ) and existing angle (θ') that the breach cut makes with the horizontal. The collapse occurs when the effective breach depth (d') exceeds the critical depth (d_c), i.e.,

$$d_c = 4C \cos\phi \sin\theta'/\left[\gamma - \gamma\cos(\theta' - \phi)\right] \tag{43}$$

The effective breach depth (d') is determined by reducing the actual breach depth (d) by Y/3 to account for the supporting influence of the water flowing through the breach. The θ' angle reduces to a new angle upon collapse which is simply $\theta = (\theta' + \phi)/2$. The model allows up to three collapses to occur.

C. Breach Erosion

Erosion is assumed to occur equally along the bottom and sides of the breach except when the sides of the breach collapse. Then, the breach bottom is assumed not to continue to erode downward until the volume of collapsed material along the length of the breach is removed at the rate of sediment transport occurring along the breach at the instant before collapse. After this characteristically short pause, the breach bottom and sides continue to erode. Material above the wetted portion of the eroding breach sides is assumed to simultaneously collapse as the sides erode. Once the breach has eroded to the specified bottom of the dam, erosion continues to occur only along the sides of the breach and thus widening the breach. The rate at which the breach is eroded depends on the capacity of the flowing water to transport the eroded material. The Meyer-Peter and Muller sediment transport relation as modified by Smart (1984) for steep channels is used, i.e.,

$$Q_s = 3.64\ (D_{90}/D_{30})^{0.2}\ \frac{D^{2/3}}{n}\ P\ S^{1.1}\ (DS - 0.0054\ D_{50}\ \tau_c) \qquad (44)$$

in which Q_s is the sediment transport rate, D_{90}, D_{30}, D_{50} are the grain sizes in (mm) at which 90, 30, and 50 percent respectively of the total weight is finer, D is the hydraulic depth of flow computed from Manning's equation for flow along the breach at any instant of time, S is the breach bottom slope which is assumed to always be parallel to the downstream face of the dam, P is the total perimeter of the breach, and τ_c is Shield's critical shear stress that must be exceeded before erosion occurs. The incremental increase in the breach bottom and sides (ΔH_c) which occurs over a very short interval of time is given by:

$$\Delta H_c = Q_s \Delta t / [P\ L\ (1-p)] \qquad (45)$$

in which L is the length of the breach through the dam, and p is the porosity of the breach material.

D. Computational Algorithm

The sequence of computations in the model are iterative since the flow into the breach is dependent on the bottom elevation of the breach and its width while the breach dimensions are dependent on the sediment transport capacity of the breach flow and the sediment transport capacity is dependent on the breach size and flow. A simple iterative algorithm is used to account for the mutual dependence of the flow, erosion, and breach properties. An estimated incremental erosion depth ($\Delta H_c'$) is used at each time step to start the iterative solution. This estimated value can be extrapolated from previously computed values. Convergence is assumed when ΔH_c computed from eq. 45 differs from $\Delta H_c'$ by an acceptable specified tolerance. Typical applications of the BREACH model require less than 2 minutes on microcomputers with a math coprocessor. The computations show very little sensitivity to a reasonable variation in the specified time step size. The model has displayed a lack of numerical instability or convergence problems.

E. Testing and Verification

BREACH was applied to the piping initiated failure of the Teton earthfill dam which breached in June 1976, releasing an estimated peak discharge of 2.3 million cfs (65,128 cms) having a range of 1.6 to 2.6 million cfs (45,450-73,860 cms). The simulated breach hydrograph is shown in fig. 6. The computed final top breach width of the trapezoidal breach was 645 ft (213 m) compared to the observed width of 650 ft (214.7 m). The computed side slope of the breach was 1:1.06 compared to 1:1.00. Additional information on this and another application of BREACH to the naturally formed landslide dam on the Mantaro River in Peru, which breached in June 1984, can be found elsewhere (Fread, 1984, 1987). The model has also been satisfactorily verified with the piping initiated failure of the 28 ft (8.5 m) high Lawn Lake dam in Colorado in 1982.

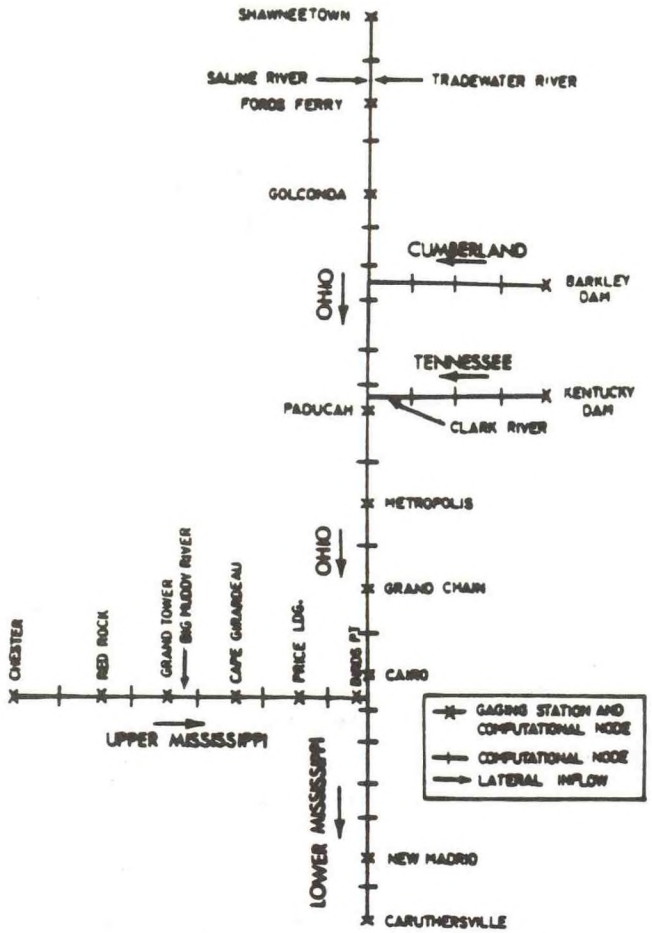

Fig. 1 Schematic of Mississippi-Ohio-Cumberland-Tennessee River System

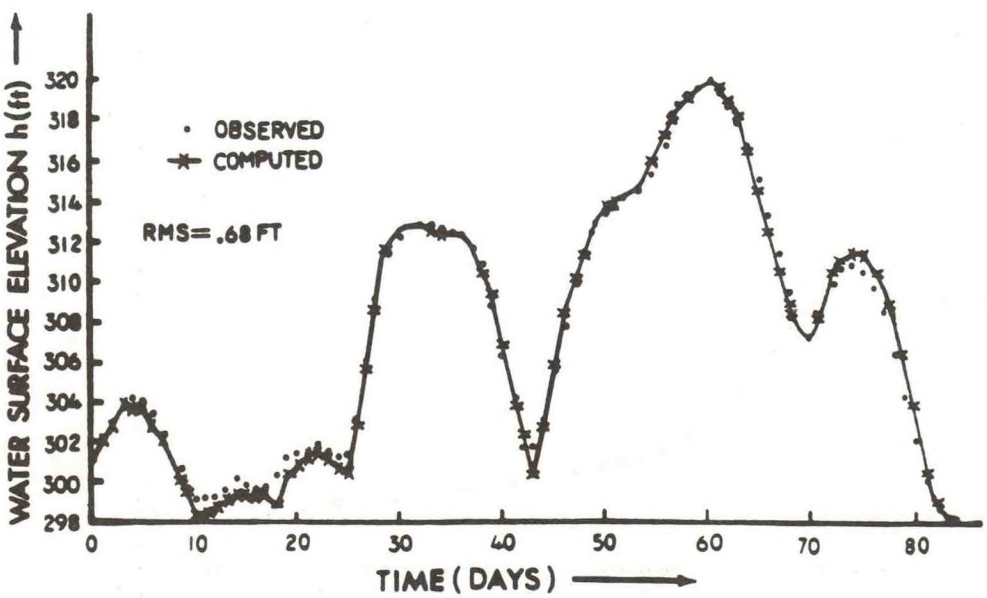

Fig. 2 Computed and Observed Stages for Cairo at Junction of Mississippi and Ohio Rivers

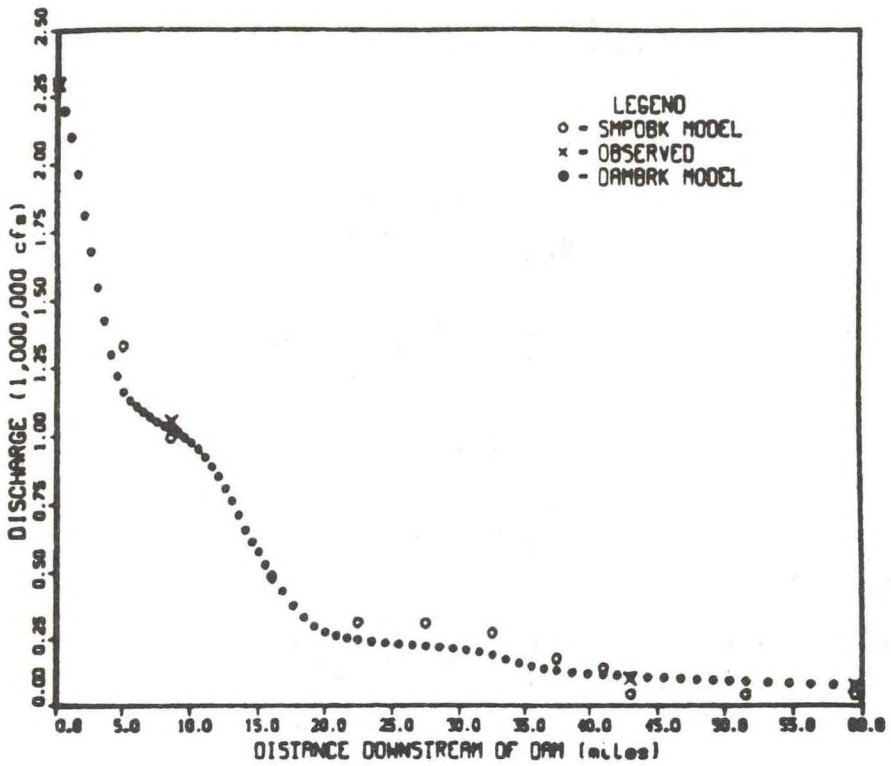

FIG. 3 PROFILE OF PEAK DISCHARGE DOWNSTREAM OF TETON.

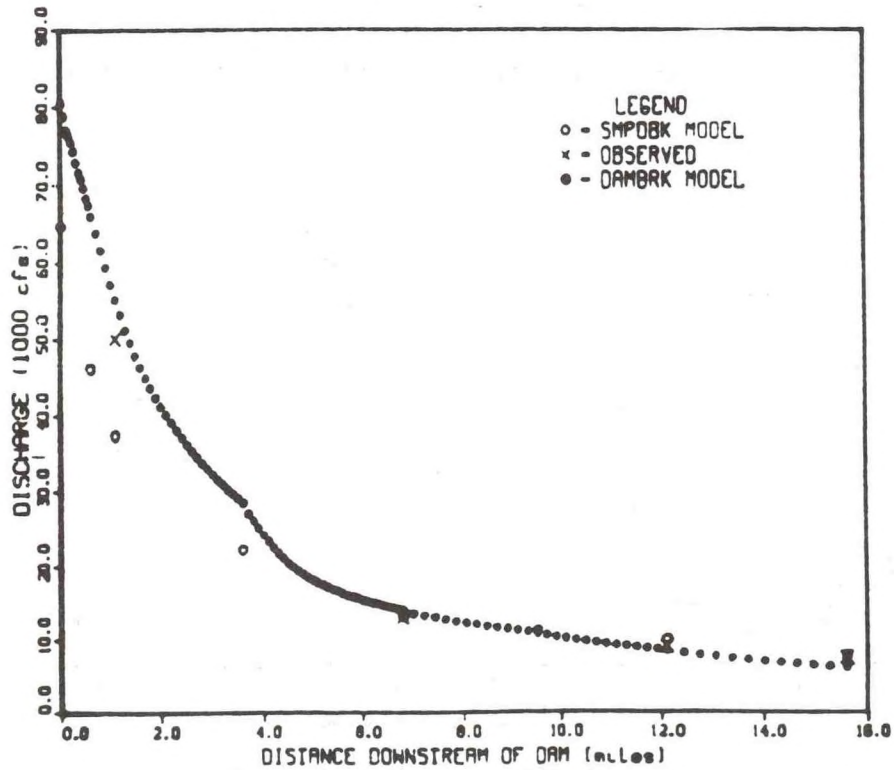

FIG. 4 PROFILE OF PEAK DISCHARGE DOWNSTREAM OF BUFFALO CREEK.

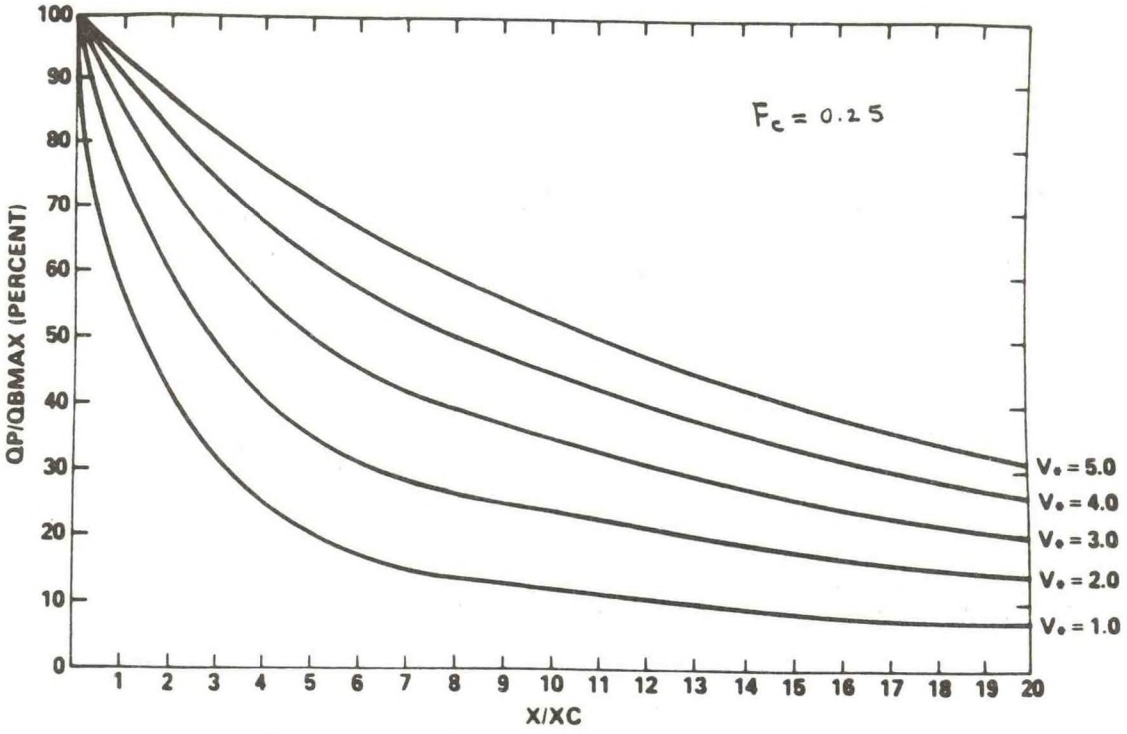

FIG. 5 ROUTING CURVES FOR SMPDBK MODEL FOR FROUDE NO = 0.25.

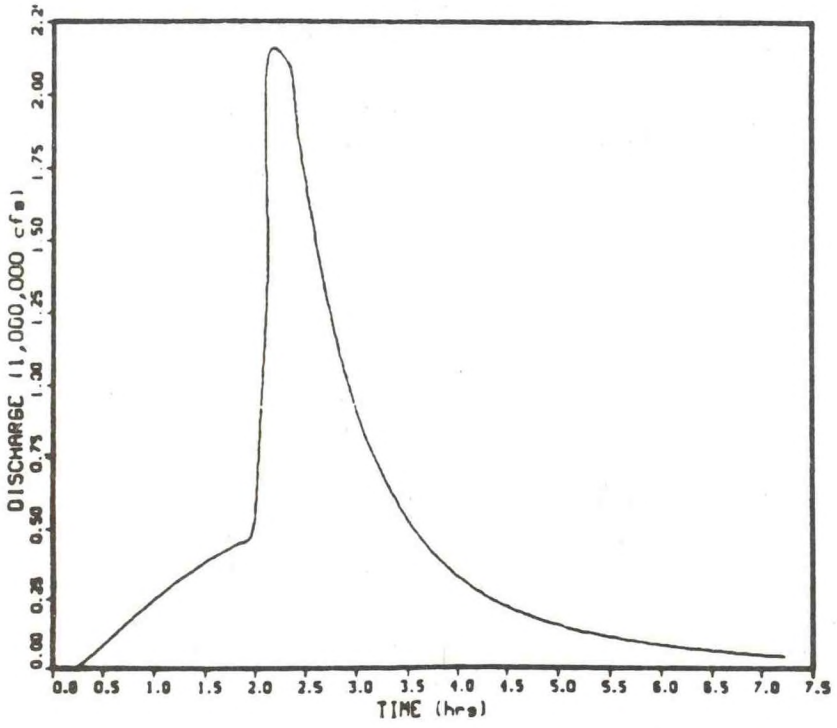

FIG 6. TETON OUTFLOW HYDROGRAPH PRODUCED BY BREACH MODEL.

REFERENCES

Davidson, D.D., and McCartney, B.L., "Water Waves Generated by Landslides in Reservoirs," Journ. Hydraulics Div., ASCE, 101, HY12, pp. 1489-1501, Dec., 1975.

Davies, W.E., Baily, J.F., and Kelly, D.B., "West Virginia's Buffalo Creek Flood: A Study of the Hydrology and Engineering Geology," Geological Survey, Circular 667, U.S. Geological Survey, 32 pp, 1975.

DeLong, L.L., "Extension of the Unsteady One-Dimensional Open Channel Flow Equations for Flow Simulation in Meandering Channels with Flood Plains," Selected Papers in HydroScience, U.S. Geological Survey Water-Supply Paper 2220, pp. 101-105, 1985.

De Saint-Venant, Barre, "Theory of Unsteady Water Flow, with Application to River Floods and to Propagation of Tides in River Channels," Acad. Sci. (Paris) Comptes rendus, 73, pp. 237-240, 1871.

Fread, D.L., "A Technique for Implicit Flood Routing in Rivers with Major Tributaries," Water Resources Research, AGU, Vol. 9, No. 4, pp. 918-926, Aug., 1973.

Fread, D.L., "The Development and Testing of a Dam-Break Flood Forecasting Model," Proceedings, Dam-Break Flood Modeling Workshop, U.S. Water Resources Council, Washington, D.C., 32 pp, Oct. 18-20, 1977.

Fread, D.L., "NWS Operational Dynamic Wave Model," Verification of Math. and Physical Models in Hydraulic Engr., Proceedings: 26th Annual Hydr. Div., Spec. Conf., ASCE, College Park, Maryland, pp. 455-464, Aug., 1978.

Fread, D.L., "DAMBRK: The NWS Dam-Break Flood Forecasting Model," Hydrologic Research Laboratory, National Weather Service, Silver Spring, Maryland, 56 pp, 1984.

Fread, D.L., "A Breach Erosion Model for Earthen Dams," Proceedings of Specialty Conference on Delineation of Landslides, Flash Flood, and Debris Flow Hazards in Utah, Utah State University, 30 pp, June 15, 1984.

Fread, D.L., "Channel Routing," Hydrological Forecasting, (Editors: M.G. Anderson and T.P. Burt), Chapter 14, John Wiley and Sons, pp. 437-503, 1985.

Fread, D.L., "BREACH: An Erosion Model for Earthen Dam Failures," Hydrologic Research Laboratory, NOAA, NWS, U.S. Department of Commerce, Silver Spring, Maryland, June, 34 pp., 1987.

Fread, D.L., and Harbaugh, T.E., "Transient Hydraulic Simulation of Breached Earth Dams," Journal of the Hydraulics Division, American Society of Civil Engineers, Vol. 99, No. HY1, pp. 139-154, Jan., 1973.

Fread, D.L., and Smith, G.F., "Calibration Technique for 1-D Unsteady Flow Models," Journal of the Hydraulics Division, ASCE, Vol. 104, No. HY7, pp. 1027-1044, July, 1978.

Fread, D.L., and Lewis, J.M. "FLDWAV: A Generalized Flood Routing Model," ASCE, Proceedings of National Conference on Hydraulic Engineering, Colorado Springs, Colorado, 6 pp., 1988.

Froehlich, D.C., "Embankment-Dam Breach Parameters," Proceedings of the 1987 National Conference of Hydraulic Engineering, ASCE, New York, New York, pp. 570-75, Aug., 1987.

Johnson, F.A., and Illes, P., "A Classification of Dam Failures," Water Power and Dam Construction, pp. 43-45, Dec., 1976.

Koutitas, C.G., "Finite Element Approach to Waves Due to Landslides," Journal of the Hydraulics Division, ASCE, 103, HY9, pp. 1021-1029, Sept., 1977.

Lin, J.O., and Soong, H.K., "Junction Losses in Open Channel Flows," Water Resources Research, AGU, Vol. 15, No. 2, pp. 414-418.

MacDonald, T.C., and Langridge-Monopolis, J., "Breaching Characteristics of Dam Failures," Journ. Hydraulics Div., ASCE, 110, No. 5, pp. 567-586, May, 1984.

Morris, H.M., and Wiggert, J.M., Applied Hydraulics in Engineering, The Ronald Press Co., New York, pp. 570-573, 1972.

Ray, H.A., Kjelstrom, L.C., Crosthwaite, E.G., and Low, W.H., "The Flood in Southeastern Idaho from Teton Dam Failure of June 5, 1976," Open File Report, U.S. Geological Survey, Boise, Idaho, 1976.

Singh, K.P., and Snorrason, A., "Sensitivity of Outflow Peaks and Flood Stages to the Selection of Dam Breach Parameters and Simulation Models, University of Illinois State Water Survey Division, Surface Water Section, Champaign, Illinois, 179 pp., June, 1982.

Smart, G.M., "Sediment Transport Formula for Steep Channels," Journal of the Hydraulics Division, American Society of Civil Engineers, Vol. 110, No. 3, pp. 267-276, 1984.

Westphal, J.A., and Thompson, D.B., "NWS Dambreak or NWS Simplified Dam Breach," Computational Hydrology '87, H17-H23, Anaheim, California, 1987.

Wetmore, J.N., and Fread, D.L., "The NWS Simplified Dam Break Flood Forecasting Model for Desk-Top and Hand-Held Microcomputers," Printed and Distributed by the Federal Emergency Management Agency (FEMA), 122 pp., 1984.

INTEGRATION SOLUTION OF THE MUSKINGUM SUCCESSIVE ROUTING METHOD AND THE LAG-AND-ROUTE METHOD

Wang Qinliang
Luo Bokun
Yangtze Valley Planning Office
Ministry of Water Resources
China

ABSTRACT. The Muskingum method of flood routing is widely used in hydrological forecasting and computation. However, it is found in practice that the satisfactory results are not frequently achieved when floods propagating through long reaches have times of travel longer than the period of rise of the inflow hydrograph. In such cases, it is desirable to adopt the method of successive routing by subreaches. In this paper, it is shown that the Muskingum model for multiple river reaches may be a lumped "strong approximation" to the quasi-diffusion wave by integrating straightforward the simplified hydrodynamic equation of flow over the reach. The analytical solutions of the quasi-diffusion wave and the Muskingum successive routing method are also derived which display a striking similarity. The range of variability of the parameter θ and the problem of the negative response are discussed in relation to the hydraulic characteristics of river channel and the ways of approximation to the flow variation over the reach, respectively.

Another hydrological method which has been studied is the lag-and-route method. Considering that the propagation of a flood wave from upstream to downstream is subject to the effects of translation and attenuation, a conceptual model has been constructed by introducing the delay element into the storage equation, which is called the model of lag-instantaneous flow concentration or the lag-and-route method. Some methods of parameter estimation are presented. This model gives good results when applied to fluctuating rivers such as the mountain

streams and the downstream reach from dam or sluice gate where the dynamic effects are nonnegligible.

I. INTRODUCTION

The theory of flood routing is based on the following equations of continuity and momentum.

$$\partial A/\partial t + \partial Q/\partial x = 0 \tag{1}$$

$$s_f - s_o + \partial h/\partial x + (1/g)\partial v/\partial t + (v/g)\partial v/\partial x = 0 \tag{2}$$

in which Q, A, h, and v are discharge, cross-sectional area, depth, and velocity of flow, respectively; s_f is friction slope; s_o is channel slope; g is the acceleration of gravity; t is time; and x is distance along the channel. These are the well-known Saint-Venant system of equations which describe the gradually varied unsteady flow in open channels without lateral inflow. Owing to their mathematical difficulties, exact integration solution for the above nonlinear hyperbolic partial equations is impossible; therefore, approximate solutions of the equations have been developed on the basis of assumptions and simplifications, such as kinematic wave models, diffusion analogy models, and complete linearized dynamic wave models, etc. These kinds of models characterize a distributing system and belong to the category of "hydraulic method." Another group of approximate flood routing methods is termed "hydrological method" which is commonly expressed in terms of the lumped form in space. The lumped water balance equation is given, from integration of the continuity equation, eq. (1), over a channel reach by

$$dS(t)/dt = I(t) - O(t) \tag{3}$$

and the dynamic equation, eq. (2), is replaced by the lumped storage-discharge relationship which may be written in a general form as follows:

$$S(t) = f[I(t), O(t)] \tag{4}$$

where I(t), O(t), and S(t) denote the inflow, outflow, and storage for the routing reach, respectively. Obviously, different forms of storage equations may lead to different models and the lumped model parameters can readily be estimated based on the observed data at the upstream and downstream ends of

the reach. A recent article presented by Fread (1985) provides a valuable summary for flood routing.

In the hydrological approach, one of the most widely applied methods is the Muskingum method. The storage equation of the method is written as:

$$S(t) = k[\theta I(t) + (1-\theta)O(t)] \tag{5}$$

in which k and θ are the routing parameters. Results in the practical application have indicated that for the long river reach where the travel time between the inflow section and the outflow section considerably exceeds the duration of the rising limb of inflow, the single Muskingum method may not accurately predict outflow hydrograph. The multiple Muskingum method has proven to be highly effective (East China Technical University of Water Resources, 1978; Yangtze Valley Planning Office, 1979; Laurenson, 1959). In the present paper, the Muskingum model for multiple river reaches will be shown to be a lumped strong-approximation solution of the quasi-diffusion model, and the analytical solutions for both the lumped model and the distributed model will be derived.

Another hydrological method involved in the paper is the lag-and-routing method. The lag-and-routing method experimentally considers the hydrodynamic characteristics of the propagation of a flood wave and has been successfully applied in some special cases.

Let us examine the general solution for the linear dynamic wave which is obtained by linearizing the Saint-Venant equations through use of the perturbation methods in fluid mechanics as follows (Dooge, 1973).

$$u(x,t) = \exp(-px)\delta(t-x/c_1) + (b/a)(x/c_1-x/c_2) \tag{06}$$
$$\exp(sx-rt)\, I_1[2ab]\, U(t-x/c_1)$$

where: $c_1 = v_0 + \sqrt{gh_o}$;

$c_2 = v_0 - \sqrt{gh_o}$;

$p = s_0(2-F)/[2h_0F(F+1)]$;

$a = \sqrt{(t-x/c_1)(t-x/c_2)}$;

$b = s_0v_0\sqrt{(4-F^2)(1-F^2)}/(4h_oF^2)$;

$s = s_o/2h_o$;

$r = s_o v_o(2+F^2)/(2h_o F^2)$;

$F = v_o/\sqrt{gh_o}$;

$\delta(t)$ = Dirac delta function;

$U(t)$ = Unit step function; and

$I_1[\,]$ = first order modified Bessel function of the first kind.

It can be seen that the solution contains the effects of pure delay and damping. The head of the wave (dynamic part) is shifting downstream at a dynamic propagation speed, c_1, while the main body of the wave (kinematic part) is moving downstream with its center of mass at a mean velocity of 1.5v and dissipating gradually with distance (Bravo et al., 1970). Therefore, for such reaches as the rivers downstream of the reservoirs, and the mountain stream where the dynamic effect of flood is significant, the storage equation may be expressed by introducing a delay element as (Wang, 1982)

$$S(t) = {}_o\int^t [I(t) - I(t-\tau)]dt + kO(t) \qquad (7)$$

Based on the above equation, we will derive the analytical result for the multiple lag-and-route flood routing method. Several methods of parameter estimation will also be described in this study.

II. QUASI-DIFFUSION WAVE AND MUSKINGUM SUCCESSIVE ROUTING METHOD

By neglecting the inertia terms, eq. (2) becomes

$$s_f = s_o[1 - (1/s_o)\partial h/\partial x] \qquad (8)$$

which can be written as

$$Q = Q_o[1 - (1/s_o)\partial h/\partial x]^{1/2} \qquad (9)$$

Differentiating eq. (9) with respect to t, a simultaneous solution with the continuity equation can be performed. If

$\omega = \omega_o\sqrt{s_f/s_o}$ convection speed

$\mu = (Q_o/2Bs_o)\sqrt{s_o/s_f}$ diffusion coefficient

We then have

$$\partial Q/\partial t + \omega \partial Q/\partial x - \mu \partial^2 Q/\partial x^2 = 0 \qquad (10)$$

This is the convection-diffusion equation, or called the diffusion equation for short.

If the term of partial derivative in eq. (9) is approximated by the kinematic wave equation, that is, $\partial h/\partial x \approx -(1/\omega_o)\, \partial h/\partial t$, the resulting equation becomes

$$\partial Q/\partial t + \omega_o \sqrt{S_f/S_o}\, \partial Q/\partial x + v_o \sqrt{S_o/S_f}\, \partial^2 Q/\partial x \partial t = 0 \qquad (11)$$

where

$$v_o = \mu_o/\omega_o \qquad (12)$$

v_o has the dimensions of distance, corresponding to half of the characteristics river length.

If further, s_f in the coefficients of the eq. (11) is approximately equal to s_o, then

$$\partial Q/\partial t + \omega_o\, \partial Q/\partial x + v_o\, \partial^2 Q/\partial x \partial t = 0 \qquad (13)$$

In order to distinguish from the diffusion equation, the above equation may be called the quasi-diffusion equation since it is closer to the dispersion of kinematic wave.

Applying the Laplace transform to eq. (13) under the following boundary conditions

$$Q(x, 0) = 0$$
$$Q(0, t) = \delta(t)$$

yields

$$\{ u(x,t)\} = \exp\{-xp/(\omega_o + v_o p)\} \qquad (14)$$

in which u(x,t) is the output resulting from the unit impulse of the upstream inflow; p is the transform variable.

By expanding the exponential function into a Taylor's series and taking the inverse transform, the impulse response of the quasi-diffusion wave can be obtained as

$$u(x,t) = \exp(-x/\nu_o)\delta(t) - \sum_{\lambda=0}^{\infty} (-x/\nu)^{\lambda} \, 1/\lambda! \; \omega_o / \nu_o \exp(-\omega_o t/\nu_o) \; L^1_{\lambda-1} (\omega_o t/\nu_o) \tag{15}$$

where $L^1_{\lambda-1}(\,)$ is a generalized Lagguerre polynomial.

The above solution indicates that the quasi-diffusion wave also possesses these two parts, say "head" and "body," of wave. The wave head is a delta function with an exponentially damping factor and the wave body is composed of generalized Laggurre polynomials with attenuation weights. However, not like the dynamic wave which moves downstream step by step, the quasi-diffusion wave seems to spread its effect immediately to very long distance at the zero time when a pulsed upstream inflow is imposed. Such phenomenon of "prompt response" is inherent in diffusion.

For the purpose of deriving the lumped expression for eq. (13), substituting from eq. (1) into eq. (13) and integrating along the reach, we obtain

$$\int_o^L \frac{\partial \Lambda}{\partial t} \, dx = \frac{1}{\omega_o} \int_o^L \frac{\partial Q}{\partial t} \, dx + \frac{\nu_o}{\omega_o} \int_o^L \frac{\partial^2 Q}{\partial x \partial t} \, dx \tag{16}$$

which is clearly equivalent to

$$\frac{dS(t)}{dt} = \frac{1}{\omega_o} \cdot \frac{d}{dt} \int_o^L Q(x,t) \, dx + \frac{\nu_o}{\omega_o} \cdot \frac{d}{dt} [O(t) - I(t)] \tag{17}$$

The first integral on the right-hand side cannot be evaluated exactly because of the unknown integrant. For this reason, the trapezoidal quadrature formula may be used here to approximate the integral, which gives

$$\int_o^L Q(x,t)dx \approx (L/2) \, [I(t) + O(t)] \tag{18}$$

The truncation error is

$$R(Q) = -(L^3/12) \, \partial^2 Q(x,t)/\partial x^2 \big|_{x=\eta} \qquad \eta \in (0,L) \tag{19}$$

Therefore, a lumped storage equation, the same as the well-known Muskingum equation, is obtained.

$$S(t) = k[\theta \, I(t) + (1-\theta)O(t)] \tag{20}$$

where

$$k = L/\omega_o \tag{21}$$

$$\theta = (1/2) - (\nu_o/L) \tag{22}$$

Notice from eq. (19) that the error of integration will increase with distance rapidly. To enhance the accuracy of integration, it is necessary to apply the composite trapezoidal formula with equal intervals of length, which physically means in the case that the total reach is divided into n subreaches and that the variations of flow for each subreach are assumed to be linear. The resulting equation then becomes

$$S(t) = \sum_{m=1}^{n} \{k_o [\theta_o Q[(m-1)L/n, t] + (1-\theta_o)Q(mL/n,t)]\} \tag{23}$$

where

$$k_o = L/(n\omega_o) \tag{24}$$

$$\theta_o = 1/2 - (n\nu_o)/L \tag{25}$$

The truncation error of the integral in eq. (17) is

$$R_\eta(Q) = -(L^3/12n^2)\, \partial^2 Q(x,t)/\partial x^2 \,|_{x=\eta} \quad \eta \in [0,L] \tag{26}$$

Solving eq. (23) simultaneously with eq. (3), and noting the fact that the inflow of a succeeding subreach is the outflow from the preceding one, we get

$$O(t) = \{(1-k_o\theta_o D)/[1+k_o(1-\theta_o)D]\}^n\, I(t) \tag{27}$$

in which D=d/dt. This equation can be written in the following form

$$O(t) = \{(-\frac{\theta_o}{1-\theta_o})^n + (-\frac{\theta_o}{1-\theta_o})^n [(1 - \frac{1/[K_o\theta_o(1-\theta_o)]}{1/[k_o(1-\theta_o)]+D})^n - 1]\}\, I(t) \tag{28}$$

Similarly, using the Laplace transformation, the analytical solution of the multiple Muskingum method may be obtained as

$$n(t) = (-\frac{\theta_o}{1-\theta_o})^n\, \delta(t) - (-\frac{\theta_o}{1-\theta_o})^n \frac{1}{K_o\theta_o(1-\theta)} \exp[-\frac{t}{K_o(1-\theta_o)}] L^1_{n-1} [\frac{1}{K_o\theta_o(1-\theta_o)}] \tag{29}$$

Comparing eq. (29) with eq. (15), the impulse response function of the Muskingum successive routing model is quite similar to that of the quasi-diffusion model. Eq. (26) shows that with the increase of the number of subreaches, the error of approximation will decrease at the dropping speed of 1/n sharply. In addition, it can be proved that the latter is just the limiting case of the former when $n \to \infty$.

III. PARAMETERS OF THE MUSKINGUM METHOD AND NEGATIVE OUTFLOWS

It is known from the preceding section, that the parameter k is referred to as the mean travel time which depends on the velocity of the kinematic wave, and that the parameter θ relates not only to the diffusion coefficient and the wave velocity but also to the length of the river reach. By using the notation

$$L_o = 2v_o \tag{30}$$

and substituting into eq. (22), it is clearer that the parameter θ stands for the relative ratio of the characteristic reach length and the actual reach length. For a certain value of L, the value of θ may be either positive or negative, depending on the length of the river reach under study. If $L \gg L_o$, then the value of θ tends to 1/2; conversely, if $L \ll L_o$, then $\theta \to -\infty$. So, under the circumstances of negligible lateral inflow and no baseflow, the allowable range of θ should be from 1/2 to $-\infty$, as discussed by Strupczewski and Kundzewicz (1980). As shown in fig. 1, for the three conditions (that is, $0 < \theta < 1/2$, $\theta = 0$, and $\theta < 0$) their differences exhibited on the discharge-storage curves and on the inflow and output hydrographs are in evidence.

In the case of successive routing by n subreaches, the condition judging $\theta_o \leq 0$ is $n \geq 1/(1-20)$ or $L_o \leq 2v_o$. When the above condition is satisfied, the negative response of the Muskingum method will be eliminated. According to the analysis in the previous section, the single Muskingum storage equation derived from the quasi-diffusion equation indicates that the water surface profile within the whole reach is approximated by a straight line. The longer the length of the river reach, the poorer the degree of the approximation. Consequently, the multiple-reach routing method is no doubt conducive to the improvement of approximation accuracy. With the increase of subreaches, the

negative response will weaken gradually. When the length of each subreach is equal to or less than the characteristic length, the negative response does not exist.

The multiple Muskingum method embodies three parameters, k_o, θ_o, and n which have relations with the first three cumulants as follows.

$$C_1 = nk_o \tag{31}$$

$$C_2 = nk_o^2 (1 - 2\theta_o) \tag{32}$$

$$C_3 = 2nk_o^3 (1 - 3\theta_o - 3\theta_o^2) \tag{33}$$

Since the higher cumulant computed from the given inflow and outflow may involve large error, the method of cumulants for the parameter estimation is rarely used in practice.

From eqs. (21), (22), (24), and (25), the following transform relations of the parameters between the multiple and the single Muskingum method can be obtained.

$$k_o = k/n \tag{34}$$

$$\theta_o = 1/2 - n (1/2 - \theta) \tag{35}$$

Thus with these related expressions, the parameters k_o and θ_o for subreaches can be evaluated from the parameters k and θ for the whole reach obtained in advance in terms of the graphical method, the method of moments, or the hydraulic method.

IV. BASIC CONCEPT AND DERIVATION OF THE LAG-AND-ROUTE METHOD

In the natural river, the propagation of a flood wave is subjected to the effects of translation and attenuation due to the influence of factors such as the variation of flow velocity, the resistance and the characteristics of river channel, etc. No matter how short the length of river reach and how fast the speed of wave head, the flood wave traveling must take some time. This is the transport delay in flood propagating. Figure 2 shows the observed hydrographs for the four major stations on the middle and lower reach of the

Han River in August 1972. It can be seen clearly that the initial wave at the Huangjiangang station, located 6 km downstream from the Danjiangkon reservoir, gradually shifts and flattens out when it is moving downstream. As mentioned earlier, these features are included in the solution of the linear dynamic wave based on the Saint-Venant equations. Therefore, take into account that the translation effect in flood routing conforms to the element of hydraulics, and can significantly increase the routing accuracy for cases where the inflow rises and recedes steeply. Otherwise, the rising limb of the calculated outflow hydrograph may move up and the peak may be underestimated (Yangtze Valley Planning Office, 1979; Wang, 1982).

On the basis of the above factors, the storage in a river reach is considered to be composed of the linear-channel storage and the linear-reservoir storage, as shown in fig. 3.

Then by introducing the delay element, the storage equation can be expressed as

$$S(t) = S_{\ell}(t) + S_r(t) = \int_o^t [I(t) - I(t-\tau)]\, dt + kO(t) \tag{36}$$

By implementing successive routing one reach after another with eqs. (36) and (3), the related expression between the inflow to the first reach and the outflow from the n^{th} reach can be obtained as

$$O(t) = \frac{1}{(1+kD)^n} I(t - n\tau) \tag{37}$$

When inflow is a delta function, $\delta(t)$, the Laplace transform of the impulse response is

$$u(p) = \frac{1}{(1+kp)^n} e^{-n\tau\gamma} \tag{38}$$

According to the Heavisde's theorem, the integration solution of the lag-and-route model for multiple reaches (Type I), or the lag IUH of Type I, is finally derived as (Wang, 1982).

$$u(t) = \begin{cases} 0 \\ \frac{1}{k\Gamma(n)} \left(\frac{t-n\tau}{k}\right)^{n-1} \exp\left(-\frac{t-n\tau}{k}\right) \end{cases} \tag{39}$$

If the storage equation is taken in the following form

$$S(t) = K(1-\theta)\, O(t) + \sum_{i-1}^{\infty} (-1)^{i-1} \frac{(K\theta)^1}{i_!} D^{i-1} I(t) \tag{40}$$

then, in a manner completely analogous to that followed in developing eq. (39), it can be shown that the formula for the IUH of another form of successive lag-and-route method (Type II), or the Type II lag IUH, is given by (Kuo Bokun and Qian Xeiwei, 1987).

$$u(t) = \begin{cases} 0 \\ \frac{1}{K(1-\theta)\Gamma(n)} \left[\frac{t-nK\theta}{k(1-\theta)}\right]^{n-1} \exp\left[-\frac{t-nK\theta}{K(1-\theta)}\right] \end{cases} \tag{41}$$

In this case, the upper limit of θ should be 1.

V. PARAMETERS OF THE MULTIPLE LAG-AND-ROUTE METHOD (TYPE-I)

The lag-and-route method for multiple river reaches (Type I) is a three-parameter model. The methods used to estimate the parameters n, k and τ include the moment method, the cumulant method, and the hydrological method.

A. Method of Moments

Differentiating eq. (38) and letting p=0, yield the first three moments about the time origin for the lag IUH of Type I.

$$M_u^{(1)} = nk + n\tau \tag{42}$$

$$M_u^{(2)} = nk^2 = (n\tau + nk)^2 \tag{43}$$

$$M_u^{(3)} = 2nk^2 + 3nk^2 (n\tau + nk) + (n\tau + nk)^3 \tag{44}$$

By using the relations between the moments about the origin and about the centroid, the second and third central moments can readily be obtained from eqs. (43) and (44). Thus the parameters can be estimated by

$$n = 4(N_u^{(2)})^3/(N_u^{(3)})^2 \tag{45}$$

$$k = N_u^{(3)}/2N_u^{(2)} \tag{46}$$

$$\tau = \frac{N_u^{(3)}}{2N_u^{(2)}} \left(\frac{M_u^{(1)} N_u^{(3)}}{2(N_u^{(2)})^2} - 1 \right) \tag{47}$$

where N_u denotes the central moments of the lag IUH.

B. Method of Cumulants

According to definition of the cumulant, the first three cumulants for the successive lag-and-route model can be derived as:

$$C_1 = M_u^{(1)} = n\tau + nk \tag{48}$$

$$C_2 = N_u^{(2)} = nk^2 \tag{49}$$

$$C_3 = N_u^{(3)} = 2nk^3 \tag{50}$$

By equating the above cumulants to the corresponding cumulants for the linear dynamic wave solution, the optimal values for the parameters n, k, and τ are given by:

$$n = (2/3)\ (4-F^2)/(2+F^2)^2\ (s_o L/h_o) \tag{51}$$

$$k = (1/3)\ (2+F^2)\ h_o/(s_o v_o) \tag{52}$$

$$\tau = (2/3)\ (2+F^2)\ [(1+2F^2)/(4-F^2)]\ h_o/(s_o v_o) \tag{53}$$

C. Hydrological Method

According to the basic concept of the IUH, the total delay time for n reaches is equal to the travel time τ_o from the beginning point of rise of the inflow to that of the outflow, that is

$$\tau = \tau_o/n \tag{54}$$

Then, solving with eqs. (42) and (49) simultaneously, we have

$$k = N_u^{(2)}/(M_u^{(1)} - \tau_o) \tag{55}$$

$$n = (M_u^{(1)} - \tau_o)^2 / N_u^{(2)} \tag{56}$$

Also, in order to avoid the third moment which is more difficult to be determined accurately in practice, we can use the following relation:

$$k = t_L - t_p \tag{57}$$

where t_L and t_p are the centroid-lag and the peak-lag of the IUH for the successive lag-and-route model, respectively. Therefore

$$k = M_u^{(1)} - t_p \tag{58}$$

$$n = N_u^{(2)} / k^2 \tag{59}$$

$$\tau = M_u^{(1)} / (n - k) \tag{60}$$

VI. CONCLUSION

The integration of the quasi-diffusion equation over the river reach leads to a lumped approximate expression which is apparently equivalent to the Muskingum storage equation. The analytical solutions derived for the quasi-diffusion model and the multiple Muskingum model show considerable similarity. Both the solutions are constituted by the head and the body of the wave. The former is a delta function with a damping factor, exponential or linear; the latter is the weighting Laggurre polynomial, complex or single. It is worth noting that, different from that of the linear dynamic wave which has the property of delay, the wave head here seems to spread promptly due to the inherent nature of diffusion.

The Muskingum successive routing method is derived from the equation for the quasi-diffusion wave by integration with the approximate representation of the entire flood profile by sectioned straight lines. For this reason, the accuracy of the approximation will improve with the increase of the number of subreaches n. When n is equal to or greater than $1/(1-2\theta)$, then θ_o for subreaches becomes negative; therefore, the negative outflow of the Muskingum method has a bearing on the approximation of the flow profile within the reach. For long reaches, the Muskingum method by successive routing is used to be more effective.

The advantage of the lag-and-route method is without negative response because of the consideration of translation effect. The model construction is based on the hydraulic characteristics of flood propagation. The integration solution for the lag-and-route method by successive routing is derived, and several methods for the parameter estimation are presented for convenience to use in practice. Since the multiple lag-and-route method contains both the effects of translation and attenuation, it is also an effective method for flood routing especially for the cases where the significant dynamic effect exists.

REFERENCES

Bravo, S.C.A., Harley, B.M., Perkins, F.E., and Eagleson, P.S., "A Linear Distributed Model of Catchment Runoff," Report No. 123, MIT, Department of Civil Engineering, R.M. Parsons Laboratory, 1970.

Dooge, J.I.C., "Linear Theory of Hydrological Systems," Technical Bulletin 1468, USDA, Agricultural Research Service, U.S. Government Printing Office, Washington, DC, 1973.

East China Technical University of Water Resources (ECTUWR), "Flood Forecasting Method for Humid Regions of China," Nanking, China, 1977.

Fread, D.L., "Channel Routing," in Anderson, M.G., and Burt, T.P. (eds.) Hydrological Forecasting, John Wiley and Sons, Ltd., Chapter 14, pp. 437-503, 1985.

Laurenson, E.M., "Storage Analysis and Flood Routing in Long River Reaches," Journal of Geophysical Research, Vol. 64, pp. 2423-24, 1959.

Luo Bokun and Qian Xuewei, "Some Problems with the Muskingum Method," Hydrologic Sciences Journal, Vol. 32, pp. 485-496, 1987.

Qian Xuewei, "Analytical Solution of Muskingum Method by Successive Routing," Water Resources and Hydropower Engineering, Hydrology Division, Beijing, China, Vol. 2, pp. 5-15, 1980.

Strupczewski, W., and Kundzewicz, Z., "Muskingum Method Revisited," Journal of Hydrology, Vol. 48, pp. 327-342, 1980.

Wang, Qinliang, "The Model of Lag-instantaneous Flow Concentration," Hydrology, Beijing, Chian, Vol. 1, pp. 13-19, 1982.

Yangtze Valley Planning Office (YVPO), "Hydrological Forecast Methods in China," China Water Resources and Electric Power Press, 1979.

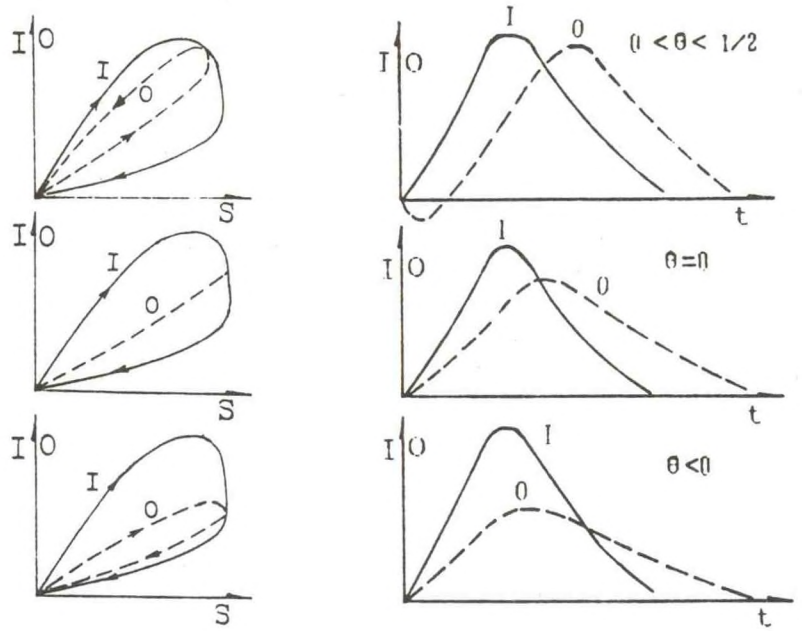

Figure 1. Differences in the storage curves and the flow hydrograph under the different values of parameter θ

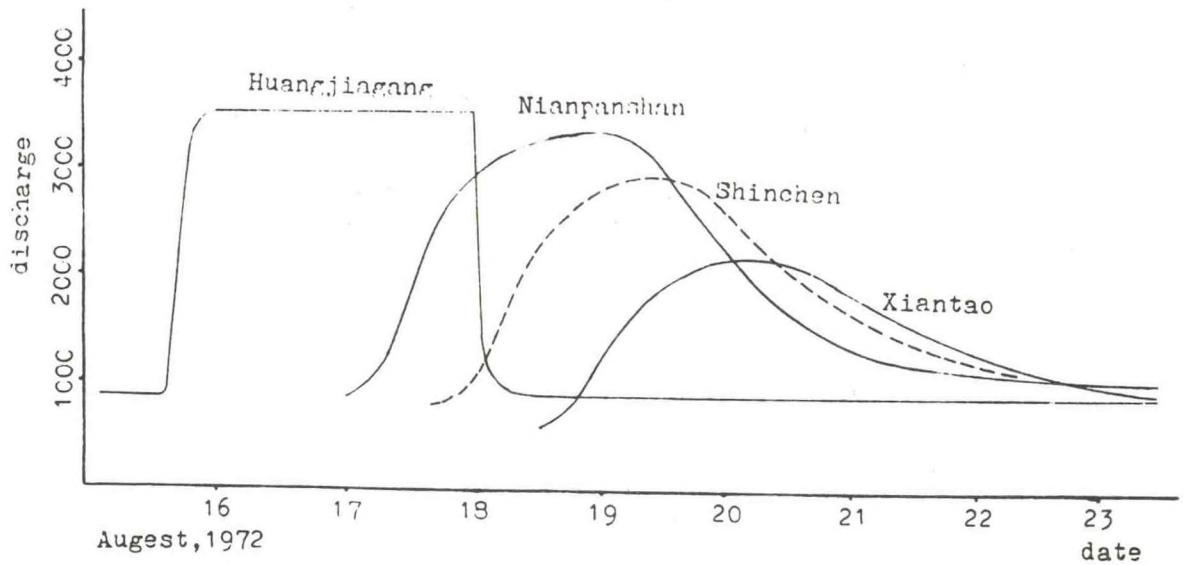

Figure 2. Observed flow hydrographs at the four stations on the middle-lower reach, the Han River, August, 1972

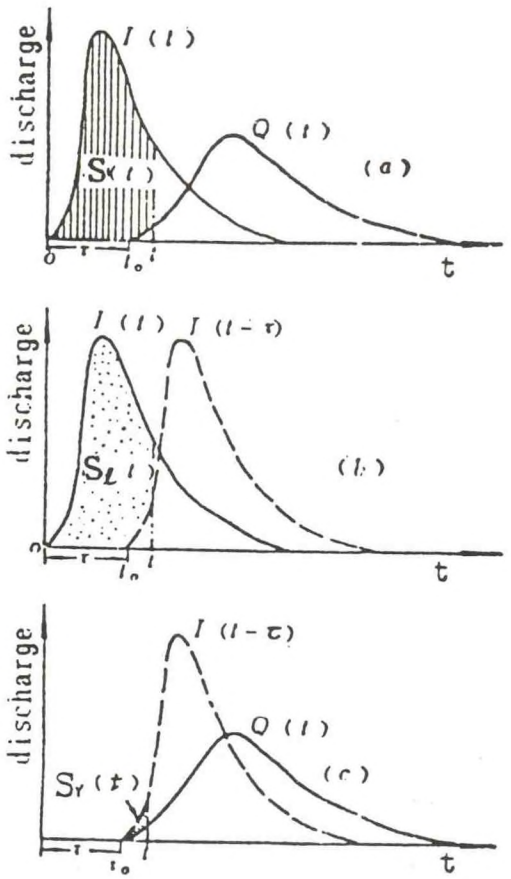

Figure 3. Analysis of the storage composition for the lag-and-route model

IMPORTANCE OF THE HRAP GRID FOR OPERATIONAL HYDROLOGY

John C. Schaake, Jr.
Office of Hydrology, NWS
Silver Spring, MD 20910

I. INTRODUCTION

Greene and Hudlow (1982) proposed a general hydrometeorological grid mapping procedure for use by the National Weather Service's (NWS) Hydrologic Rainfall Analysis Project (HRAP). This procedure, known as the HRAP grid, will be used by the NWS as the basis for organizing the digital precipitation estimates from the Next Generation Radar (NEXRAD).

The HRAP grid is a rectangular grid on a polar stereographic projection of the earth. It is nested within the National Meteorological Center's (NMC) Limited Fine Mesh (LFM) model grid. It is illustrated in fig. 1. The mesh length at 60° north latitude is 4.7625 km, one-fortieth the mesh length of the LFM grid. Mesh lengths for other latitudes may be computed from:

$$Z = 4.7625/[(1 + \sin 60°)/(1 + \sin \Phi)] \quad (1)$$

where Φ is the latitude. At 40° north, the mesh size is approximately 4.2 km; at 30°, 3.8 km. The grid is positioned so that coordinates (401, 1601) are at the North Pole. All coordinates with the United States are positive. All points with horizontal coordinate 401 lie along longitude coordinate 105° west; i.e., the grid is oriented north-south at coordinate 401.

The HRAP grid is used in the National Weather Service River Forecast System (NWSRFS) (Brazil, 1984) as part of an option to compute station weights for mean areal precipitation estimation. Basin boundaries are defined by latitude longitude coordinates. These determine which HRAP grid points lie within the basin.

II. ADVANTAGES OF THE HRAP GRID

There are many advantages to using a grid system as a basis for organizing hydrometeorological computations, especially for the new generation of

computing systems that support interactive and color graphics applications. Some advantages apply regardless of how the grid is defined. Others are specific to the HRAP grid. And there are limitations to consider of any given grid size. Following is a discussion of grid system advantages. Subsequent sections present selected analyses of potential limitations.

The most important factor in designing operational software for hydrology is to organize the total system into well-chosen modules that may be developed and modified independently of each other. Systems with interdependent modules (that must change when changes are made in other modules) become impossible to support as changes are made and the original developers move on to other work. A system composed of many small, independent, modules is far more supportable that "apparently simple" systems with only a few large modules. Good module design is equivalent to good interface design because, in an important sense, modules are defined by their interfaces.

An important interface in operational hydrology is between precipitation data modules and modules of the hydrologic models. Perhaps the most important advantage of a grid system for precipitation analysis is to serve as in interface separating models and data modules. Hydrologic models can be designed to expect input either in grid-point form, directly from point observations, or as mean areal precipitation which may be derived from grid-point data. Separately, various data analysis modules can be developed to produce grid-point estimates of precipitation from available point data, radar data, satellite data, future mesoscale precipitation modules, or combinations of these.

An important advantage of grid point fields is new graphics systems can display them so forecasters can see what the data systems are producing and what the model systems are receiving.

If a grid system is used as an interface between models and data, different data analysis procedures can easily be tested. All that is needed is a method for assigning the desired field to the model input.

As computers have become less expensive, faster, and graphically oriented, and as geographical information systems have developed, it has become

reasonable to look for improved hydrologic modeling that would take more detailed account of how water moves through a watershed. Having grid-point data available from NEXRAD will surely stimulate development of models that can use this information.

A disadvantage of a grid-point interface between data and models is that computational costs may be greater, to compute mean areal values from grid data, if all of the observations are point data. In that case, it can be shown there is no statistical advantage, in the sense of optimal interpolation theory, to doing the grid point estimates first. But if some of the gage data are missing, precomputed station weights no longer can be used -- unless all possible combinations of station failures have been planned for. In practice, the missing data are estimated and the estimated amounts are used with the original station weights. Nevertheless, the ability to display grid-point fields, to preserve more space-time information for small basins, and to further decouple data and model modules makes a grid-point interface highly attractive.

A. Computation Advantages of the HRAP Grid

An important computational advantage of the HRAP grid is that its coordinates can be transformed in either direction between latitude/longitude formulas. This preserves maximum flexibility for software developers to work in either grid system and to allow (but not require) data bases to support both systems.

Selecting a grid mesh size involves, a trade-off between computational requirements, accuracy of representation of space-time characteristics of precipitation that affect runoff, and the information content of the observed data. Ideally, one would like to have a very dense grid to minimize the "discretization error" of projecting the infinite dimensional "true" field onto a finite-dimensional array. The HRAP grid was originally planned on the basis of a subjective assessment of these factors. The radar beam of NEXRAD has a beam width of about 1° and will move in horizontal increments of 1°. At the outer range limits, the horizontal beam width will be about 4 km. Discretizing radar data to a 4 km grid, therefore, is supportable by the radar

and gives spatial average estimates of precipitation over, roughly, a 16 km^2 area.

The following sections analyze some of the "discretization errors" inherent in hydrologic applications of the RADAP grid. The analyses found little of practical operational concern for almost all services offered by the NWS. Additional analysis of the limitations of time sequences of HRAP grid fields are needed to assess the time intervals required to preserve the space-time information that is important for flood prediction, especially for small basins.

III. ESTIMATION OF DRAINAGE AREA

The most important first step in hydrology is to know what area contributes runoff to a given point on a river. Having precipitation data available on a grid system raises the possibility of doing hydrologic computations (such as defining basin boundaries) on the same grid. This raises many questions well beyond the scope of this paper. Nevertheless, the question of the accuracy of representation of drainage area will be considered in this section, and the question of the accuracy of estimation of mean areal precipitation will be considered in the next.

Suppose an area were represented in terms of grid squares or "pixels." This is how a personal computer (PC) graphics monitor displays an area. A pixel can be defined to be within an area if its centroid were in the area. Moving around the perimeter of the area, portions of pixels, defined to be outside, would actually be inside, and conversely. This means the area represented by the pixels would include a random error term and this random error would vary depending on the relative orientation of the grid with the area boundary.

A practical question is, how large is this error relative to the size of the area? To answer this question, 35 headwater basins, served by the Denver Colorado Weather Service Forecast Office (WSFO) and included in the new Denver AWIPS-90 Risk Reduction and Requirements Evaluation (DAR^3E) system, were examined. Figure 2 is a map showing the size and location of these basins in western Colorado. They ranged from 41 to 3639 km^2. The boundaries of these areas were digitized as vectors having coordinates of latitude and

longitude. Assuming these vectors define the "true" area, how accurately can pixels represent the same areas? This depends on the pixel size.

A. Area Discretization Error

A simple theoretical model of the area discretization error is as follows. Let A be the true area and let P be the length of the perimeter. Let d be the grid size, so that $a = d^2$ is the pixel area. Then, the expected number of pixels in the area would be:

$$N_a = \frac{A}{a} \tag{2}$$

and the approximate number of pixels around the perimeter would be:

$$N_p = \frac{P}{d} \tag{3}$$

Consider a hypothetical, rectangular, drainage area of width, W, and length, L. Assume:

$$L = \alpha \sqrt{A} \tag{4}$$

and,

$$W = \frac{1}{\alpha} \sqrt{A} \tag{5}$$

then,

$$P = 2 (L + W) = 2 \sqrt{A} (\alpha + \frac{1}{\alpha}) \tag{6}$$

or,

$$P = N_p \, d = 2 \, d \sqrt{N} (\alpha + \frac{1}{\alpha}) \tag{7}$$

so that,

$$N_p = 2 (\alpha + \frac{1}{\alpha}) \sqrt{N} \tag{8}$$

Around the perimeter, assume pixels occur at random to the left or to the right. If a sum is accumulated of pixel values (1 if a pixel is to the right, (i.e., inside the area), 0, otherwise); the sum will be a random variable. The standard deviation of this sum is:

$$\sigma_p = 0.5 \sqrt{N_p} \tag{9}$$

and the coefficient of variation of the error, relative to the total area is:

$$CV_e = \frac{\sigma_p}{N} \tag{10}$$

or,

$$CV_e = 0.5 \left[2 \left(\alpha + \frac{1}{\alpha}\right)\right]^{1/2} N^{-3/4} \tag{11}$$

In other words, the theoretical error is a function of the number of pixels and a shape factor, α. The shape factor term is nearly constant over a wide range of practical values.

Figure 3 shows that this equation describes the error properties of a 1 km pixel size. The standard deviations of error should be less than 10 percent for any area with enough lead time to permit forecasts to be made substantially on the basis of observed precipitation data. The 1 km grid was considered in fig. 3 because 1 km is approximately the same as 30 seconds of latitude. Readily available for the United States, 30 second terrain data can be used to generate basin boundaries automatically.

Figure 4 shows the discretization error for a 4 km grid. The errors observed by discretizing the 35 Colorado basins was generally less than the theoretical error. Basins larger than 200 km^2 can be defined on a simple grid to within a 10 percent standard error. Smaller basins should be defined on a smaller grid, but the next section will show that mean areal precipitation computations for these smaller basins may be done accurately on the basis of a simple grid point average using a 4 km grid.

IV. DISCRETIZATION ERROR IN REPRESENTING MEAN AREAL PRECIPITATION

Radar estimates of precipitation represent a spatial average over a grid cell. The goal of the following analysis is to examine how well a simple average of grid cell average precipitation agrees with the true average over the true area. This analysis does not consider the measurement error of the radar. It neglects the radar error and considers only the error introduced by using a grid size of about 4 km instead of a finer grid that would include more spatial detail.

A theoretical model for the discretization error of mean areal precipitation is:

$$CV_e = CV_p F_1 F_2 \quad (12)$$

where CV_e is the standard error as a proportion of the mean areal precipitation, CV_p is the coefficient of variation of the point precipitation process over the area, F_1 is an areal reduction factor, and F_2 is a discretization error factor. The factors on the right hand side of eq. 12 are discussed below beginning with CV_p.

A. Coefficient of Variation of Point Precipitation, CV_p

The error potential of the 4 km grid is greatest for small areas, and the flood producing storms typically are convective. A classic report on the statistical properties of such storms is Thunderstorm Rainfall (1945). Data from a dense network of recording gages for the maximum 6-hour period of rain for 38 storms over the Muskingum Basin, Ohio, during the years 1937-1941, were analyzed. An example storm over the basin is illustrated in fig. 5.

The distribution of point values over the entire basin is illustrated in fig. 6. This is the first-order distribution of rain. Different storms have different first-order distributions. A simple way to describe the storms is in terms of the mean and standard deviation of this distribution. Table 1 gives sample values for these statistics for the total basin area and two subdivisions of the total area. The statistic CV_p in eq. 12 is the ratio of the standard deviation to the mean of the first-order distribution.

Figures 7 and 8 show CV_p varied with drainage area and mean areal precipitation amounts during these storms. The center curve represents median values of CV_p. The upper and lower curves represent 1-standard deviation bounds (for individual storms) above and below the median. Notice that the point variability appears to increase with area and to decrease substantially with storm magnitude.

B. Areal Reduction Factor, F_1

In order to evaluate factor F_1, an analysis of the spatial correlation properties of the storms is required. Figure 9 shows that the daily rainfall data for these storms had an average decorrelation distance of 10 miles. The 6-hour data must have decorrelated more quickly, but that is not reported.

Table 1 -- Average Depths and Standard Deviations of Rainfall Measurements in 6-hour Storms (Muskingum Basin)

Storm No.	Storm Date	375 Sq. Mi. AD	375 Sq. Mi. SD	1500 Sq. Mi. AD	1500 Sq. Mi. SD	8000 Sq. Mi. AD	8000 Sq. Mi. SD
1	Aug. 10, 1937	0.49	0.29	0.38	0.34	0.43	0.77
2	Aug. 3, 1939	0.44	0.80	0.28	0.57	0.22	0.45
3	Sept. 12, 1938	0.27	0.23	0.61	0.53	0.93	0.77
4	June 18, 1939	1.15	0.34	1.01	0.43	0.72	0.52
5	July 4, 1939	0.74	0.19	0.70	0.21	0.73	0.47
6	June 4, 1941	0.79	0.29	0.61	0.34	0.46	0.36
7	June 12, 1941	0.33	0.58	0.34	0.87	0.30	0.37
8	June 15, 1941	0.12	0.09	0.20	0.09	0.30	0.32
9	June 29, 1941	0.51	0.27	0.49	0.29	0.36	0.42
10	July 15, 1941	0.48	0.50	0.56	0.41	0.32	0.57
11	July 29, 1941	0.40	0.39	0.71	0.63	0.51	0.58
12	Aug. 15, 1941	1.24	0.31	1.09	0.43	0.80	0.62
13	Aug. 18, 1941	0.79	0.70	0.68	0.63	0.54	0.57
14	Aug. 25, 1941	0.50	0.13	0.56	0.18	0.51	0.24
15	Aug. 25, 1941	0.08	0.16	0.16	0.21	0.29	0.47
16	Sept. 3, 1941	0.44	0.35	0.49	0.38	0.52	0.41
17	Sept. 5, 1941	0.62	0.35	0.66	0.42	0.56	0.26
18	Aug. 4, 1938	1.78	0.60	1.77	0.56	1.39	0.75
19	July 8, 1939	0.79	0.30	0.66	0.55	0.41	0.47
20	July 20, 1939	0.47	0.11	0.48	0.38	0.45	0.50
21	Aug. 7, 1939	0.20	0.12	0.40	0.50	0.49	0.52
22	July 23, 1940	0.48	0.26	0.41	0.38	0.32	0.36
23	Aug. 18, 1940	1.06	0.44	0.99	0.54	0.85	0.55
24	July 26, 1940	0.58	0.27	0.52	0.43	0.47	0.58
25	Aug. 27, 1940	0.48	0.38	0.54	0.59	0.49	0.54
26	June 7, 1940	0.26	0.17	0.30	0.25	0.29	0.37
27	June 11, 1940	0.18	0.14	0.23	0.18	0.36	0.50
28	June 18, 1940	0.72	0.36	0.55	0.47	0.38	0.44
29	June 28, 1940	0.98	0.28	0.91	0.28	0.80	0.43
30	Aug. 6, 1938	0.50	0.17	0.45	0.18	0.44	0.41
31	Sept. 4, 1937	0.46	0.27	0.40	0.34	0.68	0.66
32	Sept. 4, 1939	0.28	0.13	0.30	0.16	0.34	0.22
33	June 28, 1939	0.05	0.07	0.19	0.44	0.41	0.71
34	June 26, 1938	1.02	0.27	0.89	0.22	0.79	0.32
35	June 11, 1938	1.09	0.16	1.00	0.31	0.79	0.51
36	Aug. 9, 1938	0.32	0.08	0.38	0.13	0.37	0.25
37	June 9, 1939	0.16	0.05	0.21	0.24	0.33	0.41
38	Aug. 13, 1939	0.54	0.28	0.51	0.31	0.36	0.36

Sample functions of a standardized spatial stochastic process with a mean of zero, variance of 1.0, and an exponential correlation function with

decorrelation distance of 10 km, were generated by the turning bands method (Mantoglou and Wilson, 1981). Over each of the 35 Colorado basins, 25 sample functions (i.e., storms) were generated on a 1 km grid and areal averages were computed. A standard deviation of these areal averages was computed for each basin. These standard deviations are plotted in fig. 10. (Recall the point standard deviation was fixed at 1.0). The solid curve in this figure is based on the theoretical analysis of Rodriguez and Mehia (1974). The data presented in fig. 10 correspond to values of F_1 for each of the basins.

C. Discretization Error Factor, F_2

Grid point averages of the generated storms were computed for the 4 km grid. This was a mathematical operation analogous to the measuring process of a radar system having no measurement error. Basin averages were estimated for each storm using the 4 km grid averages. These were not exactly the same as the basin averages, according to the 1 km data, but they are well correlated. Figure 11 shows that the correlation coefficient, RHO, degenerates rapidly for basins smaller than 100 km^2. Discretization error factor F_2 is equal to:

$$F_2 = [1. - RHO^2]^{1/2} \quad (13)$$

and is illustrated in fig. 12.

D. Estimates of DV_e

The combined product (F_1) (F_2) is illustrated in fig. 13. This gives the discretization error as a proportion of the standard deviation of the point process. The measure of practical importance is the error as a proportion of the mean areal rainfall. Accordingly, the results in fig. 13 were combined with the median curve in fig. 7 to produce the estimate of error shown in fig. 14.

The final error estimates in fig. 14 take into account all of the factors affecting the discretization error and they apply to "median" storm events. Smaller events will give larger percentage errors, but these will be of little

practical importance. Larger storms will give smaller errors. Very large storms should give substantially smaller errors.

V. RELATIONSHIP BETWEEN THE HRAP GRID AND THE SPACE-TIME RESPONSE FUNCTION OF A RIVER BASIN

Geographic Information System Technology has advanced to where it is possible to construct detailed estimates of drainage systems from readily available data. Data sources include: hydrologic boundaries (for large areas); locations of larger streams, rivers, lakes, and reservoirs; and terrain data. An example of an automatically constructed drainage system for a small basin at the headwater of the Shenandoah River, Virginia, is illustrated in fig. 15. The details of how this was done are being documented in a Ph.D. theses by E. J. VanBlargan, hydrologist, Middle Atlantic River Forecast Center. With detailed information on drainage structure now readily available, studies are needed to investigate how the information should be used to represent the space-time response of the drainage system. What is the role of the HRAP grid? Is more detail required than is available from HRAP for smaller basins? These questions will be investigated during the next year.

REFERENCES

Brazil, L. E., "Description of Algorithms and Techniques," NWSRFS User's Manual, VI.3.3C, pp. 1-5, January, 1984.

Greene, D. R., and Hudlow, M. D., "Hydrometeorological Grid Mapping Procedures," AWRA International Symposium on Hydrometeorology, Denver, Colorado, June 13-17, 1982.

Hydrometeorological Section, Office of Hydrologic Director, Weather Bureau, "Thunderstorm Rainfall," Hydrometeorological Report No. 5, 1947.

Mantoglou, A., and Wilson, J. W., "Simulation of Random Fields with the Turning Bands Method," Ralph M. Parsons Laboratory, Report No. 264, MIT, July, 1981.

Rodriguez-Iturbe, I., and Mehia, J. M., "On the Transformation of Point to Areal Rainfall," Water Resources Research, Vol. 10, No. 4, pp. 729-735, 1974.

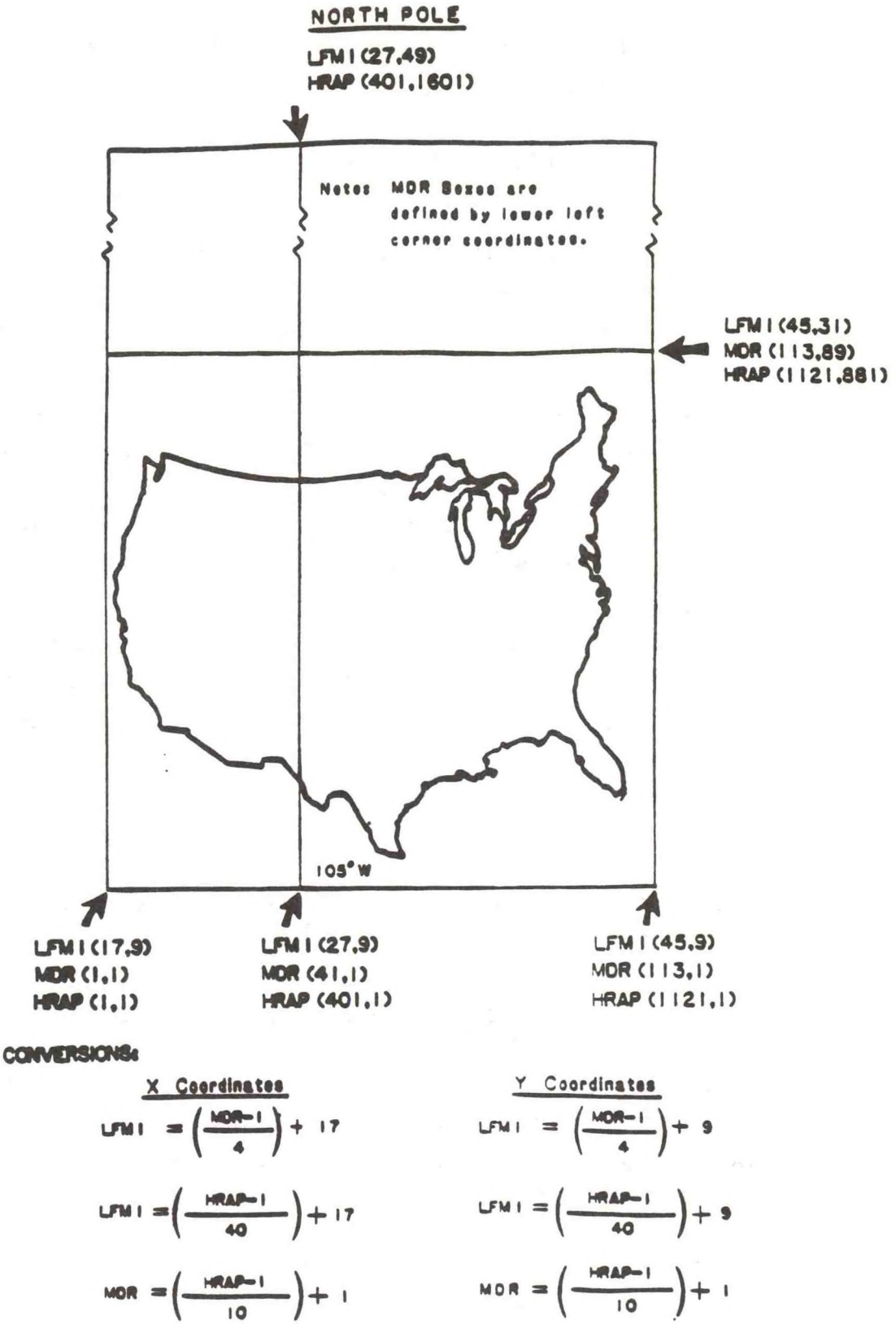

Figure 1. LFM1, MDR, and HRAP Coordinate Systems

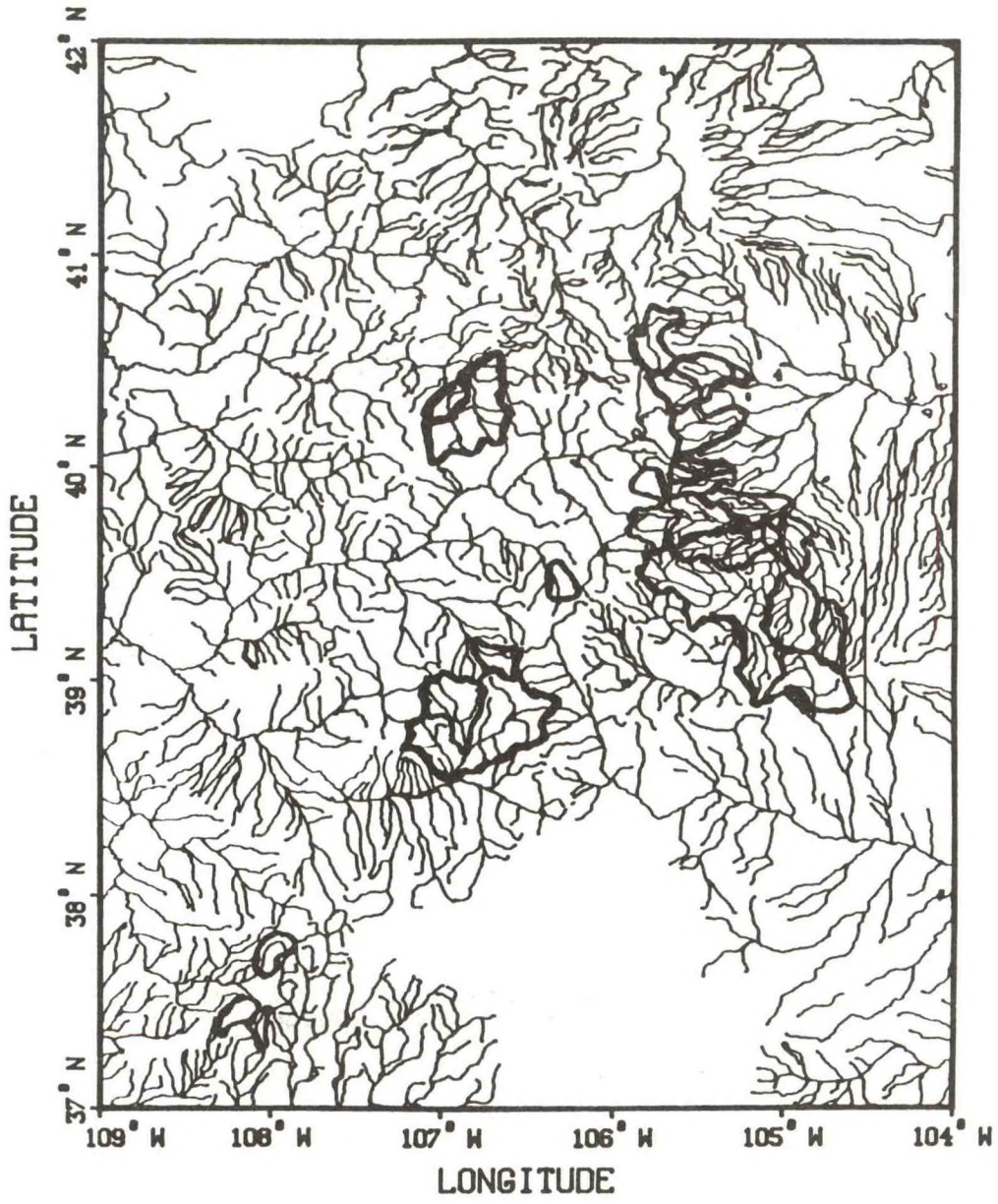

HEADWATER POINTS BASIN BOUNDARIES

Figure 2

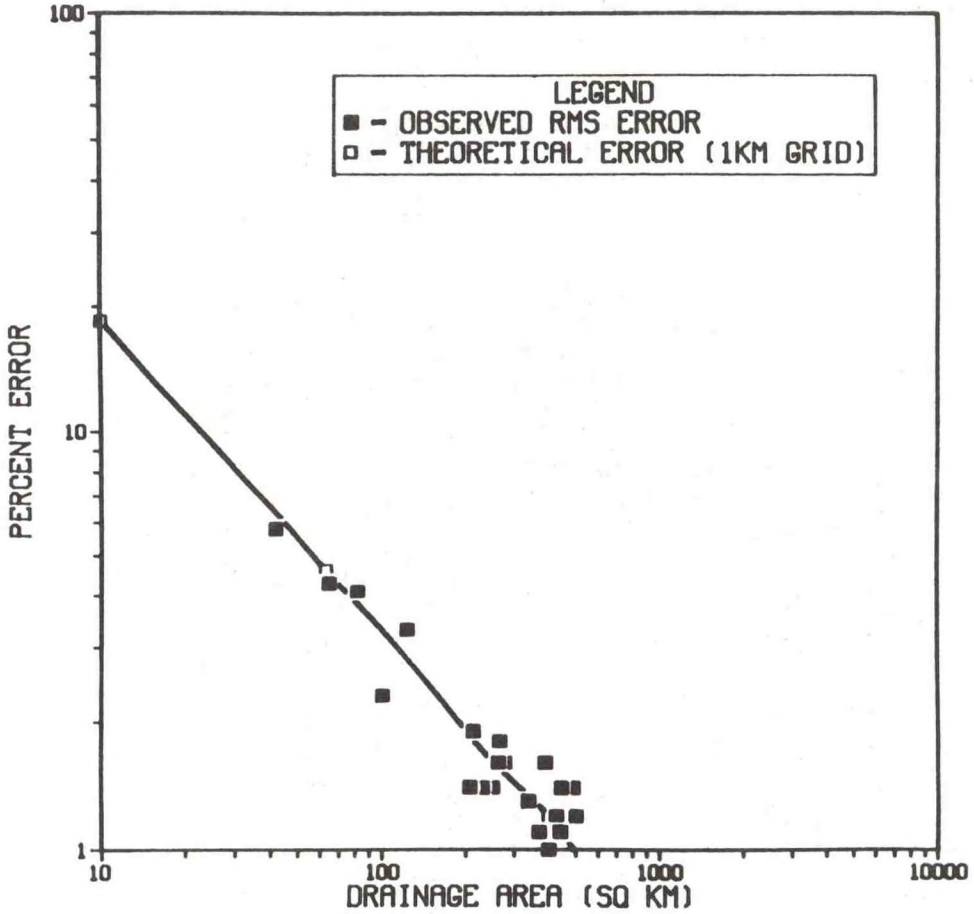

Figure 3

PERCENT ERROR OF GRID ESTIMATE OF DRAINAGE AREA (1KM GRID)
OBSERVED RMS ERRORS ARE FROM ANALYSIS OF 35 COLORADO BASINS

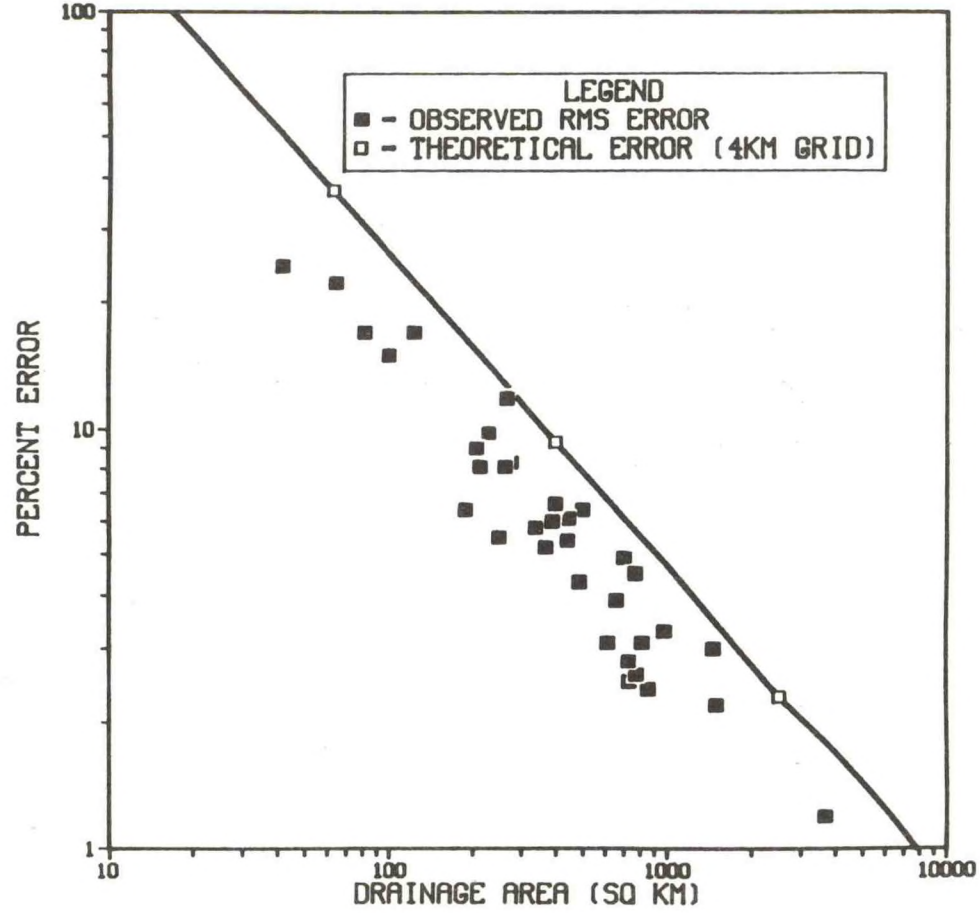

Figure 4

PERCENT ERROR OF GRID ESTIMATE OF DRAINAGE AREA (4KM GRID)
OBSERVED RMS ERRORS ARE FROM ANALYSIS OF 35 COLORADO BASINS

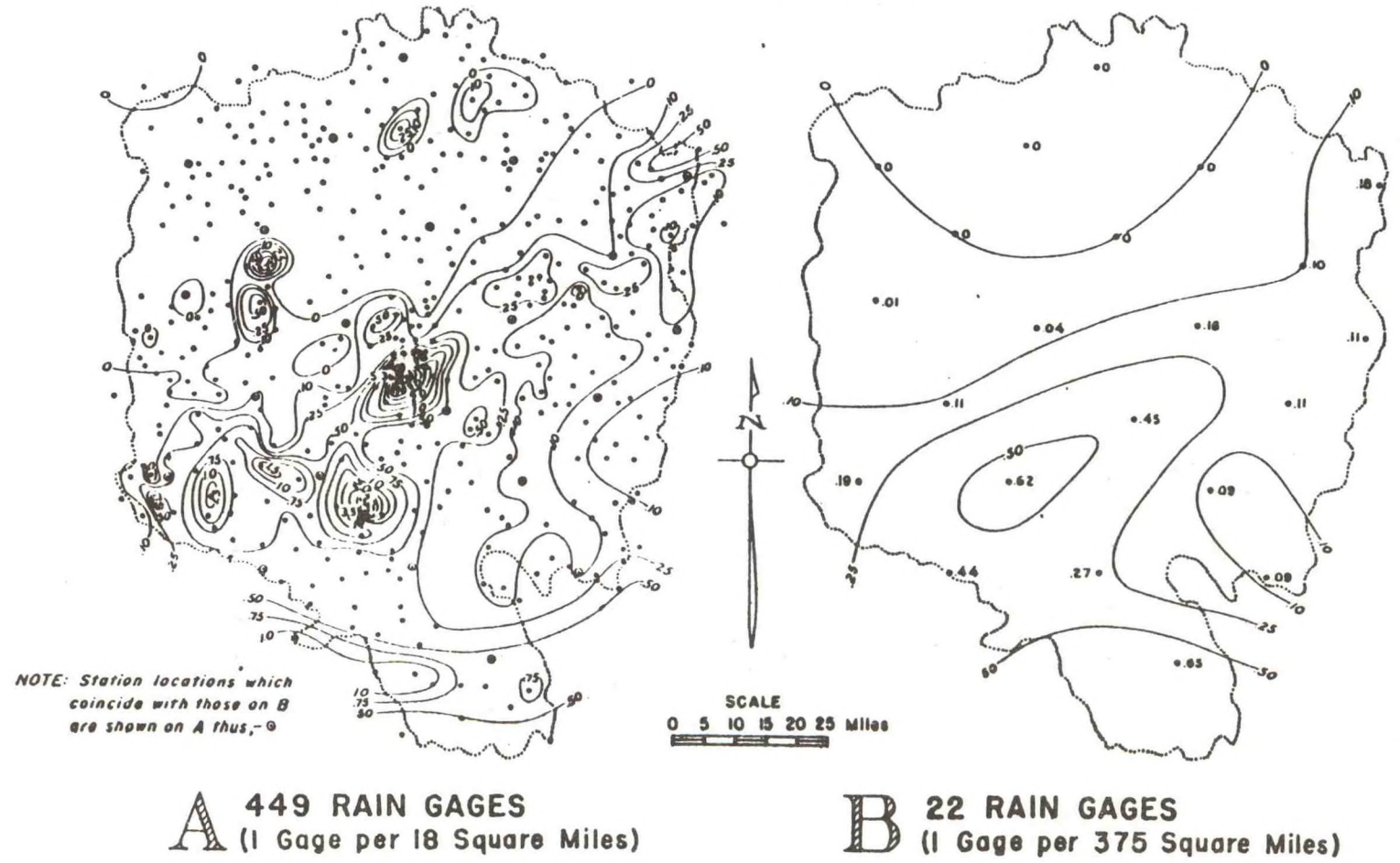
ISOHYETAL MAPS OF AUGUST 3, 1939 STORM
Muskingum Basin, Ohio
NOTE: Station locations which coincide with those on B are shown on A thus,-⊙
N
SCALE
0 5 10 15 20 25 Miles
A 449 RAIN GAGES
(1 Gage per 18 Square Miles)
B 22 RAIN GAGES
(1 Gage per 375 Square Miles)

Figure 5

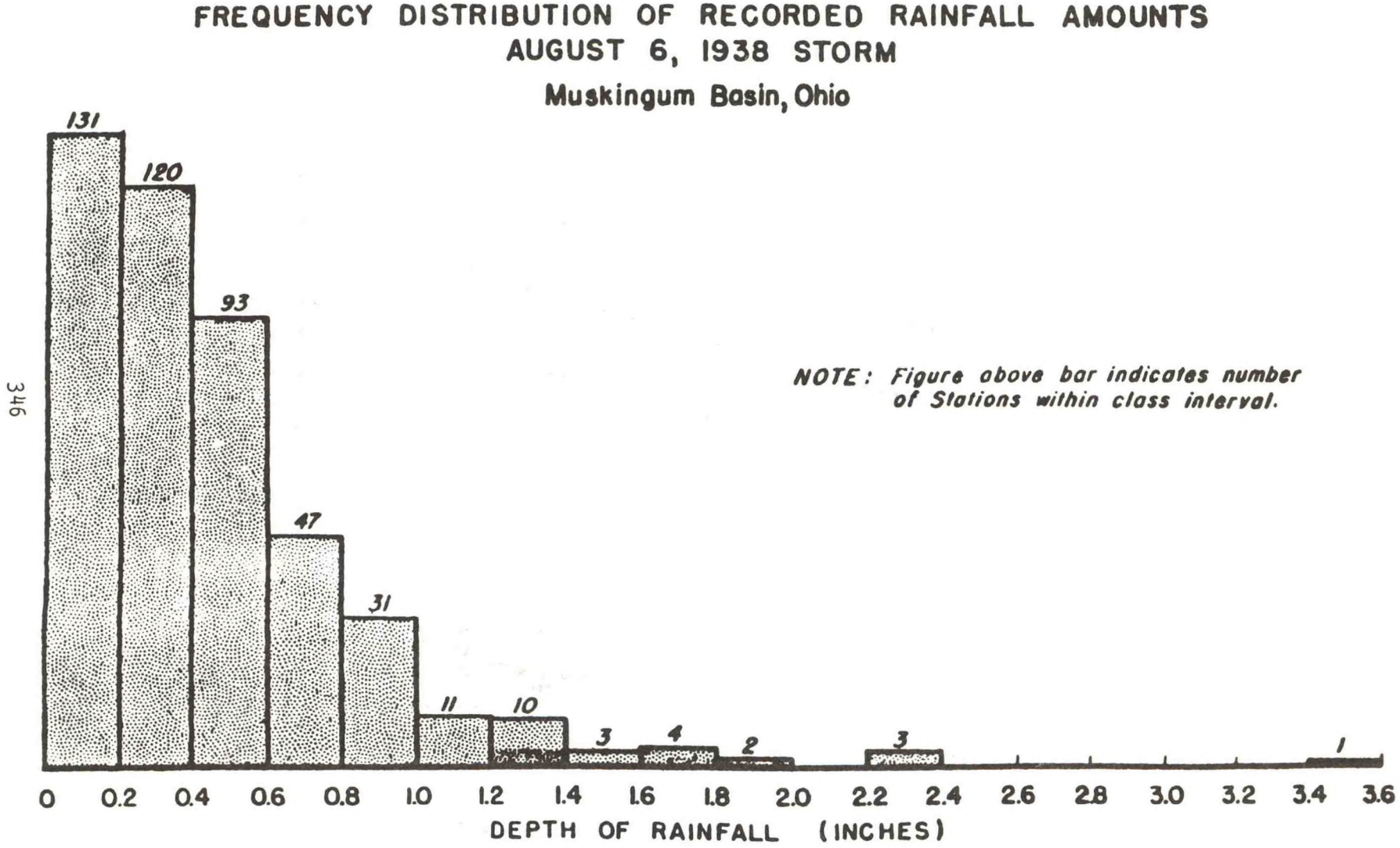
FREQUENCY DISTRIBUTION OF RECORDED RAINFALL AMOUNTS
AUGUST 6, 1938 STORM
Muskingum Basin, Ohio
131
120
93
47
31
11
10
3
4
2
3
1
NOTE: Figure above bar indicates number of Stations within class interval.
0 0.2 0.4 0.6 0.8 1.0 1.2 1.4 1.6 1.8 2.0 2.2 2.4 2.6 2.8 3.0 3.2 3.4 3.6
DEPTH OF RAINFALL (INCHES)

Figure 6

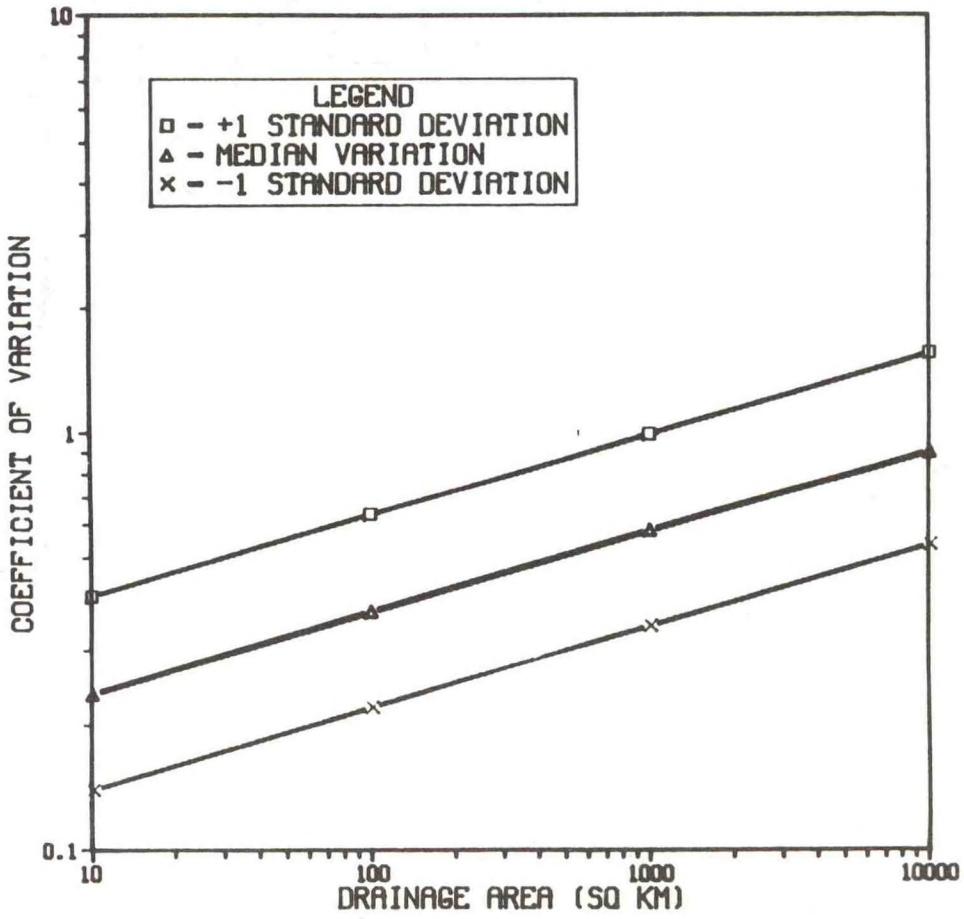

Figure 7

POINT RAINFALL COEFFICIENT OF VARIATION AS A FUNCTION OF DRAINAGE AREA
(BASED ON DATA FOR 38 6-HR STORMS, THUNDERSTORM RAINFALL PART I, P9)

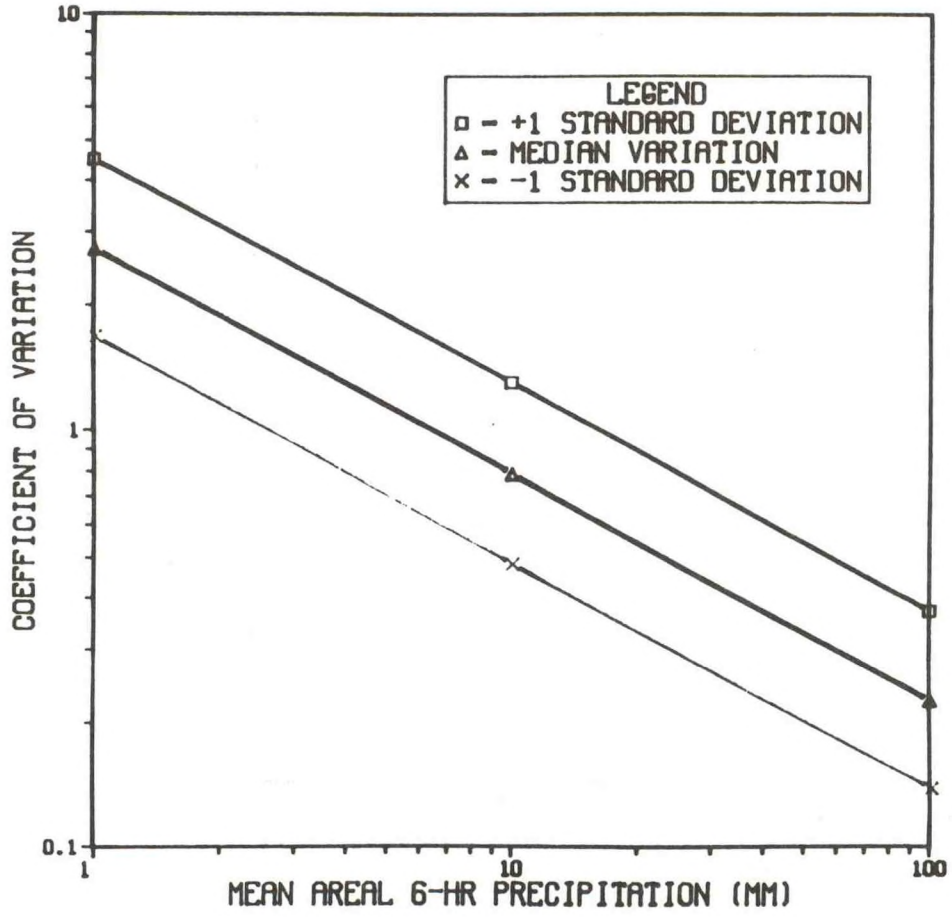

Figure 8

POINT RAINFALL COEFFICIENT OF VARIATION AS A FUNCTION OF RAINFALL AMOUNT
(BASED ON DATA FOR 38 6-HR STORMS, THUNDERSTORM RAINFALL PART I, P9)

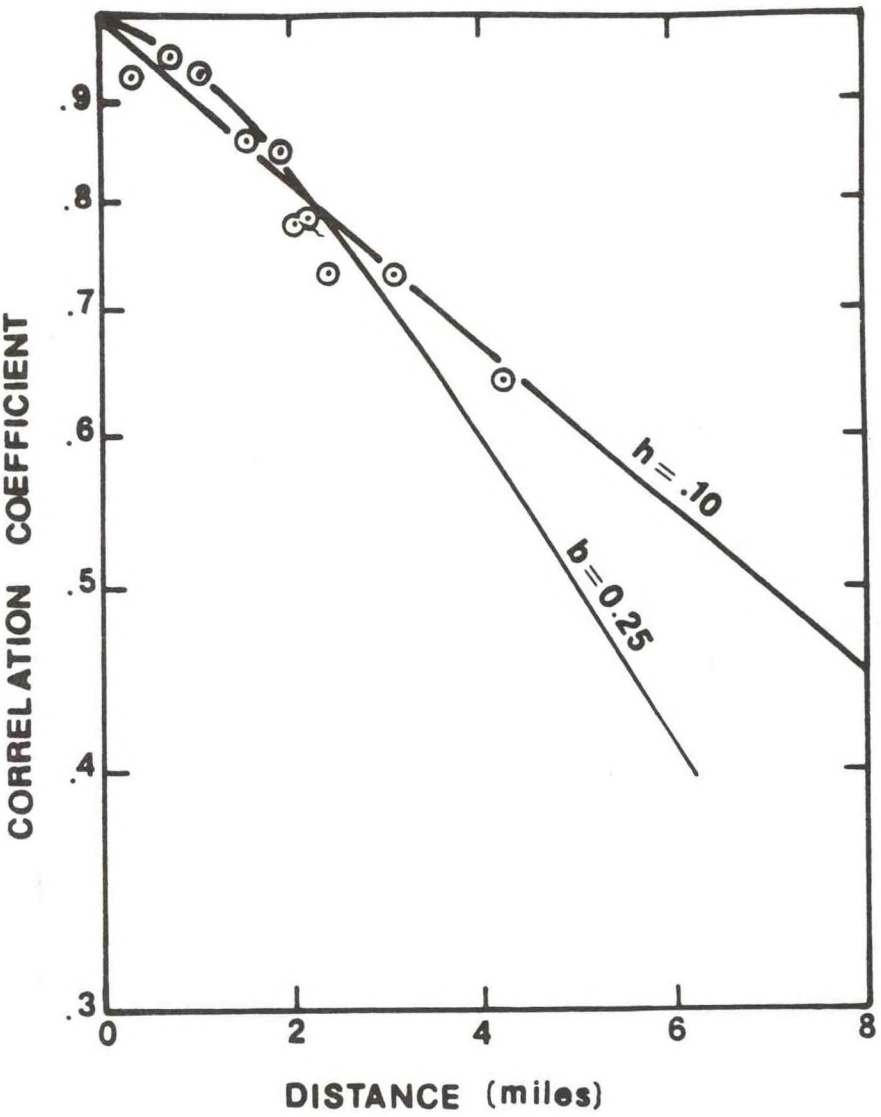

Figure 9 Spatial Correlation Function for 24-Hour Rainfall, Muskingum, Ohio

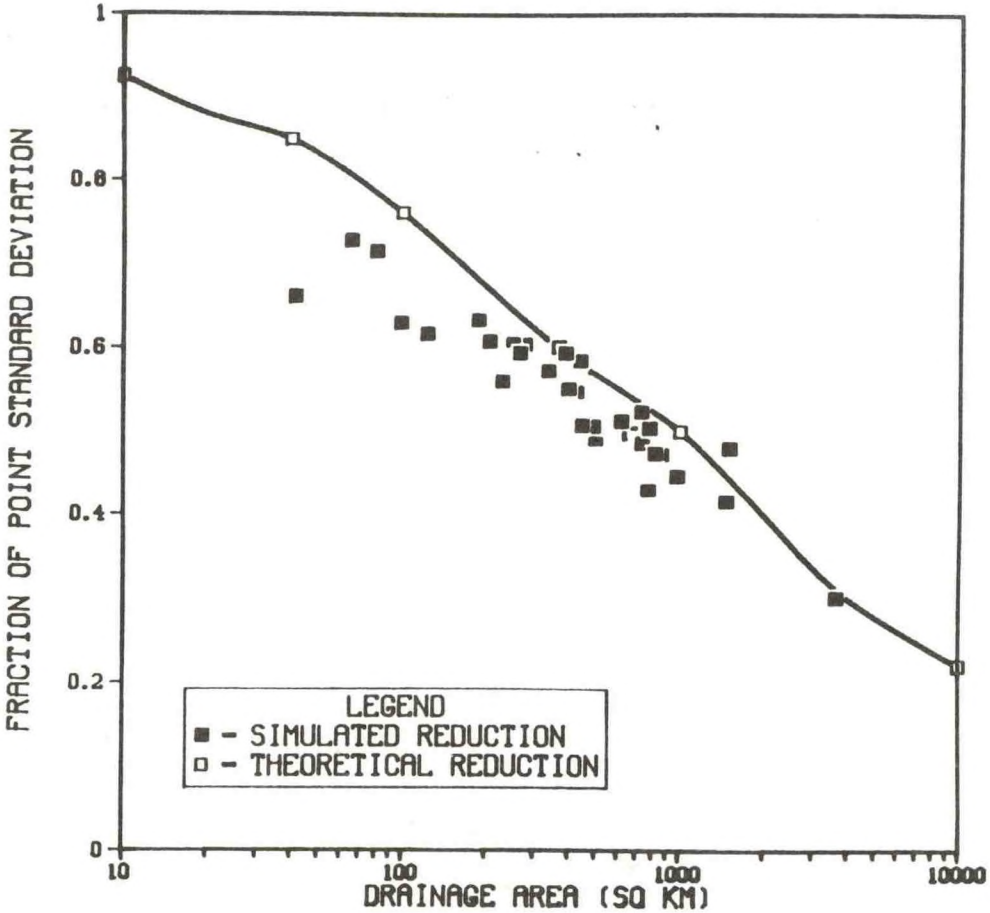

Figure 10

REDUCTION OF STANDARD DEVIATION OF MEAN AREAL RAINFALL
AS A FUNCTION OF DRAINAGE AREA
(EXPONENTIAL DECORRELATION DISTANCE - 10 KM)

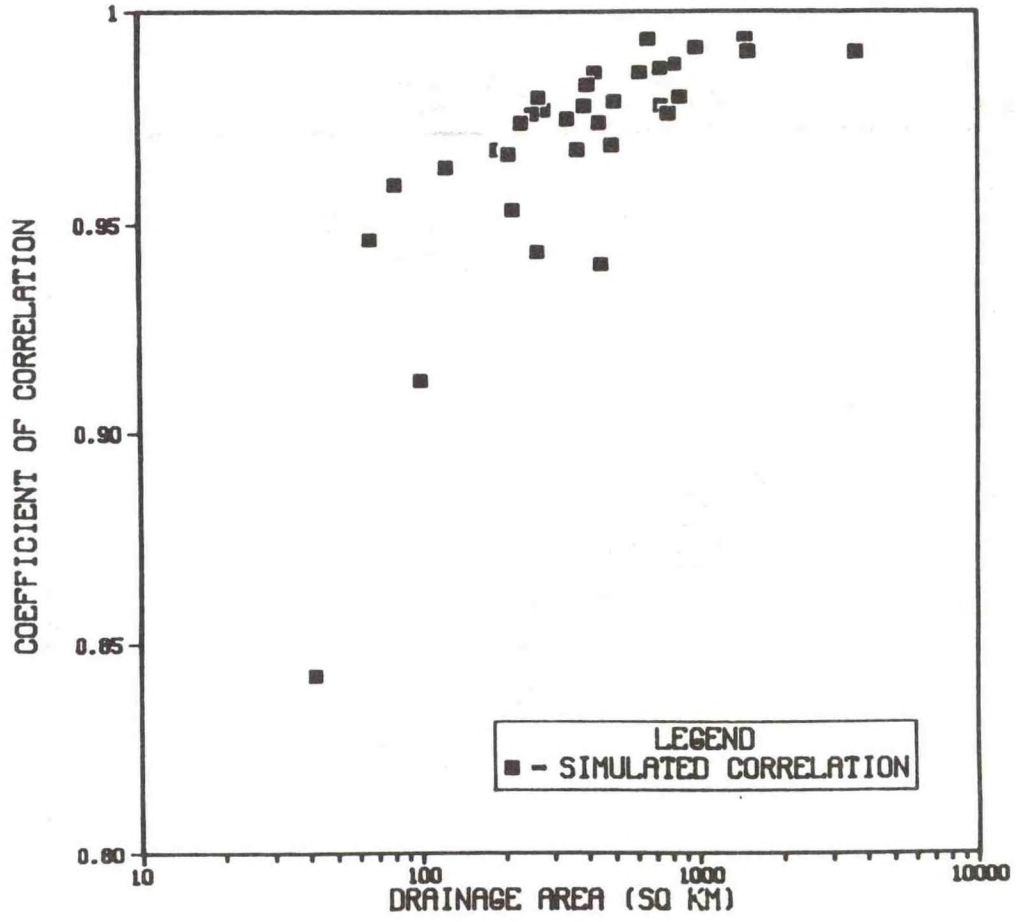

Figure 11

CORRELATION BETWEEN TRUE MEAN AREAL PRECIPITATION AND SIMPLE GRID POINT ESTIMATE AS A FUNCTION OF DRAINAGE AREA
(GRID SIZE - 4 KM EXPONENTIAL DECORRELATION DISTANCE - 10 KM)

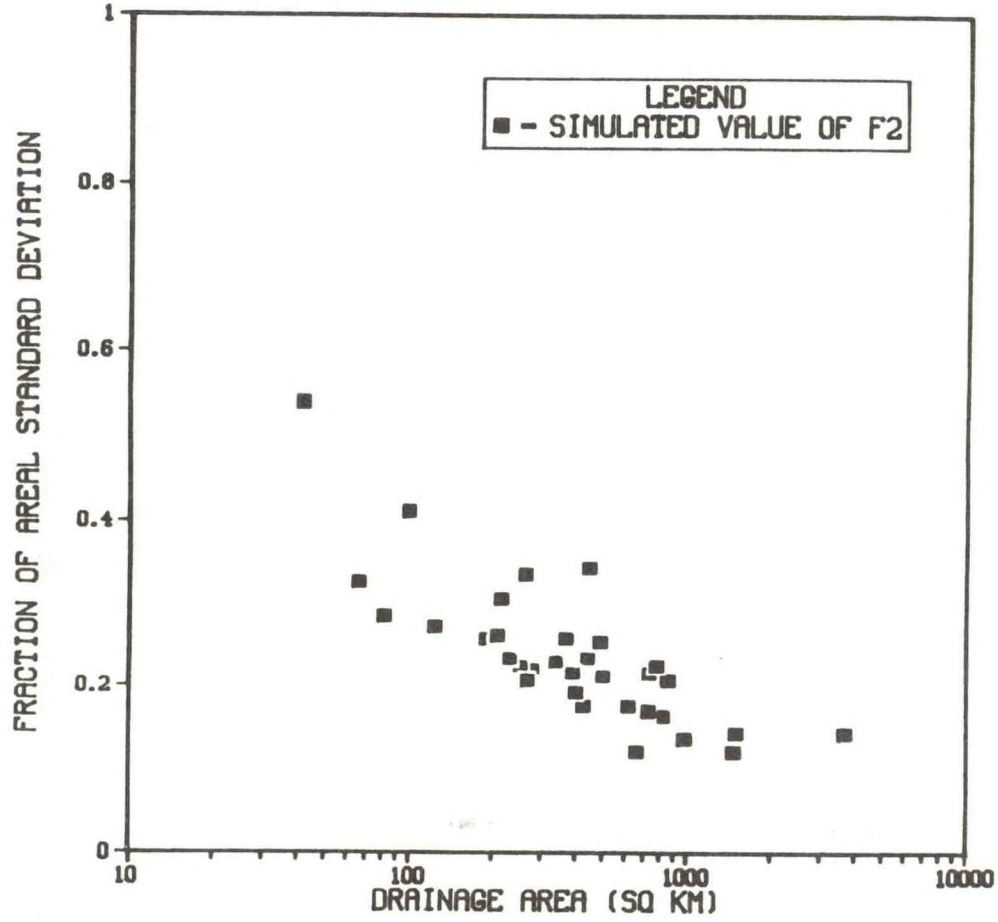

Figure 12

DISCRETIZATION ERROR FACTOR (F2) FOR SIMPLE GRID POINT ESTIMATE OF MEAN AREAL PRECIPITAION AS A FUNCTION OF DRAINAGE AREA (GRID SIZE - 4 KM EXPONENTIAL DECORRELATION DISTANCE - 10 KM)

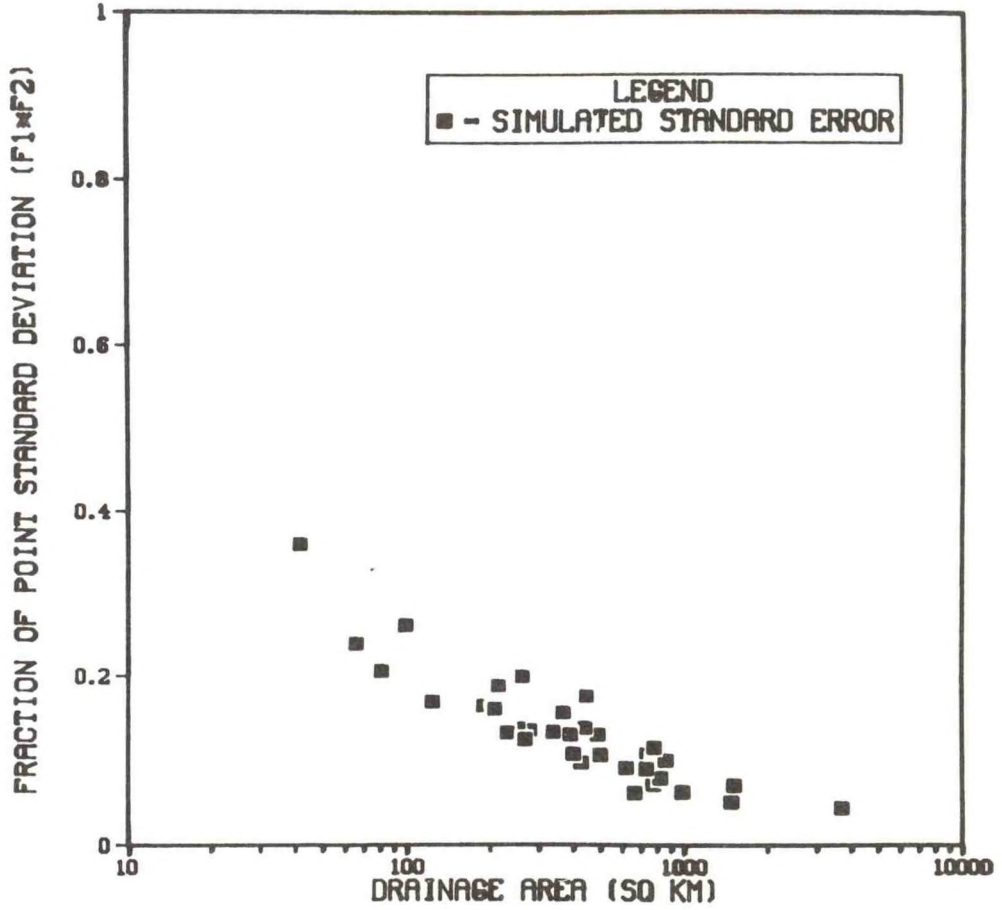

Figure 13

STANDARD DEVIATION OF ERROR IN SIMPLE GRID POINT ESTIMATE
OF MEAN AREAL PRECIPITAION AS A FUNCTION OF DRAINAGE AREA
(GRID SIZE - 4 KM EXPONENTIAL DECORRELATION DISTANCE - 10 KM)

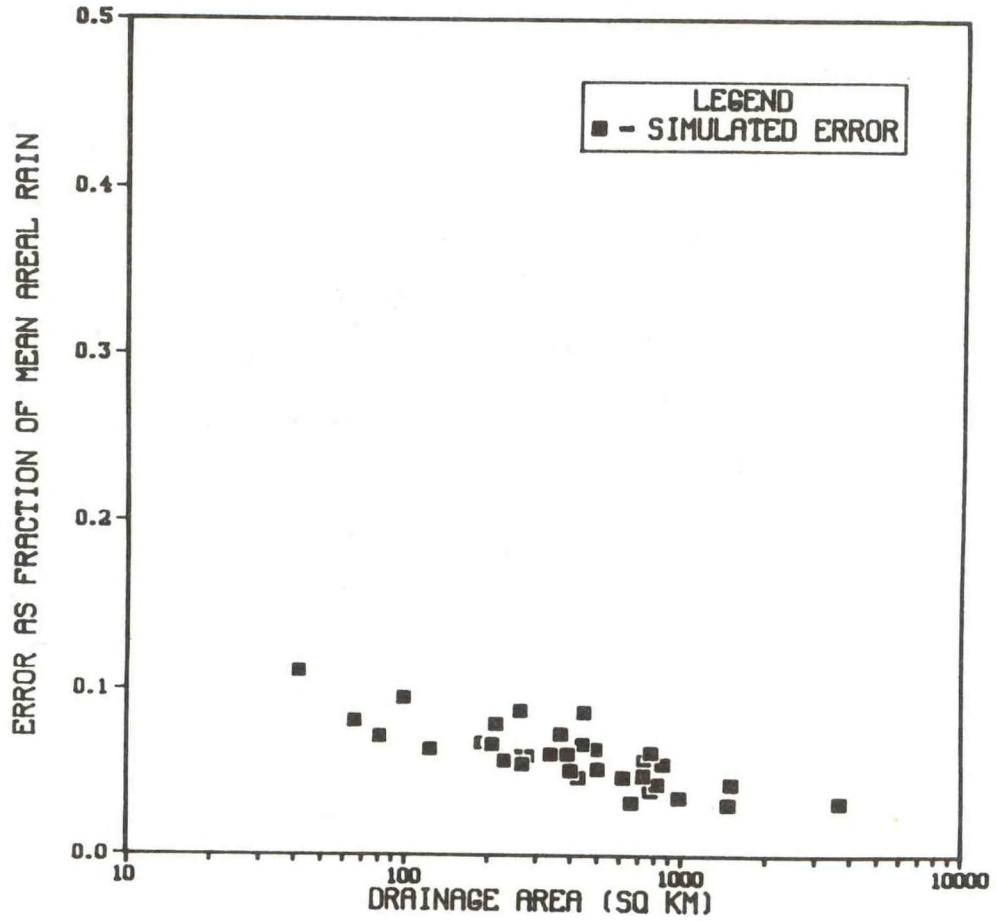

Figure 14

ERROR IN SIMPLE GRID POINT ESTIMATES OF MEAN AREAL RAINFALL
(MEDIAN STORM VARIABILITY: 6-HR STORMS)
(EXPONENTIAL DECORRELATION DISTANCE - 10 KM)

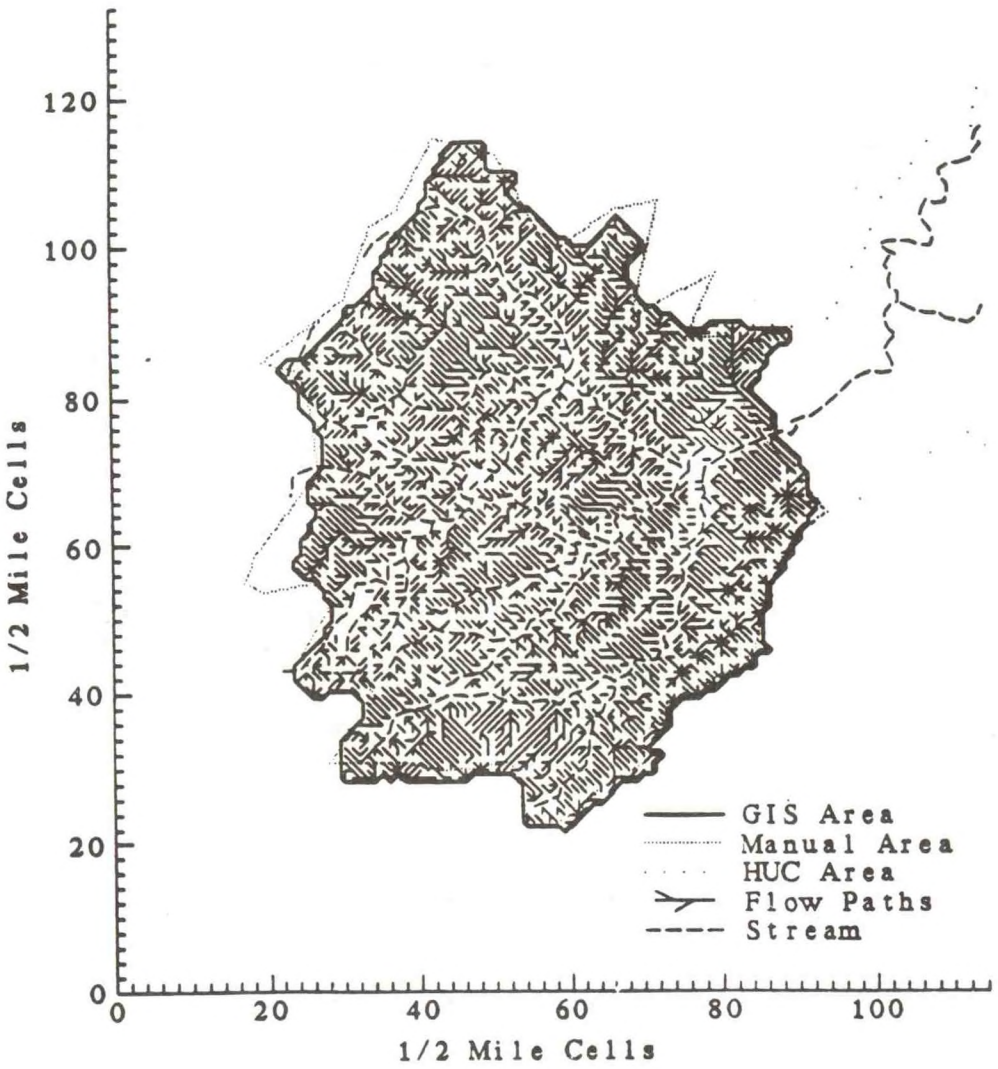

Figure 15

Gridded AREAS output for basin LYW

THE XINANJIANG MODEL AND ITS APPLICATIONS

Zhao Ren jun and Wang Pei lan
Hohai University

ABSTRACT. The Xinanjiang Model is a rainfall runoff basin model to be used in humid and semi humid regions, of which the part of evapotranspiration adopts a three soil layer model. The part of runoff production accepts the idea of runoff formation at natural storage. Runoff is produced only if the soil moisture content of the aeration zone reaches its field capacity. The part of runoff separation used the Horton concept before 1980, the two components, surface runoff and groundwater runoff, were separated, then the concept of Hillslope Hydrology is used. An additional component interflow is separated and the mechanism of surface runoff production is the saturated overland flow. The part of runoff concentration refers to unit graph or lag and route method. To flood routing, the Muskingum method is applied. There are 15 parameters in the model of which six were sensitive ones. Using structural constraints and multi-layer, multi-objective functions an optimization method is derived. The model has been widely used in China mainly for the purpose of forecasting and is beginning to be popular in other fields.

The Xinanjiang Model was established in 1973 and introduced to the world in 1980[1]. Its main feature is the concept of runoff formation at natural storage which means that runoff would not be produced unless the soil moisture content of the aeration zone reaches field capacity. While the field capacity is being reached, runoff would be equal to rainfall without loss. We put forward this idea in the early sixties and, by examination in the long run, it proves right in humid and semi humid regions of China. According to the Horton concept, the total runoff would be

separated into two components. The one infiltrated by final constant rate is groundwater runoff and the other, in excess of final constant rate, is surface runoff. This is the point of note 1. But, we found that, in many cases, unstability of the final constant rate and unit graph appears and leads to practical difficulties. This shows that the structure of the model is unsatisfactory. In fact, the Horton concept does not accord with humid conditions, so we modified the model structure by using the concept of Hillslope Hydrology [2], an additional component interflow is separated and the surface runoff is produced by saturated overland flow. This modified model is now successively and widely used in China. It will be introduced in detail in this paper. On the basis of note 1, some other attempts to modify the model have been developed, not by me, and will not be mentioned here.

I. STRUCTURE

This is a distributed model, dividing the basin into sub-basins. The outflow hydrograph of every sub-basin is first simulated and then routed down to the basin outlet. The flow chart is shown as fig. 1.

Within the blocks are inputs, outputs, and states which are variables, outside the blocks are parameters which are constants. Inputs are: P, measured rainfall; EM, measured pan evaporation. Outputs are: TQ, basin outlet discharge; E, basin evapotranspiration. E = EU (upper layer) + EL (lower layer) + ED (deep layer).

State variables in fig. 1 are:

R, runoff produced on pervious area;

RB, runoff produced on impervious area;

FR, runoff producing area, by proportion;

W, tension water storage;

S, free water storage;

RS, RI, RG, surface, interflow, groundwater runoff;

QS, QI, QG, inflow to river system from RS, RI, RG;

T, total inflow to the river system; and

Q, outflow of sub-basin.

The structure is composed of four parts: (1) Evapotranspiration -- A three soil layer model is used. Parameters are: UM, LM, tension water capacity of the upper and lower layer; C, coefficient of deep evapotranspiration; K, ratio of potential evapotranspiration to pan evaporation.

For the upper layer, evapotranspiration is equal to potential evapotranspiration.

```
IF  P+WU>K*EM  THEN  EU = K*EM
ELSE  EU = WU+P                                          (1)
```

For the lower layer, evapotranspiration is proportional to potential evapotranspiration and soil moisture content.

```
EL = (K*EM-EU)*WL/LM                                     (2)

IF  EL<C*(K*EM-EU)  THEN
    EL = C*(K*EM-EU)                                     (3)
```

For the deep layer, evapotranspiration is proportional to potential evapotranspiration.

```
IF  WL<C*(K*EM-EU)  THEN
EL = WL:  ED = C*(K*EM-EU)-EL                            (4)
```

2. Runoff production. Using the concept of runoff formation at natural storage to evaluate total runoff R per time period. In addition, to take account of the non-uniform distribution of the tension water capacity over the area, a tension water capacity curve is introduced. It is expressed by a parabola.

In fig. 2, parameters are: WM, areal mean of the tension water capacity; WM = UM(upper layer) + LM(lower layer) + DM(deep layer); B, exponent of the

tension water capacity curve; IM, ratio of impervious area to total area.

Maximum value of the tension water capacity:

$$MM = WM*(1+B)/(1-IM) \tag{5}$$

Equivalent tension water storage over the basin:

$$A = MM*[1-(1-W/WM)**(1/(1+B))] \tag{6}$$

IF P-K*EM+A<MM THEN

$$R = P-K*EM-WM+W+WM*(1-(P-K*EM+A)/MM)**(1+B) \tag{7}$$

$$\text{ELSE } R = P-K*EM-WM+W \tag{8}$$

3. Separation of runoff into components. Total runoff R is to be separated into surface runoff RS, groundwater runoff RG and interflow runoff RI. RS is produced by saturated overland flow. The free water storage in the surface soil layer is denoted by S. Storage S drained laterally becomes RI and drained downward becomes RG. Considering the non-uniform distribution of the free water capacity over the area, a free water capacity curve is introduced which is expressed by a parabola also. In fig. 3, parameters are: SM, areal mean of free water capacity; EX, exponent of the free water capacity curve; KI, outflow constant of free water storage to interflow; KG, outflow constant of free water storage to groundwater.

The formulas used are similar to eqs. (5) - (8).

Maximum value of the free water capacity

$$MS = SM*(1+EX) \tag{9}$$

Equivalent free water storage over the runoff producing area FR

$$AU = MS*[1-(1-S/SM)**(1/(1+EX))] \tag{10}$$

IF AU+P-K*EM<MS THEN

$$RS = (P-K*EM-SM+S+SM*(1-(P-K*EM+AU)/MS)**(1+EX))*FR \tag{11}$$

$$\text{ELSE } RS = (P-K*EM+S-SM)**FR \tag{12}$$

$$RG = S*KG*FR \tag{13}$$

$$RI = S*KI*FR \tag{14}$$

4. Runoff concentration. Free water storage drained laterally becomes interflow. Interflow is first produced in the upper part of surface soil layer. If the surface soil layer is thick enough then the interflow produced may infiltrate to its lower part and finally flow into the river system. The lower free water storage is simulated by a linear reservoir of which the recession constant is CI. Free water storage is drained downward and reaches the groundwater reservoir which is simulated by a linear reservoir with recession constant CG.

$$QI(I) = QI(I-1)*RI(I)*(1-CI)*U \tag{15}$$

$$QG(I) = QG(I-1)*RG(I)*(1-CG)*U \tag{16}$$

in which QI and QG are inflow to the river system caused by interflow and groundwater flow. U is a unit conversion factor.

Flow concentration of the sub-basin is computed by unit graph or by lag and route method with parameters time lag L and recession constant CG.

Flood routing from the sub-basin outlet to the basin outlet is computed by Muskingum method through successive routing by sub-reaches.

II PARAMETERS

The parameters have definite physical meanings and definitions, so theoretically they could be determined by measurements. But it is practically impossible, we have to solve the parameter values by system identification. This is quite a difficult task. To make it easy, we should investigate the sensitivity and independence of parameters. Insensitive parameters can be given value by experience, being fixed or modified individually at last. Independence of parameters is a necessary condition for identification, the solution of dependent parameters will be unstable and non-unique, unable to cope with their physical definitions.

In this model there are 15 parameters (for a sub-basin, using lag and route method) distributed in 4 parts as mentioned above.

1. Evapotranspiration. K, UM, LM, C
2. Runoff production. WM, B, IM

3. Separation of runoff into components. SM, EX, KG, KI

4. Runoff concentration. CG, CS, CI, L

The underlined parameters are sensitive ones.

Some descriptions should be given to the parameters. K is the ratio of potential evapotranspiration to pan evaporation. This is a sensitive parameter since it controls water balance. $K=k_1*k_2*k_3$. k_1 is the ratio of pond evaporation to pan evaporation. k_1 can be determined by experiments. k_2 is the ratio of potential evapotranspiration to pond evaporation. k_2 is about 1.3-1.5 in summer and 1.0 in winter. k_3 is a coefficient to correct the measured pan station value to the basin mean. Practically $k_1*k_2=1$. k_3 is a function of elevation difference between pan station and basin mean.

WM is the areal mean of tension water capacity. WM = UM(upper layer) + LM(lower layer) + DM(deep layer) is a measure of the aridity of the basin. It varies from 80mm in South China to 170mm in North China. WM is insensitive because it is irrelevant to evapotranspiration computation. But, it must be large enough to ensure the computed soil moisture content, W being positive. Parameters UM and LM are determined by experimental experience, we use UM = 5mm for deforested areas and UM = 20mm for forested areas. For LM we take 60-90mm by which we believe that in such a layer, evapotranspiration is approximately proportional to soil moisture content.

B, the exponent of tension water capacity curve, defines the non-uniformity of soil moisture condition, so generally it is a function of basin area. By experience of rainfall runoff analysis of flood events we know that B = 0.1 for basins smaller than 10 sq.km, and B = 0.4 for basins of thousands sq.km.

IM, is the ratio of impervious area to total area. For natural basins IM = 0.01-0.02 is negligible. But in semi humid areas IM is sensitive since the runoff producing area is comparatively small.

C, the coefficient of deep evapotranspiration, depends on coverage of deep root plants. It varies from 0.18 in South China to 0.08 in North China. It is inactive in humid areas and humid seasons but is important in dry areas and dry seasons. The value of C is relevant to UM and LM, but as UM+LM is usually

kept in a certain value, say 100mm or so, C can be well defined and determined.

SM, the areal mean of free water capacity of the surface soil layer, is equivalent to the maximum deficit of free water storage. This parameter is sensitive to determine surface runoff. For thin surface soil SM = 10mm and for thick and porous surface soil SM = 50mm in daily model if we take KG+KI = 0.7 and EX = 1.5. This parameter value relates to rainfall distribution in a time period, the more concentrated the rainfall, the larger the value of SM. Care must be taken in comparing the SM of the daily model with an event model.

EX, is the exponent of the free water capacity curve, dealing with its non-uniform distribution over the area. Due to Hillslope Hydrology, it determines the development of the saturated area. EX is dependent on SM, but statistical analysis shows that the value of EX lies in a small range from 1 to 2, so we may take it as 1.5.

KG, KI is the outflow constant of the free water storage to groundwater and interflow storage. KG+KI determines outflow rate of free water storage and KG/KI determines proportion of groundwater flow to interflow. KG = KI is dependent on SM, as shown in fig. 3, while KG+KI increases, SM decreases and KG/KI remains constant, the solution of runoff separation into components may be unchanged. Since they are sensitive parameters, their dependence should be avoided. As the recession duration of the upper interflow storage ordinarily lies in 2-3 days, we may take KG+KI = 0.7, the KG/KI would be independent of SM. This is called structural constraint.

CI, is the recession constant of lower interflow storage. In humid regions we find CI = 0.6-0.9.

CS, is the recession constant of river storage defined by the lag and route method. This method is easy to use and no less accurate than the unit graph. The parameter value is empirical.

L, is the lag of river storage defined by the lag and route method. It is an integer in programming and is empirical also.

KE, XE, are parameters of the Muskingum method which can be determined by hydraulic formulas.

In the following, we shall describe the optimization method of parameters. The above mentioned four parts of parameters correspond to four layers having different characteristics in optimization. The first layer is the most stable and the fourth the most active. Sensitive parameters are mostly distributed in higher layers. Parameters between layers are comparatively independent and within a layer dependent. The parameter value of a higher layer gives small effect on the solution of parameter value of the lower layer. For example, variation of parameter value of runoff concentration in a reasonable range will not influence the solution of parameter value of runoff separation, variation of parameter value of runoff separation will not influence the solution of parameter value of runoff production and evapotranspiration. In addition, objective functions for different layers are different. For the first layer it is the error of total runoff in a long term. For the second layer, it is the error of runoff of flood events. For the third and fourth layer, it is the error of the hydrograph. We can not distinguish the third layer from the fourth by different objective functions, but the information given by the hydrograph may be used to isolate these two layers. The surface runoff discharge is located at the flood part, groundwater discharge is located at the flood part, groundwater discharge at the low flow part and interflow discharge at the transitionary part of the hydrograph, their differences are quite sharp. It results that variation of parameter values of runoff concentration in a reasonable range will not influence the solution of parameter values of runoff separation. So the parameter values of the third and fourth layer can be isolatedley identified.

The objective functions we choose are:

$$\Delta R = \text{computed runoff} - \text{measured runoff} \tag{17}$$

$$ABS = \sum_{1}^{m} ABS[M(I)-Q(I)] / \sum_{1}^{m} M(I) \tag{18}$$

$$LOG = \sum_{1}^{m} ABS\{LOG[M(I)/Q(I)]\} / \sum_{1}^{m} LOG[M(I)],\ M(I)>1. \tag{19}$$

in which M(I) and Q(I) are measured and computed discharge.

The optimization procedure is as follows:

1. Assume initial value for parameters.

2. To optimize K, using daily model and eq. (17) for a long term no less than four years. If the computed W<0 then increase the value of WM.

If necessary, adjust the value of C after K is preliminarily worked out.

3. Take KG+KI = 0.7, EX = 1.5, optimization SM and KG/KI using daily model and eq. (19). Then adjust the value of CG and CI individually while SM and KG/KI remain unchanged.

Or, SM, KG/KI, CG and CI are optimized together by an automatic optimization method.

4. Using the event model to adjust SM by eq. (18). If necessary, adjust B. Then,

5. Optimize L and CS using event model and eq (18).

If a distributed model is used, parameters KE and XE would appear. They can not be optimized objectively.

III. APPLICATIONS

The Xinanjiang Model has been used in China for a long time and the efficiency is affirmed. The results cover a large territory, including almost all of the agricultural, pastural, and forested lands of China except loess areas. For the loess areas of China, another model based on the concept of runoff formation in excess of infiltration would be used.

The Xinanjiang Model in China is mainly used for hydrological forecasting. Many large projects and forecasting systems use this model. It is being extended and developed to meet with miscellaneous surface conditions such as snow cover, Karst, large plains, swamp, etc. Research work on the regional rule of model structure and parameters is being carried on.

REFERENCES

1 Zhoa etc, The Xinanjiang Model, Pro. of Oxford Symposium, AISH, 1980.

2 M.J. Kirkby, Hillslope Hydrology, 1978.

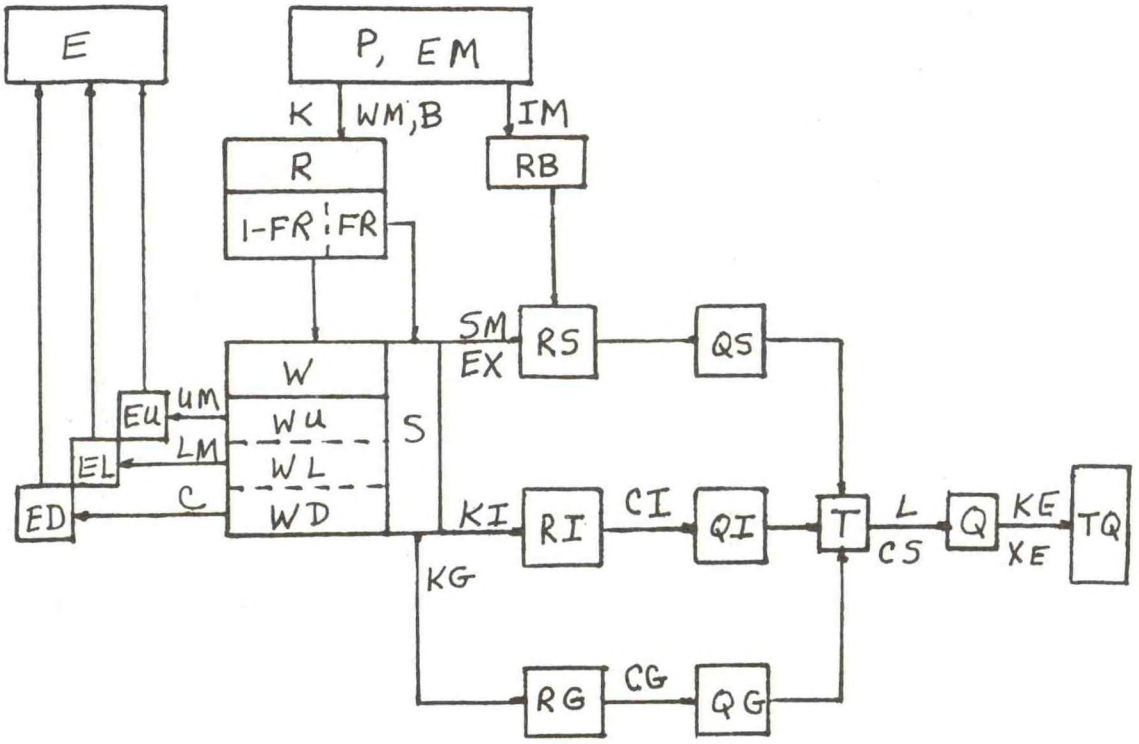

Fig.1. Flow Chart of Xinanjiang Model

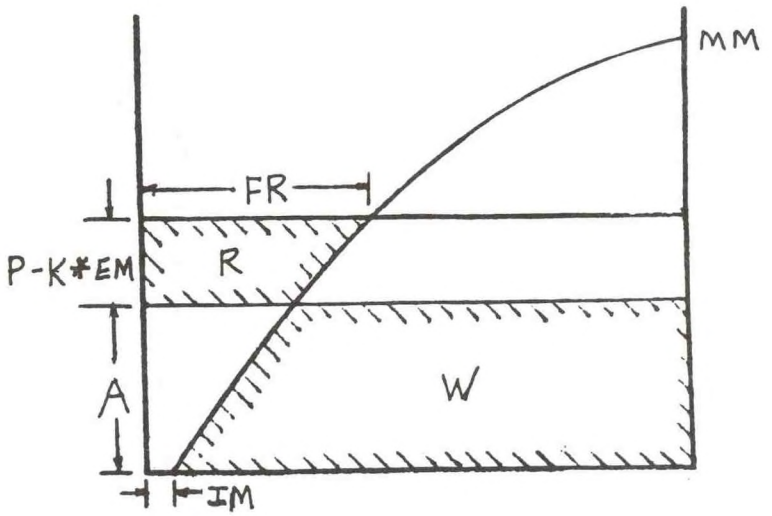

Figure 2. Rainfall runoff relation

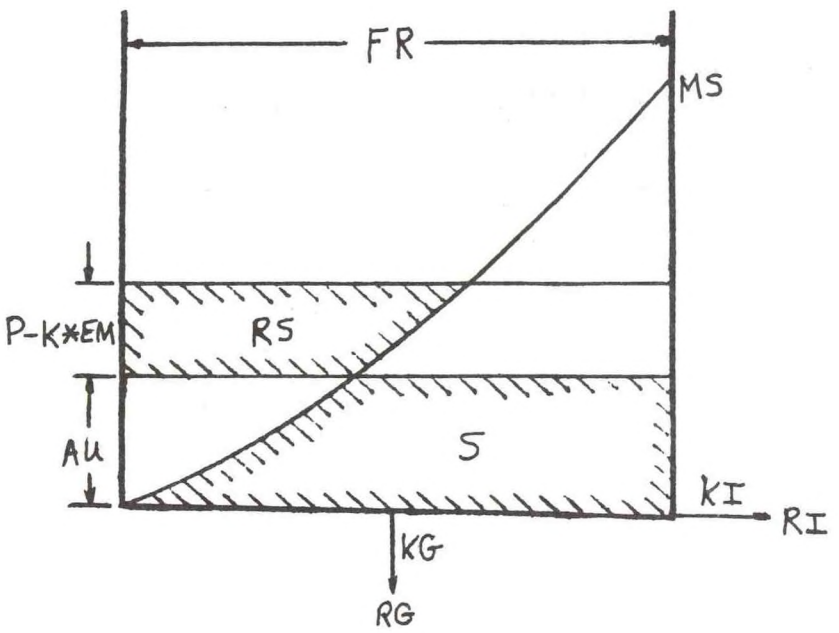

Figure 3. Separation of runoff into components

☆ U. S. GOVERNMENT PRINTING OFFICE : 1992 O - 317-145 VOL 1


DEPARTMENT OF COMMERCE
UNITED STATES OF AMERICA

Themes

Data Collection/Dissemination
Hydrologic Models
Forecasting

Participating Agencies:

People's Republic of China

Yangtze Valley Planning Office
Yellow River Conservancy Commission
Haihe River Conservancy Commission
Hohai University
General Hydrologic Station of Fujian Province
Institute of water Conservancy and Hydroelectric Power Research

United States of America

Corps of Engineers
Geological Survey
National Weather Service
Soil Conservation Service
Portland State University
San Diego State University
Iowa University